POLITECNICO
MILANO 1863

OPTIMIZATION-BASED CONTROL OF MICROGRIDS FOR ANCILLARY SERVICES PROVISION AND ISLANDED OPERATION

Doctoral Dissertation of
Alessio La Bella

Supervisor
Prof. Riccardo Scattolini

POLITECNICO DI MILANO
DEPARTMENT OF ELECTRONICS, INFORMATION AND BIOENGINEERING

DOCTORAL PROGRAMME IN INFORMATION TECHNOLOGY

Optimization-based control of microgrids for ancillary services provision and islanded operation

Doctoral Dissertation of
Alessio La Bella

Supervisor
Prof. Riccardo Scattolini

Tutor
Prof. Lorenzo Mario Fagiano

Chair of the Doctoral Program
Prof. Barbara Pernici

2019 – XXXII Cycle

As you set out for Ithaka
hope your road is a long one,
full of adventure, full of discovery.
Laistrygonians, Cyclops,
angry Poseidon—don't be afraid of them:
you'll never find things like that on your way
as long as you keep your thoughts raised high,
as long as a rare excitement
stirs your spirit and your body.

[...]

Keep Ithaka always in your mind.
Arriving there is what you're destined for.
But don't hurry the journey at all.
Better if it lasts for years,
so you're old by the time you reach the island,
wealthy with all you've gained on the way,
not expecting Ithaka to make you rich.

Ithaka gave you the marvellous journey.

[...]

And if you find her poor, Ithaka won't have fooled you.
Wise as you will have become, so full of experience,
you'll have understood by then what these Ithakas mean.

(*Ithaka*, Konstantinos Kavafis)

Aknowledgements

It is not simple to condense in few lines my gratitude to all the people who have contributed to the realization of this doctoral thesis and supported me throughout this fantastic journey.

First of all, I want to deeply thank Prof. Riccardo Scattolini for his considerable guidance and for having been more than a supervisor. His critical thinking, wide expertise and contagious passion have inspired me since my master studies. Moreover, I want to really thank him for the constant support and for having trusted me multiple times, giving me the opportunity to do research, to teach and to have significant experiences.

I sincerely thank RSE S.p.A. for having funded my research and for the valuable support in understanding many aspects of the electrical power system. In particular, I want to express my gratitude to Eng. Carlo Sandroni, for having been my reference point, for our insightful discussions and for having always supported and followed my research activity.

I want to thank all the people I had the opportunity to collaborate with during my doctoral studies. In particular, I thank Prof. Lorenzo Fagiano, Prof. Marcello Farina, Prof. Giancarlo Ferrari Trecate and Prof. Maria Prandini, for having been inspirational figures to me and for having each one supported part of my research.

Moreover, I want to express my gratitude to Fabio Bonassi, Pulkit Nahata, Stefano Raimondi Cominesi, Alessandro Falsone, Andrea Martinelli and Simone Negri for having been not only valuable collaborators, but also great friends.

I really thank my colleagues and friends at DEIB, especially for the warm, enjoyable and hilarious daily atmosphere we have been able to keep at the department. These years would have not been so amazing without them.

Surely, one of the biggest thanks go to my father Vito, my mother Aurora and my sister Noemi for their endless love. I am really indebted to them for having taught me to do always my best and for having motivated and supported me in each moment of my life.

I would like also to thank all my great and lifelong friends for the amazing time and experiences we spent together, especially Anastasia, Alessandra, Vincenzo, Marco, Eugenio, Caterina, Marcella, Andrea, Valentina and Salvo. Their sincere friendship and support have been fundamental to me and I consider them one of my greatest luck.

Last but definitely not least, I want to thank my significant other, Nina. Her continuous encouragement and enormous love are one of the key pillars of my life. I thank her to have supported me throughout this journey, and for the immense joy she has been always able to transmit me.

Thank you all, this work is dedicated to all of you.

Milan, October 2019

Alessio La Bella

Financial Support

This work has been financed by the Research Fund for the Italian Electrical System in compliance with the Decree of April 16, 2018.

Alessio La Bella
Politecnico di Milano
Dipartimento di Elettronica, Informazione e Bioingegneria
alessiolabella.alb@gmail.com

Abstract

THE interdisciplinary research presented in this doctoral thesis concerns the investigation and design of control, optimization and identification techniques to facilitate the upcoming energy transition to a more distributed and sustainable electrical system. Microgrids, i.e. small-scale grids incorporating renewable sources, storage systems, controllable loads and dispatchable units, are considered the fundamental bricks of this future electrical paradigm. This is due to their extreme flexibility, being able to operate either connected to the main grid or in islanded mode. The design of dedicated control architectures, allowing the efficient and safe operation of microgrids in these two modes, is the main focus of this doctoral thesis. Precisely, the work is structured in two parts.
Firstly, the design of optimization-based control algorithms for coordinating aggregated microgrids to provide external supporting services, usually denoted as ancillary services, is addressed. In fact, the diffusion of intermittent and non-deterministic renewable sources and the increasing world power demand require the cooperation of the different grid elements to ensure the secure operation of the whole electrical system. The second part of the doctoral thesis focuses on the design of novel hierarchical control schemes for the islanded operation. Given the absence of the main grid support, this condition is significantly critical, requiring the efficient management of the local units and the prompt regulation of the internal frequency and voltages. All the designed approaches have been tested through extensive numerical simulations considering real network benchmarks, showing their effectiveness in fostering the integration of microgrids, as well as their beneficial effects for the electrical system.

List of Acronyms

ADMM	Alternating Direction Method of Multipliers
aFRR	Automatic Frequency Restoration Reserve
AC	Alternating Current
AGS	Aggregator Supervisor
BESS	Battery Energy Storage System
BRP	Balance Responsible Party
BSP	Balancing Service Provider
CL	Controllable load
DC	Direct Current
DC-ADMM	Dual Consensus ADMM
DER	Distributed Energy Resource
DGU	Distributed Generation Unit
DSO	Distribution System Operator
EBGL	European Guideline on Electricity Balancing
EMS	Energy Management System
EU	European Union
iMG	Islanded Microgrid
FCR	Frequency Containment Reserves
HVAC	Heat, Ventilation and Air Conditioning
mFRR	Manual Frequency Restoration Reserve
mGEN	Micro-Generator
MG	Microgrid
MG-AG	Microgrids Aggregator
MGCC	MicroGrid Central Controller
MILP	Mixed-Integer Linear Program
MPC	Model Predictive Control
PV	PhotoVoltaic
RES	Renewable Energy Source
RR	Replacement Reserve
SO	System Operator
TSO	Transmission System Operator
WT	Wind Turbine

Contents

CHAPTER 1

Introduction

1.1 Motivations

Climate change is nowadays a well-recognized issue. Cutting off greenhouse gasses emissions has become a worldwide priority to stop global warming and its drastic effects on the planet. In 2015, more than 180 countries signed the *Paris Agreement*, with the goal of defining sustainable national plans to limit the global average temperature increase below 1.5 °C above pre-industrial levels [1]. Unfortunately, a single and well-defined solution to solve the climate change problem is not available as many technical, environmental, social and political aspects are involved.
Given the recent technological advances, one acknowledged strategy to reduce emissions is to reshape the electrical and the energy sector, transitioning from the standard centralized fossil-based generation paradigm to a framework where Renewable Energy Sources (RESs) cover most of the energy demand.

This necessity has been confirmed by the European Union, declaring the goal of fulfilling at least one third of the total power demand with RESs by 2030 in the Directive (EU) 2018/2001 [2].
This transition is not painless and it requires a lot of adaptation to the electrical system and the energy markets. The intermittent and unpredictable nature of most RESs, e.g. Wind Turbine (WT) and PhotoVoltaic (PV) systems, is a great limitation to their diffusion, because they cannot ensure the continuous balance of the power demand, as it is for fossil-based power plants. The power balance is of vital importance not only to guarantee the secure supply, but also because the network frequency and voltages may seriously deviate if power imbalances are not promptly restored, leading to instability events [3].
Therefore, to foster RESs penetration, the electrical system is required to become more flexible, continuously and actively adapting generation and demand patterns [4]. This flexibility characteristic can be achieved today thanks to the spread of dispatchable distributed sources, e.g. Battery Energy Storage Systems (BESSs) and Micro-Generators (mGENs), and of new controllable loads (CLs), e.g. Electric Vehicles (EVs) and Heating, Ventilation, and Air Conditioning (HVAC) systems. All these distributed generation and load units, denoted as Distributed Energy Resources (DERs), are now required to externally offer some power flexibility services to the electrical system, generally denoted as *ancillary services*, necessary to ensure the reliable, sustainable and secure energy supply [5]. Nevertheless, a decentralized and flexible electrical paradigm poses much more coordination issues with respect to the original centralized framework, requiring an efficient real-time management of the energy resources according to the grid needs.

In this context, the *MicroGrid* (MG) concept has been devised as a great solution to enhance the diffusion of distributed generation. MGs consist in autonomous small-scale grids equipped with mGENs, BESSs, RESs and loads, properly coordinated by control units, usually denoted as Microgrid Central Controllers (MGCCs) [1].

[1] The MG concept is here assumed to comprehend also smart buildings and industrial facilities, regulated by central controllers to optimize the management of available DERs, RESs and CLs.

The introduction of MGs into the electrical system brings many advantages under several economical, environmental and operational perspectives [6]. Among them, the following ones are here highlighted.

- MGs, equipped with DERs installed in proximity of loads, allow to considerably reduce the amounts of power flowing in transmission networks and consequently to curtail line losses.

- Deploying RESs with co-located BESSs and CLs in MGs makes the renewable diffusion more manageable. Rather than coordinating thousands or millions of individual distributed resources, each MG appears to the main utility as a single entity able to modify its power profile [7].

- MGCCs can use weather forecasts for a more efficient management of local RESs and other dispatchable units. Moreover, the future trends of energy prices can be also taken into account to optimize the power trade with the main grid, see [8], [9].

- MGs can interact each other to compensate for their energy needs and to achieve a more efficient resource management [10].

- A MG can also operate in isolated, or islanded, mode, without the support of the main grid. This may ensure the local power supply also in case of transmission line failures and in remote areas, where building an electric infrastructure can be costly or impracticable [11].

A high-level schematic of a generic MG is represented in Figure 1.1.

MGs have shown to be a great opportunity to enhance the flexibility of the electrical system, acting both as energy consumers or providers when connected to the main grid, or operating in islanded mode if necessary. According to Navigant Research, the global capacity of MGs, considering both installed and planned projects, reached about 19 GW in 2018 and it is expected to grow [12].

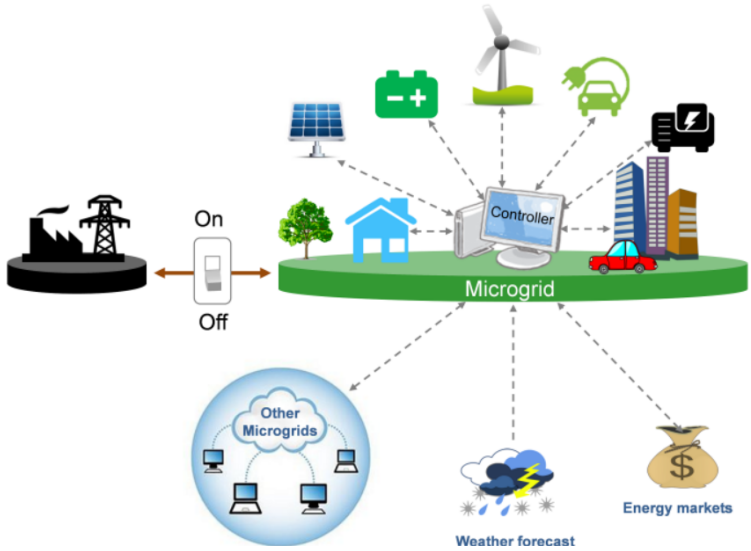

Figure 1.1: High-level scheme of a microgrid. Source: Berkeley Lab, https://building-microgrid.lbl.gov.

Nevertheless, MGs are still not considered a competitive and valuable alternative to big power plants for the provision of ancillary services, due to their reduced power capability. In fact, as it will be evident in the next section, the actual regulations on the provision of most services are characterized by minimum power requirements which can be hardly met by single MGs, having also to satisfy their internal loads.

It has been also mentioned that MG can operate in isolated mode, not requiring any support from the main utility. This possibility enhances the flexibility and decentralization of the electrical system but it is characterized by many technical issues which may affect the MG reliability.

To better comprehend the main contributions of this Thesis, a brief overview of the actual energy markets and of the ancillary services provision is firstly presented. Then, the main issues concerning islanded MG operations are described.

1.2 European electricity markets: an overview

The purpose of this section is to give a brief overview of the main mechanisms governing energy markets and ancillary services provision in Europe. For a more detailed comprehension, the reader is referred to [13–18].

Energy markets have dramatically changed in the last decades, adapting their mechanisms to accommodate the wide diffusion of variable and distributed energy resources. The transition from several national monopolies to a single liberalized European energy market, devised by the *European Union* in 1996, and then recasted in 2003 and in 2009 [18–20], opened the opportunity to small-scale producers and consumers to trade energy in a unique and competitive energy market. This brought several benefits to the whole electrical system, guaranteeing affordable energy prices and fostering the penetration of RESs [13].

Two important phases of the European energy market model are the *day-ahead* and the *intra-day* markets.
The *day-ahead* market closes at 12 pm of the day before the delivery. In this phase, market participants submit their demand and supply energy bids and take part to an auction process, where eventually generation and demand are matched to define the energy prices for each hour of the next day. Since this auction process is carried out on a day ahead basis, each participant relies on the available power schedules and forecasts for the next day, e.g. for loads consumption and RESs production.
Then, the *intra-day* market is periodically performed, generally until one hour before delivery. The rationale is that the declared power programs should be respected despite uncertainties. Therefore, market participants are periodically allowed to re-trade energy during the day, adjusting the declared programs with updated forecasts and schedules.

As mentioned in the previous section, the procurement of ancillary services to the electrical system is today regarded necessary and fundamental to ensure its proper operation. There are different type of services that

can be provided to the electrical system, e.g. voltage control, stability control, black-start capability etc. [21]. Among them, the so-called *balancing services*, entitled to ensure the real-time balance between active power generation and demand, are today gaining more and more importance given the wide of variable and nondeterministic energy resources. These services are regulated through another market, performed in parallel to the previously mentioned energy markets, i.e. the *balancing market*. It should be underlined that the network frequency plays a central role in this context. In fact, the frequency is a direct and instantaneous measure of active power imbalance in Alternating Current (AC) networks, so that a value above the nominal (50 Hz in Europe) indicates a surplus of energy, while a value below is a symptom of shortage. Because of this, it can be affirmed that the main objective of the *balancing market* mechanisms is to always keep the network frequency at its nominal value, implying that generation and demand are continuously matched.
The *balancing market* has still not reached the harmonization and standardization of the *day-ahead* and *intra-day* markets and there are still some severe zonal differences among the European countries that should be addressed [14]. However, in November 2017, the European Commission approved the *European Guideline on Electricity Balancing* (EBGL), identifying the main characteristics and conditions to provide balancing services [15].

Three main actors interact in the *balancing market*:

- *Balance Responsible Parties* (BRPs) have the responsibility of balancing a portfolio of grid units, e.g. generators, RESs and loads. They are called to address the power deviations with respect to the declared schedules and they are generally financially accountable for them.
- *Transmission System Operator* (TSO) is an entity entrusted of transporting electrical power on national or regional levels through the transmission network and it is responsible of guaranteeing its proper operation. The TSO activates the balancing power services as the sum of BRPs imbalances is non-zero, i.e. as the network frequency deviates from the nominal value.

- *Balancing Service Providers* (BSPs) are market parties called to provide balancing services to the TSO acting on a portfolio of grid units.

BSPs can provide both capacity and energy balancing service products. The first correspond to the pre-allocation of power reserves that can be later used to regulate the network frequency, usually denoted as *frequency control reserves*. The energy products correspond to the actual real-time delivery of balancing services.
Depending on the required activation speed and service duration, the *European Network of Transmission System Operators* (ENTSO-E) identifies different types of frequency control reserves [16].

- *Frequency Containment Reserves* (FCR) are employed to quickly and automatically address imbalances and contain frequency deviations. They are subjected to an automatic decentralized activation and they must be delivered within few seconds after the power contingency.
- *Automatic Frequency Restoration Reserves* (aFRR) are used to bring the frequency to its nominal value and to recover the delivered FCR. Their activation response time must be between some seconds and few minutes. aFRR are generally activated in automatic and centralized fashion, using a regulating signal sent by the TSO.
- *Manual Frequency Restoration Reserves* (mFRR) serve to restore aFRR with an activation response time of maximum 15 minutes. They are activated with manual request from the TSO.
- *Replacement Reserves* (RR) are generally used resolve consistent contingencies and congestion in the transmission lines. RR are activated manually by the TSO and a larger response time is generally requested (between 15 minutes and hours).

Traditionally, FCR have been named as *Primary control reserves*, aFRR as *Secondary control reserves*, while manually activated services, i.e. mFRR and RR, have been denoted as *Tertiary control reserves* [17], [22]. Given their different purposes and response times, these reserves are usually activated in sequence as far as it is necessary to restore network frequency and power imbalances, as shown in Figure 1.2.

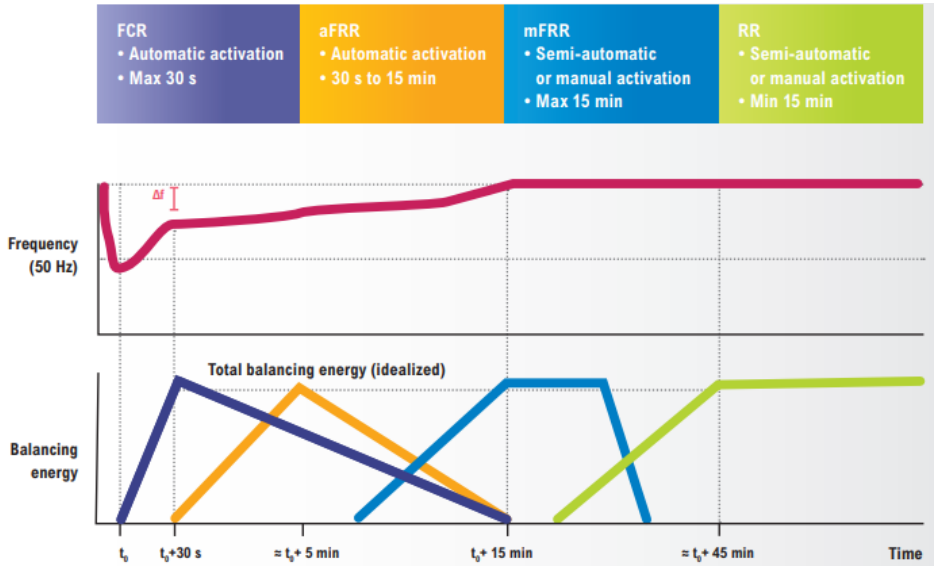

Figure 1.2: Sequential activation of frequency control reserves. Source: [16].

There are still consistent differences on the procurement of balancing services among the national *balancing markets*. In few countries some services are still mandatory, implying that just large dispatchable generation units can continuously provide them. On the other hand, the EBGL expressively states the strong need in shifting to a full market-based approach, giving the opportunity to flexible DERs to offer balancing services based on their availability [15].
Despite some zonal differences, the following common phases can be identified in *balancing markets*:

- *Balance planning:* The BRPs send to the TSO the expected power schedules, defined through the *day-ahead* and *intra-day* markets [23].
- *Balancing service provision:* The BSPs send balancing capacity and energy bids to the TSO, declaring their availability for the different services[2]. Depending on the specific national regulation, BSPs can

[2]In some countries capacity and energy bids are procured jointly, implying that the energy bid is already specified with the capacity bid, while, for others, it also possible to provide split capacity and energy bids [17]

send balancing bids both ex-ante, i.e. in the days before the delivery, and during the day if periodic bid adjustments are allowed. The procured bids are ranked according to some merit order and the TSO selects the needed amount of allocated balancing capacity, usually defined through some statistical criteria [24]. The selected capacity bids are generally denoted as *precontracted* bids, meaning that the BSPs are financially responsible of guaranteeing the declared availability in case of necessity. During the day, some countries allow BSPs also to submit *non-precontracted bids* for some services, also denoted as free energy bids. These bids allow BSPs to offer their near real-time energy availability to the TSO, without pre-allocating it as power reserve. In this case, BSPs are rewarded just if the offered balancing energy is activated and delivered [17].

- *Real-time balancing:* Based on the current BRPs imbalances, the BSPs are called to deliver the promised balancing services. As already mentioned, some services are automatically activated, while others through a direct request from the TSO.

A basic schematic on the main interactions between the actors of energy and balancing markets is depicted in Figure 1.3[3], considering references in [23, 25].

As evident from the Figure, the balancing service provision phase spans from the days before the delivery to the online operation. Apart from specific national regulations, this phase of the balancing market is generally carried out sequentially to the day-ahead or intra-day market sessions.
For instance, in Italy, pre-contracted reserve bids are offered on a day-ahead basis, after the day-ahead market session is closed, through the so-called *Mercato del Dispacciamento*. Then, during the day, the offered balancing bids can be updated periodically, right after the intra-day market sessions, through the so-called *Mercato del Bilanciamento* [26].

[3] Another core element of the *balancing markets*, which is not discussed here, is the *Imbalance Settlement* phase, where the BRPs are charged or paid for their imbalances, see [23].

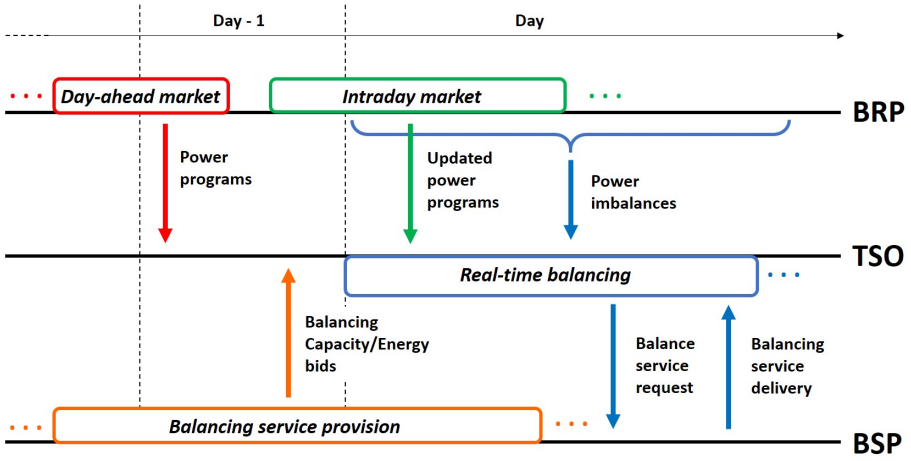

Figure 1.3: Generic schematic of energy and balancing markets operations.

Although *balancing markets* have been mainly introduced to foster the spread of DERs, there are still some regulatory barriers that limit their contribution in the balancing service provision [17, 22]. The following market design variables have a fundamental role in this context.

- *Bidding frequency*: This variable determines how often BSPs can submit balancing capacity and energy bids, and so it is strictly related to the duration of declared availability. Long-term bids allow to a simpler management of the balancing system, but it is a strict barrier for non-deterministic and variable DERs, since they cannot guarantee power reserves in large advance due to forecasts' uncertainty. The EGBL states that the BSPs should be allowed to provide balancing services bids as close as possible to the actual delivery, implying that the bidding frequency should be high [15].

- *Bid symmetry*: Balancing bids can be either symmetric or asymmetric, depending if the offered upward and downward regulation reserves have the same size or not. Asymmetric bids are beneficial for DERs diffusion since some resources can just provide unidirectional regulation. For instance, PV and WT systems can just decrease their power if necessary.

Table 1.1: Current balancing market variables in Italy [26], Austria, Germany and Netherlands [17].

	Italy	**Austria**	**Germany**	**Netherlands**
Frequency Containment Reserves (FCR)				
Procurement	Mandatory [5]	Market	Market	Market
Bid symmetry	Symmetric	Symmetric	Symmetric	Symmetric
Minimum bid volume	*N.A.*	10 MW	1 MW	1 MW
Capacity bid frequency	*N.A.*	Week	Week	Week
Energy bid frequency	*N.A.*	*N.A.*	*N.A.*	*N.A.*
Automatic Frequency Restoration Reserves (aFRR)				
Procurement	Market	Market	Market	Market
Bid symmetry	Symmetric	Asymmetric	Asymmetric	Asymmetric
Minimum bid volume	10 MW	5 MW	5 MW	4 MW
Capacity bid frequency	Day	Week	Week	Month
Energy bid frequency	4 hours	Week	Week	15 min
Manual Frequency Restoration Reserves (mFRR)				
Procurement	Market	Market	Market	Market
Bid symmetry	Asymmetric	Asymmetric	Asymmetric	Asymmetric
Minimum bid volume	1 MW	5 MW	5 MW	4 MW
Capacity bid frequency	Day	Day	Day	*N.A.*
Energy bid frequency	4 hours	Day	Day	15 min

- *Minimum bid volume*: Balancing bids are commonly characterized by minimum size requirements to have a significant impact on the electrical system. According to the actual regulations, minimum bidding volumes are still to high for small-scale DERs and just large generation plants are able to actually provide most services.

Table 1.1 shows how the mentioned design variables differ among some EU countries for the provision of FCR, aFRR and mFRR services [4]. As evident, minimum bid volumes are a great barrier for small-scale DERs as an extra power reserve in the order of MW is needed for the balancing service provision. The same limitation applies to MGs, as real implemen-

[4] *Replacement Reserves* are not explicitly considered since not all countries apply them, e.g. Netherlands, and other countries do not distinguish between mFRR and RR, denoting both as tertiary reserves, e.g. Italy.

[5] The provision of FCR in Italy, denoted as *primary reserve*, is mandatory for dispatchable production units with capacity larger than 10 MVA

tations hardly meet such a large amount of extra reserve capability to be used just for external balancing services [27].
An interesting solution to overcome this issue is to jointly coordinate multiple smart grid elements, e.g. MGs and smart buildings, as part of a unique BSP, potentially capable of providing the required amount of balancing services. These energy communities have been recently introduced and denoted as Aggregators.

1.3 Aggregators: a key solution to provide balancing services

Aggregators are considered a great opportunity to exploit the flexibility of many small-scale *prosumers*[6] and to promote their access to the balancing market. This is also an advantage for system operators, since they can directly send signals and interact with an aggregation supervising system, here denoted as Aggregator Supervisor (AGS), instead of singularly considering multiple grid units [21], as shown in Figure 1.4.

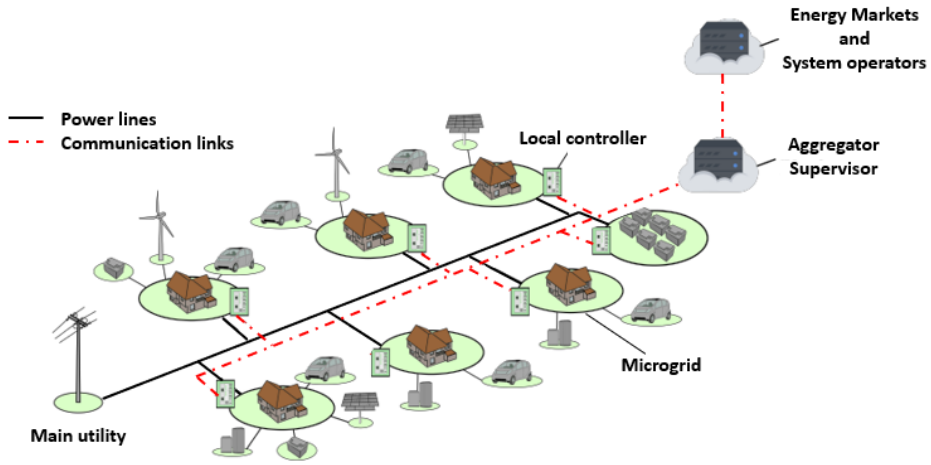

Figure 1.4: Example of a MGs Aggregator. Source: [28].

[6]The term *prosumer* is generically referred to systems that can both produce and consumer power based on the management of their resources, e.g. MGs.

The EGBL explicitly affirms that aggregations of DERs and loads should be allowed to provide balancing services [15], and actually some national markets are progressively regularizing their access. In Italy, the participation of aggregators was approved by the national authority[7] in 2018, giving the permission to start pilot projects [29]. The Italian TSO[8] then published a detailed document with all the technical specifications that aggregators of DERs and loads, generally named as UVAM[9], should respect for the balancing service provision [30].

Considering the actual regulations, aggregation of DERs are not suitable to provide FCR and aFRR products, as reported in [17,22]. This is mainly due to the bidding frequency, which for these services is generally in the order of weeks or days, meaning that DERs must guarantee a long-term reserve availability, see Table 1.1. This is not the case of mFRR, where BSPs are allowed to send their capacity/energy bids more often, reducing the effect of forecasts errors. Moreover, mFRR allows also asymmetric bids, which enhances the participation of DERs.
In fact, DERs aggregators in Italy and Netherlands started to enter in the balancing markets just for the provision of mFRR and, if applicable, of RR services [30], [31]. It should be also considered that mFRR and RR services require a larger activation time with respect to FCR and aFRR, facilitating the coordination of multiple aggregated resources.

Giving the importance of aggregators, many research studies are aiming to define efficient control and coordination algorithms. Management frameworks for optimizing the operations of interconnected MGs are presented in [32,33].
The provision of frequency control reserves from aggregation of buildings has been widely addressed, mainly using the flexibility offered by HVAC systems in regulating the internal temperature [34–36]. A framework where multiple MGs equipped with DERs are aggregated and jointly coordinated to reach minimum bid sizes to provide balancing services is discussed in [37].

[7] ARERA, *Autorità di Regolazione per l'Energia Reti e Ambiente*
[8] TERNA
[9] *Unità Virtuali Abilitate Miste*

The mentioned contributions rely on centralized control frameworks, where the upper-layer coordinating unit, i.e. the AGS, is in charge of scheduling the operations of its aggregate to provide balancing services. This implies that the elements of the aggregator have to share with the AGS all their internal information such as DERs characteristics, RESs production and load consumption profiles. Since MGs and smart building are usually private facilities, this could be no a desirable aspect, leading some elements to not join aggregators in order to keep the full control and knowledge of their own resources. On the other hand, centralized approaches are not scalable and they may lead to computational issues as the aggregator size grows.

Given the mentioned issues, one of the main contribution of this thesis is the design of optimization-based control frameworks for the provision balancing services from aggregators using *distributed*, *hierarchical* and *cluster-based*[10] approaches. This has the great advantage of ensuring the scalability of the approach, preserving at the same time MGs internal information and the full control of local resources.

1.4 Microgrid islanded operating mode

Being a site of both energy production and consumption, MGs can also operate in islanded mode. This condition involves different technical issues that must be addressed to ensure reliable operation.
In fact, without the support of the main grid, the continuous balance between generation and absorption must be locally ensured, which can be critical due to the presence of non-deterministic RESs and loads. Moreover, the islanded condition requires MGs to regulate the internal frequency and voltages, since this task is no more carried out by the main utility. This aspect can become critical in such low-inertia networks, since these electrical variables are extremely sensitive to power imbalances and can seriously diverge, leading to electrical faults.

[10] The meaning of the *cluster-based* approach will be clearer in next chapters

These issues motivated many research studies on the design of control architectures ensuring the reliable operation of islanded MGs. A consistent part of the literature focuses on stability studies, designing efficient low-level controllers to regulate voltage and frequency [38–41].
On the other hand, the presence of uncertain elements, e.g. RESs and loads, and of dispatchable DERs, e.g. BESSs, calls for the design of efficient Energy Management Systems (EMSs), necessary to ensure the continuous power supply and the proper management of MG resources. Few optimization-based EMS for islanded MGs have been proposed in the literature, and a reduced attention to the interaction between the EMS and the stabilizing low-layer controllers is usually given, see [42, 43].

Considering that the islanded operating mode requires the MGCC to both ensure the optimal management of resources and the low-level regulation of frequency and voltages, and moreover these tasks involve different time scales and system modelling, *hierarchical control architectures* are proposed in this thesis. These multi-layer control architectures are designed both for MGs with standard AC networks and also for MGs with Direct-Current (DC) networks. Indeed, DC MGs, due to their ability to interface naturally with most RESs, BESSs and many electronic loads (e.g. electric vehicles, LED systems) have gained a lot of attraction in recent years and they are expected to become a future standard [44].

In both cases, a Model Predictive Control (MPC) approach is adopted for the EMS layer, since this technique allows to include units capability constraints, economic objectives and forecasts of RESs and loads. Then, fast decentralized controllers, properly interfaced with the high-level EMS, are entitled of the low-level regulation of MG frequency and voltages.

1.5 Main contributions and structure of the thesis

The doctoral thesis is structured in two parts.

Part I - Microgrids aggregators providing ancillary services

The first part focuses on the design of optimization-based control algorithms for coordinating MGs Aggregators (MG-AGs), so that the they can interact as unique entity in the described market mechanisms and provide ancillary services to the main grid. As discussed, a MG-AG is supposed to be coordinated by an Aggregator Supervisor (AGS), which acts as an intermediate between the MGs and the System Operators (SOs) (see Figure 1.4). Common desired features for all the designed control strategies are the confidentiality of MGs internal information and enhanced scalability properties, so that the algorithm performances do not depend on the aggregation size. Because of this, different distributed and hierarchical methods are proposed in this first part, allowing the AGS to efficiently perform all the required operations for participating to the energy markets and the ancillary service provision.

Precisely, the following MG-AG operations are here addressed[11]:

- During the offline operation (e.g. day-ahead market), the AGS optimally schedules the overall power profile of the MG-AG, considering the energy prices and the internal MGs' costs. Moreover, it also defines the *precontracted* amounts of power reserves respecting the required *minimum bid volumes*. These operations are addressed in Chapter 2.
- During the online operation, the AGS acts as a proper BSP, effectively providing balancing services to the SOs. Moreover, the AGS periodically submit, according to a predefined *bidding frequency*, additional *non-precontracted* reserve bids considering the updated availability of power reserves in MGs. To accomplish these tasks, different control architectures are proposed in Chapter 3.

[11] It is underlined that the market procedures external to the MG-AG, e.g. offers, auctions and interactions with the SOs, are not modelled in this thesis but it is assumed that the AGS sends and receives the corresponding signals and information for the provision of ancillary services.

- During the online operation, the AGS also operates as a BRP, using the remaining power reserves in MGs to compensate the power variability caused by loads and RESs internal to the MG-AG, so that to maintain the pre-scheduled MG-AG power profile. This required the design of suitable algorithms, which are described in Chapter 4.
- During the offline operation, the AGS can also directly participate to the energy markets' auctions for the effective definition of the energy prices. This implies that the AGS has to submit supply/demand bids, i.e. evaluating the MG-AG optimal output power for each realization of the energy prices. To efficiently accomplish this task, an estimation procedure is proposed in Chapter 5, allowing to characterize the input/output model of each MG using just historical data.

The main contents and contributions of each chapter of the first part are described in the following.

Chapter 2 - Economic dispatch and procurement of active and reactive power services

This chapter concerns the design of an offline coordination framework, where the AGS and the interconnected MGs interact for defining the optimal power program of the MG-AG, provided that specific power requirements on pre-contracted reserves are globally respected. Moreover, supposing that all MGs are connected to the same distribution network, also line congestion issues are avoided, properly regulating the MG-AG active and reactive power operations.

The main novelty of Chapter 2 is the definition of a new three-phase optimization scheme, with guaranteed scalability properties and confidentiality requirements. In the first phase, a distributed optimization algorithm, based on a iterative negotiation between the AGS and the MGs, computes the active power profile of the MG-AG. Then, the second phase addresses the reactive power management so that the active power trends planned in the first phase do not compromise voltage/current limitations in the

distribution network. The third phase is used to schedule the active and reactive power profiles of the generation units of each MG to make them consistent with the requirements and results of the previous two phases.

The contents of this chapter have been presented in the following papers

- A. La Bella, M. Farina, C. Sandroni, R. Scattolini. *Microgrids aggregation management providing ancillary services*. European Control Conference (ECC) - Limassol (Cyprus), 12-15 June 2018.

- A. La Bella, M. Farina, C. Sandroni, R. Scattolini. *On the design of a microgrids aggregation framework to provide ancillary services*. CIRED Workshop on "Microgrids and local communities"- Ljubjana (Slovenia), 2-8 June 2018.

- A. La Bella, M. Farina, C. Sandroni, R. Scattolini. (in press) *Design of aggregators for the day-ahead management of microgrids providing active and reactive power services*. IEEE Transactions on Control Systems Technology. Extensive version available at https://arxiv.org/abs/1804.02195.

Chapter 3 - Management of real-time balancing service provision

This chapter addresses the online provision of balancing services to the main grid, supposing the MG-AG acts as a proper BSP, and considering the pre-programmed operations and reserves through the techniques described in Chapter 2. The MG-AG is also coordinated to offer additional reserves during the online operation, not declared as pre-contracted reserves in the offline scheduling phase. The formulated optimization problems are mixed-integer, as discrete variables are introduced for the online management of controllable loads.

The main novelties of Chapter 3 are the definition of two different optimization-based strategies for the balancing services provision.

- The first approach is based on a hierarchical scheme, where MGs initially communicate to the AGS a measure of their degree of power flexibility, introducing the concept of *flexibility functions*. This information is used by the AGS both to offer non-precontracted reserves, and also for dispatching the online balancing power requests from the TSO. The use of flexibility functions reveals to be an efficient alternative to centralized approaches, achieving nearly optimal solutions also in presence of mixed-integer variables.

- The second approach consist in the design of a properly defined distributed optimization algorithm for mixed-integer linear problems. Indeed, applying the standard distributed techniques to mixed-integer problems can lead to unfeasibility and non-convergence issues. The proposed algorithm shows enhanced scalability properties, which reduced optimality gap with respect to the centralized solution.

The first approach has been described in the following paper

- A. La Bella, F. Bonassi, C. Sandroni, L. Fagiano, R. Scattolini. *A hierarchical approach for balancing service provision by microgrids aggregators*. IFAC World Congress 2020 - Berlin (Germany), (under review).

The second approach is reported in the following paper

- A. La Bella, A. Falsone, D. Ioli. M. Prandini, R. Scattolini. *A mixed-integer distributed approach to prosumers aggregation for providing balancing services*. IEEE Transactions on Smart Grid, (under review).

Chapter 4 - Control and clustering strategies for self-balancing in distribution networks

This chapter focuses on the control of a MG-AG to actively and locally compensate the power variability introduced by loads and RES, acting as a proper BRP. The approach is applied during the online operation, with the aim of respecting the pre-declared power profile of the MG-AG, defined through the methods described in Chapter 2. A prompt control action and enhanced scalability are required, so as to ensure the efficient self-balancing in the MG-AG despite its size. To do this, the distribution network where MGs are connected is partitioned in areas, and coordinated by a properly defined control architecture.

The main novelties of Chapter 4 are the following.

- The design of a new two-layer control architecture, suitable for networked systems with shared resources. This is constituted by a decentralized low-level MPC framework, entitled of self balancing each area of the distribution network, and by a fully distributed supervisory layer, entitled of optimally defining the power exchanges among the areas. Moreover, the low-level MPC regulators are implemented with a novel flexible horizon approach, allowing to take into account updated forecasts.

- The definition of a novel technique to decompose large-scale networks into areas, such that each area is as self-sufficient as possible considering the local sources and sinks. The approach is tested on large-scale electrical distribution networks, but it can be generalized to different types of networks.

The proposed two-layer control architecture has been analysed from the theoretical perspective in the following paper

- A. La Bella, F. Bonassi, M. Farina, R. Scattolini. *Two-layer model predictive control of independent systems with shared control sources*. IFAC Symposium on Large Scale Complex Systems - Delft (Netherlands), 26-28 May 2019.

The application of the proposed architecture for the self-balancing of MG-AGs interconnected by hybrid AC-DC distribution grids has been reported in the following paper

- F. Bonassi, A. La Bella, R. Lazzari, C. Sandroni, R. Scattolini. *A supervised MPC architecture for power balance restoration in hybrid AC-DC grids*. International Journal of Electrical Power and Energy Systems, (under review).

A generalization of the two-layer architecture for controlling pure AC grids has been described in

- A. La Bella, F. Bonassi, K. Pascal, R. Scattolini. *A fully distributed control scheme for power balancing in distribution networks*. IFAC World Congress 2020 - Berlin (Germany), (under review).

The partition algorithm technique has been not yet submitted for publication, but it is described in details in the following Master Thesis

- Klaus Pascal. *Clustering and Multi-Level Control of Networked Systems and its Application to AC and Mixed AC-DC Grids*. École Polytechnique Fédérale de Lausanne, Switzerland, 2019.

cosupervised by the author.

Chapter 5 - A data-driven approach to estimate microgrids internal scheduling

This chapter concerns the design of an estimation method, so that the AGS can quickly evaluate the MG-AGs optimal power scheduling for a pre-determined trend of energy prices. This can be an efficient tool since it allows AGS to submit the supply/demand energy bids of the MG-AGs, without the necessity of performing an optimization problem or of knowing MGs internal information.

The main novelty of Chapter 5 relies on the use of the nonlinear Set Membership identification approach to derive MGs models using just historical data of output power vs. energy prices, which are available to the AGS. This identification technique provides both a nominal estimate and guaranteed uncertainty bounds. An important feature of the proposed method

is that it requires rather mild assumptions on the uncertain components of produced/consumed power, which are simply required to be bounded. Moreover, a novel tuning method is proposed in this chapter, allowing to obtain reduced uncertainty bounds.

The contents of this chapter have been presented in the following paper

- A. La Bella, L. Fagiano, R. Scattolini. *Set-membership identification of day-ahead microgrids scheduling*. European Control Conference - Naples (Italy), 24-28 June 2019.

Part II - Hierarchical control architectures for islanded MGs

The second part concerns the design of control architectures for MGs in islanded operation. As mentioned, this condition is the more critical as, without the support of the main grid, it must be ensured both the efficient frequency/voltage regulation and the proper management of the internal resources. Since different time scales and control objectives are involved, multi-layer hierarchical control architectures are designed, applied to MGs with either AC or DC networks.

The main contents and contributions of each chapter of the second part are described in the following.

Chapter 6 - Two-layer control of AC islanded microgrids with energy storage systems

This chapter addresses the design of a two-layer architecture for islanded AC Microgrids, equipped just with BESSs and RESs. The low-layer is based on a decentralized control framework, where one BESS unit, denoted as slack generator, regulates the MG internal voltage and frequency, while the other BESS units, named PQ generators, are controlled to track pre-defined active and reactive power references. At the top level, a MPC regulator is designed, coordinating the power references of PQ generators, ensuring that voltages lie in the required bounds, the minimization of power losses and the efficient management of BESSs.

The main novelty of Chapter 6 is the definition of the described two-layer architecture. Moreover, a novel high-level modelling of the MG electrical variables is proposed, allowing to optimize the MG economic objectives while ensuring the proper system operation.

The contents of this chapter have been reported in the following papers

- A. La Bella, S. Raimondi Cominesi, C. Sandroni, R. Scattolini. (2017) *Hierarchical predictive control of microgrids in islanded operation*. IEEE Transactions on Automation Science and Engineering, 14(2), 536-546.
- A. La Bella, S. Negri, R. Scattolini, E. Tironi. *A architecture for islanded AC microgrids with storage devices*. IEEE Conference on Control Technology and Applications - Copenhagen (Denmark), 21-24 August 2018.

Chapter 7 - Three-layer control of DC islanded microgrids with flexible structure

This chapter concerns the design of a hierarchical control structure for islanded DC Microgrids, allowing a more efficient resource management where respect to Chapter 6, allowing DERs to disconnect and reconnect based on economic objectives, without spoiling the MG stable operation and the low-level voltage regulation.

The main novelties of the chapter are the following.

- The definition of a novel and flexible hierarchical control architecture, comprising of three layers. The low-level is based on Plug-and-Play decentralized primary control framework, equipped at each DER to track pre-defined voltage references. Then, a secondary layer is proposed, which translates power references into voltage references for the primary controllers. This layer solves a non-linear optimization problem based on the power flow equations. Finally a tertiary layer is devised, based on a mixed-integer MPC problem,

which defines the optimal power references and operation mode of each DER.

- The second contribution relies on the theoretical analysis of the secondary layer, which is a nonlinear optimization problem entitled of translating the decision variables of the tertiary layer into primary voltage references. It is proved that a simplified version of the secondary optimization problem is guaranteed to be always feasible. Moreover, since the voltages can only be enforced at the DERs nodes, a novel condition is provided, guaranteeing the uniqueness of the solution for load voltages and power injection of DERs units.

The research results reported in this chapter have been described in the following papers

- A. Martinelli, A. La Bella, R. Scattolini. *Secondary control strategies for DC islanded microgrids operations*. European Control Conference - Naples (Italy), 24-28 June 2019.
- A. La Bella, P. Nahata, G. Ferrari-Trecate. *A Supervisory Control Structure for Voltage-Controlled Islanded DC Microgrids*. IEEE Conference on Decision and Control - Nice (France), 11-13 December 2019.
- P. Nahata, A. La Bella, R. Scattolini, G. Ferrari-Trecate. *Hierarchical Control in Islanded DC Micogrids with Flexible Structures*. IEEE Transactions on Control Systems Technology (under review). Technical Report available at `https://arxiv.org/pdf/1910.05107`.

Part I

Microgrids Aggregators providing ancillary services

CHAPTER 2

Economic dispatch and procurement of active and reactive power services

2.1 Introduction

The purpose of this chapter is to develop an optimization framework for the design of a MGs Aggregator (MG-AG), scheduling and coordinating the optimal operations of its units and, at the same time, jointly providing an adequate amount of frequency control reserve.
The developed coordination scheme is assumed to be executed on a day-ahead basis, right after the energy prices are defined through the *day-ahead* energy market, so that the Aggregator Supervisor (AGS) can communicate the next-day power program of the MG-AG to the TSO. The proposed approach can be also easily adapted to be executed right after the *intra-day* market sessions, using updated forecasts and energy prices.
It is assumed that the AGS manages a MG-AG, where MGs are all in-

terconnected to the same distribution network. This implies that MGs operations should be also coordinated to avoid over-voltage and line current congestion issues, properly regulating the active and reactive power flows in the network.

2.1.1 Literature review

Based on centralized approaches, the design of aggregator frameworks providing frequency control reserves has been described in [37] for MGs, and in [34–36] for smart buildings. However, centralized solutions could be inapplicable due to the large size of the overall system, leading to computational and scalability issues. Moreover, confidentiality requirements motivate possible restrictions on the information to be transmitted by the MGs, such as their internal costs, generator characteristics and load demand profiles. For these reasons, and considering that MGs are already locally managed by their own MGs Central Controllers (MGCC), distributed approaches are an effective solution, where the MGs operations are coordinated without requiring the transmission of internal sensitive information. Distributed optimization approaches for multi-microgrids have been proposed in [33,45,46], neglecting however the provision of ancillary services. A distributed management scheme of commercial buildings for the reserve provision service is presented in [47].
Notably, no one of the previous contributions deals with the design of aggregator management frameworks also considering the electrical feasibility in terms of voltage and current regulation.
Concerning this aspect, distributed optimization approaches become critical due to the nonlinearity and non-convexity of the underlying power flow equations, which negatively impact on the convergence of most distributed optimization-based algorithms [48]. Possible solution algorithms exist, but they usually have a complex structure, e.g. through the communication of gradients and Hessians of the local cost functions and constraints [49] or through convexification and approximation procedures [50–52]. Because of this, these methods are not recognized as viable and realistic solutions for the considered electrical application, and an easily implementable approach must be devised.

2.1.2 Proposed solution

Motivated by the previous analysis and state of the art, a novel method is proposed for the design of an AGS planning in a distributed way the active power production/absorption of MGs considering also the ancillary services provision. Specifically, the MGs autonomously manage their internal resources, while the AGS coordinates their operations to guarantee the best economic management of the MG-AG and the minimum power requirements to provide upward and downward power reserve. Additionally, MGs are also managed to operate as reactive power producers/consumers, regulating the voltages and the line currents of the distribution grid. This second task is addressed in a separate phase through an equivalent MG representation, allowing to solve the power flow problem in a centralized way while preserving the MGs internal sensitive data. In fact, a distributed approach is not necessary in this phase, since the reactive power management does not affect the MGs production costs but it just involves the regulation of inverters or excitation systems of DERs. Therefore, this phase can be performed by an external entity without interfering with the MGs internal economy and information. The scheduling process is structured according to the following phases, see also the flowchart in Figure 2.1.

Phase 1: **Distributed active power and reserve dispatch.** The day-ahead active power profiles of the MG generation units, minimizing the internal production costs and globally providing the minimum required active power reserve, are computed with a distributed optimization algorithm, i.e. the Alternating Direction Method of Multipliers (ADMM) [53].

Phase 2: **Power flow feasibility and reactive power planning.** Each MG communicates its equivalent active and reactive power reserves to the AGS. The MGs' reactive power output is then scheduled to satisfy the voltage/current limits and to minimize the overall power losses inside the considered distribution network. If necessary, the AGS can also request the MGs to vary the active power profiles scheduled in *Phase 1* considering line limitations and network topology.

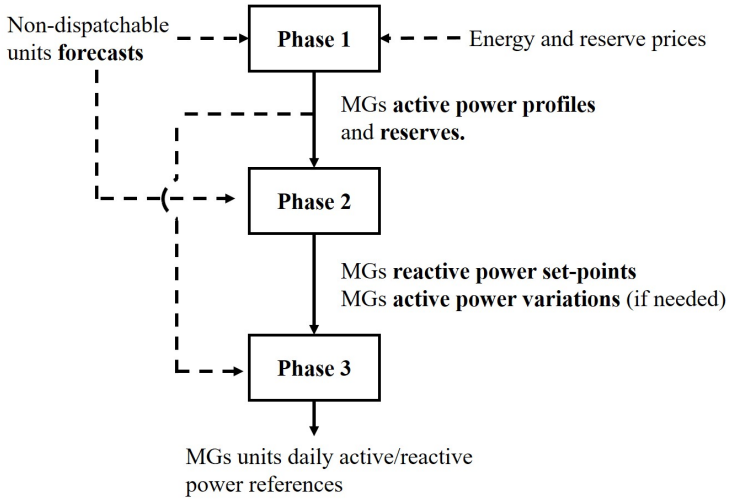

Figure 2.1: Flowchart of the MG-AG scheduling process

Phase 3: **Final scheduling of MG generation units.** Each MG must schedule the active and reactive power daily trends of its generation units considering the requirements from *Phase 1* and *Phase 2*.

As mentioned, the proposed algorithm is intended to be performed off-line, relying on the day-ahead energy prices and forecasts. In this way, the AGS manages the MG-AG achieving the best internal economic profit respecting both the ancillary services and the electrical requirements. Then, the optimal MG-AG total power output and provided reserve can be communicated to the system operators, e.g. the TSO. This method is an effective solution since it allows the AGS to interact in the energy market knowing how much its aggregation is going to produce/absorb based on the energy prices, without the need of solving a huge centralized problem or knowing all internal information of its aggregation.
The chapter is structured as follows: in Section 2.2, the MGs modelling is presented and the proposed distributed optimization algorithm used in Phase 1 is described. The reactive power management aimed at guaranteeing the feasibility of the proposed solution is presented in Section 2.3. In Section 2.4, the final optimization performed in Phase 3 is described.

Table 2.1: Optimization variables and system parameters

Symbol	Description
p^g, q^g	MG mGEN active/reactive power outputs [kW, kVar]
p^b, q^b	MG BESS active/reactive power outputs [kW, kVar]
p^l, q^l	MG load active/reactive power forecast [kW,kVar]
p^r, q^r	MG RES active/reactive power forecast [kW,kVar]
p^{mg}, q^{mg}	MG active/reactive output power [kW, kVar]
s^b	MG BESS state of charge (SOC) [%]
$C^b, \bar{E}^b$	MG BESS capacity and energy throughput [kWh]
a^b, b^b, c^b	MG BESS cost coefficients [€/kWh^2]
a^g, b^g, c^g	MG mGEN cost coefficients [€/kWh^2, €/kWh, €]
$r_p^{g\uparrow}, r_p^{g\downarrow}$	MG mGEN up/down active power reserves [kW]
$r_p^{b\uparrow}, r_p^{b\downarrow}$	MG BESS up/down active power reserves [kW]
$r_p^{mg\uparrow}, r_p^{mg\downarrow}$	MG total up/down active power reserves [kW]
$r_q^{mg\uparrow}, r_q^{mg\downarrow}$	MG total up/down reactive power reserves [kVar]
ρ_e^s, ρ_e^b	Grid energy selling and buying price [€/kWh]
p^L, q^L	Active/reactive power of an external load node [kW, kVar]
$p^{\text{AG}}, r_p^{\text{AG}\uparrow}, r_p^{\text{AG}\downarrow}$	MG-AG total active power output and reserves [kW]

The results achieved by applying the proposed framework to the IEEE 37-bus network, configured to include MGs, are extensively discussed in Section 2.5. Finally, some conclusions are drawn in Section 2.6.

2.2 Phase 1: active power and reserve dispatch

The considered distribution network is modelled as a bi-directional graph $\mathcal{G}(\mathcal{N}, \mathcal{E})$ with nodes $\mathcal{N} = \{1, \ldots, n\}$ and edges $\mathcal{E} \subseteq \mathcal{N} \times \mathcal{N}$, where the first node is conventionally named as *slack node*. This network includes a set $\mathcal{N}_\mathcal{M} = \{1, \ldots, M\}$ of flexible elements (e.g. the MGs) and a set $\mathcal{N}_\mathcal{L} = \{1, \ldots, n_L\}$ of non-dispatchable load elements (e.g., commercial buildings). The variables used in the next sections are described in Table 2.1. As a convention, all the power values are positive if delivered and negative if absorbed. The maximum and minimum limits of each variable are denoted with a bar over or below the variable, respectively.

2.2.1 Microgrid modelling and problem formulation

MGs are modelled as discrete-time systems with sampling time $\tau = 15$ min, being grid energy prices and weather forecasts usually provided with the same time rate. In view of the adopted time horizon of 24 hours, $N = 96$ steps must be considered in the optimization problem. The i-th microgrid, denoted as MG$_i$ with $i \in \mathcal{N}_{\mathcal{M}}$, is equipped with n_i^g Micro-Generators (mGENs), n_i^b Battery Energy Storage Systems (BESSs), n_i^r Renewable Energy Sources (RESs) and has a given load demand. During this offline phase, it is assumed that loads cannot be shifted or interrupted, but they are kept at the preferred position. The active power constraints for generation units are

$$\underline{p}_{j_i}^{g} \;\leq\; p_{j_i}^{g}(t) \;\leq\; \bar{p}_{j_i}^{g}\,, \tag{2.1}$$

$$\underline{p}_{k_i}^{b} \leq\; p_{k_i}^{b}(t) \;\leq\; \bar{p}_{k_i}^{b}\,, \tag{2.2}$$

where t is the time index, while $j_i \in [1, \ldots, n_i^g]$ and $k_i \in [1, \ldots, n_i^b]$ represent the j-th mGEN and the k-th BESS installed in MG$_i$, respectively. The dynamics of the state of charge (SOC) of the BESSs is

$$s_{k_i}^{b}(t+1) \;= s_{k_i}^{b}(t) \;-\; 100\,\frac{\tau}{C_{k_i}^{b}}\,p_{k_i}^{b}(t)\,, \tag{2.3}$$

where, for simplicity, the charge-discharge efficiencies have been neglected. The SOC must be constrained between minimum and maximum bounds

$$\underline{s}_{k_i}^{b} \;\leq\; s_{k_i}^{b}(t) \;\leq\; \bar{s}_{k_i}^{b}\,. \tag{2.4}$$

The overall MG output active power is given by the internal power balance. Moreover, it is expected that the output active power of MG$_i$ must respect some bounds, dictated for instance by an electrical contract with the DNO. It follows that

$$p_i^{mg}(t) \;= \sum_{k_i=1}^{n_i^b} p_{k_i}^{b}(t) + \sum_{j_i=1}^{n_i^g} p_{j_i}^{g}(t) + \sum_{p_i=1}^{n_i^r} p_{p_i}^{r} + p_i^{l}(t)\,, \tag{2.5}$$

$$\underline{p}_i^{mg} \leq p_i^{mg}(t) \leq \bar{p}_i^{mg}\,. \tag{2.6}$$

The active power reserves provided by dispatchable mGENs correspond to the remaining power margins with respect to the actual production as follows

$$r^{g\uparrow}_{p,j_i}(t) = \bar{p}^{g}_{j_i} - p^{g}_{j_i}(t), \qquad r^{g\downarrow}_{p,j_i}(t) = p^{g}_{j_i}(t) - \underline{p}^{g}_{j_i}. \tag{2.7}$$

As for the active power reserves of BESSs, not only the capability limits must be considered, but also the amount of available stored energy. At each time instant, the total active power reserve can be computed as

$$r^{b\uparrow}_{p,k_i}(t) = \min\left\{ \bar{p}^{b}_{k_i}, \ \frac{\left(s^{b}_{k_i}(t) - \underline{s}^{b}_{k_i}\right)}{100}\frac{C^{b}_{k_i}}{\tau} \right\} - p^{b}_{k_i}(t)\,,$$

$$r^{b\downarrow}_{p,k_i}(t) = \min\left\{ -\underline{p}^{b}_{k_i}, \ \frac{\left(\bar{s}^{b}_{k_i} - s^{b}_{k_i}(t)\right)}{100}\frac{C^{b}_{k_i}}{\tau} \right\} + p^{b}_{k_i}(t)\,.$$

However, the dependence of BESS power reserves on the amount of stored energy implies that, if at a certain time instant some power reserve is requested, in the future time instants the available reserve may vary. To ensure that the reserve externally offered to the TSO is guaranteed for each time instant, despite unexpected balancing service requests, a conservative strategy can be implemented. It consists in taking just the minimum values of the available stored energy reserves achieved over the whole optimization horizon, dividing them by N, and considering these fractions as active power reserves that can be externally offered at each time instant. This corresponds to replace the previous defined expressions with the following

$$r^{b\uparrow}_{p,k_i}(t) = \min\left\{ \bar{p}^{b}_{k_i}, \ \min_{\forall k\in[1,N]} \frac{1}{N}\left\{ \frac{\left(s^{b}_{k_i}(k) - \underline{s}^{b}_{k_i}\right)}{100}\frac{C^{b}_{k_i}}{\tau} \right\} \right\} - p^{b}_{k_i}(t)\,, \tag{2.8}$$

$$r^{b\downarrow}_{p,k_i}(t) = \min\left\{ -\underline{p}^{b}_{k_i}, \ \min_{\forall k\in[1,N]} \frac{1}{N}\left\{ \frac{\left(\bar{s}^{b}_{k_i} - s^{b}_{k_i}(k)\right)}{100}\frac{C^{b}_{k_i}}{\tau} \right\} \right\} + p^{b}_{k_i}(t)\,. \tag{2.9}$$

The expressions (2.8)-(2.9) can be easily transformed in linear inequalities as shown in Appendix A of this chapter.

The MG overall reserves are obtained by summing all the contributions, assuming that power production of RES can be used as down active power reserve

$$r_{p,i}^{mg\uparrow}(t) = \sum_{k_i=1}^{n_i^b} r_{p,k_i}^{b\uparrow}(t) \; + \; \sum_{j_i=1}^{n_i^g} r_{p,j_i}^{g\uparrow}(t)\,, \tag{2.10}$$

$$r_{p,i}^{mg\downarrow}(t) = \sum_{k_i=1}^{n_i^b} r_{p,k_i}^{b\downarrow}(t) + \sum_{j_i=1}^{n_i^g} r_{p,j_i}^{g\downarrow}(t) + \sum_{p_i=1}^{n_i^b} p_{p_i}^{r}(t)\,. \tag{2.11}$$

The goal of the MG internal management is to minimize the production costs and maximize the gain from the external trading. Therefore, a quadratic cost function is considered for the generic MG_i management as follows

$$\begin{aligned} J_i^{mg} = & \sum_{t=1}^{N} \sum_{j_i=1}^{n_i^g} \underbrace{(a_{j_i}^g \tau^2 (p_{j_i}^g(t))^2 + b_{j_i}^g \, \tau \, p_{j_i}^g(t) + c_{j_i}^g)}_{\alpha} \\ & + \sum_{t=2}^{N} \sum_{k_i=1}^{n_i^b} \Big[\underbrace{a_{k_i}^b \tau^2 (p_{k_i}^b(t) - p_{k_i}^b(t-1))^2}_{\beta_1} \\ & + \underbrace{b_{k_i}^b \left(\frac{p_{k_i}^b(t)\,\tau}{\bar{E}_{k_i}^b} \right)^2}_{\beta_2} + \underbrace{c_{k_i}^b (s_{k_i}^b(N) - s_{k_i}^b(1))^2}_{\beta_3} \Big] \\ & - \sum_{t=1}^{N} \underbrace{h_i^p \left(p_i^{mg}(t),\, r_{p,i}^{mg\uparrow}(t),\, r_{p,i}^{mg\downarrow}(t) \right)}_{\eta}\,. \end{aligned} \tag{2.12}$$

In (2.12), α includes the mGENs' fuel cost, expressed as a second-order polynomial function with respect to the generated power [54], while β_1 weights the BESSs' power variations to avoid frequent and excessive charges and discharges. The term β_2 is introduced to minimize the stored/absorbed energy with respect to the available energy throughput of the BESS, considering its remaining life. β_3 is included since it often required that the state at the end of the day equals the one at the beginning.

Finally, η is a term including the MG gain/cost for the overall produced/absorbed power and the provided upward and downward reserves; this will be defined later since it depends on the AGS management.

For the sake of clarity, MG_i is now compactly represented by defining the following vectors

$$x_i^p = [(p_{j_i}^g, r_{p,j_i}^{g\uparrow}, r_{p,j_i}^{g\downarrow})_{\forall j_i \in \{1,n_i^g\}}, (p_{k_i}^b, r_{p,k_i}^{b\uparrow}, r_{p,k_i}^{b\downarrow})_{\forall k_i \in \{1,n_i^b\}}]',$$

$$d_i^p = [\, p_i^l \,,\, p_{\forall p_i \in \{1,n_i^r\}}^r \,]',$$

$$y_i^p = [\, p_i^{mg},\, r_p^{mg\uparrow},\, r_p^{mg\downarrow} \,]',$$

where x_i^p includes the MG_i internal active power variables, d_i^p is the vector of non-dispatchable active power trends and y_i^p is the vector of the MG_i output variables. For compactness, the variables referred to the whole time horizon are expressed with bold symbols, e.g. $\mathbf{x_i^p} = [x_i^p(1)', \ldots, x_i^p(N)']'$. Similarly, the MG_i cost function can be rewritten as

$$J_i^{mg} = f_i^p(\mathbf{x_i^p}) \,-\, h_i^p(\mathbf{y_i^p})\,, \tag{2.13a}$$

where f_i^p includes the production cost of MG_i, i.e. the terms α and β in (2.12). The MG_i constraints and output expressions (2.1)-(2.11) can be reformulated as

$$\boldsymbol{A_i^p}\, \mathbf{x_i^p} \,\leq\, \boldsymbol{b_i^p}\,, \tag{2.13b}$$

$$\mathbf{y_i^p} \,=\, \boldsymbol{C_i^p}\, \mathbf{x_i^p} \,+\, \boldsymbol{M_i^p}\, \mathbf{d_i^p}\,, \tag{2.13c}$$

where $\boldsymbol{A_i^p}$, $\boldsymbol{b_i^p}$, $\boldsymbol{C_i^p}$ and $\boldsymbol{M_i^p}$ are properly defined matrices.
For the description of the AGS scheduling process, the MG_i compact optimization problem (2.13) will be considered. This is not only related to the notational compactness, but also because MGs can be characterized by different cost functions, constraints and composition of generations units and this must not have an impact on the AGS management.

2.2.2 AGS problem formulation and distributed algorithm

At a collective level, the AGS must consider the selling/buying energy prices and the gain for the provided active power reserve. The centralized AGS cost function is defined as follows

$$\mathbf{J}^{\text{AG}} = \sum_{\forall i \in \mathcal{N}_{\mathcal{M}}} f_i^p(\mathbf{x}_i^{\mathbf{p}}) - \tau \boldsymbol{\rho}_{\boldsymbol{e}}^{\boldsymbol{s}\prime} \max\left(\mathbf{p}^{\text{AG}}, \mathbf{0}\right) + \tau \boldsymbol{\rho}_{\boldsymbol{e}}^{\boldsymbol{b}\prime} \max(-\mathbf{p}^{\text{AG}}, \mathbf{0}) \,. \tag{2.14a}$$

Note that the MG-AG at time t can either absorb ($p^{\text{AG}}(t) < 0$) or release ($p^{\text{AG}}(t) > 0$) power. The functions $\max\left(\pm\mathbf{p}^{\text{AG}}, \mathbf{0}\right)$ in (2.14a) compute the element-wise maximum between the output power profile $\pm\mathbf{p}^{\text{AG}}$ and the zero column vector, in order to differently price the power considering either the selling or the buying energy prices.
The constraints (2.13b)-(2.13c) must be considered for all $i \in \mathcal{N}_{\mathcal{M}}$, together with constraints for the minimum up and down power reserve that can be externally provided

$$\mathbf{r}_{\mathbf{p}}^{\text{AG}\uparrow} \geq \underline{\mathbf{r}}_{\mathbf{p}}^{\text{AG}\uparrow} \,, \quad \mathbf{r}_{\mathbf{p}}^{\text{AG}\downarrow} \geq \underline{\mathbf{r}}_{\mathbf{p}}^{\text{AG}\downarrow} \,. \tag{2.14b}$$

Finally, the following expressions are used

$$\mathbf{r}_{\mathbf{p}}^{\text{AG}\uparrow} = \sum_{\forall i \in \mathcal{N}_{\mathcal{M}}} \mathbf{r}_{\mathbf{p},i}^{\mathbf{mg}\uparrow} \,, \quad \mathbf{r}_{\mathbf{p}}^{\text{AG}\downarrow} = \sum_{\forall i \in \mathcal{N}_{\mathcal{M}}} \mathbf{r}_{\mathbf{p},i}^{\mathbf{mg}\downarrow} \,, \tag{2.14c}$$

$$\mathbf{p}^{\text{AG}} = \sum_{\forall i \in \mathcal{N}_{\mathcal{M}}} \mathbf{p}_i^{\mathbf{mg}} \,, \tag{2.14d}$$

defining the total up and down power reserve and the active power balance for the whole MG-AG. From (2.14), it is clear that the AGS objective is to minimize the MGs production costs and maximize the overall profit due to the external trade with the main grid respecting the MGs internal constraints and the minimum up and down MG-AG power reserve constraints.

The overall optimization problem can be stated as follows

$$\min_{\substack{\mathbf{x}^{\mathrm{P}}_{\forall i},\mathbf{y}^{\mathrm{P}}_{\forall i}\\ \mathbf{z}^{\mathrm{P}}}} \{ \sum_{\forall i \in \mathcal{N}_{\mathcal{M}}} f_i^p(\mathbf{x}_i^{\mathrm{P}}) \; + \; g_z^p(\mathbf{z}^{\mathrm{P}}) \} \tag{2.15a}$$

subject to

$$\begin{aligned} & \boldsymbol{A}_i^{\mathrm{P}}\, \mathbf{x}_i^{\mathrm{P}} \; \leq \; \boldsymbol{b}_i^{\mathrm{P}} \\ & \mathbf{y}_i^{\mathrm{P}} \; = \; \boldsymbol{C}_i^{\mathrm{P}}\, \mathbf{x}_i^{\mathrm{P}} \; + \; \boldsymbol{M}_i^{\mathrm{P}}\, \mathbf{d}_i^{\mathrm{P}} \qquad \forall i \in \mathcal{N}_{\mathcal{M}} \end{aligned} \tag{2.15b}$$

$$\mathbf{z}^{\mathrm{P}} \; \in \mathcal{Z}^p \tag{2.15c}$$

$$\mathbf{z}^{\mathrm{P}} \; = \sum_{\forall i \in \mathcal{N}_{\mathcal{M}}} \mathbf{y}_i^{\mathrm{P}} \, , \tag{2.15d}$$

where $\mathbf{z}^{\mathrm{P}} = [\mathbf{p}^{\mathrm{AG}\,\prime}, \mathbf{r}_{\mathbf{p}}^{\mathrm{AG}\uparrow\,\prime}, \mathbf{r}_{\mathbf{p}}^{\mathrm{AG}\downarrow\,\prime}]'$ and

$$g_z^p(\mathbf{z}^{\mathrm{P}}) = - \; \tau \boldsymbol{\rho}_{\boldsymbol{e}}^{\boldsymbol{s}\prime} \max\left(\mathbf{p}^{\mathrm{AG}}, \mathbf{0}\right) \; + \; \tau \boldsymbol{\rho}_{\boldsymbol{e}}^{\boldsymbol{b}\prime} \max(-\mathbf{p}^{\mathrm{AG}}, \mathbf{0}) \, .$$

The MG-AG reserve requirements (2.14b) have been condensed in (2.15c) properly defining the set $\mathcal{Z}^p \subset \mathbb{R}^{3N,1}$, while the constraints (2.14c)-(2.14d) have been compacted in (2.15d). Note that the optimization problem (2.15) includes the coupling constraint (2.15d) which collect the MGs optimization variables, i.e. $\mathbf{y}_i^{\mathrm{P}}$ and the AGS ones, i.e. $\mathbf{z}^{\mathrm{P}}$. Finally, we denote by $\mathbf{J}^{\mathrm{AG},*}$ the optimal value of the cost function (2.15a), corresponding to the optimal centralized solution of (2.15).
As previously discussed, the centralized approach is not advisable since the AGS should know everything about the MGs internal structure so as to be able to provide the set-points to their units. To overcome this drawback and to confer scalability to the solution of (2.15), it is here proposed to rely on ADMM, a distributed optimization algorithm with enhanced properties with respect to standard *dual-decomposition* [53]. To reach convergence, ADMM requires the convexity of the cost function of the centralized problem. To this regard, considering (2.15a), the terms $f_i(\mathbf{x}_i^{\mathrm{P}})$ have been defined to be convex, while, regarding $g_z^p(\mathbf{z}^{\mathrm{P}})$, its piece-wise structure does not directly guarantee any convexity property. However, the following result can be stated.

Proposition 2.1. *If $\rho_e^b(t) \geq \rho_e^s(t) \;\; \forall t$, then the function $g_z^p(z^p(t))$ is convex (but not strictly).*

The proof of Proposition 2.1 is reported in Appendix B of this chapter. The requirement that, at each time instant, the buying price must be greater than the selling one is realistic and quite common in the literature, e.g. [55]. Indeed, if the MG-AG absorbs active power, the system operators afford some fixed costs to transport the needed power additionally to the generation ones, due to transmission or power losses. This is not the case when the nergy is produced *in loco* by the MGs resources and sold to the main grid.
Therefore, the ADMM method can be now applied, defining the following *Augmented Lagrangian* function

$$L_\mu(\mathbf{x}^{\mathbf{p}}_{\forall i}, \mathbf{y}^{\mathbf{p}}_{\forall i}, \mathbf{z}^{\mathbf{p}}, \boldsymbol{\lambda}) = \sum_{\forall i \in \mathcal{N}_\mathcal{M}} f_i^p(\mathbf{x}_i^{\mathbf{p}}) + g_z^p(\mathbf{z}^{\mathbf{p}}) + \boldsymbol{\lambda}'(\mathbf{z}^{\mathbf{p}} - \sum_{\forall i \in \mathcal{N}_\mathcal{M}} \mathbf{y}_i^{\mathbf{p}}) + \\ + \frac{\mu}{2} ||\mathbf{z}^{\mathbf{p}} - \sum_{\forall i \in \mathcal{N}_\mathcal{M}} \mathbf{y}_i^{\mathbf{p}} ||_2^2 , \tag{2.16}$$

where $\mu > 0$ is a tuning parameter and $\boldsymbol{\lambda}$ is named *dual variable* or *shadow price*. Being (2.16) not fully separable among the agents due to the presence of the quadratic term, the sequential iterative procedure described in Algorithm 1 must be followed according to ADMM procedure. In principle, Step 1 of Algorithm 1 does not allow to preserve the confidentiality since each i-th MGCC needs information about the optimal outputs of the other agents at the previous iteration, i.e. $(\mathbf{y}^{\mathbf{p},k-1}_{\forall j \neq i},\ \mathbf{z}^{\mathbf{p},k-1})$, in order to minimize L_μ. However, defining the constraint residual as $\mathbf{r}^{\mathbf{p}} = \mathbf{z}^{\mathbf{p}} - \sum_{\forall i \in \mathcal{N}_\mathcal{M}} \mathbf{y}_i^{\mathbf{p}}$, it holds that

$$\begin{aligned} &L_\mu(\mathbf{x}_i^{\mathbf{p}}, \mathbf{y}_i^{\mathbf{p}}, \boldsymbol{\lambda}^{k-1}, \mathbf{y}^{\mathbf{p},k-1}_{\forall j \neq i}, \mathbf{z}^{\mathbf{p},k-1}) = \ f_i^p(\mathbf{x}_i^{\mathbf{p}}) \ - \ \boldsymbol{\lambda}^{k-1\prime}\mathbf{y}_i^{\mathbf{p}} + \\ &+ \ \frac{\mu}{2} ||\mathbf{z}^{\mathbf{p},k-1} - \sum_{\forall j \neq i \in \mathcal{N}_\mathcal{M}} \mathbf{y}_j^{\mathbf{p},k-1} - \mathbf{y}_i^{\mathbf{p}}||_2^2 = \\ &= f_i^p(\mathbf{x}_i^{\mathbf{p}}) - \boldsymbol{\lambda}^{k-1\prime}\mathbf{y}_i^{\mathbf{p}} - \frac{\mu}{2} || \ \mathbf{r}^{\mathbf{p},k-1} + \mathbf{y}_i^{\mathbf{p},k-1} - \mathbf{y}_i^{\mathbf{p}} \ ||_2^2 \ = \\ &= L_\mu(\mathbf{x}_i^{\mathbf{p}}, \mathbf{y}_i^{\mathbf{p}}, \boldsymbol{\lambda}^{k-1}, \mathbf{y}_i^{\mathbf{p},k-1}, \mathbf{r}^{\mathbf{p},k-1}) \, . \end{aligned} \tag{2.17}$$

Algorithm 1 Distributed economic dispatch through ADMM

While *convergence* is not met

1) The MGCCs solve in parallel the following sub-problems using information about the previous iteration:

for all $i \in \mathcal{N}_{\mathcal{M}}$

$$(\mathbf{x}_i^{\mathbf{p},k}, \mathbf{y}_i^{\mathbf{p},k}) = \underset{\text{s.t. (2.13b)-(2.13c)}}{\operatorname{argmin}} L_\mu(\mathbf{x}_i^{\mathbf{p}}, \mathbf{y}_i^{\mathbf{p}}, \boldsymbol{\lambda}^{k-1}, \mathbf{y}_{\forall j \neq i}^{\mathbf{p},k-1}, \mathbf{z}^{\mathbf{p},k-1})$$

end for

2) The AGS gathers the optimal outputs of the MGs sub-problems, i.e. $\mathbf{y}_i^{\mathbf{p},k}$, and solves the following sub-problem

$$\mathbf{z}^{\mathbf{p},k} = \underset{\text{s.t. (2.15c)}}{\operatorname{argmin}} L_\mu(\mathbf{z}^{\mathbf{p}},\ \mathbf{y}_{\forall i}^{\mathbf{p},k},\ \boldsymbol{\lambda}^{k-1})$$

3) The dual variable $\boldsymbol{\lambda}$ is updated by the AGS based on the updated constraint residual

$$\boldsymbol{\lambda}^k = \boldsymbol{\lambda}^{k-1} + \mu \cdot (\mathbf{z}^{\mathbf{p},k} - \sum_{\forall i \in \mathcal{N}_{\mathcal{M}}} \mathbf{y}_i^{\mathbf{p},k})$$

Next iteration update: $k = k + 1$

end while

Therefore, to perform Step 1 it is enough that the AGS provides each i-th MGCC with information about the dual variable and the coupling constraint residual. The MG_i cost function to minimize is therefore defined by (2.17), and it includes the internal production costs $f_i^p(\mathbf{x}_i^{\mathbf{p}})$ and some other terms related to the output variables $\mathbf{y}_i^{\mathbf{p}}$. These terms were denoted in (2.13a) with the generic function $h_i^p(\mathbf{y}_i^{\mathbf{p}})$ and, at convergence, they express the cost/gain of the MG_i for the provided active power output and power reserves.
The optimality of Algorithm 1 is guaranteed by the following proposition, which can be straightforwardly proven based on [56, Section 3.4].

Proposition 2.2. *The sequence* $\{\mathbf{x}_{\forall i}^{\mathbf{p}}, \mathbf{y}_{\forall i}^{\mathbf{p}}, \mathbf{z}^{\mathbf{p}}\}^k$ *generated by Algorithm 1 is bounded and its limit points are in the set of the optimal solutions of the original problem* (2.15).

Therefore, the sequence of the optimal values of the overall cost function, generated by Algorithm 1 and defined as

$$\mathbf{J}^{\text{AG},\mathbf{k}} = \sum_{\forall i \in \mathcal{N}_{\mathcal{M}}} f_i^p(\mathbf{x}_i^{\mathbf{p},k}) + g_z^p(\mathbf{z}^{\mathbf{p},k}) \,,$$

converges to the optimal objective of the primal problem, i.e. $\mathbf{J}^{\text{AG},\mathbf{k}} \longrightarrow \mathbf{J}^{\text{AG},*}$ as $k \to \infty$. Although this is an asymptotic result, ADMM often converges in few tens of iterations with satisfactory accuracy, and the following termination criterion can be used

$$||\mathbf{r}^{\mathbf{p},k}||_2 \leq \epsilon_r \wedge ||\mathbf{z}^{\mathbf{p},k+1} - \mathbf{z}^{\mathbf{p},k}||_2 \leq \epsilon_z \,,$$

where $\epsilon_r > 0$ and $\epsilon_z > 0$ are predefined tolerances.
In a practical implementation, ADMM applied to the MG-AG management consists of the following iterative procedure: firstly the MGCCs perform in parallel their local optimization problems, based on the previous values of the constraint residual $\mathbf{r}^{\mathbf{p}}$, and of the internal shadow price $\boldsymbol{\lambda}$. Then, the AGS gathers the optimal values of the MGs output variables and solves its sub-problem, considering minimum reserve requirements and the external grid prices. Notice that the MGs internal information and optimization variables $\mathbf{x}_i^{\mathbf{p}}$ are not externally shared. Finally, the AGS updates the internal price $\boldsymbol{\lambda}$ based on the coupling constraint residual which is sent back to the MGs such that they can start again performing Step 1. The dual variable $\boldsymbol{\lambda} = [\boldsymbol{\lambda}^{r_p\uparrow\prime}, \boldsymbol{\lambda}^{r_p\downarrow\prime}, \boldsymbol{\lambda}^{p\prime}]'$ can be therefore interpreted as the vector of the internal negotiation prices between the AGS and the MGs, for the output active power ($\boldsymbol{\lambda}^{p\prime}$) and for the power reserves ($\boldsymbol{\lambda}^{r_p\uparrow\prime}, \boldsymbol{\lambda}^{r_p\downarrow\prime}$). Differently from the external trade with the main utility where the selling and the buying prices are different, just one internal price exists for the MGs output active power. This is done on purpose since additional transmission-related fixed costs are not relevant internally to the MG-AG network, meaning that selling or buying power do not imply differential costs for MGs.

2.3 Phase 2: power flow feasibility and reactive power planning

Phase 2 is necessary to ensure that the active power flows computed by Algorithm 1 are consistent with the constraints on nodal voltages and line currents. In addition, it allows to regulate the reactive power flows inside the distribution network, minimizing the power losses and ensuring the network electrical feasibility. This is possible since MGs can have a significant role as reactive power producers/consumers, being clusters of several inverter-interfaced generation sources. As mentioned in Section **??**, since each MG is regarded as a single equivalent mGEN, this phase can be carried out by the AGS through a centralized approach, without compromising the computational feasibility and violating the MGs privacy constraints. For clarity, from now on the optimal values of the variables computed in Section 2.2 by Algorithm 1 will be denoted with the superscript *, e.g. $\mathbf{p}_i^{\mathbf{mg},*}$.

2.3.1 MGs representation as equivalent generators

At this stage, the MG output reactive power coincides with the internal load demand since the reactive power set-points have not been yet scheduled, i.e. $\mathbf{q}_i^{\mathbf{mg},*} = \mathbf{q}_i^{\mathbf{l}}$. The MG reactive power capability can be represented by aggregating the capabilities of each generation unit. For consistency with Section 2.2, the overall MG reactive power capability is expressed through up/down reserves. The following relations hold

$$\mathbf{r}_{\mathbf{q},i}^{\mathbf{mg}\uparrow *} = \sum_{j_i=1}^{n_i^g} \bar{\mathbf{q}}_{j_i}^{\mathbf{g}}(\mathbf{p}_{j_i}^{\mathbf{g},*}) + \sum_{k_i=1}^{n_i^b} \bar{\mathbf{q}}_{k_i}^{\mathbf{b}} + \sum_{p_i=1}^{n_i^r} \bar{\mathbf{q}}_{p_i}^{\mathbf{r}}\,, \tag{2.18}$$

$$\mathbf{r}_{\mathbf{q},i}^{\mathbf{mg}\downarrow *} = -\sum_{j_i=1}^{n_i^g} \underline{\mathbf{q}}_{j_i}^{\mathbf{g}}(\mathbf{p}_{j_i}^{\mathbf{g},*}) - \sum_{k_i=1}^{n_i^b} \underline{\mathbf{q}}_{k_i}^{\mathbf{b}} - \sum_{p_i=1}^{n_i^r} \underline{\mathbf{q}}_{p_i}^{\mathbf{r}}\,, \tag{2.19}$$

where the mGENs reactive power limits are expressed as functions of the active power production, as usual for fuel-based mGENs. The MG reactive power reserves defined in (2.18)-(2.19) have been also denoted with the superscript $*$ since their values are computed based on the outcomes

of *Phase 1*. Actually, prior to perform *Phase 2*, MGs must communicate to the AGS not only their optimal active power trends, but also the active and reactive reserve capabilities. The reactive power variation $\mathbf{\Delta q^{mg}}$ with respect to $\mathbf{q^{mg,*}}$ is then scheduled in *Phase 2*, and this must be bounded by the up/down reserves

$$-\mathbf{r}_{\mathbf{q},i}^{\mathbf{mg}\downarrow *} \;\leq\; \mathbf{\Delta q}_i^{\mathbf{mg}} \;\leq\; \mathbf{r}_{\mathbf{q},i}^{\mathbf{mg}\uparrow *}\,. \tag{2.20}$$

It would be desirable that the optimal active power trends achieved by Algorithm 1 are not varied. To this regard, since the MG active power output has been locally constrained, see (2.6), it is expected that just small active power variations may be needed, e.g. in case many MGs are injecting an excessive amount of active power in the same line leading to over-current issues. Also in this case, the active power reserves scheduled in *Phase 1* can be used to limit the active power variations of each MG. Therefore, denoting by $\Delta\mathbf{p}_i^{\mathbf{mg}}$ the active power variation with respect to $\mathbf{p}_i^{\mathbf{mg},*}$, it holds that

$$-\mathbf{r}_{\mathbf{p},i}^{\mathbf{mg}\downarrow,*} \;\leq\; \mathbf{\Delta p}_i^{\mathbf{mg}} \;\leq\; \mathbf{r}_{\mathbf{p},i}^{\mathbf{mg}\uparrow,*}\,. \tag{2.21}$$

The variation of the MGs active power outputs should not compromise the minimum MG-AG frequency reserve requirements (2.14b) defined in Section 2.2. Therefore the following additional constraints must be considered:

$$\sum_{\forall i\in\mathcal{N}_{\mathcal{M}}} \left(\mathbf{r}_{\mathbf{p},i}^{\mathbf{mg}\uparrow,*} - \Delta\mathbf{p}_i^{\mathbf{mg}}\right) \;\geq\; \underline{\mathbf{r}}_{\mathbf{p}}^{\mathbf{AG}\uparrow}\,, \tag{2.22}$$

$$\sum_{\forall i\in\mathcal{N}_{\mathcal{M}}} \left(\mathbf{r}_{\mathbf{p},i}^{\mathbf{mg}\downarrow,*} + \Delta\mathbf{p}_i^{\mathbf{mg}}\right) \;\geq\; \underline{\mathbf{r}}_{\mathbf{p}}^{\mathbf{AG}\downarrow}\,. \tag{2.23}$$

To sum up, through these expressions the MGs are modelled as PQ generation nodes with predefined active and reactive power trends, i.e. $\mathbf{p^{mg,*}}$ and $\mathbf{q^{mg,*}}$, allowing for active and reactive power set-points variations, $\Delta\mathbf{p^{mg,*}}$ and $\Delta\mathbf{q^{mg,*}}$ which must respect predefined capability limits, defined by (2.20)-(2.23).

2.3.2 Network model

The network is modelled using the power flow equations, i.e. nonlinear static functions defining the nodal powers based on the network voltages and on the *nodal admittance matrix*. By means of these equations, also some other variables can be calculated, such as the active power losses and the magnitude of the flowing current in the lines of the network. These equations are not explicitly expressed here as they be easily recovered from the literature, see [57]. The following generic notation is used

$$\mathbf{P}_j = \boldsymbol{f}_j^{\boldsymbol{P}}(\mathbf{V}_{1,\dots,n}, \boldsymbol{\delta}_{1,\dots,n}, Y)\,, \qquad \forall j \in \mathcal{N}\,, \tag{2.24}$$

$$\mathbf{Q}_j = \boldsymbol{f}_j^{\boldsymbol{Q}}(\mathbf{V}_{1,\dots,n}, \boldsymbol{\delta}_{1,\dots,n}, Y)\,, \qquad \forall j \in \mathcal{N}\,, \tag{2.25}$$

$$\mathbf{P}_{i,j}^{\mathbf{loss}} = \boldsymbol{f}_{i,j}^{\boldsymbol{loss}}(\mathbf{V}_i, \boldsymbol{\delta}_i, \mathbf{V}_j, \boldsymbol{\delta}_j, Y)\,, \qquad \forall (i,j) \in \mathcal{E}\,, \tag{2.26}$$

$$\mathbf{I}_{i,j} = \boldsymbol{f}_{i,j}^{\boldsymbol{I}}(\mathbf{V}_i, \boldsymbol{\delta}_i, \mathbf{V}_j, \boldsymbol{\delta}_j, Y)\,, \qquad \forall (i,j) \in \mathcal{E}\,, \tag{2.27}$$

where $\boldsymbol{f}_j^{\boldsymbol{P}}$, $\boldsymbol{f}_j^{\boldsymbol{Q}}$, $\boldsymbol{f}_{i,j}^{\boldsymbol{loss}}$ and $\boldsymbol{f}_{i,j}^{\boldsymbol{I}}$ are vectors of static nonlinear functions expressing the j-th nodal active power, the j-th nodal reactive power, the (i,j) line active power loss and the (i,j) line current magnitude over the whole optimization horizon, respectively. For each node of the distribution network, the output powers defined in (2.24)-(2.25) must be linked with the MGs and loads output powers; it follows that $\forall j \in \mathcal{N}$

$$\mathbf{P}_j = \sum_{\forall i \in \mathcal{N}_{\mathcal{M}}} \sigma_{i,j}^{M} (\mathbf{p}_i^{\mathbf{mg},*} + \boldsymbol{\Delta}\mathbf{p}_i^{\mathbf{mg}}) \; + \sum_{\forall j_l \in \mathcal{N}_{\mathcal{L}}} \sigma_{j_l,j}^{L}\, \mathbf{p}_{j_l}^{\mathbf{L}}\,, \tag{2.28}$$

$$\mathbf{Q}_j = \sum_{\forall i \in \mathcal{N}_{\mathcal{M}}} \sigma_{i,j}^{M} (\mathbf{q}_i^{\mathbf{mg},*} + \boldsymbol{\Delta}\mathbf{q}_i^{\mathbf{mg}}) + \sum_{\forall j_l \in \mathcal{N}_{\mathcal{L}}} \sigma_{j_l,j}^{L}\, \mathbf{q}_{j_l}^{\mathbf{L}}\,, \tag{2.29}$$

where $\sigma_{\alpha,\beta}^{M,L}$ are boolean scalars defined to be equal to 1 only if the α-th element is connected to the β-th node.
As common in practice, the slack voltage, i.e. V_1, is assumed to be fixed to the nominal grid value, and imposed by the whole external network.

Finally, electrical constraints are introduced to force voltages and line currents to remain inside the allowed ranges

$$\underline{\mathbf{V}}_j \leq \mathbf{V}_j \leq \bar{\mathbf{V}}_j\,, \quad \forall\, j \in \mathcal{N}\,, \tag{2.30}$$

$$\mathbf{I}_{i,j} \leq \bar{\mathbf{I}}_{i,j}\,, \quad \forall\,(i,j) \in \mathcal{E}\,. \tag{2.31}$$

2.3.3 Optimization problem of Phase 2

Having defined all the constraints, the optimization problem to be solved in *Phase 2* is stated.

$$\min_{\substack{\Delta\mathbf{p}^{\mathbf{mg}}_{\forall i} \\ \Delta\mathbf{q}^{\mathbf{mg}}_{\forall i}}} \left\{ \sum_{\forall (i,j)\in\mathcal{E}} \zeta_i^l ||\mathbf{P}^{\mathbf{loss}}_{i,j}||_2^2 + \sum_{\forall i \in \mathcal{N}_\mathcal{M}} \zeta_i^p \,||\Delta\mathbf{p}_i^{\mathbf{mg}}||_2^2 \; + \sum_{\forall i \in \mathcal{N}_\mathcal{M}} \zeta_i^q \,||\Delta\mathbf{q}_i^{\mathbf{mg}}||_2^2 \right\} \tag{2.32}$$

subject to (2.20) - (2.31) .

The first term in (2.32) penalizes the active power losses, while the last two terms involve the minimization of the MG active power and reactive power variations, respectively. The parameters are set as $\zeta_i^p \gg \zeta_i^l > \zeta_i^q > 0$, so that active power variations are requested just if the problem feasibility is compromised.

2.4 Phase 3: Final scheduling of the MGs units

Phase 3 is needed to schedule the final power references of the MGs generation units consistently with the active and reactive optimal profiles obtained in *Phases 1* and *2*. Denote the optimal variables computed in *Phase 2* with the superscript $**$. Note that, given the constraints (2.8)-(2.9) and (2.22)-(2.23), the minimum requirements on the MG-AG power reserve ensured in *Phase 1* are not compromised despite the active power variations committed in *Phase 2*.

Therefore, there is no need of solving *Phase 3* using a distributed approach but it can be performed in a pure decentralized mode, where each MG_i independently solve the following optimization problem

$$\min_{\substack{\mathbf{x}_i^{\mathbf{p}},\mathbf{y}_i^{\mathbf{p}} \\ \mathbf{x}_i^{\mathbf{q}},\mathbf{y}_i^{\mathbf{q}}}} \left\{ f_i^p(\mathbf{x}_i^{\mathbf{p}}) + f_i^q(\mathbf{x}_i^{\mathbf{q}}) + \gamma_i^p \, ||\boldsymbol{\epsilon}_i^{\boldsymbol{p}}||_2^2 + \gamma_i^q \, ||\boldsymbol{\epsilon}_i^{\boldsymbol{q}}||_2^2 \right\} \tag{2.33a}$$

subject to

$$\begin{aligned} A_i^p \, \mathbf{x}_i^{\mathbf{p}} &\leq b_i^p \\ \mathbf{y}_i^{\mathbf{p}} &= C_i \, \mathbf{x}_i^{\mathbf{p}} + M_i \, \mathbf{d}_i^{\mathbf{p}} \end{aligned} \tag{2.33b}$$

$$\begin{aligned} A_i^q \, \mathbf{x}_i^{\mathbf{q}} &\leq b_i^q(\mathbf{x}_i^{\mathbf{p}}) \\ \mathbf{y}_i^{\mathbf{q}} &= C_i^q \, \mathbf{x}_i^{\mathbf{q}} + M_i^q \, \mathbf{d}_i^{\mathbf{q}} \end{aligned} \tag{2.33c}$$

$$\begin{aligned} \mathbf{p}_i^{\mathbf{mg}} &= \mathbf{p}_i^{\mathbf{mg},*} + \boldsymbol{\Delta}\mathbf{p}_i^{\mathbf{mg},**} + \boldsymbol{\epsilon}_i^{\boldsymbol{p}} \\ \mathbf{q}_i^{\mathbf{mg}} &= \mathbf{q}_i^{\mathbf{mg},*} + \boldsymbol{\Delta}\mathbf{q}_i^{\mathbf{mg},**} + \boldsymbol{\epsilon}_i^{\boldsymbol{q}} \, . \end{aligned} \tag{2.33d}$$

Following the same reasoning of Section 2.2, the internal and output reactive power variables are compactly defined as $\mathbf{x}_i^{\mathbf{q}}$ and $\mathbf{y}_i^{\mathbf{q}}$, while the MGs internal reactive power constraints are given by (2.33c). The constraints (2.33d) are introduced to make the MGs follow the active and reactive power outputs dictated by the optimization problems in Phases 1 and 2. Two slack variables are used in (2.33d), i.e. $\boldsymbol{\epsilon}_i^{\boldsymbol{p}}$ and $\boldsymbol{\epsilon}_i^{\boldsymbol{q}}$, to avoid infeasibility problems, and they are minimized in the cost function (2.33a) through the weights $\gamma_i^p \gg 0$ and $\gamma_i^q \gg 0$. In (2.33d), the MG productions cost are included through the function f_i^p, already defined in Section 2.2, while a function f_i^q is also introduced to equally distribute the reactive power burden among the MG units. For the sake of compactness, the explicit expressions of f_i^q and of (2.33c) are not stated, and they actually depends on the MG internal management strategy.

Final considerations

It could be argued that separating the whole scheduling problem in three different phases may be not necessary and it could lead to a sub-optimal solution. Actually, the problem constraints and cost functions of Phase 1, 2 and 3 can be clustered in a unique non-convex optimization problem which, in principle, could be solved through a distributed algorithm.
However, it has been chosen to adopt this three steps procedure for two main reasons:

1. Applying distributed optimization algorithms to non-convex problems leads to sub-optimal solution, and not-generalized convergence results [48, 53]. As shown, a distributed algorithm for solving Phase 2 is not needed and it can be performed in centralized fashion, while preserving MG internal economy and sensitive information through the equivalent representation proposed in Paragraph 2.3.1.

2. Dividing the convex dynamic scheduling problem (Phase 1) from the non-convex power flow part (Phase 2) allows to use an efficient distributed method for the first, while the second, being a static optimization problem, can be efficiently solved by decomposing it in N different optimization problems, one for each time instant of the day.

3. The proposed structure allows to perform the optimization phases in different time instants and at different time rates. For instance, Phase 2 and 3 can be periodically performed in the online management of the MGs, using updated information about the load and renewable power trends, ensuring the MGs support for the voltage and current regulation, and for the minimization of power losses. The same holds for Phase 1, which may be used to reschedule the MG-AG active power production in case the energy prices or the reserve requirements are varied over the day.

2.5 Numerical results

The proposed method has been tested on the standard IEEE 37-bus system, which characteristics are derived from [58]. As shown in Figure 2.2, 4 MGs and 25 loads are connected to the considered distribution network. The characteristics of MGs dispatchable units, i.e. mGENs and BESSs, are shown in Table 2.2; all BESSs are operated with SOCs bounded between 10% and 90%. Moreover, each MG is endowed with PV system and a WT system, which power trends are depicted Figure 2.3(a) and Figure 2.3(b), respectively. Finally, the active power absorption profiles of MGs loads are shown in Figure 2.3(c), while the ones of loads directly connected to the distribution network in 2.3(d). Concerning the reactive power profiles, all loads are simulated with a 0.8 constant power factor. Consistently with the actual regulations for Aggregators in Italy [30], the MG-AG must provide a minimum active power reserve bid of 1 MW. Considering the voltage and current regulation service, it is assumed that line currents are limited at 350 A and the nodal voltages at a maximum variation of 10%. The overall scheduling approach has been implemented in MATLAB, using the CPLEX solver for *Phases 1* and *3* and the FMINCON solver for *Phase 2*.

The optimization problem stated in *Phase 1* has been solved also in a centralized fashion to check the validity of *Proposition 1*. In the considered case, ADMM converges to the global optimum in about 70 iterations. The total output power of the MG-AG, i.e. $\mathbf{p}^{\text{AG}}$, and of the total upward power reserve, i.e. $\mathbf{r}_{\mathbf{p}}^{\text{AG}\uparrow}$, are shown in Figure 2.4(a) and (b), respectively, computed both using the centralized and the distributed approach. It is evident that the same optimal solution is obtained and that the minimum required amount of power reserve is always globally provided. This means that the AGS is able to optimally manage the MG-AG without any information about the MGs composition and internal optimization problems. As described in the previous sections, the AGS uses the dual variables, which can be interpreted as negotiation internal prices, to coordinate the MGs operations. The selling and buying energy price are shown in Figure 2.4 (a), together with the steady-state value of $\boldsymbol{\lambda}^{\boldsymbol{p}}/\tau$. This converges to the selling prices when the MG-AG exports power, to the buying price when

the MG-AG absorb power, while it takes an intermediate optimal value if the MG-AG overall output power is zero. Figure 2.4 (d) shows the convergent value of $\boldsymbol{\lambda}^{r_P\uparrow}$, which takes values greater than zero at the beginning and at the end of the day so that MGs are incentivised to provide the minimum required amount of active power reserve.
Once the active power profile of each MG has been scheduled, *Phase 2* has been performed to check if electrical feasibility is compromised by the optimal active power flows computed in *Phase 1*.
Considering Figure 2.2, it can be noted that line 22-23 could be one of the most critical since three MGs inject power through it. In Figure 2.4(e), the current magnitude profile in line 22-23 is shown both in case the current constraints are considered and in case they are not. It is evident that the MGs power flows scheduled in *Phase 1* would violate the maximum current bound between 8:00 and 12:00. On the contrary, if *Phase 2* is performed, the electrical feasibility can be achieved by asking the MGs a small active power reduction. For the reported numerical results, MG2, MG3 and MG4 are asked to reduce their active power production, while MG1 is just requested to produce an extra amount of reactive power, see Figure 2.5. The nodal voltages after execution of *Phase 2* are reported in Figure 2.4 (f), showing that they respect the operational limits. Finally, *Phase 3* is executed such that the MGs reschedule their units according to the final active and reactive power set-points computed after *Phases 1* and *2*. As shown in Figure 2.5, all the MGs perfectly track the active and reactive power profiles. Moreover, in Figure 2.6, the scheduled profiles for the resources of MG2 are shown, both after the execution of *Phase 1* and of *Phase 3*.

Analysis of convergence and scalability properties of the distributed algorithm in Phase 1

The scalability of Algorithm 1 has been tested considering larger number of MGs, connected to the IEEE 37-bus system. Figure 2.7 shows the differences between the optimal values of the cost function of the centralized solution and the one of the distributed algorithm also for 8-MGs, 12-MGs, 16-MGs and 32 MGs aggregation sizes, using the units characteristics shown in Table 2.2 and varying accordingly the minimum power

reserve. The distributed algorithm achieves the same optimal objective of the centralized solution in about 70 iterations, even though a varying number of MGs are considered. This result has been obtained by properly tuning the step update of Algorithm 1 as follows $\mu = 0.5e^{-5}/M$, where M represents the number of MGs in the aggregation, i.e. $M = |\mathcal{N}_{\mathcal{M}}|$.
The test-cases have been simulated using a laptop with an Intel Core i7-6500u processor. The average computational time for each iteration of *Phase 1* is $t_{1,k} = 1$ s, the whole scheduling of *Phase 2* requires $t_2 = 300$ s, while for Phase 3 the computational time is $t_3 = 1$ s. These results witness the potentiality of the distributed approach since the total computational time does not depend on the size of the aggregation. In particular, *Phase 1* involves $1344\,M$ optimization variables for each tested aggregation size. On the other hand, although *Phase 2* is centralized, its complexity is marginally affected by the size of the aggregation thanks to the proposed MG equivalent modelling. Indeed, it involves $(21120{+}2\,M)$ optimization variables for each tested case.

Table 2.2: MGs generation units

Owner	Unit	$(\underline{p},\, \bar{p})$	$(\underline{q},\, \bar{q})$	$(C^b, \bar{E}^b)$	Costs
MG_1	mGEN 1	$(75, 500)$	$\pm\sqrt{(670 - p^{g\,2})}$	–	$(0.05,\ 2,\ 30)e^{-3}$
MG_1	mGEN 2	$(50, 700)$	$\pm\sqrt{(920 - p^{g\,2})}$	–	$(0.02,\ 4,\ 25)e^{-3}$
MG_1	BESS 1	± 80	± 80	$(150, 20e^3)$	$(6e^{-5}, 8.8e^{-2}, 1e^5)$
MG_1	BESS 2	± 125	± 125	$(225, 20e^3)$	$(9e^{-5}, 8e^{-2}, 1e^5)$
MG_2	mGEN 1	$(25, 375)$	$\pm\sqrt{(480 - p^{g\,2})}$	–	$(0.04, 3, 35)e^{-3}$
MG_2	mGEN 2	$(75, 450)$	$\pm\sqrt{(600 - p^{g\,2})}$	–	$(0.03, 3, 25)e^{-3}$
MG_2	BESS 1	± 150	± 150	$(300, 20e^3)$	$(7e^{-5}, 9.6e^{-2}, 1e^5)$
MG_2	BESS 2	± 125	± 125	$(225, 20e^3)$	$(8e^{-5}, 7.2e^{-2}, 1e^5)$
MG_3	mGEN 1	$(50, 500)$	$\pm\sqrt{(670 - p^{g\,2})}$	–	$(0.05, 1, 27.5)e^{-3}$
MG_3	mGEN 2	$(75, 400)$	$\pm\sqrt{(850 - p^{g\,2})}$	–	$(0.03, 1, 25)e^{-3}$
MG_3	BESS 1	± 80	± 80	$(175, 20e^3)$	$(8e^{-5}, 7.2e^{-2}, 1e^5)$
MG_3	BESS 2	± 125	± 125	$(225, 20e^3)$	$(5e^{-5}, 8e^{-2}, 1e^5)$
MG_4	mGEN 1	$(25, 400)$	$\pm\sqrt{(500 - p^{g\,2})}$	–	$(0.04, 4, 30)e^{-3}$
MG_4	mGEN 2	$(100, 725)$	$\pm\sqrt{(910 - p^{g\,2})}$	–	$(0.03, 2, 25)e^{-3}$
MG_4	BESS 1	± 75	± 75	$(175, 20e^3)$	$(4e^{-5}, 8e^{-2}, 1e^5)$
MG_4	BESS 2	± 125	± 125	$(225, 20e^3)$	$(4e^{-5}, 9.6e^{-2}, 1e^5)$

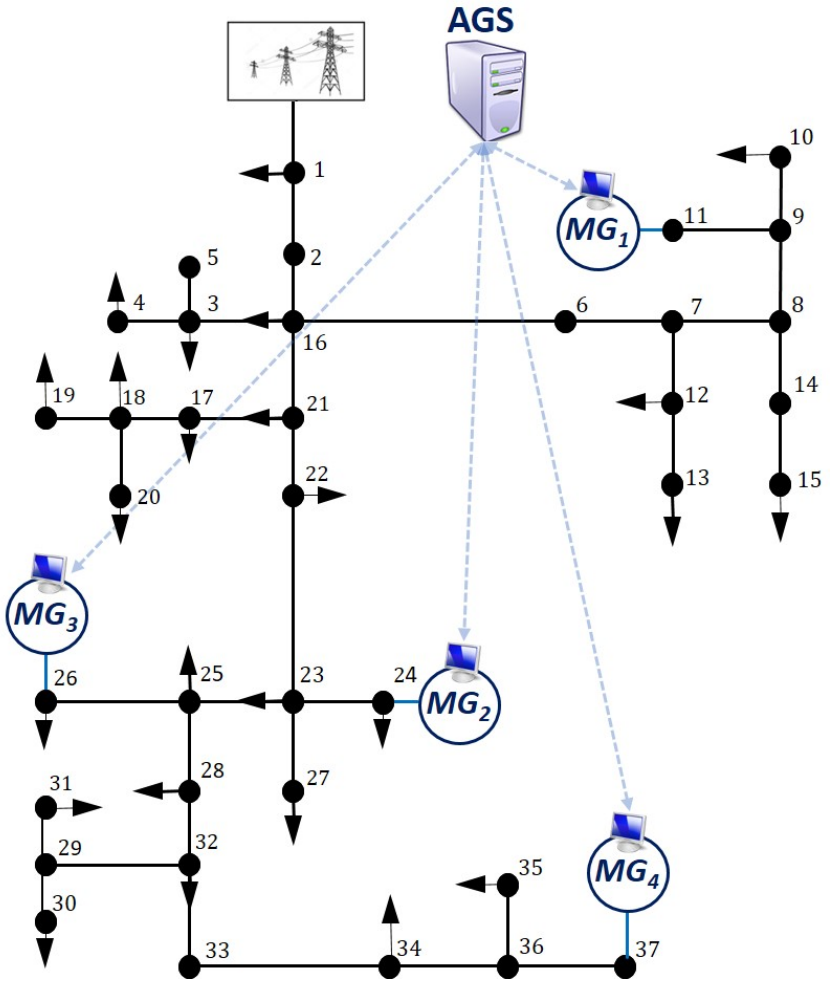

Figure 2.2: Distribution network where MGs are connected: IEEE 37 bus system

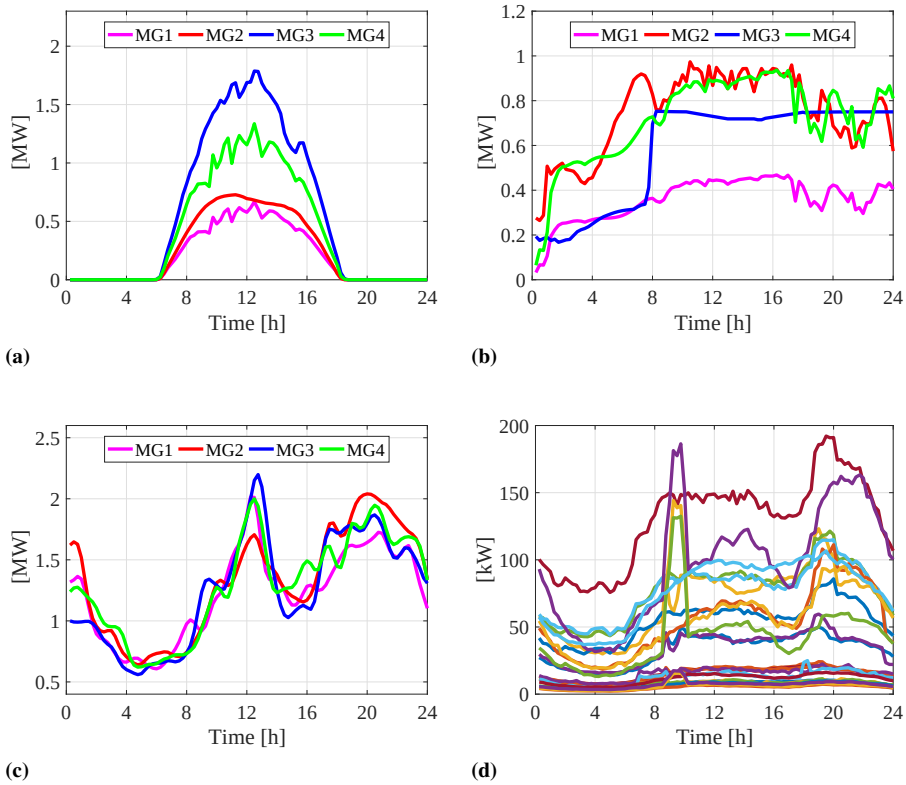

Figure 2.3: (a) Power production of MGs PV systems; (b) Power production of MGs WT systems; (c) Power absorption of MGs loads; (d) Power absorption of loads directly connected to the distribution network.

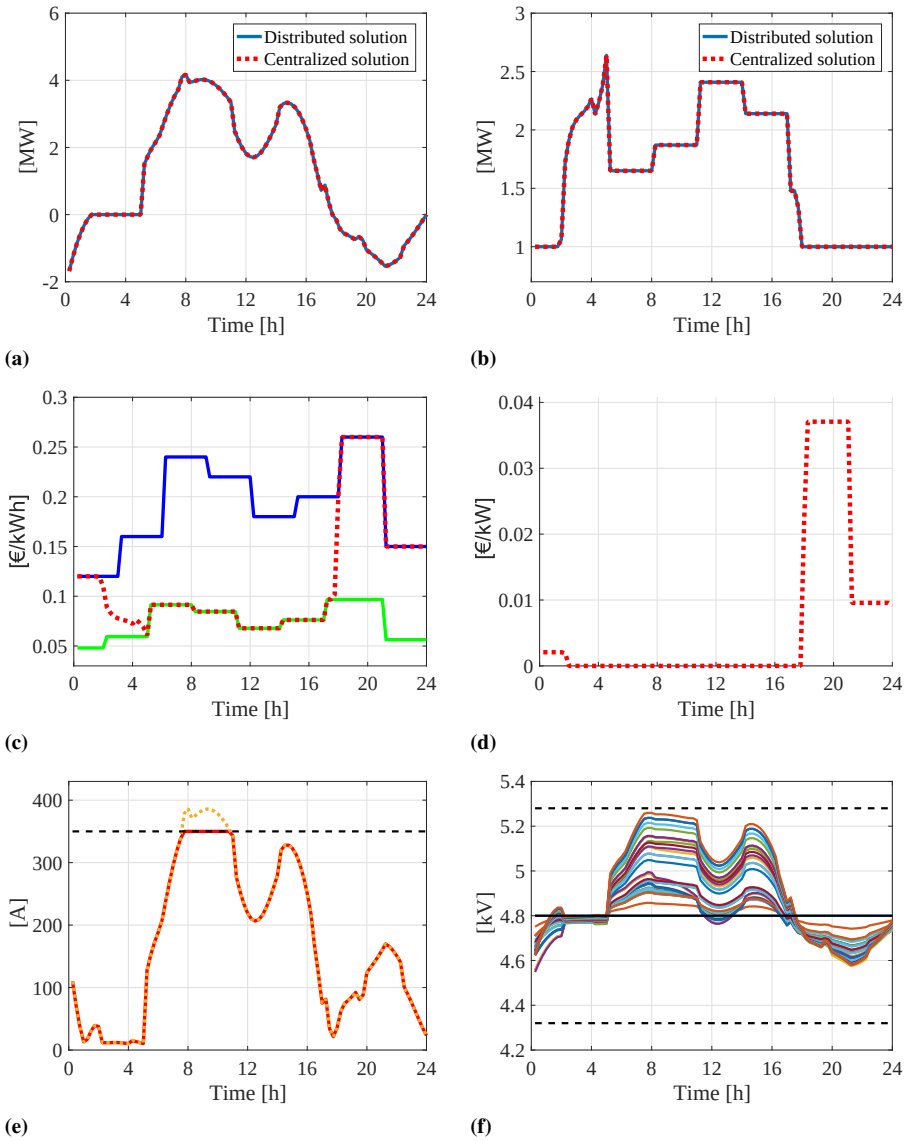

Figure 2.4: (a) MG-AG output power; (b) MG-AG upward active power reserve; (c) Buying price (dashed blue), selling price (solid green), internal energy price $\boldsymbol{\lambda}^{\boldsymbol{p}}/\tau$; (d) Internal price for upward power reserve $\boldsymbol{\lambda}^{r_{\mathcal{P}}\uparrow}$; (e) Current magnitude of line 22-23 in case limits are considered (solid red) and not (dashed yellow); (f) Nodal voltages after *Phase 2*.

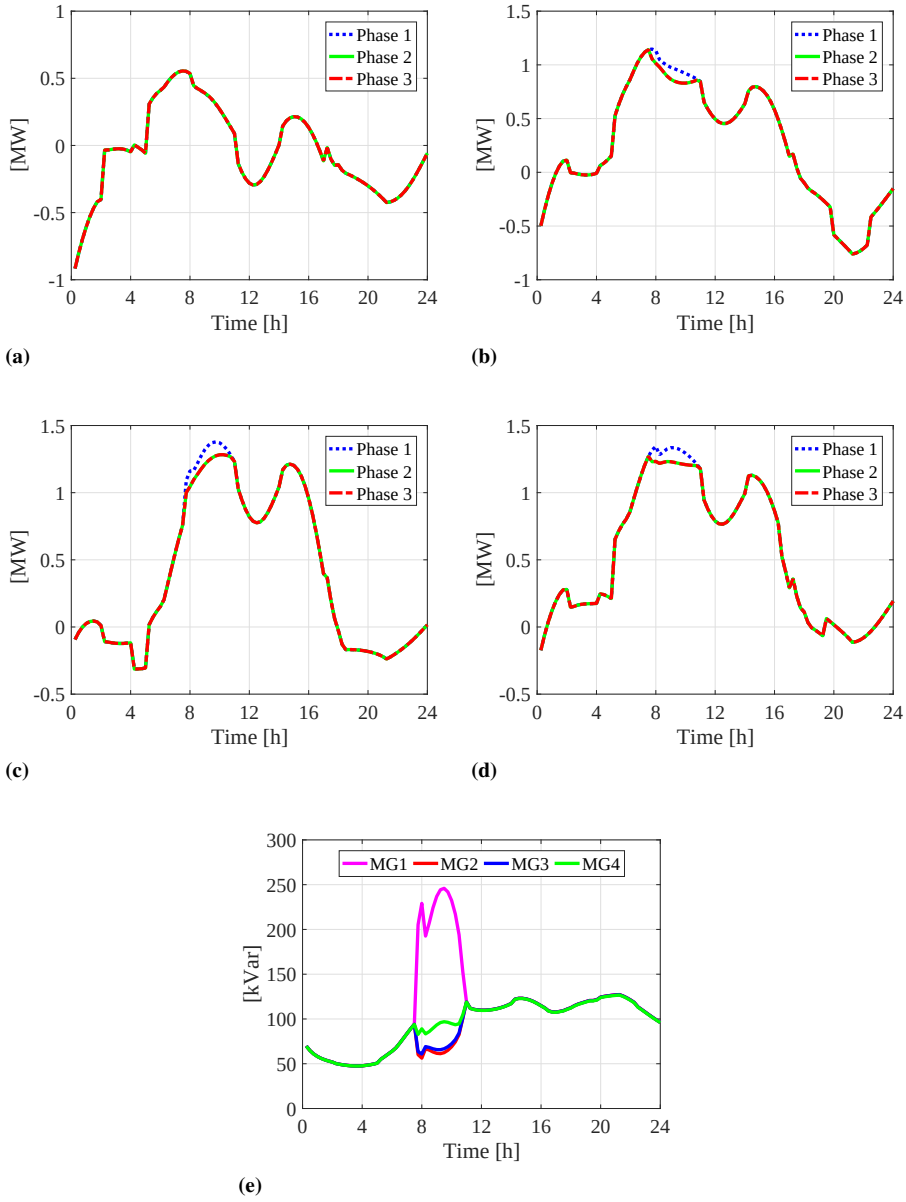

Figure 2.5: MGs output active power at each phase: (a) MG1, (b) MG2 , (c) MG3, (d) MG4; (e) MGs output reactive power at *Phase 3*.

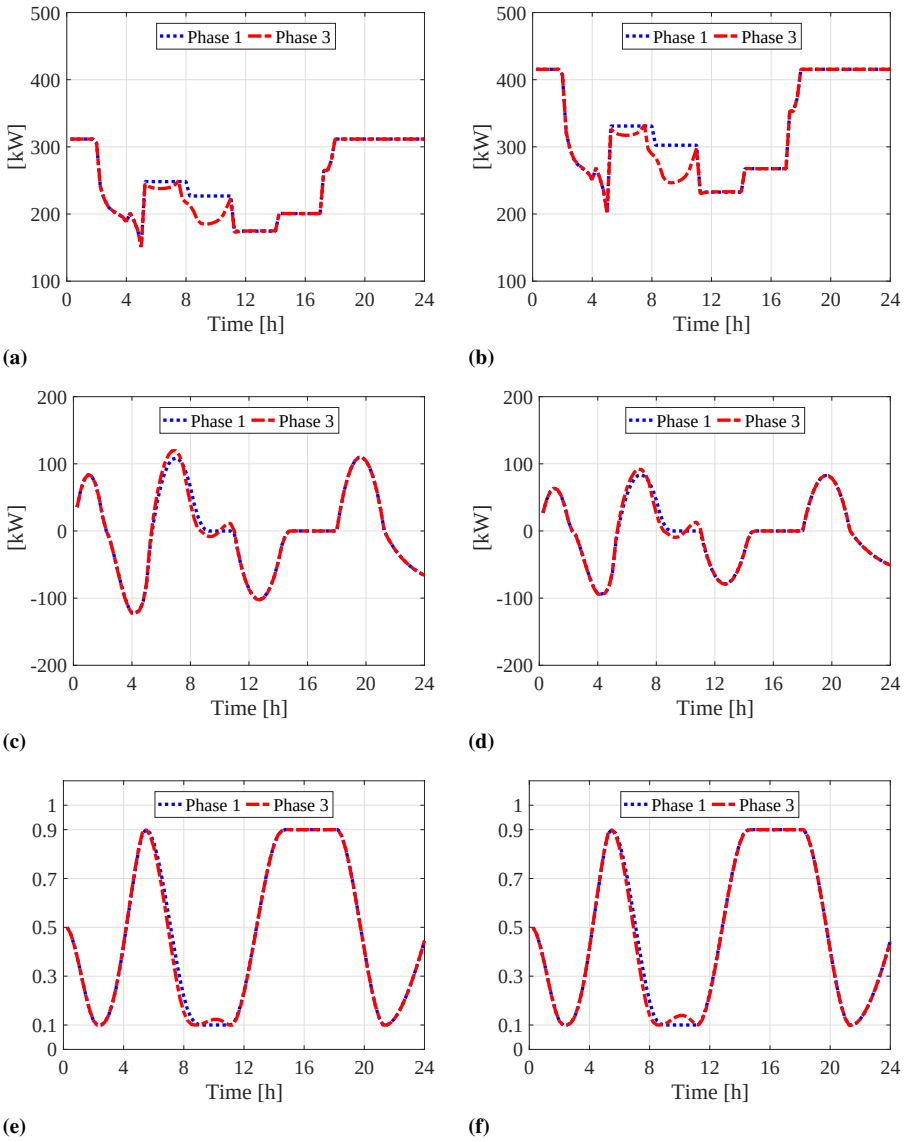

Figure 2.6: Output of MG2 resources at *Phase 1* and *Phase 3*: (a) Active power of mGEN 1, (b) Active power of mGEN 2, (c) Active power of BESS 1, (d) Active power of BESS 2, (e) SOC of BESS 1, (f) SOC of BESS 2.

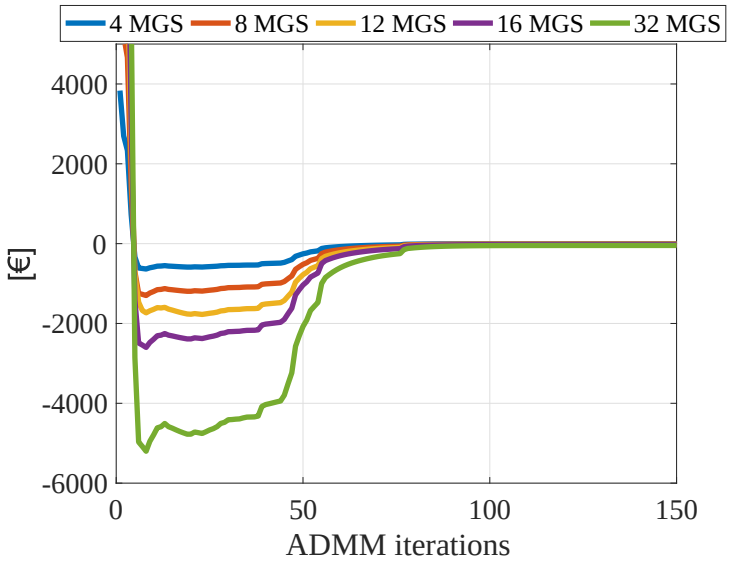

Figure 2.7: Optimal objective gap between centralized and distributed solution at *Phase 1*, i.e. $(\mathbf{J}^{\mathrm{AG},*} - \mathbf{J}^{\mathrm{AG},\mathbf{k}})$, for varying MGs aggregation size.

2.6 Conclusion

An approach for the offline scheduling of microgrids grouped to form an aggregation has been described. The goal is to allow microgrids to provide ancillary services to the main utility, e.g. in terms of power reserve and voltage regulation. The method has been structured in three phases. Scalability of the optimization problem and confidentiality requirements are guaranteed by resorting to a suitable distributed optimization algorithm.

Appendix A

Expressing active power reserves of BESSs as linear inequalities

It is shown how to transform BESSs active power reserves expressions, defined in (2.8)-(2.9), into a set of linear inequalities.
First of all, the variables $r^{b\uparrow}_{e,k_i}$ and $r^{b\downarrow}_{e,k_i}$ are introduced, expressing the minimum amount of available energy reserves with respect to the whole time horizon. These are constrained as follows

$$r^{b\uparrow}_{e,k_i} \leq C^b_{k_i} \frac{s^b_{k_i}(k) - \underline{s}^b_{k_i}}{100}, \quad \forall k \in [1, \dots, N], \tag{2.34}$$

$$r^{b\downarrow}_{e,k_i} \leq C^b_{k_i} \frac{\bar{s}^b_{k_i} - s^b_{k_i}(k)}{100}, \quad \forall k \in [1, \dots, N]. \tag{2.35}$$

Then, according to the proposed conservative strategy, the following constraints are introduced to bound the offered power reserves from BESSs

$$r^{b\uparrow}_{p,k_i}(t) \leq \bar{p}^b_{k_i} - p^b_{k_i}(t), \qquad r^{b\uparrow}_{p,k_i}(t) \leq \frac{r^{b\uparrow}_{e,k_i}}{\tau N} - p^b_{k_i}(t), \tag{2.36}$$

$$r^{b\downarrow}_{p,k_i}(t) \leq \underline{p}^b_{k_i} + p^b_{k_i}(t), \qquad r^{b\downarrow}_{p,k_i}(t) \leq \frac{r^{b\downarrow}_{e,k_i}}{\tau N} + p^b_{k_i}(t). \tag{2.37}$$

At this stage, it is sufficient to add a sufficiently small and positive weighting term for the variables $r^{b\uparrow}_{p,k_i}(t)$ and $r^{b\downarrow}_{p,k_i}(t)$ to the cost function of the optimization problem, defined for the MG case in (2.12). In this way, the optimal value of the variables $r^{b\uparrow}_{p,k_i}(t)$ and $r^{b\downarrow}_{p,k_i}(t)$ will coincide with the more restrictive of constraints (2.36)-(2.37), achieving so the same value of the minimum function used for the expressions (2.8)-(2.9).
Therefore, the expressions (2.34)-(2.37) can be included in the compact version of MGs constraints (2.13b), replacing (2.8)-(2.9).

Appendix B

Proof of Proposition 1

Proof. Proposition 1 holds $\forall t$, therefore the time index is neglected in the following.
The function

$$g_z^p(z^p) = -\ \rho_e^s\ \tau \max\left(p^{\text{AG}}, 0\right) + \rho_e^b\ \tau \max(-p^{\text{AG}}, 0)\,,$$

is said to be convex over $\mathcal{Z}^p$ if and only if

$$g_z^p(z_2^p)\ \geq\ g_z^p(z_1^p)\ +\ (z_2^p - z_1^p)'\,\nabla g_z^p(z_1) \quad \forall z_1^p, z_2^p \in \mathcal{Z}^p \tag{2.38}$$

Moreover, if the inequality (2.38) is strict with $z_1^p \neq z_2^p$, then $g_z(z^p)$ is said to be strictly convex over $\mathcal{Z}^p$.

Take two instances $z_1^p = [(p^{\text{AG}})_1, (r_p^{\text{AG}\uparrow})_1, (r_p^{\text{AG}\downarrow})_1]'$ and $z_2^p = [(p^{\text{AG}})_2, (r_p^{\text{AG}\uparrow})_2, (r_p^{\text{AG}\downarrow})_2]'$. If $(p^{\text{AG}})_2 \leq 0 \leq (p^{\text{AG}})_1$, it can be verified that (2.38) becomes $(\rho_e^b - \rho_e^s) \cdot (p^{\text{AG}})_2 \leq 0$. Since $(p^{\text{AG}})_2 \leq 0$, this implies that $g_z(z^p)$ is convex if and only if $\rho_e^b \geq \rho_e^s$. The same result can be easily obtained in case $(p^{\text{AG}})_1 \leq 0 \leq (p^{\text{AG}})_2$. On the other hand, if $(p^{\text{AG}})_1$ and $(p^{\text{AG}})_2$ have the same sign, e.g. $(p^{\text{AG}})_1 \geq (p^{\text{AG}})_2 \geq 0$, (2.38) collapses in a trivial equality. This implies that $g_z(z^p)$ is convex but not strictly. □

CHAPTER 3

Management of real-time balancing service provision

3.1 Introduction

It has been described in Chapter 2 how a Microgrids Aggregator (MG-AG) can optimally schedule its resources and jointly allocate the required amount of active power reserve. During the online operation, the MG-AG, acting as a proper Balancing Service Provider (BSP), is called to exploit this reserve to support the frequency regulation in the electrical system. This chapter focuses on the design of coordination schemes for aggregated Microgrids (MGs) to accomplish this task. Also in this case, the designed algorithms ensure scalability properties and the confidentiality of MGs internal information.
Moreover, it is considered that MGs can offer other sources of flexibility during the online management, other than relying just on Micro-

Generators (mGENs) and Battery Energy Storage Systems (BESSs). This consists in acting on controllable loads, which can be shifted, modulated or interrupted. However, although this additional degree of freedom can be a great advantage, it adds further complexity in the management of the MG-AG since it involves the introduction of mixed-integer decision variables and constraints.

3.1.1 Literature Review

The online provision of frequency regulating power from commercial buildings, equipped with BESSs and HVACs, is addressed in [59, 60], adopting centralized optimization approaches. As previously mentioned, centralized methods are not advisable for coordinating aggregated resources and MGs since they lead to poor scalability properties and to the share of all MGs internal information. Distributed optimization schemes for satisfying balancing service requests sent from the TSO are proposed in [61, 62]. Nevertheless, the previous mentioned contributions address cases where resources are modelled just using continuous variables, which is not always a realistic assumption. Indeed, some units can be switched on/off, while loads can be shifted, interrupted or curtailed. Unfortunately, feasibility and convergence issues arise when distributed approaches are applied to non-convex optimization frameworks, like those when mixed-integer variables are involved. Heuristic methods addressing the mixed-integer case have been proposed in [63] and in [64], where local units react based on the energy prices and they are not managed to satisfy balancing services request from the TSO. Moreover, the mentioned heuristic methods do not guarantee to converge and find a feasible solution.

3.1.2 Proposed solution

Consistently with the actual balancing market regulations, described in Chapter 1, and considering the mentioned literature, the following solution is here proposed.
It is assumed that, through the methods described in Chapter 2, the MG-AG has already scheduled its optimal operations defining the output power profile for the whole day and guaranteeing that the minimum required amount of power reserve is ensured at each time instant.

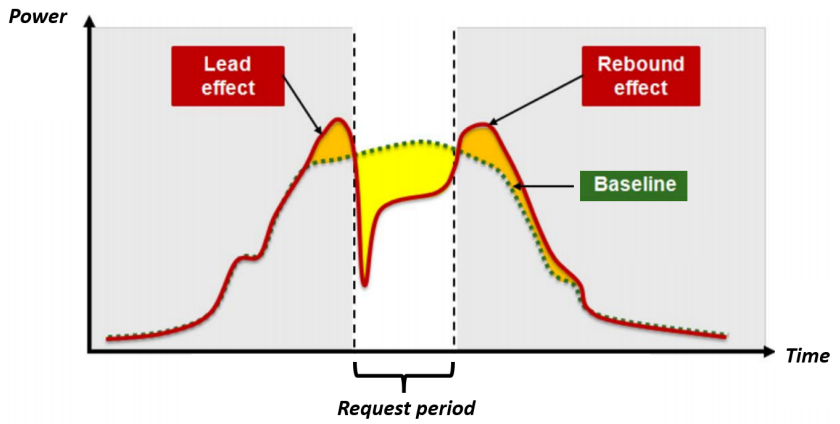

Figure 3.1: Lead and rebound effects. Source: [65].

As described in Chapter 1, the AGS can decide to submit the power reserves to the TSO either as *precontracted* or *non-precontracted* bids. The first are declared ex-ante and must be guaranteed also during the online operations. The second are periodically offered during the day and the TSO, based on the grid needs, can decide to ask for their provision or not. In this Chapter, it is assumed that the AGS submits just the minimum required amount of reserves as *precontracted* bids, while the remaining extra-reserve, together with the additional flexibility given by controllable loads, is offered during the day as *non-precontracted* balancing bids. It is reminded, as discussed in Section 1.3, that MG-AGs are more indicated for the provision of mFRR services. In this framework, during the real-time operation, the TSO can request to vary the MG-AG power output with respect to the pre-scheduled power baseline for a defined time period. This service request is assumed to be sent directly to the AGS, which must accordingly coordinate MGs operations at the minimum cost. The power variation request must be satisfied avoiding the so-called *lead* or *rebound effects*, i.e. when MGs are not able to maintain the pre-declared baseline in the time instants outside the request period because of the satisfaction of the power variation request, see Figure 3.1. Moreover, even though multiple power requests are received from the TSO, the MG-AG must always guarantee the availability of the pre-contracted power reserves.

Given the presence of mixed-integer variables, the distributed optimization method presented in Chapter 2 cannot be directly applied to accomplish these tasks. Therefore, two alternative and novel solution approaches are here designed and proposed.
The first consists in a hierarchical optimization framework where initially MGs communicate to the AGS their degree of flexibility, described by properly defined *flexibility functions* expressing the power variation each MG can provide and the associated cost. The AGS uses this information both to submit non-precontracted balancing bids to the TSO and to dispatch the effective power request at the minimum global cost. The advantages of the approach are that the MGs internal information is preserved and that this solution is extremely efficient from a computational point of view, not requiring iterative procedures as for distributed approaches. Moreover, its performances have been compared to the centralized optimization framework, where the AGS has a complete knowledge of each MG, showing satisfactory results in terms of optimality of the solution.
A second approach is also proposed, where the balancing service provision is addressed through a proper distributed optimization approach. Indeed, a distributed algorithm has been recently introduced for Mixed-Integer Linear Programs (MILPs) in [66], with finite-time convergence and feasibility properties under suitable assumption. Yet, the algorithm in [66] is too conservative in some cases, failing to find a feasible solution or determining a solution far from being optimal. Therefore, a less conservative variant of the algorithm is here designed, applying it for the AGS dispatch of TSO balancing power requests. Also in this case, the results show satisfying scalability and optimality performances compared to the centralized case.

Before describing the two approaches in details, the following common considerations are presented. As for Chapter 2, MGs models are defined as discrete-time systems with sampling time $\tau = 15$ min, while $N = 24h/\tau = 96$ denotes the number of time steps during the whole day. As a convention, all the power values are positive if delivered and negative if absorbed, while maximum and minimum limits of each variable are denoted with a bar over or below the variable, respectively.

Table 3.1: Optimization variables and system parameters

Symbol	Description
p^{g}	MG mGEN active power output [kW]
p^{b}	MG BESS active power output [kW]
p^{cl}	MG controllable load active power output [kW]
δ^{cl}	MG controllable load consumption level [integer]
p^{l}	MG load active power forecast [kW]
p^{r}	MG RES active power forecast [kW]
p^{mg}	MG active output power [kW]
s^{b}	MG BESS state of charge (SOC) [%]
$C^{b}, \bar{E}^{b}$	MG BESS capacity and energy throughput [kWh]
a^{b}, b^{b}, c^{b}	MG BESS cost coefficients [€/kWh^2]
a^{g}, b^{g}, c^{g}	MG mGEN cost coefficients [€/kWh^2, €/kWh, €]
c^{cl}	MG load cost coefficient [€/kWh]
$r_p^{g\uparrow}, r_p^{g\downarrow}$	MG mGEN up/down active power reserves [kW]
$r_p^{b\uparrow}, r_p^{b\downarrow}$	MG BESS up/down active power reserves [kW]
$r_p^{mg\uparrow}, r_p^{mg\downarrow}$	MG total up/down active power reserves [kW]
λ^{p}	MG-AG energy price [€/kWh]
$\Gamma_{\tilde{t}}^{\text{TSO}}$	TSO power variation request received at time $\widetilde{t}$ [kW]
$\Gamma_{\tilde{t}}^{mg}$	MG active power variation scheduled at time $\widetilde{t}$ [kW]

The two approaches described in the following are supposed to be executed during the daily management at the generic time instant $\tilde{t} \in (1, \dots, N)$. The hat symbol is used to denote optimally pre-scheduled variables, for instance through the methods described in Chapter 2, e.g. $\hat{p}_i^{mg}$. When variables are referred to the whole daily time horizon, these are expressed in bold, e.g. $\mathbf{p^{mg}}_i = [p_i^{mg}(1), \dots, p^{mg}(N)]$, while, when variables span from the time instant $\tilde{t}$ to the end of the horizon N, they are expressed in bold and with the subscript $\tilde{t}$, e.g. $\mathbf{p}_{i,\tilde{t}}^{\mathbf{mg}} = [p_i^{mg}(\tilde{t}), \dots, p_i^{mg}(N)]$. The optimization variables used in this Chapter are reported in Table 3.1. Moreover, the MG-AG is supposed to be composed of M MGs, included in the set $\mathcal{N}_{\mathcal{M}} = \{1, \dots, M\}$.

3.2 Hierarchical approach using flexibility functions

Consistently with the actual regulations on balancing market, the following framework is considered.
The AGS communicates the power reserve availability of the MG-AG with a bidding frequency of T_R time steps. Then, the TSO, based on the grid needs and compatibly with the offered reserves, can require a power variation $\Gamma^{\text{TSO}}_{\tilde{t}}$ with respect to the pre-scheduled MG-AG power baseline for the request period $\{\tilde{t}, \dots, \tilde{t} + T_R - 1\}$. MGs are therefore entitled of rescheduling their internal units to provide their contribution $\Gamma^{mg}_{i,\tilde{t}}$ to satisfy the TSO request. For the sake of clarity, it is assumed that both the TSO request $\Gamma^{\text{TSO}}_{\tilde{t}}$ and the MGs power variations $\Gamma^{mg}_{i,\tilde{t}}$ are constant for the whole the request period. This does not compromise the validity of the proposed approach and the assumption can be easily removed in case the TSO, or the MGs, are supposed to provide a power variation profile over the request period.

It is reminded that these operations must be performed avoiding rebound/lead effects and unavailability of the pre-contracted reserve outside the request period. As mentioned, it is supposed that just the minimum required power reserves, denoted in Chapter 2 as $\underline{\mathbf{r}}_{\mathbf{p}}^{\text{AG}\uparrow}$ and $\underline{\mathbf{r}}_{\mathbf{p}}^{\text{AG}\downarrow}$, are submitted as pre-contracted reserves. To ensure that these are guaranteed also without the need of an online coordination scheme, these reserves are proportionally redistributed among MGs based on their pre-scheduled total power reserves, denoted as $\hat{\mathbf{r}}_{\mathbf{p},i}^{\text{mg}\uparrow}$ and $\hat{\mathbf{r}}_{\mathbf{p},i}^{\text{mg}\downarrow}$, with respect to MG-AG total pre-scheduled power reserves of the MG-AG, i.e. $\hat{\mathbf{r}}_{\mathbf{p}}^{\text{AG}\uparrow}$ and $\hat{\mathbf{r}}_{\mathbf{p}}^{\text{AG}\downarrow}$. The following variables are therefore introduced

$$\underline{\mathbf{r}}_{\mathbf{p},i}^{\text{mg}\uparrow} = \frac{\hat{\mathbf{r}}_{\mathbf{p},\mathbf{i}}^{\text{mg}\uparrow}}{\hat{\mathbf{r}}_{\mathbf{p}}^{\text{AG}\uparrow}} \underline{\mathbf{r}}_{\mathbf{p}}^{\text{AG}\uparrow}, \qquad \underline{\mathbf{r}}_{\mathbf{p},i}^{\text{mg}\downarrow} = \frac{\hat{\mathbf{r}}_{\mathbf{p},\mathbf{i}}^{\text{mg}\downarrow}}{\hat{\mathbf{r}}_{\mathbf{p}}^{\text{AG}\downarrow}} \underline{\mathbf{r}}_{\mathbf{p}}^{\text{AG}\downarrow}, \qquad \forall i \in \mathcal{N}_{\mathcal{M}}, \tag{3.1}$$

where $\underline{\mathbf{r}}_{\mathbf{p},i}^{\text{mg}\uparrow}$ and $\underline{\mathbf{r}}_{\mathbf{p},i}^{\text{mg}\downarrow}$ now indicate the fractions of pre-contracted reserves that each MG must independently guarantee during the online operation.

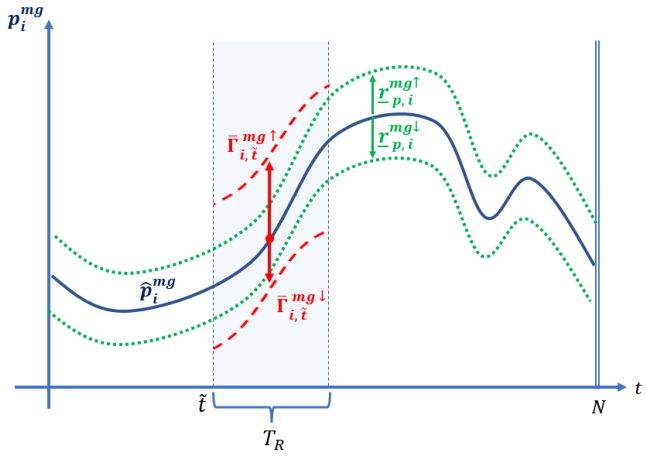

Figure 3.2: Power flexibility that each MG can offer during the online management.

The proposed approach for the real-time balancing service provision relies on the following operations performed at the time instant $\widetilde{t}$.

1. **MG flexibility evaluation:** Each MG independently computes the maximum upward and downward power variations that it can continuously provide for the next T_R time steps, denoted as $\bar{\Gamma}_{i,\tilde{t}}^{mg\uparrow}$ and $\bar{\Gamma}_{i,\tilde{t}}^{mg\downarrow}$, respectively, see Figure 3.2. These are computed such that, even though these power variations are requested for the time period $\{\tilde{t},\dots,\tilde{t}+T_R-1\}$, the following requirements are respected

   - Each MG is able to singularly maintain its pre-scheduled power baseline $\hat{p}_i^{mg}(t)$ for $t \in \{\tilde{t}+T_R,\dots,N\}$, avoiding to cause imbalances after satisfying the power request (rebound effect).
   - Each MG is able to guarantee the pre-contracted minimum reserves $\underline{r}_{p,i}^{mg\uparrow}(t)$, $\underline{r}_{p,i}^{mg\downarrow}(t)$, defined in (3.1), for $t \in \{\tilde{t}+T_R,\dots,N\}$.

   MG power flexibility is also associated to the corresponding cost so that the AGS can optimally dispatch the TSO request. In order to avoid sharing the characteristics and costs of each MG unit, here the concept of *flexibility functions* is introduced.

A *flexibility function* $f^{\Gamma}_{i,\widetilde{t}}$ is defined as the following static map

$$J^{mg,*}_{i,\widetilde{t}} = f^{\Gamma}_{i,\widetilde{t}}(\Gamma^{mg,*}_{i,\widetilde{t}}), \tag{3.2}$$

where $J^{mg,*}_{i,\widetilde{t}}$ is the minimum operational cost that MG_i would afford to provide the power variation $\Gamma^{mg}_{i,\widetilde{t}}$ at time $\tilde{t}$ for the following T_R steps. Characterizing the shape and the properties of $f^{\Gamma}_{i,\widetilde{t}}$ is not a trivial task and it would require much information about MG internal optimization objectives and constraints. However, in Paragraph 3.2.3, a procedure to compute a convex approximation of $f^{\Gamma}_{i,\widetilde{t}}$ is proposed. This will be then communicated to the AGS, together with the power variations bounds $\bar{\Gamma}^{mg\uparrow}_{i,\widetilde{t}}$ and $\bar{\Gamma}^{mg\downarrow}_{i,\widetilde{t}}$, allowing MGs to preserve the internal information, and to simplify the AGS management from a computational point of view.

2. **AGS bidding and TSO balancing power request:** The AGS gathers the MGs approximated *flexibility functions* and the power variations bounds and it uses this information to submit *non-precontracted* reserve bids in the balancing market. The TSO, according to the grid needs, can send a power variation request to the MG-AG for the time period $\{\widetilde{t}, \ldots, \widetilde{t}+T_R-1\}$. These market operations are not modelled in this Chapter.

3. **Dispatch of the TSO request:** If the TSO requires a power variation $\Gamma^{\text{TSO}}_{\widetilde{t}}$ to the MG-AG, the AGS must dispatch it minimizing the MGs operational costs. To do this, it will exploit the *flexibility functions* that the MGs have previously communicated.

4. **MGs rescheduling:** Finally, each MG independently reschedules its internal operations to satisfy the power variation committed by the AGS, maintaining the pre-declared power baseline and reserves for the future time instants.

This Section is structured as follows. MG models in presence of controllable loads are presented in Paragraph 3.2.1, while the centralized MG-AG management for providing balancing services is formulated in Paragraph 3.2.2. The procedure to approximate flexibility functions is

described in Paragraph 3.2.3, while the final dispatch of TSO requests using flexibility functions is discussed in 3.2.4. Finally, simulation tests of the proposed approach are presented in Paragraph 3.2.5.

3.2.1 Microgrid modelling in presence of flexible loads

First of all, the modelling of MG loads is addressed, which are here supposed to be controllable, meaning that the power consumption can be modulated and/or deferred in time. For notational simplicity and without compromising the validity of the approach, it is assumed that each MG is endowed with just one controllable load. Consistently with the reality, controllable loads cannot be continuously modulated, but they can be operated only at specific levels, which correspond to certain fractions of the maximum power consumption $\bar{p}^{cl}$ per time slot. Therefore, the integer variable $\delta^{cl}(t) \in \{0, 1, \dots, n^{cl}\}$ is introduced, denoting the level of consumption of the load at time step t. Moreover, controllable loads usually allow to be modulated just in a pre-defined time interval, denoted as $\{\underline{\tau}_i^{cl}, \bar{\tau}_i^{cl}\}$. Therefore, the following constraints are stated $\forall i \in \mathcal{N}_{\mathcal{M}}$,

$$p_i^{cl}(t) = \frac{\delta_i^{cl}(t)}{n_i^{cl}} \bar{p}_i^{cl} \qquad t \in \{\underline{\tau}_i^{cl}, \bar{\tau}_i^{cl}\}, \tag{3.3a}$$

$$p_i^{cl}(t) = \hat{p}_i^{cl}(t), \qquad t \notin \{\underline{\tau}_i^{cl}, \bar{\tau}_i^{cl}\}, \tag{3.3b}$$

where $\hat{p}_i^{cl}(t)$ represent the pre-scheduled power absorption of the load. Finally, it must be also ensured that the load, although modulated, receives however the pre-scheduled energy demand. It follows that

$$\sum_{t=\widetilde{t}}^{N} \tau \, p_i^{cl}(t) = \sum_{t=\widetilde{t}}^{N} \tau \, \hat{p}_i^{cl}(t) \,. \tag{3.3c}$$

Figure 3.3 depicts an example of controllable load modulation, respecting all the presented constraints. Concerning the other MGs resources, e.g. mGENs and BESSs, their models have been already described in Paragraph 3.2.1, and these are here represented for completeness.

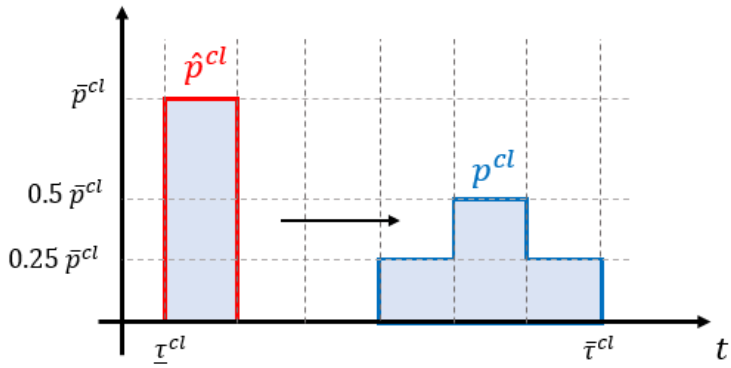

Figure 3.3: Load controlled with 25% modulation steps, i.e. $n^{cl} = 4$.

Considering dispatchable mGENs, $\forall j_i \in \{1, \ldots, n_i^g\}$ it must hold that

$$\underline{p}_{j_i}^{g} \leq p_{j_i}^{g}(t) \leq \bar{p}_{j_i}^{g}\,, \tag{3.4}$$

$$r_{p,j_i}^{g\uparrow}(t) = \bar{p}_{j_i}^{g} - p_{j_i}^{g}(t), \tag{3.5}$$

$$r_{p,j_i}^{g\downarrow}(t) = p_{j_i}^{g}(t) - \underline{p}_{j_i}^{g}\,. \tag{3.6}$$

For BESS systems, the following expressions must be stated $\forall k_i \in \{1, \ldots, n_i^b\}$

$$\underline{p}_{k_i}^{b} \leq p_{k_i}^{b}(t) \leq \bar{p}_{k_i}^{b}\,, \tag{3.7}$$

$$s_{k_i}^{b}(t+1) = s_{k_i}^{b}(t) - 100\,\frac{\tau}{C_{k_i}^{b}}\,p_{k_i}^{b}(t)\,, \tag{3.8}$$

$$\underline{s}_{k_i}^{b} \leq s_{k_i}^{b}(t) \leq \bar{s}_{k_i}^{b}\,, \tag{3.9}$$

$$r_{p,k_i}^{b\uparrow}(t) = \min\left\{\bar{p}_{k_i}^{b},\ \min_{\forall k\in[1,N]}\frac{1}{N}\left\{\frac{\left(s_{k_i}^{b}(k) - \underline{s}_{k_i}^{b}\right)}{100}\frac{C_{k_i}^{b}}{\tau}\right\}\right\} - p_{k_i}^{b}(t)\,, \tag{3.10}$$

$$r_{p,k_i}^{b\downarrow}(t) = \min\left\{-\underline{p}_{k_i}^{b},\ \min_{\forall k\in[1,N]}\frac{1}{N}\left\{\frac{\left(\bar{s}_{k_i}^{b} - s_{k_i}^{b}(k)\right)}{100}\frac{C_{k_i}^{b}}{\tau}\right\}\right\} + p_{k_i}^{b}(t)\,. \tag{3.11}$$

Finally, the MGs output variables are defined as follows

$$p_i^{mg}(t) = \sum_{k_i=1}^{n_i^b} p_{k_i}^b(t) + \sum_{j_i=1}^{n_i^g} p_{j_i}^g(t) + \sum_{p_i=1}^{n_i^r} p_{p_i}^r + p_i^l(t) - p_i^{cl}(t)\,, \tag{3.12}$$

$$\underline{p}_i^{mg} \leq p_i^{mg}(t) \leq \bar{p}_i^{mg}\,, \tag{3.13}$$

$$r_{p,i}^{mg\uparrow}(t) = \sum_{k_i=1}^{n_i^b} r_{p,k_i}^{b\uparrow}(t) \; + \; \sum_{j_i=1}^{n_i^g} r_{p,j_i}^{g\uparrow}(t)\,, \tag{3.14}$$

$$r_{p,i}^{mg\downarrow}(t) = \sum_{k_i=1}^{n_i^b} r_{p,k_i}^{b\downarrow}(t) + \; \sum_{j_i=1}^{n_i^g} r_{p,j_i}^{g\downarrow}(t) + \sum_{p_i=1}^{n_i^b} p_{p_i}^r(t)\,. \tag{3.15}$$

Therefore, the following cost function can be stated for the online MG scheduling

$$\begin{aligned} J_{i,\widetilde{t}}^{mg} = \sum_{t=\widetilde{t}}^{N} \Bigg\{ & \sum_{j_i=1}^{n_i^g} \Big[\underbrace{a_{j_i}^g \tau^2 (p_{j_i}^g(t))^2 + b_{j_i}^g \, \tau \, p_{j_i}^g(t) + c_{j_i}^g}_{\alpha} \Big] \\ & + \sum_{k_i=1}^{n_i^b} \Big[\underbrace{a_{k_i}^b \tau^2 (p_{k_i}^b(t) - p_{k_i}^b(t-1))^2}_{\beta_1} + \underbrace{b_{k_i}^b \left(\frac{p_{k_i}^b(t)\,\tau}{\bar{E}_{k_i}^b} \right)^2}_{\beta_2} \\ & + \underbrace{c_{k_i}^b (s_{k_i}^b(N) - s_{k_i}^b(1))^2}_{\beta_3} \Big] + \underbrace{c_i^l \, |p_i^{cl}(t) - \hat{p}_i^{cl}(t)|}_{\omega} - \underbrace{\lambda^p(t)\, p_i^{mg}(t)}_{\eta} \Bigg\}\,, \end{aligned} \tag{3.16}$$

where α includes the mGENs' fuel cost, while β_1 weights the BESSs' power variations to avoid frequent and excessive charges and discharges. The term β_2 is introduced to minimize the stored/absorbed energy with respect to the available energy throughput of the BESS, considering its remaining life. β_3 is included since it often required that the state at the end of the day equals the one at the beginning. Finally, the term ω expresses the discomfort cost for the load modulation, while η the gain/cost for the

energy trade. It is worth noticing that the price $\lambda^p(t)$ can be assumed to be either set by the energy market or defined through the distributed optimization algorithm presented in Chapter 2 as dual variable.

For the sake of notational compactness, MG variables are condensed in the following vectors

$$x_i^p = [(p_{j_i}^g, r_{p,j_i}^{g\uparrow}, r_{p,j_i}^{g\downarrow})_{\forall j_i \in \{1,n_i^g\}}, (p_{k_i}^b, r_{p,k_i}^{b\uparrow}, r_{p,k_i}^{b\downarrow})_{\forall k_i \in \{1,n_i^b\}}, p_i^{cl}, \delta_i^{cl}]',$$

$$d_i^p = [p_i^l, p_{\forall p_i \in \{1,n_i^r\}}^r]', \qquad y_i^p = [p_i^{mg}, r_{p,i}^{mg\uparrow}, r_{p,i}^{mg\downarrow}]',$$

where x_i^p includes the internal optimization variables, d_i^p the nondispatchable power profiles, while y_i^p refers to the MG_i output variables.
Therefore, MG constraints and variable expressions (3.3)-(3.15), imposed for $\forall t \in \{\widetilde{t}, \dots, N\}$, are formulated in compact form as follows

$$\boldsymbol{A}_{i,\widetilde{t}}^{\mathbf{p}} \mathbf{x}_{i,\widetilde{t}}^{\mathbf{p}} \leq \boldsymbol{b}_{i,\widetilde{t}}^{\mathbf{p}}, \tag{3.17a}$$

$$\mathbf{y}_{i,\widetilde{t}}^{\mathbf{p}} = \boldsymbol{C}_{i,\widetilde{t}}^{\mathbf{p}} \mathbf{x}_{i,\widetilde{t}}^{\mathbf{p}} + \boldsymbol{M}_{i,\widetilde{t}}^{\mathbf{p}} \mathbf{d}_{i,\widetilde{t}}^{\mathbf{p}}, \tag{3.17b}$$

where $\boldsymbol{A}_{i,\widetilde{t}}^{\mathbf{p}}$, $\boldsymbol{b}_{i,\widetilde{t}}^{\mathbf{p}}$, $\boldsymbol{C}_{i,\widetilde{t}}^{\mathbf{p}}$ and $\boldsymbol{M}_{i,\widetilde{t}}^{\mathbf{p}}$ are properly defined matrices. On the other hand, the cost function (3.16) is compacted as

$$J_{i,\widetilde{t}}^{mg} = f_{i,\widetilde{t}}^{p}(\mathbf{x}_{i,\widetilde{t}}^{\mathbf{p}}) - h_{i,\widetilde{t}}^{p}(\mathbf{y}_{i,\widetilde{t}}^{\mathbf{p}}), \tag{3.18}$$

where $f_{i,\widetilde{t}}^{p}(\mathbf{x}_{i,\widetilde{t}}^{\mathbf{p}})$ contains the operational costs for mGENs, BESSs and loads, i.e. the terms α, β_1, β_2, β_3, ω in (3.16), while $h_{i,\widetilde{t}}^{p}(\mathbf{y}_{i,\widetilde{t}}^{\mathbf{p}})$ expresses the cost/gain related to the output variables, i.e. the term η.

3.2.2 Centralized balancing service provision

At this stage, the centralized dispatch of TSO power variation requests is formulated. This, as mentioned, is not an efficient method from a computational point of view, given also the presence of mixed-integer variables, and from the privacy perspective since the AGS must have a complete knowledge of MGs internal pre-schedules, constraints and units characteristics. Nevertheless, its formulation is presented to better comprehend the balancing service provision objectives and constraints.

Suppose that the TSO sends a power variation request $\Gamma^{\text{TSO}}_{\tilde{t}}$ that must be provided the next T_R time steps.
The AGS can dispatch this request, scheduling the optimal power variations $\Gamma^{mg}_{i,\tilde{t}}$, $\forall i \in \mathcal{N}_{\mathcal{M}}$ at the minimum cost, through the following optimization problem

$$\min_{\substack{\mathbf{x}^{\mathbf{p}}_{\forall i,\tilde{t}},\mathbf{y}^{\mathbf{p}}_{\forall i,\tilde{t}},\\ \Gamma^{mg}_{\forall i,\tilde{t}},\,\epsilon}} \; \{ \sum_{\forall i \in \mathcal{N}_{\mathcal{M}}} J^{mg}_{i,\tilde{t}} \; + \; \sigma\,\epsilon^2 \} \tag{3.19a}$$

s.t. , $\forall i \in \mathcal{N}_{\mathcal{M}}$,

$$\boldsymbol{A}^{\mathbf{p}}_{i,\tilde{t}}\,\mathbf{x}^{\mathbf{p}}_{i,\tilde{t}} \leq \boldsymbol{b}^{\mathbf{p}}_{i,\tilde{t}}, \tag{3.19b}$$

$$\mathbf{y}^{\mathbf{p}}_{i,\tilde{t}} = \boldsymbol{C}^{\mathbf{p}}_{i,\tilde{t}}\,\mathbf{x}^{\mathbf{p}}_{i,\tilde{t}} + \boldsymbol{M}^{\mathbf{p}}_{i,\tilde{t}}\mathbf{d}^{\mathbf{p}}_{i,\tilde{t}}, \tag{3.19c}$$

$$p^{mg}_i(t) = \hat{p}^{mg}_i(t) + \Gamma^{mg}_{i,\tilde{t}}, \qquad \forall t \in \{\tilde{t},\dots,\tilde{t}+T_R-1\}, \tag{3.19d}$$

$$p^{mg}_i(t) = \hat{p}^{mg}_i(t), \qquad \forall t \in \{\tilde{t}+T_R,\dots,N\}, \tag{3.19e}$$

$$r^{mg\uparrow}_{p,i}(t) \geq \underline{r}^{mg\uparrow}_{p,i}(t), \qquad \forall t \in \{\tilde{t}+T_R,\dots,N\}, \tag{3.19f}$$

$$r^{mg\downarrow}_{p,i}(t) \geq \underline{r}^{mg\downarrow}_{p,i}(t), \qquad \forall t \in \{\tilde{t}+T_R,\dots,N\}, \tag{3.19g}$$

$$\sum_{\forall i \in \mathcal{N}_{\mathcal{M}}} \Gamma^{mg}_{i,\tilde{t}} + \epsilon = \Gamma^{\text{TSO}}_{\tilde{t}}. \tag{3.19h}$$

Considering constraint (3.19h) and the cost function(3.19a), it is evident that the objective of the AGS is to schedule MG power variations to satisfy the TSO power variation request, minimizing the MGs internal costs. The slack variable ϵ is introduced to avoid unfeasibility issues; therefore the term σ in (3.19a) must be chosen to a very high value. MGs optimal power variations must be provided for the whole request period, as stated in (3.19d). Constraints (3.19e)-(3.19g) enforce that the MGs operations are rescheduled such that each MG is able to maintain its pre-scheduled baseline and the pre-contracted reserves in the future time instants.
Nevertheless, MGs must share with the AGS all their internal characteristics, profiles and constraints to solve the optimization problem (3.19), see (3.19b)-(3.19c). This could be an undesired feature of the approach and moreover it leads the AGS to centrally solve a large-scale mixed-integer

optimization problem. Therefore, the idea of using flexibility functions is described in the following.

3.2.3 MGs flexibility functions

The objective of this section is to describe a procedure to provide a simple approximation of the flexibility function (3.2), which expresses the cost that a MG must sustain to provide a required power variation $\Gamma^{mg}_{\tilde{t},i}$.
Initially, each MG computes the maximum upward and downward power variations that can be provided in the next T_R steps, respecting the previously mentioned requirements. To do this, two separate optimization problems are stated.
Problem (3.20) concerns the maximization of the upward power variation that each MG_i can provide

$$\bar{\Gamma}^{mg\uparrow}_{i,\tilde{t}} = \min_{\mathbf{x}^{\mathbf{p}}_{i,\tilde{t}}, \mathbf{y}^{\mathbf{p}}_{i,\tilde{t}}, \Gamma^{mg}_{i,\tilde{t}}} \{ -\Gamma^{mg}_{i,\tilde{t}} \} \tag{3.20a}$$

s.t.

$$\boldsymbol{A}^{\mathbf{p}}_{i,\tilde{t}}\, \mathbf{x}^{\mathbf{p}}_{i,\tilde{t}} \leq \boldsymbol{b}^{\mathbf{p}}_{i,\tilde{t}}, \tag{3.20b}$$

$$\mathbf{y}^{\mathbf{p}}_{i,\tilde{t}} = \boldsymbol{C}^{\mathbf{p}}_{i,\tilde{t}}\, \mathbf{x}^{\mathbf{p}}_{i,\tilde{t}} + \boldsymbol{M}^{\mathbf{p}}_{i,\tilde{t}} \mathbf{d}^{\mathbf{p}}_{i,\tilde{t}}, \tag{3.20c}$$

$$p^{mg}_i(t) = \hat{p}^{mg}_i(t) + \Gamma^{mg}_{i,\tilde{t}}, \qquad \forall t \in \{\tilde{t}, \dots, \tilde{t} + T_R - 1\}, \tag{3.20d}$$

$$p^{mg}_i(t) = \hat{p}^{mg}_i(t), \qquad \forall t \in \{\tilde{t} + T_R, \dots, N\}, \tag{3.20e}$$

$$r^{mg\uparrow}_{p,i}(t) \geq \underline{r}^{mg\uparrow}_{p,i}(t), \qquad \forall t \in \{\tilde{t} + T_R, \dots, N\}, \tag{3.20f}$$

$$r^{mg\downarrow}_{p,i}(t) \geq \underline{r}^{mg\downarrow}_{p,i}(t), \qquad \forall t \in \{\tilde{t} + T_R, \dots, N\}, \tag{3.20g}$$

while problem (3.21) aims to compute the maximum downward power variation

$$\begin{aligned} \bar{\Gamma}^{mg\downarrow}_{i,\tilde{t}} &= \min_{\mathbf{x}^{\mathbf{p}}_{i,\tilde{t}}, \mathbf{y}^{\mathbf{p}}_{i,\tilde{t}}, \Gamma^{mg}_{i,\tilde{t}}} \{ \Gamma^{mg}_{i,\tilde{t}} \} \\ &\text{s.t.} \\ &\text{(3.20b)-(3.20g)} \end{aligned} \tag{3.21}$$

As noticeable, the maximum power variations are computed such that each MG singularly maintains the pre-declared power baseline and reserves in the future time instants.

Then, the cost associated to the maximum power variations are evaluated. To do this, each MG solves the following problems, where (3.22) computes the minimum cost that each MG_i affords to provide $\bar{\Gamma}^{mg\uparrow}_{\tilde{t},i}$

$$\begin{aligned} \bar{J}^{mg\uparrow}_{i,\tilde{t}} \; = \; & \min_{\mathbf{x}^{\mathbf{P}}_{i,\tilde{t}},\, \mathbf{y}^{\mathbf{P}}_{i,\tilde{t}},\, \Gamma^{mg}_{i,\tilde{t}}} \{\; J^{mg}_{i,\tilde{t}} \;\} \\ & \text{s.t.} \\ & (3.20b)\text{-}(3.20g) \\ & \Gamma^{mg}_{i,\tilde{t}} \; = \; \bar{\Gamma}^{mg\uparrow}_{i,\tilde{t}}\,, \end{aligned} \tag{3.22}$$

while problem (3.23) computes the minimum cost to provide the power variation $\bar{\Gamma}^{mg\downarrow}_{i,\tilde{t}}$

$$\begin{aligned} \bar{J}^{mg\downarrow}_{i,\tilde{t}} \; = \; & \min_{\mathbf{x}^{\mathbf{P}}_{i,\tilde{t}},\, \mathbf{y}^{\mathbf{P}}_{i,\tilde{t}},\, \Gamma^{mg}_{i,\tilde{t}}} \{\; J^{mg}_{i,\tilde{t}} \;\} \\ & \text{s.t.} \\ & (3.20b)\text{-}(3.20g) \\ & \Gamma^{mg}_{i,\tilde{t}} \; = \; \bar{\Gamma}^{mg\downarrow}_{i,\tilde{t}}\,, \end{aligned} \tag{3.23}$$

After having computed the maximum and minimum power variations, and the associated costs, a last optimization problem is performed. This serves to assess which is the optimal power variation for each MG_i, i.e. the one that achieves the minimum value of $J^{mg}_{i,\tilde{t}}$. Indeed, it may happen that, due to forecasts updates or because of previous power variation requests, the pre-scheduled power baseline is no more the optimal operating point. Therefore, it follows that

$$\begin{aligned} J^{mg,\text{min}}_{i,\tilde{t}} \; = \; & \min_{\mathbf{x}^{\mathbf{P}}_{i,\tilde{t}},\, \mathbf{y}^{\mathbf{P}}_{i,\tilde{t}},\, \Gamma^{mg}_{i,\tilde{t}}} \{\; J^{mg}_{i,\tilde{t}} \;\} \\ & \text{s.t.} \\ & (3.20b)\text{-}(3.20g) \end{aligned} \tag{3.24}$$

The optimal values of the cost function and of the power variation computed by (3.24), are denoted as $J^{mg,\,\text{min}}_{i,\tilde{t}}$ and $\Gamma^{mg,\,\text{min}}_{i,\tilde{t}}$, respectively.
After solving the sequence of optimization problems (3.20)-(3.24), each MG has available three important operating points: the maximum, the

minimum and the optimal power variation that can be provided for the next T_R steps, with the associated values of $J^{mg}_{i,\tilde{t}}$. This information is enough to compute a convex approximation of the flexibility function (3.2). Here, it is proposed to use a piece-wise quadratic approximation defined as follows

$$J^{mg}_{i,\tilde{t}}(\Gamma^{mg}_{i,\tilde{t}}) \;=\; f^{\Gamma}_{i,\tilde{t}}(\Gamma^{mg}_{i,\tilde{t}}) \;\approx\; \tilde{f}^{\Gamma}_{i,\tilde{t}}(\Gamma^{mg}_{i,\tilde{t}}) \;=$$

$$= \begin{cases} \frac{\bar{J}^{mg\uparrow}_{i,\tilde{t}} - J^{mg,\min}_{i,\tilde{t}}}{(\bar{\Gamma}^{mg\uparrow}_{i,\tilde{t}} - \Gamma^{mg\,\min}_{i,\tilde{t}})^2} (\Gamma^{mg}_{i,\tilde{t}} - \Gamma^{mg,\min}_{i,\tilde{t}})^2 + J^{mg,\min}_{i,\tilde{t}}, & \text{if } \Gamma^{mg}_{i,\tilde{t}} \geq \Gamma^{mg\,\min}_{i,\tilde{t}} \\ \frac{\bar{J}^{mg,\downarrow}_{i,\tilde{t}} - J^{mg,\min}_{i,\tilde{t}}}{(\bar{\Gamma}^{mg\downarrow}_{i,\tilde{t}} - \Gamma^{mg,\min}_{i,\tilde{t}})^2} (\Gamma^{mg}_{i,\tilde{t}} - \Gamma^{mg,\min}_{i,\tilde{t}})^2 + J^{mg,\min}_{i,\tilde{t}}, & \text{if } \Gamma^{mg}_{i,\tilde{t}} < \Gamma^{mg,\min}_{i,\tilde{t}} \end{cases}$$

The convex quadratic approximation is also motivated by the fact that the optimal cost of parametric quadratic problems (such as the MG one assuming fixed integer variables) is indeed a piece-wise quadratic function with respect to the parameters, as discussed in [67]. In Figure 3.4, the piece-wise quadratic approximation is shown. Obviously, using more information on MGs internal characteristics and using more operating points, the approximation of function (3.2) can be significantly improved.

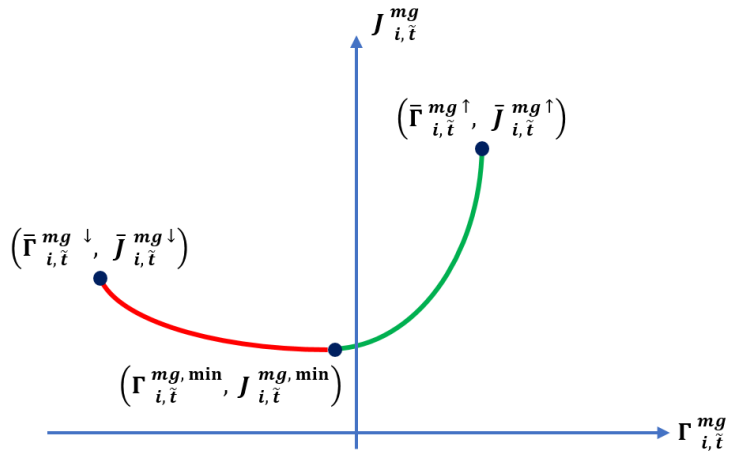

Figure 3.4: Approximated flexibility function.

However, as it will shown in Paragraph 3.2.5, satisfactory performances are obtained also using the described rough approximation.

3.2.4 Dispatching balancing power requests using flexibility functions

The AGS is supposed to receive the flexibility functions from all the MGs, together with the maximum and minimum power variations that each MG can provide. Using this information, it can offer on the balancing market the total upward and downward power flexibility of the MG-AG as *non-precontracted* reserve bids, which can be accepted or not by the TSO based on the actual grid needs. As mentioned, these market processes are out of the scope of this work. It is instead assumed that, at the generic time instant $\widetilde{t}$, the TSO can send a balancing power variation $\Gamma^{\text{TSO}}_{\widetilde{t}}$ with respect to the total pre-scheduled baseline to the AGS, that must be delivered by the whole MG-AG. At this stage, instead of relying on centralized or distributed approaches, the AGS can use the approximated MGs flexibility functions to dispatch the TSO power request, as follows

$$\min_{\substack{\Gamma^{mg}_{\forall i,\widetilde{t}}}} \{ \sum_{\forall i \in \mathcal{N}_{\mathcal{M}}} \tilde{f}^{\Gamma}_{i,\widetilde{t}}(\Gamma^{mg}_{i,\widetilde{t}}) \} \tag{3.25a}$$

s.t.

$$\bar{\Gamma}^{mg\downarrow}_{i,\widetilde{t}} \leq \Gamma^{mg}_{i,\widetilde{t}} \leq \bar{\Gamma}^{mg\uparrow}_{i,\widetilde{t}}, \tag{3.25b}$$

$$\sum_{\forall i \in \mathcal{N}_{\mathcal{M}}} \Gamma^{mg}_{i,\widetilde{t}} = \Gamma^{\text{TSO}}_{\widetilde{t}} \,. \tag{3.25c}$$

The optimization problem (3.25) aims to find the optimal power variations for each MG, denoted as $\Gamma^{mg,*}_{i,\widetilde{t}}$, such that the total request from the TSO is satisfied, see (3.25c), compatibly with the availability that each MG has previously communicated, see (3.25b). It is evident that, through the approximated MGs information, the AGS is able to efficiently dispatch the balancing power solving (3.25), which is a static and convex optimization problem with M optimization variables.
Once the optimal power variations $\Gamma^{mg,*}_{i,\widetilde{t}}$ are computed through (3.25), each MG_i must reschedule its internal operation to satisfy the request.

This is performed through the following optimization problem

$$\min_{\substack{\mathbf{x}^{\mathbf{P}}_{i,\widetilde{t}},\mathbf{y}^{\mathbf{P}}_{i,\widetilde{t}},\\ \Gamma^{mg}_{i,\widetilde{t}},\,\epsilon_i}} \; \{\; J^{mg}_{i,\widetilde{t}} \;+\; \sigma_i\,\epsilon_i^2 \;\} \tag{3.26a}$$

s.t.

(3.20b)-(3.20g)

$$\Gamma^{mg}_{i,\widetilde{t}} = \Gamma^{mg,*}_{i,\widetilde{t}} + \epsilon_i \;. \tag{3.26b}$$

As evident, (3.26b) is defined as a soft constraint through the use of the slack variable ϵ_i, which is significantly weighted in the cost function choosing a high value for σ_i. This is because, since MGs optimization problems are mixed-integer, it cannot be *a-priori* certified that each MG_i is able to perfectly provide each value of the power variation $\Gamma^{mg,*}_{i,\widetilde{t}}$ in the pre-defined range $[\bar{\Gamma}^{mg\downarrow}_{i,\widetilde{t}},\ \bar{\Gamma}^{mg\uparrow}_{i,\widetilde{t}}]$. Through the actual formulation of (3.26b), even though $\Gamma^{mg,*}_{i,\widetilde{t}}$ is not feasible to some MG_i, the closest power variation to the set-point will be computed.

Remark 3.1. *If, the solution (3.26) includes a $\epsilon_i \neq 0$, different heuristic approaches can be proposed to find a feasible solution. For instance, the AGS can measure the violation ϵ_i and commit it to other MGs based on the available total power reserves $r_p^{mg\uparrow}$ and $r_p^{mg\downarrow}$ which are given by mGENs and BESSs. Generation units are in fact modelled as continuous variables and therefore they can exactly track requested power references compatibly with their capabilities.*

3.2.5 Numerical results

The approach is tested on the same simulation benchmark presented in Section 2.5 with $M = 4$ MGs. The units characteristics are re-presented in Table 3.2, including also controllable loads (CL) which are supposed to be operated with $n_i^{cl} = 5$ consumption levels, $\forall i \in \mathcal{N}_{\mathcal{M}}$.
The pre-scheduled profiles of each unit have been defined using the methods described in Chapter 2. It is here reminded that the MG-AG opera-

Table 3.2: MGs dispatchable units

Owner	Unit	$(\underline{p},\ \bar{p})$	$(\tau_0^{cl}, \tau_f^{cl})$	$(C^b, \bar{E}^b)$	Costs
MG_1	mGEN 1	$(75, 500)$	–	–	$(0.05,\ 2,\ 30)e^{-3}$
MG_1	mGEN 2	$(50, 700)$	–	–	$(0.02,\ 4,\ 25)e^{-3}$
MG_1	BESS 1	± 80	–	$(150, 20e^3)$	$(6e^{-5}, 8.8e^{-2}, 1e^5)$
MG_1	BESS 2	± 125	–	$(225, 20e^3)$	$(9e^{-5}, 8e^{-2}, 1e^5)$
MG_1	CL	$(0, 500)$	$(1, 24)$	–	0.05
MG_2	mGEN 1	$(25, 375)$	–	–	$(0.04, 3, 35)e^{-3}$
MG_2	mGEN 2	$(75, 450)$	–	–	$(0.03, 3, 25)e^{-3}$
MG_2	BESS 1	± 150	–	$(300, 20e^3)$	$(7e^{-5}, 9.6e^{-2}, 1e^5)$
MG_2	BESS 2	± 125	–	$(225, 20e^3)$	$(8e^{-5}, 7.2e^{-2}, 1e^5)$
MG_2	CL	$(0, 225)$	$(76, 96)$	–	0.05
MG_3	mGEN 1	$(50, 500)$	–	–	$(0.05, 1, 27.5)e^{-3}$
MG_3	mGEN 2	$(75, 400)$	–	–	$(0.03, 1, 25)e^{-3}$
MG_3	BESS 1	± 80	–	$(175, 20e^3)$	$(8e^{-5}, 7.2e^{-2}, 1e^5)$
MG_3	BESS 2	± 125	–	$(225, 20e^3)$	$(5e^{-5}, 8e^{-2}, 1e^5)$
MG_3	CL	$(0, 250)$	$(12, 40)$	–	0.05
MG_4	mGEN 1	$(25, 400)$	–	–	$(0.04, 4, 30)e^{-3}$
MG_4	mGEN 2	$(100, 725)$	–	–	$(0.03, 2, 25)e^{-3}$
MG_4	BESS 1	± 75	–	$(175, 20e^3)$	$(4e^{-5}, 8e^{-2}, 1e^5)$
MG_4	BESS 2	± 125	–	$(225, 20e^3)$	$(4e^{-5}, 9.6e^{-2}, 1e^5)$
MG_4	CL	$(0, 150)$	$(65, 96)$	–	0.05

tions have been scheduled guaranteeing 1 MW of upward and downward reserves at each time instants. These must also be respected during the online operations since they are submitted as pre-contracted reserves. In the following numerical results, it is supposed that the TSO sends two power balancing requests to the MG-AG throughout the day. The first is issued at 04:00 and it consists in a power increase of $\Gamma^{\text{TSO}}_{4h/\tau} = 3.8$ MW with respect to the baseline, that must be maintained for one hour, i.e. $T_R = \frac{1h}{\tau} = 4$. The second is sent at 16:00 and it consists in a power decrease of $\Gamma^{\text{TSO}}_{16h/\tau} = -1.5$ MW, required to be provided for one hour.

To assess the performances of the proposed approach, also the centralized optimization problem (3.19) is solved. As shown in Figure 3.5(a), the proposed hierarchical approach perfectly tracks the TSO required power variations with respect to the pre-scheduled baseline, as it is for the centralized case. The single contributions of the MGs are reported in Figures 3.5(c)-(f), where it can be noted that the optimal power variations computed by the hierarchical and the centralized approach slightly differ. Moreover, it is evident that lead and rebound effects are avoided, as the MG output power is varied with respect to pre-scheduled baseline only during the TSO request periods. In Figure 3.5(b) the total upward reserve of the MG-AG, computed using the hierarchical approach, is shown for the whole day and it is apparent that the pre-contracted quantity of power reserve is always available despite the TSO requests.

Figures 3.6 report the scheduling of some units of MG3 and MG4. Considering the first TSO power request, both MGs increase the production of their mGENs and discharge the stored energy in BESSs systems. Moreover, MG3 reduces the consumption of its controllable load at 4:00, shifting it ahead in time. Considering the second request, both MGs reduce the power production of their mGENs, while BESSs are not operated since they already reached their maximum charge limit. Moreover, MG4 anticipates the activation of its controllable load, so as to further decrease its output power profile. As notable, controllable loads are operated at specific consumption levels according to their mixed-integer modelling.

The flexibility functions communicated by MG3 and MG4 for both requests are shown in Figure 3.7. The proposed procedure, although simple, satisfactory describes the real dependence between the MG offered power flexibility and its cost. However, the quality of the approximation significantly depends on which variables MGs manipulate to provide the power variation. For instance, power flexibilities offered by MG3 for the first power request and by MG4 for the second rely on the mixed-integer modulation of controllable loads, see Figures 3.6(e) and (f), implying that real MGs costs vary with a non-smooth behaviour, as reported in Figures 3.7 (a) and (d).
Considering the optimality gap between the solution computed by the centralized and the hierarchical approach the following index is introduced

$$\Delta J_{\%} = \frac{\tilde{J}_H - J^*}{J^*} \cdot 100.$$

where J^* is the optimal value of the cost function (3.19a) computed using the centralized approach, while $\tilde{J}_H$ is the value computed using the solution found by the proposed hierarchical approach.
Concerning the first TSO request, both approaches achieve the same optimal solution, therefore $\Delta J_{\%} = 0\%$. Concerning the second TSO request, the solutions slightly differ, e.g. see Figure 3.6(f), however the optimality gap is $\Delta J_{\%} = 0.006\%$.
The benchmark has been simulated using a laptop equipped with an Intel Core i7-6500U process and 8 GB of RAM. The centralized approach executed the first request in 2.99 sec and the second in 1.13 sec. The hierarchical approach performed the effective dispatch of the first request in 0.5 sec and the second in 0.38 sec. The evaluation of the flexibility functions, performed in advance with respect to the TSO request, has been executed in 1.75 sec for the first request and in 1.3 sec for the second.
An advantage of the proposed hierarchical approach is that it performs all the operations in parallel, apart from the AGS dispatch, see (3.25), which is a simple static and convex problem. Moreover, the centralized approach is not scalable, therefore if the MGs number increases also the computational time will raise, considering also that a mixed-integer optimization problem must be solved.

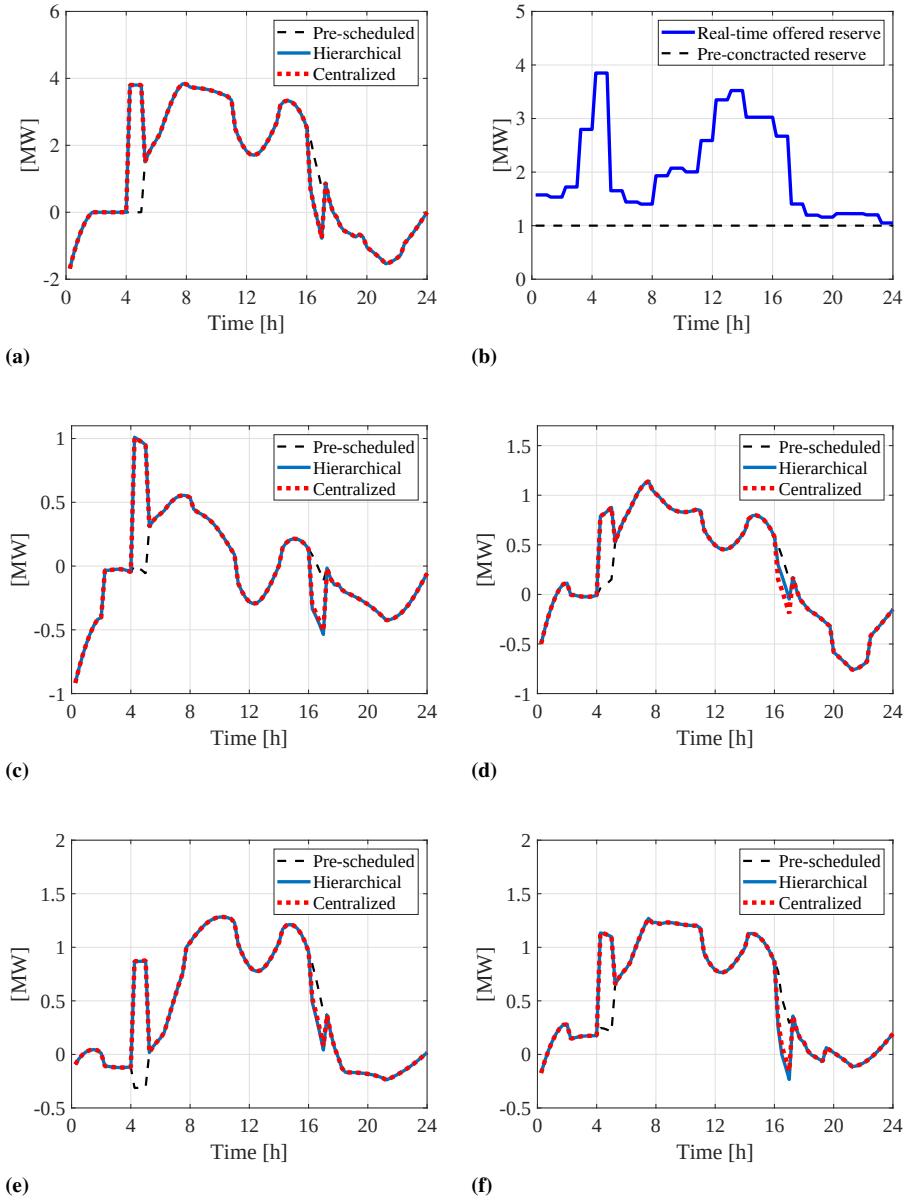

Figure 3.5: (a) MG-AG output power profile; (b) MG-AG upward power reserve; (c) MG1 output power profile; (d) MG2 output power profile; (e) MG3 output power profile; (f) MG4 output power profile.

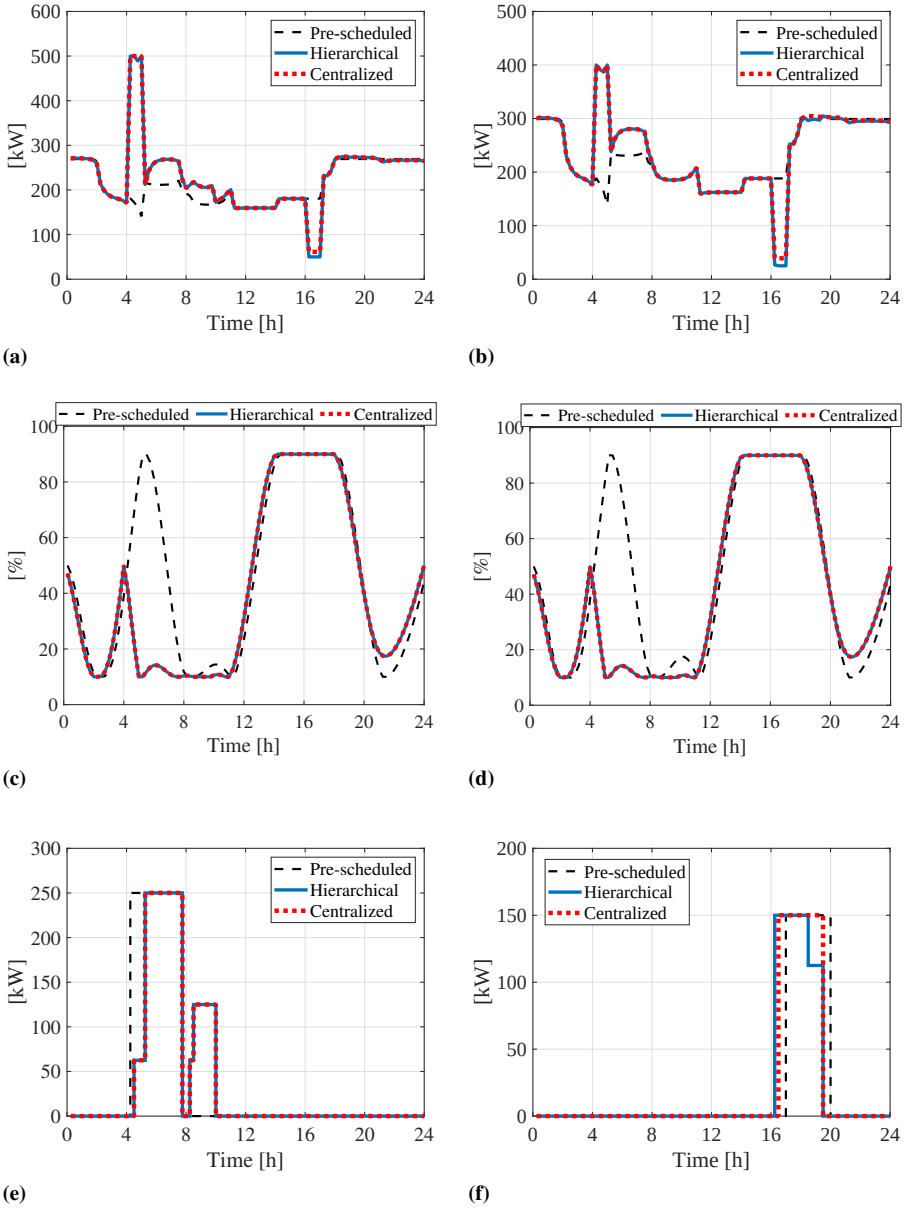

Figure 3.6: MG3: (a) mGEN 1 generated power, (c) BESS 1 state of charge, (e) CL absorbed power. MG4: (b) mGEN 1 generated power, (d) BESS 1 state of charge, (f) CL absorbed power.

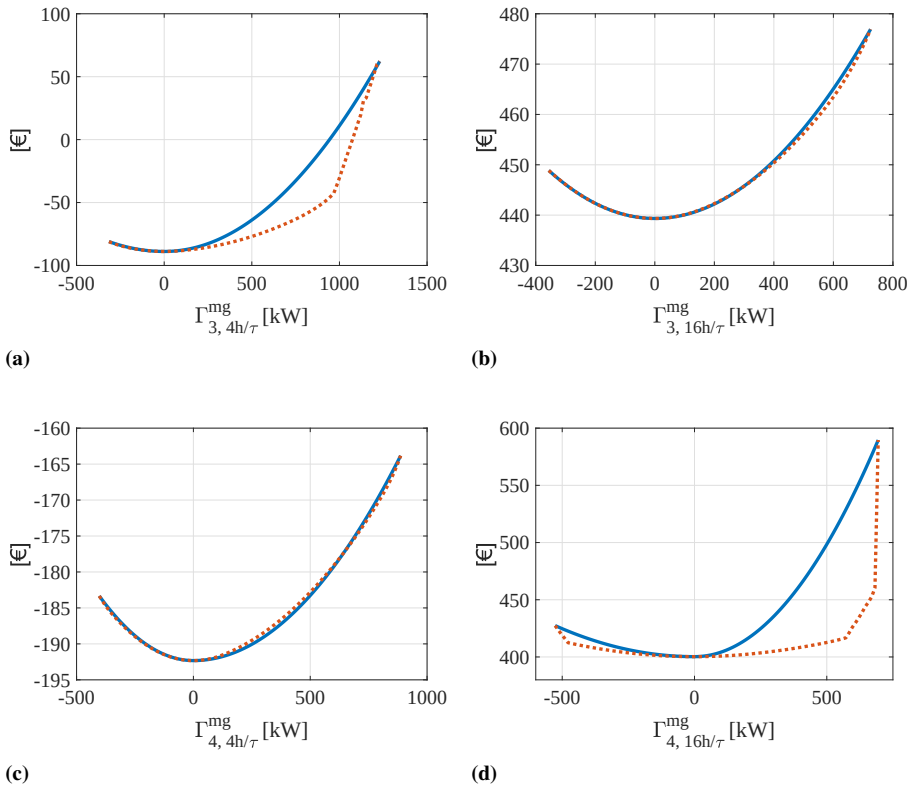

Figure 3.7: Real (dashed line) and approximated (solid line) flexibility functions for MG3, (a) first power request and (b) second power request, and for MG4, (c) first power request and (d) second power request.

3.3 Distributed optimization approach using MILPs

In this Section, the distributed dispatch of the TSO power requests is addressed. As discussed in the Section 3.1, using standard distributed optimization techniques for mixed-integer optimization problems may lead to feasibility and convergence issues. A novel distributed algorithm for mixed-integer linear problems (MILPs) with guaranteed feasibility and convergence properties is presented in [66], which however is too conservative in some cases, determining solution too far from the optimal one. Because of this, here a variant of this algorithm is proposed, and applied to real-time dispatch of TSO power requests.
The advantage is that through this approach MGs can protect the knowledge of all their characteristics, avoiding also to communicate approximated internal information as in the previous Section.
Nevertheless, the distributed approach works just for mixed-integer linear systems, while the MGs optimization problems presented so far have quadratic terms. Therefore, a linear formulation of the MG-AG balancing service provision problem is firstly presented.

3.3.1 Mixed-integer linear problem formulation

For the sake of simplicity, it is here assumed that each MG is equipped with one dispatchable mGEN, one BESS and one controllable load. Moreover, the management of power reserves is not addressed here, and MGs are just requested to maintain the pre-scheduled power baseline after the power variation request period. These assumptions do not compromise the validity of the proposed approach and they can be easily removed, including the proper constraints.
With respect to the solution described in Section 3.2, an additional degree of freedom is considered in this paragraph, as mGENs are supposed to be switched on or off, if necessary. Let's the binary variable $\delta_i^G \in \{0,1\}$ denote the status of the mGEN of MG$_i$ (1 being the on and 0 the off status), then, it follows that

$$\delta_i^g(t)\,\underline{p}_i^g \;\leq p_i^g(t) \leq \bar{p}_i^g \delta_i^g(t)\,. \tag{3.27}$$

The BESS and controllable loads are modelled as in the previous Section, therefore the same corresponding constraints are here represented

$$\underline{p}_i^{\,b} \leq p_i^b(t) \leq \bar{p}_i^{\,b}\,, \tag{3.28a}$$

$$s_i^b(t+1) = s_i^b(t) - 100\,\frac{\tau}{C_i^b}\,p_i^b(t)\,, \tag{3.28b}$$

$$\underline{s}_i^{\,b} \leq s_i^b(t) \leq \bar{s}_i^{\,b}\,, \tag{3.28c}$$

$$p_i^{cl}(t) = \frac{\delta_i^{cl}(t)}{n_i^{cl}}\,\bar{p}_i^{\,l} \qquad t \in \{\underline{\tau}_i^{cl}, \bar{\tau}_i^{cl}\}\,, \tag{3.29a}$$

$$p_i^{cl}(t) = \hat{p}_i^{cl}(t), \qquad t \notin \{\underline{\tau}_i^{cl}, \bar{\tau}_i^{cl}\}\,, \tag{3.29b}$$

$$\sum_{t=\widetilde{t}}^{N} \tau\, p_i^{cl}(t) = \sum_{t=\widetilde{t}}^{N} \tau\, \hat{p}_i^{cl}(t)\,. \tag{3.29c}$$

The total output power of MG_i can be expressed as

$$p_i^{mg}(t) = p_i^g(t) + p_i^b(t) - p_i^{cl}(t)\,. \tag{3.30}$$

The MG cost function is also reformulated, transforming the quadratic terms in linear to be compatible with the proposed distributed MILP algorithm. This is defined as follows

$$\begin{aligned} J_{i,\widetilde{t}}^{mg} = \sum_{t=\widetilde{t}}^{N} \Big\{ & c_i^g\, p_i^g(t) + c_i^b\, |p_i^b(t) - p_i^b(t-1)| + \\ & + c_i^{cl}\, |p_i^{cl}(t) - \hat{p}_i^{cl}(t)| - \lambda^p(t)\, p_i^{mg}(t) \Big\}\,, \end{aligned} \tag{3.31}$$

where $c_i^g > 0$ is the production cost of the mGEN, $c_i^b > 0$ is a cost associated to the ageing of the BESS, $c_i^{cl} > 0$ is a cost that penalizes changes in a programmable load consumption profile with respect to its original schedule and λ^p is the energy price.
The cost function (3.31) is not linear since it contains absolute values, however, it can be rewritten in a linear form by adopting an epigraphic

reformulation. To this end, the auxiliary variables h_i^b and h_i^{cl} and the following additional local constraints are introduced

$$\begin{aligned} &p_i^b(t) - p_i^b(t-1) \leq h_i^b(t)\,, \\ &p_i^b(t-1) - p_i^b(t) \leq h_i^b(t)\,, \\ &p_i^{cl}(t) - \hat{p}_i^{cl}(t) \leq h_i^{cl}(t)\,, \\ &\hat{p}_i^{cl}(t) - p_i^{cl}(t) \leq h_i^{cl}(t)\,. \end{aligned} \tag{3.32}$$

Therefore, the linear formulation of the cost function (3.31) follows

$$J_{i,\widetilde{t}}^{mg} \;=\; \sum_{t=\widetilde{t}}^{N} \left\{ c_i^g\, p_i^g(t) \;+\; c_i^b\, h_i^b(t) \;+\; c_i^{cl}\, h_i^{cl}(t) \;-\; \mu^p(t)\, p_i^{mg}(t) \right\}. \tag{3.33}$$

It is considered that the TSO at the generic time $\widetilde{t}$ can send to the AGS a power variation profile $\Gamma_{\widetilde{t}}^{\text{TSO}}(t)$ for $t \in \{\widetilde{t}, \ldots, \widetilde{t} + T_R - 1\}$ with respect to the pre-scheduled baseline.
The AGS has to reschedule each MG operations by suitably choosing the values of $p_i^g(t), \delta_i^g(t),\ p_i^b(t),\ p_i^{cl}(t)$ and $\delta_i^{cl}(t)$, $t \in \{\tilde{t}, \ldots, N\}$ and $i \in \{1, \ldots, M\}$, such that each MG$_i$ optimally varies its power baseline by a quantity $\Gamma_{i,\tilde{t}}^{mg}(t)$. Moreover, rebound effects must be avoided, meaning that each MG must maintain its original power profile after satisfying the TSO request. The following constraints are therefore introduced concerning the single MG$_i$

$$p_i^{mg}(t) = \hat{p}_i^{mg}(t) \;+\; \Gamma_{i,\tilde{t}}^{mg}(t)\,, \qquad t \in \{\tilde{t}, \ldots, \tilde{t} + T_R - 1\}\,, \tag{3.34}$$

$$p_i^{mg}(t) = \hat{p}_i^{mg}(t)\,, \qquad t \in \{\tilde{t} + T_R, \ldots, N\}\,. \tag{3.35}$$

The satisfaction of the TSO request is instead expressed as follows

$$\begin{aligned} &(1-\epsilon)\,\Gamma_{\tilde{t}}^{\text{TSO}}(t) \;\leq\; \sum_{i \in \mathcal{N}_{\mathcal{M}}} \Gamma_{i,\tilde{t}}^{mg}(t) \;\leq\; (1+\epsilon)\,\Gamma_{\tilde{t}}^{\text{TSO}}(t)\,, \\ &t \in \{\tilde{t}, \ldots, \tilde{t} + T_R - 1\}\,, \end{aligned} \tag{3.36}$$

where $\epsilon > 0$ is introduced as a tolerance parameter, selected at a sufficient small value.

For notational compactness, MGs optimization variables are condensed in the following vector $x_i^p(t) = [p_i^g(t), \delta_i^g(t), p_i^b(t), p_i^{cl}(t), \delta_i^{cl}(t)]'$.

At this stage, the overall centralized AGS dispatch problem, formulated as MILP, follows

$$\begin{aligned} &\min_{\substack{\mathbf{x}_{i,\widetilde{t}}^{\mathbf{P}},\, \Gamma_{i,\widetilde{t}}^{mg} \\ \forall i \in \mathcal{N}_{\mathcal{M}}}} \Big\{ \sum_{\forall i \in \mathcal{N}_{\mathcal{M}}} J_{i,\widetilde{t}}^{mg} \Big\} \\ &\text{s.t.} \\ &\quad (3.27)\text{-}(3.30)\,, (3.32)\,, \quad \forall i \in \mathcal{N}_{\mathcal{M}}\,, \quad \forall t \in \{\widetilde{t}, \dots, N\}\,, \\ &\quad (3.34)\text{-}(3.35)\,, \qquad\qquad \forall i \in \mathcal{N}_{\mathcal{M}}\,, \\ &\quad (3.36)\,. \end{aligned} \tag{3.37}$$

which involves both continuous (p_i^g, p_i^b, p_i^{cl} and $\Gamma_{i,\widetilde{t}}^{mg}$) and discrete ($\delta_i^g$ and δ_i^{cl}) decision variables for each MG. Note that the cost function of (3.37) is additive over the MGs, so that if constraint (3.36) is removed, then problem (3.37) becomes separable and, hence, easier to solve. Therefore, constraint (3.36) is referred as the *coupling* constraint since it couples the MGs decisions, whereas the other constraints are referred to as *local* constraints.
For the sake of clarity, the optimization problem (3.37) is expressed in a more standard form, collecting the decision variables of each MG_i in the variable x_i. Therefore, (3.37) can be compactly rewritten as

$$\begin{aligned} \min_{x_1,\dots,x_M} \quad & \sum_{i=1}^{M} {c_i}'\, x_i \\ \text{subject to:} \quad & \sum_{i=1}^{M} A_i x_i \leq b \\ & x_i \in X_i, \quad i \in \mathcal{N}_{\mathcal{M}}\,, \end{aligned} \tag{3.38}$$

where X_i is the mixed-integer polyhedral set defined by constraints (3.27)-(3.30) and (3.32) together with relations (3.34)-(3.35), while $\sum_{i=1}^{M} A_i x_i \leq b$ represents the coupling constraint (3.36).

3.3.2 Distributed dispatch of balancing power requests

The optimization problem in (3.38) fits the framework proposed in [66], which provides a scalable distributed strategy for its approximate resolution. The iterative algorithm proposed in [66] exploits the dual decomposition method to obtain a scalable and privacy preserving solution, see [68]. In particular, agents, i.e. MGs, have to solve in parallel a lower dimensional MILP involving their local decision variables, cost, and constraints, while a central entity, i.e. the AGS, is in charge of enforcing the coupling constraint by updating the dual variable based on the tentative solutions of the agents. A constraint tightening technique is here integrated within dual decomposition in order to ensure that a feasible solution to (3.38) is found after a finite number of iterations.
Duality theory, see e.g. [68], plays a central role in the distributed resolution of multi-agent optimization problems in the form of (3.38) as it allows to decompose the problem across the agents by softening the coupling constraint and incorporating it as an additive term in the cost function. More precisely, let $\mu \geq 0$ be a vector of Lagrange multipliers (named as dual variable) and

$$L(x_{\forall i}, \mu) = \sum_{i=1}^{M} {c_i}' x_i + \mu' \left(\sum_{i=1}^{M} A_i x_i - b \right) \tag{3.39}$$

the Lagrangian function obtained augmenting the cost function of (3.38) with a term that penalizes the amount of violation of the coupling constraint weighted by μ. The dual problem of (3.38) is then given by

$$\max_{\mu \geq 0} \; -\mu' b + \sum_{i=1}^{M} \underbrace{\min_{x_i \in X_i} ({c_i}' + \mu' A_i) x_i}_{\varphi_i(\mu)} . \tag{3.40}$$

It is worth noticing that despite (3.38) is a non-convex program, given the presence of discrete variables, problem (3.40) is convex as each $\varphi_i(\mu)$ is a concave function since it is the minimum of affine functions of μ, see also [68, Proposition 5.1.2].

A distributed approach to solve (3.40) is the well-known dual subgradient algorithm, see [68, Section 6.3]. Using the index k to denote the iteration number, the algorithm iterates between the following two steps:

$$x_i^{k+1} \in \underset{x_i \in X_i}{\operatorname{argmin}} \left(c_i{}' + \mu^k A_i\right) x_i, \tag{3.41a}$$

$$\mu^{k+1} = \left[\mu^k + \alpha^k \left(\sum_{i=1}^{M} A_i x_i^{k+1} - b\right)\right]_+, \tag{3.41b}$$

where α^k is a step-size parameter satisfying $\sum_{k=0}^{\infty} \alpha^k = \infty$ and $\sum_{k=0}^{\infty} \left(\alpha^k\right)^2 < \infty$, and $[\,\cdot\,]_+$ denotes the projection of its argument onto the non-negative orthant. Update (3.41a) can be performed in parallel by the agents, while step (3.41b) has to be performed by a central entity, in our setting the MGs and the AGS, respectively.

It is worth noticing that each MG_i needs to communicate to the AGS only its contribution $A_i\, x_i^{k+1}$ to the coupling constraint (i.e., its optimal power variation $\Gamma_{i,\tilde{t}}^{mg}$, see (3.36)) and is not required to disclose any private information regarding operating costs (coded in c_i) nor device characteristics and limitations (coded in X_i).

Typical choices for α^k are given by

$$\alpha^k = \frac{\alpha_1}{(k+1)^{\alpha_2}}, \tag{3.42}$$

with $\alpha_1 > 0$ and $\alpha_2 \in (0.5, 1]$.

Unfortunately, applying (3.41) does not provide a way to recover the optimal solution x_i^* of (3.38), $\forall i \in \mathcal{N}_{\mathcal{M}}$. While [69] provides a recovery procedure in the convex case, in the non-convex case it may return a solution which is not feasible for (3.38).

The approach in [66] overcomes this issue by replacing the b vector in (3.41b) with the term $b - \rho^k$, where $\rho^k > 0$ is a properly defined tightening vector with the same dimension of b. The role of ρ^k is to progressively reduce some components of b to enforce the algorithm to obtain a feasible solution for all the components of the coupling constraint. The term ρ^k is progressively updated based on the tentative solutions x_i^k explored by (3.41) across iterations.

The approach in [66] is guaranteed to return a feasible solution after a finite number of iterations provided that ρ does not grow too much as the algorithm progresses, see [66] for a detailed discussion. This issue is particularly critical for our problem (3.37) since constraint (3.36) poses a limit on the amount of growth of the tightening ρ, as better explained hereafter.
The tightened version of the coupling constraint, for a generic ρ vector, is given by

$$(1-\epsilon)\,\Gamma_{\tilde{t}}^{\text{TSO}}(t)+\rho_t^{lb}(t)\leq\sum_{i\in\mathcal{N}_{\mathcal{M}}}\Gamma_{i,\tilde{t}}^{mg}(t)\leq(1+\epsilon)\,\Gamma_{\tilde{t}}^{\text{TSO}}(t)-\rho_t^{ub}(t) \tag{3.43}$$

where $\rho_t^{ub}(t)$ and $\rho_t^{lb}(t)$ are the components of ρ associated with the right and left constraints in (3.36) respectively, for a given $t\in\{\widetilde{t},\ldots,\widetilde{t}+T_R-1\}$. From (3.43) it is clear that an excessive tightening would quickly lead to infeasibility since

$$\rho_t^{ub}(t)+\rho_t^{lb}(t)\leq 2\,\epsilon\,\Gamma_{\tilde{t}}^{\text{TSO}}(t), \tag{3.44}$$

$t\in\{\widetilde{t},\ldots,\widetilde{t}+T_R-1\}$, must hold.
Because of this, here Algorithm 2 reported in the following is devised, which is inspired by [66], but it updates the tightening vector ρ more cautiously, based on a nested loop strategy. The inner loop, indexed by k_i, runs (3.41) until convergence keeping ρ fixed (see Steps 6-13 noticing that Steps 10 and 11 are equivalent to (3.41b) with $b-\rho^{k_o}$ in place of b), while the outer loop, indexed by k_o, is responsible for updating the tightening vector ρ. The same privacy-related considerations for (3.41) apply to Algorithm 2. The rationale behind this is to ignore the tentative primal solutions x_i^k explored during the transient phase of μ^k and update ρ based on those tentative primal solutions that are computed when μ^k reaches a steady state for the given ρ, so as to reduce the tightening. Within the inner loop, the AGS keeps monitoring the coupling constraints by computing (see Step 10)

$$v^{k_i}=\sum_{i=1}^{M}A_jx_j^{k_i}-b, \tag{3.45}$$

Algorithm 2 Distributed MILP for AGS dispatch

1: $\mu^0 = 0$
2: $\rho^0 = 0$
3: $k_o = 0$
4: **repeat**
5: $\quad k_i = 0$
6: $\quad$ **repeat**
7: $\quad\quad$ **for** $j = 1, \ldots, M$ **do**
8: $\quad\quad\quad x_j^{k_i+1} \in \underset{x_j \in X_j}{\text{argmin}} (c_j{}' + \mu^{k_i}{}' A_j)\, x_j$
9: $\quad\quad$ **end for**
10: $\quad\quad v^{k_i+1} = \sum_{j=1}^{M} A_j x_j^{k_i+1} - b$
11: $\quad\quad \mu^{k_i+1} = \left[\mu^{k_i} + \alpha^{k_i}(v^{k_i} + \rho^{k_o})\right]_+$
12: $\quad\quad k_i \leftarrow k_i + 1$
13: $\quad$ **until** μ^{k_i} converges **or** $x_j^{k_i}$ is feasible for $j = 1, \ldots, M$
14: $\quad \bar{k}_i = \underset{k > k_i - w}{\text{argmin}} \,||\, [v^k]_+ \,||_\infty$
15: $\quad \rho^{k_o+1} = \rho^{k_o} + [v^{\bar{k}_i}]_+$
16: $\quad \mu(0) = \mu^{k_i}$
17: $\quad k_o \leftarrow k_o + 1$
18: **until** $x_j^{k_i}$ is feasible for $j = 1, \ldots, M$

whose r-th component is positive if the r-th joint constraint is violated and is negative or zero otherwise. If, for some k_i, all components of v^{k_i} are non-positive, then the algorithm terminates and returns the optimal solution $\tilde{x}_1, \ldots, \tilde{x}_M$, which is feasible. Otherwise the inner loop keeps running until μ^{k_i} converges. When the inner loop has converged, the AGS looks at the latest w values of v^k, and computes, for each $k = k_i - w + 1, \ldots, k_i$, the amount of maximum violation $||\, [v^k]_+ \,||_\infty$ (i.e., the highest among the positive components of v^k), and then selects the inner iteration index corresponding to the lowest $||\, [v^k]_+ \,||_\infty$ in Step 14. This translates into selecting the tentative primal solution among the latest w with the least maximum violation of the coupling constraints.
Finally, the update of the tightening coefficient ρ is performed by taking the integral of the violation $[v^{\bar{k}_i}]_+$ associated with the least violating ten-

tative primal solution (see Step 15). The rationale behind this consists in trying to increase the tightening vector ρ by a small amount at each outer iteration to avoid being overly conservative. In the unfortunate event that ρ^{k_o} is such that (3.44) is not satisfied for some $t \in \{\tilde{t}, \ldots, \tilde{t}+T_R-1\}$, then a feasible solution could not be found. One can then stop the algorithm and restart it with a larger value for the tolerance ϵ in (3.36) thus softening the TSO request and possibly providing an approximate yet guaranteed solution to its original request.

3.3.3 Numerical results

In order to test the potentiality of the proposed distributed strategy, a MG-AG with $M = 50$ MGs is considered.
In principle, the baseline power profiles of each MG_i should be obtained using optimization-based strategies explicitly accounting for the provided balancing service, e.g. with the methods described in Chapter 2. Here, to show the effectiveness of the proposed approach irrespectively to the profile generation mechanism, the baseline power profiles (together with devices physical limits and operating costs) are generated at random according to the procedure described in Appendix A of this Section.
It is assumed that the AGS receives two power requests from the TSO. The first, issued at 07:00, requires to increase by $\Gamma^{\text{TSO}}_{7h/\tau} = 800$ kW the amount of power produced by the MG-AG, whereas the second request, issued at 15:00, the TSO asks to reduce the power baseline by $\Gamma^{\text{TSO}}_{15h/\tau} = -700$ kW. In both cases the relative tolerance level for the satisfaction of the TSO request is $\epsilon = 0.05$ and the requested power variation must be maintained for two hours, i.e. $T_R = 8$. The Algorithm 2 is therefore run twice, using in both cases α^k given by (3.42), with $\alpha_1 = 0.15/M$ and $\alpha_2 = 0.51$, and $w = 8$.

In all the following figures the following color code is adopted: red lines represent the original power profiles (before receiving any TSO request), blue lines represent the power profiles computed so as to meet the first TSO request, and green lines represent the power profiles computed based on the second TSO request. Solid lines are used for actual profiles and dotted lines for scheduled ones that are not implemented.

Figure 3.8 shows how the power profile of the MG-AG properly varies throughout the day as the two TSO requests are received and processed by the AGS. The yellow band around the solid lines between 7:00 and 9:00 and 15:00 and 17:00 represent the allowed deviation from the TSO request based on the relative tolerance $\epsilon = 0.05$, see (3.36). As it can be seen from Figure 3.8, for both events, the algorithm is able to reschedule in a distributed fashion the usage of the MGs units so as to meet the TSO request while avoiding the rebound effect. This is achieved without any need of sharing MGs internal information and in presence of mixed-integer variables.

Close-up views of the power profile of the MG-AG in the time frames 7:00-9:00 and 15:00-17:00 related to the two requests are shown in Figures 3.9(a) and 3.9(b), respectively. Besides the yellow band representing the request satisfaction tolerance bound coded by constraint (3.36), we also report the tightened tolerance upper and lower bounds (black dashed lines) representing constraint (3.43) for the last value of ρ before the algorithm returned a feasible solution. It is interesting to note that the solution found by the algorithm is feasible for the original constraint (3.36) but not necessarily for its tightened counterpart (3.43), as clearly discussed in detail in [66].

In Figure 3.10 we also report the power profiles of one of the MGs: its output power profile in Figure 3.10(a), the profile of the mGEN in Figure 3.10(b), the charging/discharging profile of the BESS in Figure 3.10(c), and the modulation of the load in Figure 3.10(d). From Figures 3.10(b)-(d) it is evident how the MGs changes the schedule of its internal units to accommodate part of the TSO request while avoiding any rebound effect (the green solid line in Figure 3.10(a) matches the reference profile represented by the red dotted line). Specifically, to satisfy the power request between 7:00 and 9:00, the mGEN and the BESS output power are increased, while the controllable load is switched off. During the second TSO request, the mGEN is switched off, the BESS is operated in charging mode, while the load is kept at its pre-scheduled operating point.

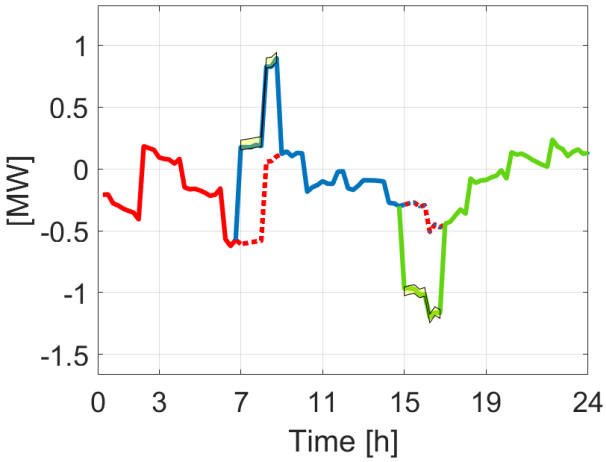

Figure 3.8: MG-AG output power profile. Original baseline (red), profile based on the first request (blue), profile based on the second request (green): pre-scheduled (dotted lines) and effective (solid lines) profiles, and tolerance bounds (yellow band).

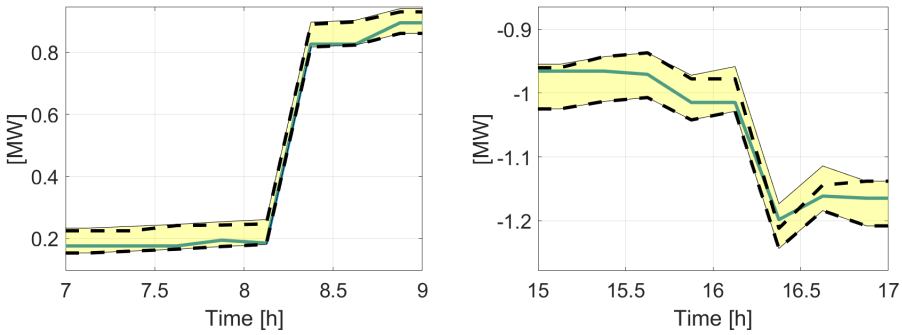

(a) **(b)**

Figure 3.9: Close-up of the power profile of the consumer pool (blue solid line) in the time frames 7:00-9:00 (a) and 15:00-17:00 (b), together with the tolerance bounds (yellow band) and tightened tolerance bounds (black dashed lines).

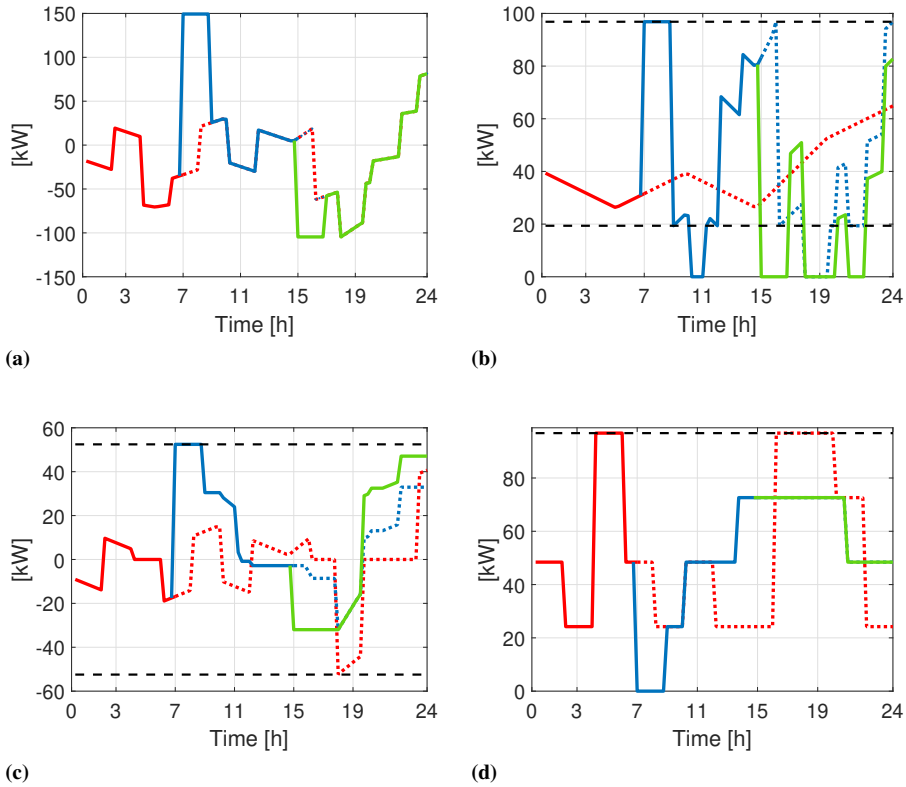

Figure 3.10: Power profiles of MG_{10}: total (a), mGEN (b), BESS (c), controllable load (d). Original reference profile (red), profile based on the first TSO request (blue), profile based on the second TSO request (green): scheduled (dotted lines) and actual (solid lines) profiles, capability limits (dashed lines).

In order to quantify the quality of the feasible solution $\tilde{x}_1, \ldots, \tilde{x}_M$ returned by Algorithm 2, let's denote the value $\tilde{J}$ of the total MG-AG cost function defined in (3.37) obtained for the solution $\tilde{x}_1, \ldots, \tilde{x}_M$ and the optimal value of the total cost function J^* of (3.37), supposed to be solved through a centralized approach.

These two optimal values of the total cost function can be compared computing the following relative optimality gap

$$\Delta J_{\%} = \frac{\tilde{J} - J^*}{J^*} \cdot 100.$$

In case of a large number of MGs in the MG-AG, however, it can happen that problem (3.37) cannot be centrally solved with standard computational resources, mainly due to the combinatorial complexity of the problem. In the considered case study, for example, a laptop equipped with an Intel Core i7-6500U processor and 8 GB of RAM has been used, encountering out-of-memory issues when trying to compute J^* solving (3.37) . In fact, the overall problem (3.37) involves M boolean variables $\delta_i^g(t)$ and M integer variables $\delta_i^{cl}(t)$, taking $n_i^{cl} + 1$ discrete values, for $t \in \{\tilde{t}, \dots, N\}$, thus amounting to a total of $2^{(N-\tilde{t})M} \cdot \prod_{i=1}^{M} (n_i^{cl} + 1)^{(N-\tilde{t})}$ possible combinations to be explored in a centralized solution. On the other hand, the proposed distributed approach allows to decompose the overall problem and solve (in parallel!) M sub-problems with only $2^{(N-\tilde{t})} \cdot (n_i^{cl} + 1)^{(N-\tilde{t})}$ possible combinations each. This translates to 10^{3400} possible combinations for the centralized problem, and only 10^{68} for each MG, for the first request; and 10^{1800} and 10^{36} for the second request.

Nevertheless, even though J^* cannot be directly computed, an estimate can be evaluated by resorting on the dual problem, expressed in (3.40). In fact, by weak duality, it is known that the optimal value J_D^* of the dual problem (3.40) constitutes a lower bound for J^* (see [68, Proposition 5.1.3]). Therefore, since the solution $\tilde{x}_1, \dots, \tilde{x}_M$ computed by Algorithm 2 is feasible for the centralized problem (3.37), it follows that

$$J_D^* \leq J^* \leq \tilde{J},$$

and the relative optimality gap can therefore be estimated as follows

$$\Delta J_{\%} = \frac{\tilde{J} - J_D^*}{J_D^*} \cdot 100.$$

where the value of J_D^* can be easily computed iterating (3.41) until convergence.

TSO request	Estimated $\Delta J_{\%}$	Outer iterations	Inner iterations	Execution time [sec]
1-st	0.17%	4	125	38.7
2-nd	0.79%	3	98	3.8

Table 3.3: Assessment of the performance of Algorithm 2 when applied to satisfy the two TSO requests with $M = 50$.

In Table 3.3, the estimated relative optimality gap $\Delta J_{\%}$ for the two TSO requests is reported, along with the number of outer iterations performed, which also corresponds to the number of times the value of ρ has been updated, the total number of inner iterations, which corresponds to the number of times each agent has performed Step 8, and the time elapsed before Algorithm 2 returned a feasible solution divided by the number M of MGs. The latter being a good indicator of how long the algorithm will take in practice as the time elapsed performing Steps 10-15 is negligible with respect to the time needed by each MG to perform (in parallel) Step 8.

Remarkably, for the two cases reported in Table 3.3, the relative optimality gap is lower than 1%, showing the effectiveness of the approach in returning a feasible solution with close-to-optimality performance. Note also how the first request exhibits a much higher execution time with respect to the second one. This is due to the longer time horizon the prosumer have to consider for the rescheduling phase after the first TSO request, with respect to the second one.
It is worth noticing that, in both cases, the number of outer iterations is greater than one (i.e. the final ρ is different from zero). This witnesses that the standard dual subgradient method, executed in the first outer iteration of Algorithm 1 (i.e. Steps 6-13 with $\rho^0 = 0$), is not able to find a feasible solution.
For comparison purposes, we also used the original algorithm in [66], but it resulted in constraint (3.36) becoming infeasible after the first few iterations.

M	Estimated $\Delta J_{\%}$	Outer iterations	Inner iterations	Execution time [sec]
30	0.49%	3	120	8.7
40	0.82%	2	125	5.0
50	0.55%	1	65	2.5
60	0.36%	11	219	9.4
70	0.39%	2	191	5.9
80	0.33%	3	164	8.4

Table 3.4: Assessment of the performance of Algorithm 2 as a function of the number M of MGs in the MG-AG.

Finally, the proposed distributed strategy has been tested for a growing number M of MGs in the MG-AG, to assess its scalability properties. A TSO request of $\Gamma_{\tilde{t}}^{\text{TSO}} = 18M$ kW between 15:00 and 17:00 has been assumed for each test case, with all the other parameters set as previously discussed. Note that in this case problem (3.37) involves $252M$ variables: $180M$ continuous, $36M$ boolean, and $36M$ integer assuming 5 possible values. The total number of possible combinations is thus 10^{36M}, which will eventually lead to an intractable problem as M grows, if addressed centrally.
The performance of Algorithm 2 is evaluated based on the same indicators of Table 3.3 for different values of M and the results are reported in Table 3.4. As it appears from the table, for each M, the proposed approach is able to find a feasible solution with close-to-optimal performance ($\Delta J_{\%} < 1\%$) in a handful of iterations and in less than 10 seconds.

Appendix A: Generation of the simulation set-up for distributed MILP strategy

Consider the generic MG$_i$. As for the controllable load, $\bar{p}_i^{cl}$ is extracted at random according to the uniform distribution over the interval $[10, 100]$ kW and the reference profile $\hat{p}_i^{cl}$ is set equal to a piecewise constant function with intervals of 2-hour duration each and amount of power per interval computed according to (3.3a) with δ_i^{cl} extracted uniformly at random in $\{1, \ldots, n_i^{cl}\}$ with $n_i^{cl} = 4$.

The load flexibility limits are set to the entire optimization horizon, i.e., $\underline{\tau}_i^{cl} = \tilde{t}$ and $\bar{\tau}_i^{cl} = N$. As for the mGEN, we set $\bar{p}_i^g = \bar{p}_i^{cl}$, $\underline{p}_i^g = 0.2\,\bar{p}_i^g$, and the reference profile as a piecewise linear function with hinging points every 4 hours with values given by the average power consumption of the load scaled by a factor chosen uniformly at random from the set $\{0.5, 0.75, 1, 1.25, 1.5\}$. As for the BESS capacity limits, the BESS is set to be able to provide 25% of the energy needed by the controllable load. The BESS reference power profile $\hat{p}_i^b$ is defined so as to match $\hat{p}_i^g - \hat{p}_i^{cl}$ compatibly with its constraints.
Finally, the terms c_i^{cl}, c_i^g, and c_i^b appearing in the cost function (3.37) are extracted at random according to a uniform distribution over the interval $[0, 35]$ e/kW for c_i^{cl}, and over the interval $[0, 1]$ e/kW for both c_i^g and c_i^b.

3.4 Conclusion

In this chapter, the actual provision of balancing services from MGs aggregators have been addressed. Precisely, algorithms for the satisfaction of TSO manual power requests (mFRR service) have been designed, with the objective of preserving MGs internal information and the scalability of the approach. Moreover, the MGs scheduling problem is modelled as a mixed-integer problem, allowing the step-wise modulation of loads and the switching of dispatchable mGENs. Two different approaches have been proposed. The first relies on a approximated description of the power flexibility that each MG can offer, properly associated with its cost. Having this information, the AGS can communicate to the TSO the overall availability of the MG-AG and it can efficiently dispatch the balancing power request at the minimum cost. The second approach concerns the design of a distributed algorithm for mixed-integer linear problems, allowing MGs to completely preserve their internal information. The method allows the AGS to properly dispatch the TSO requests, without the need of any information of MGs flexibility and characteristics.
Both approaches have been tested in simulation, showing their ability to find feasible solutions with null, or significantly small, optimality gaps with respect to the optimal solution found by a centralized AGS management.

CHAPTER 4

Control and clustering strategies for self-balancing in distribution networks

4.1 Introduction

The intermittent and non-deterministic nature of Renewable Energy Sources (RESs) and of new electric loads, such as charging stations of electric vehicles, causes continuous active power imbalances between generation and demand, which, if not promptly restored may lead to serious frequency deviations [3]. Chapters 2 and 3 focused on how aggregated Microgrids (MGs) can serve as Balancing Service Providers (BSP), optimally scheduling their operations to initially preserve, and then provide, active power reserves to the TSO for the overall network frequency regulation. As discussed in Chapter 1, another fundamental figure of the balancing market is the Balance Responsible Party (BRP), entitled to address power imbalances of a portfolio of grid units (e.g. DERs and loads).

This actor is needed since the declared power programs in the day-ahead and intra-day markets rely on forecasted power profiles for loads and RESs, which can significantly differ from reality becoming one of the main causes of network power variability [24].
This chapter focuses on the design of a coordination framework for Microgrids Aggregators (MG-AGs) to serve as a proper BRP. Precisely, MGs will be coordinated to share part of the reserves to compensate imbalances caused by external non-dispatchable elements.
The method is supposed to be applied to MGs interconnected to the same distribution network, with the aim of respecting the overall programmed power exchange with the main grid. The control strategy must be designed to act promptly, to avoid the propagation of power variability to the main utility, and with also enhanced scalability properties, so that its performances do not depend on the size of the considered distribution network.

4.1.1 Literature Review

The design of a low-level controller for a single MG to compensate the fluctuations of an external load is presented in [70]. In [71], a MG is controlled to balance the power variability in a distribution feeder in presence of multiple consumers. Centralized MPC methods have been adopted for the compensation of power deviations in [8, 72], but, in light of the low-scalability of the approaches, these solutions are applicable only to small scale systems. A well-known method to overcome scalability issues in large-scale networks consists in decomposing the grid in multiple areas and properly regulating their operations and power exchanges. Distributed optimization frameworks for the coordination of different grid areas have been proposed in the literature as in [73], for the power flow optimization, and in [74], using a distributed MPC scheme for the efficient management of Battery Energy Storage Systems (BESSs) and generations units. However, distributed approaches are characterized by iterative and communicationally-intensive procedures, especially when many variables must be optimized, and therefore they are not considered as the best solution to quickly compensate power unbalances. Because of this, an alternative and novel control architecture will be proposed in this chapter,

particularly suited for the coordination of networks partitioned in areas. Concerning network partitioning algorithms, many methods are discussed in the literature, based either on topological properties, as proposed in [75–77], or with the aim of partitioning the network in self-sufficient areas, as discussed in [78–80]. Partitioning techniques are not applied only in the electrical sector but also in other fields, e.g. for drinking water networks as discussed in [81] and in [82]. In this chapter, an efficient decomposition method will be also proposed, generalizable for many types of networked applications and adaptable to different partitioning purposes, as it will be discussed in the following.

4.1.2 Proposed solution

Considering the objective of coordinating different interconnected MGs to balance unexpected power variations of non-dispatchable elements, here a novel supervised Model Predictive Control (MPC) architecture is proposed. To ensure a prompt control action, not depending on the size of the considered network and on the number of interconnected MGs, the designed control scheme is supposed to be applied to a distribution network properly decomposed in several non-overlapping areas, denoted as grid *clusters*. The proposed control strategy is structured in two control layers.

At the low level, each cluster is controlled by a decentralized MPC regulator, named C-MPC, designed to compensate the local power variability by requesting balancing services to the MGs connected to the cluster. The rationale is that, from an external perspective, the active power exchanged by each cluster with the rest of the distribution network should exactly match a reference power profile, supposed to be previously programmed. Moreover, C-MPC regulators are designed using a novel technique with flexible prediction horizon, allowing to take into account updated information of forecasts and MGs schedules. This decentralized approach allows each C-MPC to act autonomously and with a prompt control action, just considering the elements inside its cluster. To enhance the applicability of the approach, the C-MPC regulators are designed such that they do not need to measure the instantaneous output power of each local unit, but just the exchanged power among clusters.

Furthermore, a supervisory layer is introduced, named C-SUP. This is designed to ensure that each cluster is always able to operate autonomously, having enough power reserve in MGs to balance the local power variability. The C-SUP layer is not continuously executed and it is activated just in case a cluster k needs an external power support from the other clusters. In this case, the corresponding C-MPC$_k$ sends an emergency signal to the C-SUP layer, which will dispatch the optimal power exchanges between the clusters, based on the offered availability, so that the overall power imbalances are compensated.
To enhance the scalability of the control architecture, the C-SUP layer is not designed as centralized, but a fully distributed optimization approach is adopted. The implemented method relies on a properly defined communication network graph, where each agent directly interacts with its neighbours, without needing a total communication among agents or a coordination entity[1]. The method is based on the distributed Dual Consensus ADMM (DC-ADMM) algorithm, presented in [83, Sec. IV]. Each agent of the C-SUP layer is implemented at the top of each C-MPC regulator, and it is denoted as C-SUP$_k$ for the generic cluster k. A schematic of the proposed control architecture is depicted in Figure 4.1.

The proposed event-triggered hierarchical control architecture has several advantages with respect to traditional approaches, allowing to achieve both a prompt control action and scalability properties. Moreover, the C-SUP layer is formulated to solve a simple optimization problem with reduced clusters models, which allows, when activated, to find the optimal power exchanges between clusters in a very few number of iterations. On the other hand, the C-MPC regulators are autonomously executed at each sampling time, so as to quickly counteract the power variability in each grid cluster.
The approach is described in Section 4.2. Precisely, Paragraph 4.2.1 concerns the modelling of MGs and grid clusters, while the formulation of the C-MPC and C-SUP optimization problems are described in Paragraph 4.2.2 and Paragraph 4.2.3, respectively. Finally, the approach is tested on

[1] Differently, the distributed optimization approaches presented in Chapter 2 and Chapter 3 require a supervising unit to update the dual variables (the AGS), which must communicate with all the agents (the MGs).

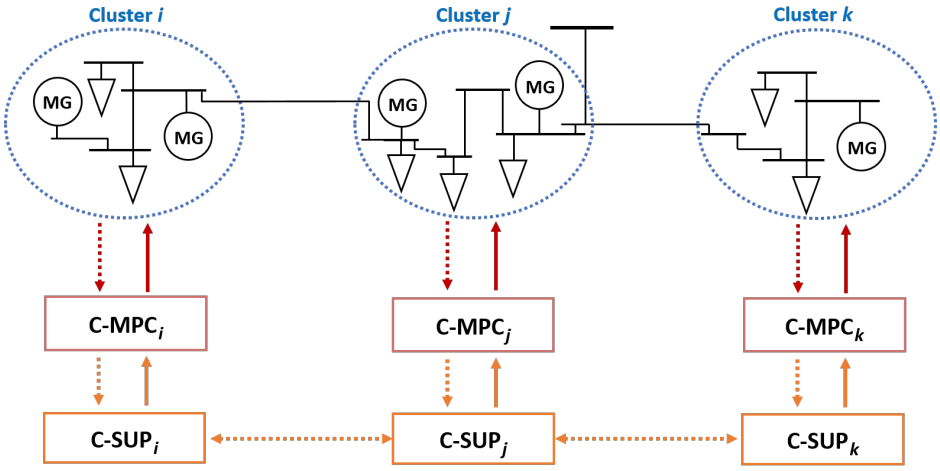

Figure 4.1: Schematic of the proposed control architecture applied to a network decomposed in three clusters.

a distribution network composed of the interconnection between the IEEE 37-bus and the IEEE 13-bus systems, whose numerical results are shown in Paragraph 4.2.4.

The proposed control solution is applied to a distribution network already decomposed into grid clusters according to some predefined criteria. Consistently, a novel partitioning algorithm for large-scale networks is devised and described in Section 4.3. The proposed decomposition method allows to obtain clusters as self-sufficient as possible so that, if the previously described control architecture is applied, the C-SUP layer is rarely activated and the C-MPC regulators can ensure the continuous balance of power variability.
The partitioning algorithm is described from a conceptual point of view, so that it can be applied to different types of networks where different sources, e.g. dispatchable generators, and sinks, e.g. loads, are present. Moreover, clusters can be created with different purposes, e.g. such that local sources are able to satisfy the nominal sinks demand or to balance the maximum demand variability.

The method is structured in three main steps. Firstly, sources and sinks are associated, defining the optimal flow transactions among them. Then, these transactions are projected in the original network graph with the aim of defining the weight of each edge. The higher the weight of an edge, the more important is the edge itself. Finally, a standard graph partitioning procedure is applied, using a well-known software toolbox named METIS, so as to minimize the sum of weights of the removed edges. The procedure is tested on large-scale electrical networks and the numerical results witness the potentiality of the approach.
The proposed decomposition algorithm is described in Section 4.3. Precisely, Paragraph 4.3.1 describes the optimal transactions computations, while Paragraph 4.3.2 shows how these can be projected on the shortest paths connecting sources and sinks, giving the proper weights on the edges. The METIS toolbox is then described in Paragraph 4.3.3, while the overall procedure is tested on real large-scale electrical networks and the results are shown in Paragraph 4.3.4.

4.2 A novel supervised MPC architecture for balance restoration in distribution grids

The main variables and parameters used in the following are reported in Table 4.1. Fixed quantities, such as pre-scheduled or forecasted power outputs, are marked with an upper hat, e.g. $\hat{p}_i^{mg}$. The variations of variables with respect to the pre-scheduled or forecasted values are denoted by Δ, e.g. $\Delta p_i^{mg} = p_i^{mg} - \hat{p}_i^{mg}$. Moreover, all the power values are positive if delivered and negative if absorbed, while maximum and minimum limits of each variable are denoted by a bar over or below the variable, respectively.
The designed control scheme is supposed to be applied to a distribution network, and $\mathcal{N}$ denotes the set of nodes. The nodes where MGs are connected are grouped in the set $\mathcal{N}_M \subseteq \mathcal{N}$, while those of external non-dispatchable elements, external to the MGs, are collected in $\mathcal{N}_L \subseteq \mathcal{N}$. The network is partitioned into n_c non-overlapping clusters of connected sub-networks, i.e. $\mathcal{N} = \mathcal{N}_{C1} \cup ... \cup \mathcal{N}_{Cn_c}$. In this Section, it is supposed that the network partition is performed offline according to some criteria.

Table 4.1: Main optimization variables and parameters

Symbol	Description
p^g	MG mGEN power output [kW]
p^b	MG BESS power output [kW]
s^b	MG BESS state of charge [%]
C^b	MG BESS capacity [kWh]
p^{mg}	MG power output [kW]
$r_p^{g\uparrow}, r_p^{g\downarrow}$	MG mGEN upward/downward active power reserves [kW]
$r_p^{b\uparrow}, r_p^{b\downarrow}$	MG BESS upward/downward active power reserves [kW]
$r_e^{b\uparrow}, r_e^{b\downarrow}$	MG BESS upward/downward energy reserves [kWh]
P^g	Total MG mGEN power output [kW]
P^b	Total MG BESS power output [kW]
E^b	Total MG BESS stored energy [kWh]
$R_P^{g\uparrow}, R_P^{g\downarrow}$	Total MG mGEN upward/downward active power reserves [kW]
$R_P^{b\uparrow}, R_P^{b\downarrow}$	Total MG BESS upward/downward active power reserves [kW]
$R_E^{b\uparrow}, R_E^{b\downarrow}$	Total MG mGEN upward/downward energy reserves [kWh]
$R_P^{mg\uparrow}, R_P^{mg\downarrow}$	Total MG upward/downward active power reserves [kW]
p^c	Cluster net power output [kW]
p^L	Output power of non-dispatchable element [kW]
D^c	Total aggregated disturbance in cluster [kW]
$R_P^{c\uparrow}, R_P^{c\downarrow}$	Total cluster upward/downward active power reserves [kW]
P^p	Power flow at the interconnection points of clusters [kW]
ΔP^{req}	Requested power variation by C-MPC regulator [kW]
ΔP^{sup}	Committed power variation by C-SUP regulator [kW]

To identify the nodes of the generic cluster k where local MGs and non-dispatchable elements are connected, the sets $\mathcal{N}_{Mk} = \mathcal{N}_M \cap \mathcal{N}_{Ck}$ and $\mathcal{N}_{Lk} = \mathcal{N}_L \cap \mathcal{N}_{Ck}$ are respectively introduced. Being a partition of the overall distribution network, each cluster k is generally connected to the rest of the grid through multiple interconnection points, which are collected in the set $\mathcal{I}_k^p = \{1, ..., n_k^p\}$.

Finally, the proposed control structure is supposed to run with sampling time $\tau_s = 90\,\text{s}$, to both ensure a prompt balance action and to have sufficient computational time to solve the optimization problems. Denoting by t the generic time index and assuming the proposed algorithm to operate for the whole day, one has $t = \{1, ..., T\}$, where $T = 24\,\text{h}/\tau_s = 960$.

4.2.1 Modelling and problem statement

First of all, MGs are modelled using a reduced description, allowing them to be employed by the C-MPC without requiring, for the sake of privacy, the disclosure of internal units' information and power profile scheduling. Then, the overall model of each cluster is presented.

Microgrid model description

MGs are supposed to have already scheduled their internal units and the output power program, considering the production costs and the energy prices, for example with the methods described in Chapter 2. The generic MG_i, with $i \in \mathcal{N}_M$, is supposed to be equipped with n_i^g mGENs, n_i^b BESSs and other non-dispatchable elements. It is assumed that controllable loads, if present, are not manipulated to compensate external power variability, given also the adopted reduced sampling time.
Considering mGENs and BESSs, their models have been widely discussed in the previous Chapters, see (2.13b)-(2.13c). The pre-scheduled upward and downward active power reserves are defined as the remaining power margins with respect to the capability limits, as follows

$$\hat{r}^{g\uparrow}_{p,j_i}(t) = \bar{p}^g_{j_i} - \hat{p}^g_{j_i}(t)\,, \qquad \hat{r}^{g\downarrow}_{p,j_i}(t) = \hat{p}^g_{j_i}(t) - \underline{p}^g_{j_i}\,, \tag{4.1}$$

$$\hat{r}^{b\uparrow}_{p,k_i}(t) = \bar{p}^b_{k_i} - \hat{p}^b_{k_i}(t)\,, \qquad \hat{r}^{b\downarrow}_{p,k_i}(t) = \hat{p}^b_{k_i}(t) - \underline{p}^b_{k_i}\,, \tag{4.2}$$

where $j_i \in [1, \ldots, n_i^g]$ and $k_i \in [1, \ldots, n_i^b]$ represent the j-th mGEN and the k-th BESS installed in MG_i, respectively. Concerning BESS, not only the power margins, but also the stored energy must be considered. The energy reserves that can be externally offered by each k_i-th BESS at each

time instant are defined as

$$\hat{r}^{b\uparrow}_{e,k_i}(t) = (\,\bar{s}^{\,b}_{k_i} \;-\; \hat{s}^{\,b}_{k_i}(t)\,)\,C^b_{k_i}\,, \tag{4.3}$$

$$\hat{r}^{b\downarrow}_{e,k_i}(t) = (\,\hat{s}^{\,b}_{j_i}(t) \;-\; \underline{s}^{\,b}_{k_i}\,)\,C^b_{k_i}\,. \tag{4.4}$$

To preserve MG internal information, it is supposed that just the aggregated reserves provided by mGENs and BESSs are communicated to the C-MPC. Therefore, the following variables are introduced

$$\hat{R}^{g\uparrow}_{P,i}(t) = \sum_{j_i=1}^{n^g_i} \hat{r}^{\,g\uparrow}_{p,j_i}(t)\,, \quad \hat{R}^{g\downarrow}_{P,i}(t) = \sum_{j_i=1}^{n^g_i} \hat{r}^{\,g\downarrow}_{p,j_i}(t)\,,$$

$$\hat{R}^{b\uparrow}_{P,i}(t) = \sum_{j_i=1}^{n^b_i} \hat{r}^{\,b\uparrow}_{p,j_i}(t)\,, \quad \hat{R}^{b\downarrow}_{P,i}(t) = \sum_{j_i=1}^{n^b_i} \hat{r}^{\,b\downarrow}_{p,j_i}(t)\,,$$

$$\hat{R}^{b\uparrow}_{E,i}(t) = \sum_{j_i=1}^{n^b_i} \hat{r}^{\,b\uparrow}_{e,j_i}(t)\,, \quad \hat{R}^{b\downarrow}_{E,i}(t) = \sum_{j_i=1}^{n^b_i} \hat{r}^{\,b\downarrow}_{e,j_i}(t)\,,$$

representing the pre-scheduled total upward and downward power and energy reserves of MG_i.
The C-MPC, to compensate the power variability inside the cluster, is designed to require the generic MG_i to vary the output power of mGENs and BESSs with respect to the pre-scheduled profiles; these power variations are denoted as ΔP^g_i and ΔP^b_i for mGENs and BESSs, respectively.

The variation of the stored energy in BESSs, denoted by ΔE^b_i and caused by ΔP^b_i, is also modelled as follows

$$\Delta E^b_i(t+1) \;=\; \Delta E^b_i(t) \;-\; \tau_s\,\Delta P^b_i(t)\,. \tag{4.5}$$

Based on the power variations committed by the C-MPC, the effective MGs reserves will be reduced, or increased, with respect to the pre-scheduled values. Therefore, it follows that

$$R^{g\uparrow}_{P,i}(t) = \hat{R}^{g\uparrow}_{P,i}(t) - \Delta P^g_i(t)\,, \quad R^{g\downarrow}_{P,i}(t) = \hat{R}^{g\downarrow}_{P,i}(t) + \Delta P^g_i(t)\,, \tag{4.6}$$

$$R^{b\uparrow}_{P,i}(t) = \hat{R}^{b\uparrow}_{P,i}(t) - \Delta P^b_i(t)\,, \quad R^{b\downarrow}_{P,i}(t) = \hat{R}^{b\downarrow}_{P,i}(t) + \Delta P^b_i(t)\,, \tag{4.7}$$

$$R^{b\uparrow}_{E,i}(t) = \hat{R}^{b\uparrow}_{E,i}(t) - \Delta E^b_i(t)\,, \quad R^{b\downarrow}_{E,i}(t) = \hat{R}^{b\downarrow}_{E,i}(t) + \Delta E^b_i(t)\,. \tag{4.8}$$

Moreover, active power variations requested by the C-MPC regulators must not exceed the pre-scheduled power reserves at each time instant. Therefore, it must hold that

$$-\hat{R}_{P,i}^{g\downarrow}(t) \;\leq\; \Delta P_i^g(t) \;\leq\; \hat{R}_{P,i}^{g\uparrow}(t)\,, \tag{4.9}$$

$$-\hat{R}_{P,i}^{b\downarrow}(t) \;\leq\; \Delta P_i^b(t) \;\leq\; \hat{R}_{P,i}^{b\uparrow}(t)\,, \tag{4.10}$$

$$-\hat{R}_{E,i}^{b\downarrow}(t) \;\leq\; \Delta E_i^b(t) \;\leq\; \hat{R}_{E,i}^{b\uparrow}(t)\,, \tag{4.11}$$

The total MG active power reserves are also defined, since they will be needed to easily assess the overall power capability in the corresponding cluster,

$$R_{P,i}^{mg\uparrow}(t) = R_{P,i}^{g\uparrow}(t) \;+\; \min\left(R_{P,i}^{b\uparrow}(t),\, \frac{R_{E,i}^{b\downarrow}(t+1)}{\tau_s} \right), \tag{4.12}$$

$$R_{P,i}^{mg\downarrow}(t) = R_{P,i}^{g\downarrow}(t) \;+\; \min\left(R_{P,i}^{b\downarrow}(t),\, \frac{R_{E,i}^{b\uparrow}(t+1)}{\tau_s} \right), \tag{4.13}$$

where for BESSs the minimum between the effective power margin and the deliverable/absorbable power based on the stored energy must be considered; the energy reserves are considered at the next time instant given the state update (4.5).

Finally, the total output power of the generic MG_i is defined as the sum of the pre-scheduled profile, plus the committed power variations by the C-MPC regulator, as follows

$$p_i^{mg}(t) \;=\; \hat{p}_i^{\,mg}(t) \;+\; \Delta P_i^g(t) \;+\; \Delta P_i^b(t)\,. \tag{4.14}$$

It is worth noticing that, through the proposed modelling, MGs are not requested to communicate all their internal characteristics to the respective C-MPC, but just the scheduled output power and the available power and energy reserves such that constraints (4.5)-(4.14) can be stated.
Then, as the C-MPC defines the optimal power variation $\Delta P_i^{g\,*}(t)$ and $\Delta P_i^{b\,*}(t)$, the MG_i, through its MGCC, must coordinate its internal mGENs and BESSs to satisfy the power requests, minimizing the operative costs.

The corresponding MG tracking optimization problem to satisfy the C-MPC requests is not described here, as its formulation is straightforward.

Remark 4.1. *The available power and energy reserves have been supposed to be entirely offered to the C-MPC to balance the variability of the cluster. However, MGs can be also modelled to communicate just a fraction of the available reserves, keeping an internal pre-defined amount for providing external power services to the TSO, using the techniques described in Chapter 3.*

Cluster model description

The grid cluster is a connected portion of the distribution network, where both MGs and external non-dispatchable elements are connected. Therefore, the net active power of cluster k can be defined as follows

$$p_k^c(t) = \sum_{i \in \mathcal{N}_{Mk}} p_i^{mg}(t) \; + \sum_{j \in \mathcal{N}_{Lk}} p_i^L(t)\,, \tag{4.15}$$

where internal power losses are neglected for the sake of simplicity. Consistently with the MG output power expression (4.14), the external load power absorption can be also modelled as the sum of two terms

$$p_j^L(t) \;=\; \hat{p}_j^L(t) \;+\; \Delta p_j^L(t)\,, \qquad \forall j \in \mathcal{N}_{\mathcal{L}}\,, \tag{4.16}$$

where the first term expresses the forecasted power profile, while the second the unexpected power variation that must be balanced. The total unknown power variability acting on cluster k is aggregated in the following variable

$$D_k^c(t) = \sum_{j \in \mathcal{N}_{Lk}} \Delta p_j^L(t)\,. \tag{4.17}$$

Therefore, the pre-scheduled/forecasted power program of cluster k is defined as

$$\hat{p}_k^c(t) = \sum_{i \in \mathcal{N}_{Mk}} \hat{p}_i^{mg}(t) \; + \sum_{j \in \mathcal{N}_{Lk}} \hat{p}_i^L(t)\,, \tag{4.18}$$

while, combining (4.14)-(4.18), the net power output of cluster k can be reformulated as

$$p_k^c(t) \;=\; \hat{p}_k^c(t) \;+\; \sum_{i \in \mathcal{N}_{Mk}} \big(\Delta P_i^g(t) \;+\; \Delta P_i^b(t)\big) \;+\; D_k^c(t)\,. \tag{4.19}$$

Remark 4.2. *The power variability of MGs internal loads and RESs is not modelled for the sake of simplicity, but it can be easily included considering additional non-dispatchable elements connected to the same nodes of MGs.*

The total power reserves in cluster k at the generic time instant t are expressed, defined as the sum of the available reserves in MGs

$$R_{P,k}^{c\uparrow}(t) = \sum_{\forall i \in \mathcal{N}_{Mk}} R_{P,i}^{mg\uparrow}(t)\,, \qquad R_{P,k}^{c\downarrow}(t) = \sum_{\forall i \in \mathcal{N}_{Mk}} R_{P,i}^{mg\downarrow}(t)\,. \tag{4.20}$$

As mentioned, to enhance the applicability of the approach, it is assumed that the output power of all non-dispatchable elements is not measured at each time-step τ_s to estimate the aggregated disturbance $D_k^c(t)$. On the other hand, the power flows through the points connecting cluster k to the rest of the network, i.e. $P_{k,i}^p$ with $i \in \mathcal{I}_k^p$, are supposed to be measurable. The power flows $P_{k,i}^p$ are defined to be positive (negative) when exported from (absorbed by) cluster k. The net power of cluster k can be therefore defined as

$$p_k^c(t) = \sum_{i \in \mathcal{I}_k^p} P_{k,i}^p(t)\,. \tag{4.21}$$

The C-MPC, before computing the optimal control action at the generic time instant t, can estimate the aggregated disturbance acting on cluster k, denoted by $\tilde{D}_k^c(t)$, as the difference between the measured cluster net power (4.21), the pre-scheduled/forecasted one (4.18) and the active power variations committed at the previous control iteration, as follows

$$\tilde{D}_k^c(t) \;\approx \sum_{i \in \mathcal{I}_k^p} P_{k,i}^p(t) \;-\; \hat{p}_k^c(t) \;-\; \sum_{i \in \mathcal{N}_{Mk}} \big(\Delta P_i^g(t-1) \;+\; \Delta P_i^b(t-1)\big)\,. \tag{4.22}$$

4.2.2 Clusters' control using MPC with flexible prediction horizon

The proposed control architecture is structured in two layers, named as C-MPC and C-SUP, which are executed as follows.

- The C-MPC regulators compute the optimal MGs power variations with a sampling time τ_s, so as to balance the local power variability. Specifically, they are designed to track a pre-defined reference for the net cluster power output, denoted as $p_k^{c,0}(t)$ for the generic cluster k. In case the power variability acting on cluster k is too large to be compensated by local MGs, not allowing to track the pre-defined reference, the corresponding C-MPC regulator issues a power support request $\Delta P_k^{req}(t)$ to the C-SUP layer.
- The C-SUP layer is activated as $\Delta P_k^{req*}(t) \neq 0$ for a generic cluster k, and it is executed right after the C-MPC layer, within the sampling time τ_s. Its main goal is to define the power variations of clusters' net power outputs, with objective of compensating the power deficit in cluster k. The optimal power variations are denoted by $\Delta P_k^{sup,*}(t)$, and they are supposed to be executed by the C-MPC regulators at the next sampling time, i.e. at $t+1$.

The C-MPC problem is now more formally stated. Conversely to standard predictive approaches, a flexible prediction horizon is adopted, denoted by $N(t)$ to express its dependence on the current time instant. The reason behind this choice will be explained later. Moreover, the time index h is introduced, spanning the whole prediction horizon from the current time instant t, i.e. $h \in T_N(t) = \{t, \dots, t + N(t) - 1\}$.

As the main objective of the C-MPC regulator is to track the cluster net power reference $p_k^{c,0}(h)$, the following constraint should be stated for each generic cluster k

$$p_k^c(h) = p_k^{c,0}(h), \quad \forall h \in T_N(t).$$

However, the power variability acting on the cluster may be too large to be compensated by local MGs, causing the unfeasibility of the above

defined constraint. Because of this, the slack variable ΔP_k^{req} is included as follows

$$p_k^c(h) = p_k^{c,0}(h) \; - \; \Delta P_k^{req}(h), \quad \forall h \in T_N(t), \tag{4.23}$$

where $\Delta P_k^{req}(h)$ can become different from zero just in case it is not possible to track $p_k^{c,0}(h)$ using local MGs. Precisely, if the C-MPC of cluster k selects $\Delta P_k^{req}(h) \geq 0$, it means that local power imbalances cause a power shortage in cluster k, implying that $p_k^c(h) \leq p_k^{c,0}(h)$. On the other hand, if $\Delta P_k^{req}(h) < 0$, it means that cluster k records an excess of power that cannot be internally absorbed.

The optimal value of the slack variable $\Delta P_k^{req*}(t)$ denotes the power support request of cluster k, which is transmitted by the corresponding C-MPC regulator to the C-SUP layer.

If $\Delta P_k^{req*}(t) \neq 0$ for a generic cluster k, the C-SUP layer is activated. This optimally dispatches power variations to the net power output of the clusters, denoted as ΔP^{sup}, so that the power requests of the C-MPC regulators are satisfied. To impose that the clusters track the power variations committed by the C-SUP layer, the expression (4.23) is substituted with the following

$$p_k^c(h) \; = \; p_k^{c,0}(h) \; - \; \Delta P_k^{req}(h) + \; \Delta P_k^{sup,*}(t-1)\,, \tag{4.24}$$

where the variables $\Delta P_k^{sup,*}(t-1)$ are considered as parameters at the C-MPC level. A time shift is introduced since they are supposed to be computed by the C-SUP layer at the previous time instant with respect to the C-MPC execution. If the C-SUP selects $\Delta P_k^{sup,*}(t-1) \geq 0$, it implies that cluster k must increase its net power output with respect to the reference at time t, while, if $\Delta P_k^{sup,*}(t-1) < 0$, it has to decrease it.

The C-MPC problem formulation must include the reduced models of MGs, i.e. the expressions (4.5), (4.14). Moreover, a zero terminal constraint is also introduced to enforce the restoration of the scheduled stored energy in the MG BESS at the end of the optimization horizon.

$$\Delta E_i^b(t+N(t)) = 0\,, \qquad \forall i \in \mathcal{N}_{Mk} \tag{4.25}$$

The expressions of the cluster net power output and reserves, i.e. (4.19) and (4.20), are also included in the C-MPC problem formulation. Since the net power trajectory depends on the future realization of the disturbance, which is supposed to be unknown in advance, it is customarily assumed that the disturbance remains constant for the whole prediction horizon and, specifically, it is equal to the value estimated by (4.22) at time t. It follows that

$$D_k^c(h) = \tilde{D}_k^c(t), \qquad \forall h \in T_N(t) \tag{4.26}$$

The cost function of the C-MPC is therefore stated as follows

$$J_k^c(t) = \sum_{h=t}^{N(t)} \Big\{ r_{req}(\Delta P_k^{req}(h))^2 + \sum_{\forall i \in \mathcal{N}_{Mk}} \Big[r_i^b(\Delta P_i^b(h))^2 + r_i^g(\Delta P_i^g(h))^2 + \\ + r_i^{\delta g}\left(\Delta P_i^g(h) - \Delta P_i^g(h-1)\right)^2 \Big] \Big\} \tag{4.27}$$

where r_i^g, r_i^b, $r_i^{\delta g}$ and r_{req} are positive non-null weights.
The proposed cost function aims to minimize the cost related to the power variations committed to MGs, such that the pre-defined constraints are respected. To this regard, it is worth noticing that the mGENs and BESSs costs can be communicated directly by the MGs in accordance to some internal economic policy. Moreover, the variation of mGENs active power adjustments between consecutive time instants is also penalized, to avoid an unnecessary variability of mGENs' set-points, encouraging the exploitation of BESSs to compensate the fast component of power fluctuations. Finally, since the C-MPC must request external power support just in case constraint (4.24) cannot be respected using local MGs, the use of ΔP_k^{req} must be strongly discouraged. This means that its cost must is set to be much higher with respect to other terms, i.e. $r_{req} \gg r_i^g,\, r_i^b,\, r_i^{\delta g}$.

In summary, at each time instant t, the C-MPC of cluster k must solve the following optimization problem

$$\begin{aligned} \min_{\substack{\Delta P^{g}_{\forall i \in \mathcal{N}_{Mk}} \Delta P^{b}_{\forall i \in \mathcal{N}_{Mk}} \\ \Delta P^{req}_{k}}} \quad & J^{c}_{k}(t) \\ \text{subject to} \quad & \\ & (4.5)\text{-}(4.14)\,,\ \forall i \in \mathcal{N}_{Mk}\,,\ \forall h \in T_N(t)\,, \\ & (4.19),\ (4.20),\ (4.24)\,,\ \forall h \in T_N(t)\,, \\ & (4.25),\ (4.26)\,. \end{aligned} \tag{4.28}$$

The optimal variables computed by the C-MPC are denoted by the superscript *. According to standard predictive approaches, the C-MPC implements the first step of the optimal input sequence, i.e. $\Delta P^{g*}_{\forall i}(t), \Delta P^{b*}_{\forall i}(t), \forall i \in \mathcal{N}_{Mk}$.
At each time instant, the C-MPC of cluster k communicates to the supervisory layer the optimal value of power request $\Delta P^{req*}_{k}(t)$ and the effective available power reserves, i.e. $R^{c\uparrow *}_{P,k}(t)$ and $R^{c\downarrow *}_{P,k}(t)$.

Choice of the prediction horizon for the C-MPC

Differently from standard MPC approaches, a time-varying prediction horizon is here proposed in view of the following considerations:

- As common in practice, MGs scheduled profiles and load/RES forecasts are provided with a resolution of $\tau_f = 15$ min. The same holds for the MGs' power and energy reserves.
- It is supposed that the forecasts, schedules and reserves are updated with a sampling time equal to τ_f.
- Updated forecasts are considered to be reliable just for the next hour, $T_f = 1$ h. Therefore, the prediction horizon will never exceed one hour, i.e. $N(t) \leq T_f/\tau_s$.

Because of this, a flexible evolution of the prediction horizon is adopted. A sketch of its evolution is shown in Figure 4.2, and it works according to the following procedure. At the beginning, $N(t)$ is set to the maximum length for which reliable predictions are available, i.e. $N(t) = T_f/\tau_s = 40$. Then, a shrinking horizon approach is adopted, where $N(t)$ is reduced by one step at each C-MPC iteration. After $\tau_f = 15$ minutes, updated information are available for the entire next hour, therefore the prediction horizon is extended again to T_f, i.e $N(t) = 40$.

Precisely, at each C-MPC iteration, the prediction horizon can be computed according to the following formula:

$$N(t) = \left(\left\lfloor \frac{\tau_s\, t}{\tau_f} \right\rfloor \frac{\tau_f}{\tau_s} + \frac{T_f}{\tau_s} \right) - t$$

The adoption of this flexible prediction horizon allows to exploit always the most reliable and updated schedules/forecasts. Moreover, differently from pure shrinking MPC methods, the proposed approach prevent the terminal constraint (4.25) from being excessively strict, as the horizon is always longer than 45 minutes.

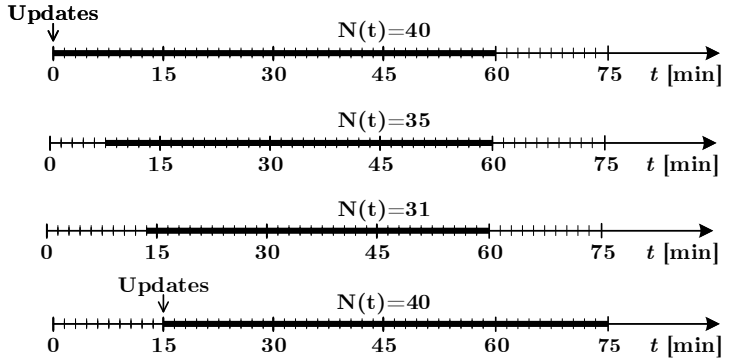

Figure 4.2: Flexible prediction horizon

4.2.3 Clusters' Supervisor design using DC-ADMM

The C-SUP is designed to regulate power exchanges among clusters. It is supposed to be executed right after the C-MPC layer just if one, or more, clusters are not able to counteract the local power variability using MGs reserves.
As discussed in Paragraph 4.1.2, the C-SUP layer is implemented through a fully distributed approach, meaning that a central coordination entity is not required and each C-SUP agent, implemented at the top of each cluster, directly interacts with the others. Moreover, the implemented distributed algorithm does not require a total communication. Therefore, it is supposed that the C-SUP agent exchanges messages just with its neighbouring clusters, eventually finding the optimal power exchanges among all clusters.
Before describing in detail the adopted distributed algorithm, the centralized formulation of the C-SUP layer is firstly presented.

C-SUP problem formulation

As shown in the previous section, the C-MPC of cluster k computes the optimal power request $\Delta P_k^{req,*}(t)$, taking values different than zero just in case of necessity. At this stage, the C-SUP layer must select the committed power variations to other clusters, selecting the variables $\Delta P_j^{sup}(t)$, $\forall j \in \{1, \dots, n_c\} \setminus k$.
First of all, the following constraint must be respected, where it is reminded that at the C-SUP level, $\Delta P_k^{req,*}(t)$ are fixed parameters.

$$\sum_{k=1}^{n_c} \Delta P_k^{sup}(t) \;=\; \sum_{k=1}^{n_c} \Delta P_k^{req,*}(t)\,. \tag{4.29}$$

Expression (4.29) ensures that the balance between the C-MPC requests and the committed power variations by the C-SUP layer is respected. It is worth noticing that if two C-MPC regulators send two opposite requests, the overall request is null. This is a desired feature since it means that the overall distribution network is self-balanced, even though the single clusters are not.

As previously described, a request $\Delta P_k^{req,*}(t) < 0$ indicates that there is an excess power in the cluster that cannot be compensated by local MGs, while $\Delta P_k^{sup}(t) \geq 0$ means that cluster k is requested to increase its net power output. Therefore, if the C-MPC of cluster k sends a request $\Delta P_k^{req,*}(t) < 0$, the C-SUP layer cannot ask the cluster to absorb extra-power from other clusters and it must be enforced that $\Delta P_k^{sup}(t) \geq 0$. On the other hand, if $\Delta P_k^{req,*}(t) > 0$, meaning that cluster k is facing a power shortage, it cannot be requested to export extra-power to the others, i.e. $\Delta P_k^{sup}(t) \leq 0$. The following constraint is therefore stated

$$\text{sign}(\Delta P_k^{req,*}(t))\, \Delta P_k^{sup}(t) \;\leq\; 0\,, \tag{4.30}$$

where it is reminded that $\Delta P_k^{req,*}(t)$ is a fixed parameter at this level, implying that (4.30) is a linear constraint.

Remark 4.3. *It is worth noticing that the exact power exchanges among clusters are not specified. Indeed, being all clusters part of the same distribution network, if a cluster k increases its net power output and another cluster j decreases its output by the same quantity, it will result in a power transfer from resources of cluster k to the ones of cluster j.*

The committed power variations by the C-SUP layer obviously have an impact on the effective power reserves of clusters. To have an estimation of this effect, the following variables are introduced

$$R_k^{sup\uparrow}(t) \;=\; R_k^{c\uparrow *}(t) \;-\; \Delta P_k^{sup}(t)\,, \tag{4.31}$$

$$R_k^{sup\downarrow}(t) \;=\; R_k^{c\downarrow *}(t) \;+\; \Delta P_k^{sup}(t)\,. \tag{4.32}$$

The shortage of clusters' reserves is prevented forcing them to be larger than a fixed threshold $\bar{\varphi}$ of the pre-scheduled values. However, to avoid feasibility issues, the threshold can be decreased by means of a slack variable $\Delta\varphi_k(t)$, which will be strongly penalized in the C-SUP cost function.

$$\begin{aligned} R_k^{sup\uparrow}(t) &\geq (\,\bar{\varphi} - \Delta\varphi_k(t)\,)\;\hat{R}_k^{c\uparrow}(t)\,,\\ R_k^{sup\downarrow}(t) &\geq (\,\bar{\varphi} - \Delta\varphi_k(t)\,)\;\hat{R}_k^{c\downarrow}(t)\,. \end{aligned} \tag{4.33}$$

Obviously, the slack variable $\Delta\varphi_k$ must be bounded between 0, corresponding to no relaxation, and $\bar{\varphi}$, i.e. a complete constraint relaxation, as follows

$$0 \leq \Delta\varphi_k(t) \leq \bar{\varphi}\,, \tag{4.34}$$

Constraints (4.31)-(4.34) are defined so that, when the C-SUP layer is activated, it commits the power variations to clusters such that each one has a sufficient amount of reserve, imposed to be greater than a threshold. This avoids chattering phenomena, i.e. cases where the C-MPC regulators make consecutive requests of small amounts of power.

Thee C-SUP is designed to minimize the following cost function for each cluster k

$$\begin{aligned} J_k^{sup}(t) = \; & \gamma_p\, c_k\, (\Delta P_k^{sup}(t))^2 \; + \; \gamma_r\, (\Delta P_k^{sup}(t) - \Delta P_k^{sup}(t-1))^2 \; + \\ & + \; \gamma_\varphi\, (\Delta\varphi_k)^2\,, \end{aligned} \tag{4.35}$$

where the following terms are penalized:

- the power variation committed to cluster k, i.e. ΔP_k^{sup}, to avoid perturbing clusters unless it is necessary to satisfy constraints,
- the variation of ΔP_k^{sup} with respect to the previous time instant, to enhance the steadiness of these variables
- the slack variables $\Delta\varphi_k$, such that the power reserves' thresholds are attempted to be respected,

The terms γ_p, γ_φ and γ_r are introduced to differently penalize the described contribution. As mentioned, it is set $\gamma_\varphi \gg \gamma_p, \gamma_r$ to avoid an unmotivated relaxation of minimum reserve constraints. The coefficients c_k are also introduced since the clusters may involve different costs for the provided power. Here, it has been chosen to use time-varying costs, defined as

$$c_k(t) = \frac{1}{R_k^{c\uparrow *}(t) + R_k^{c\downarrow *}(t)}\,,$$

such that the larger the power reserves that cluster k owns, the lower the cost associated to the committed power variation $\Delta P_k^{sup}(t)$.

Therefore, the C-SUP must solve the following optimization problem

$$\begin{aligned} \min_{\Delta P_k^{sup}(t), \Delta\varphi_k(t)} \quad & \sum_{k=1}^{n_c} J_k^{sup}(t) \\ \text{subject to} \quad & \\ & (4.30) \text{ - } (4.34), \quad \forall\, k = \{1, \ldots, n_c\} \\ & (4.29)\,, \end{aligned} \tag{4.36}$$

which is a static optimization problem, that must be solved just in case one of the C-MPC regulators issues a power request. As the optimal values $\Delta P_k^{sup*}(t)$ are computed for each cluster, these are sent to the C-MPC regulators to be executed at the next time instant, through the constraint (4.24). Problem (4.36) is constituted by an additive cost function, see (4.35), by local constraints defined for each cluster, i.e. (4.30) -(4.34), and by a power balance constraint which couples clusters' optimization variables, i.e. (4.29).

Introducing the variable $x_k = [\,\Delta P_k^{sup}(t),\, \Delta\varphi_k(t)\,]'$, the optimization problem (4.36) can be expressed in the following standard form

$$\begin{aligned} \min_{x_1, \ldots, x_{n_c}} \quad & \sum_{k=1}^{n_c} f_k(\,x_k\,) \\ \text{subject to:} \quad & \\ & x_k \in X_k\,, \quad k \in \{1, \ldots, n_c\}\,, \\ & \sum_{k=1}^{n_c} E_k x_k = q\,, \end{aligned} \tag{4.37}$$

where $f_k(x_k)$ expresses the cluster cost function defined in (4.35), X_k is a polyhedral set defined by constraints (4.30)-(4.34), while $\sum_{k=1}^{n_c} E_k x_k = q$ represents the coupling constraint (4.29).

Fully distributed solution of the C-SUP problem

The optimization problem (4.37) is named *primal problem* and it can be solved using a fully distributed approach, meaning that each agent directly interacts with the others, without the need of any central supervising entity.
The implemented algorithm is based on the Dual Consensus ADMM (DC-ADMM) method described in [83]. The purpose of this paragraph is to present a general overview of this method, since its actual derivation requires detailed mathematical development. The reader is referred to [83–85] for more details on Dual Consensus ADMM approaches.
Let's model a multi-agent communication network as an undirected graph $\mathcal{G} = \{\mathcal{V}, \mathcal{E}\}$, where $\mathcal{V} = \{1, \dots, n_c\}$ is the set of nodes (i.e. the agents) and $\mathcal{E}$ is the set of edges. Precisely, an edge $(i, j) \in \mathcal{E}$ if, and only if, agent i and agent j are neighbours, meaning that they can exchange messages between each other. Thus, it is possible to define the index subset of neighbours for each agent i as $\mathcal{N}_i = \{j \in \mathcal{V} \,|(i, j) \in \mathcal{E}\}$, and the number of neighbours for agent i as $n_i = |\mathcal{N}_i|$.

The approach requires two assumptions: 1) the undirected graph $\mathcal{G} = \{\mathcal{V}, \mathcal{E}\}$ must be connected and, 2) the primal problem must be convex. If the mentioned assumptions hold, the DC-ADMM algorithm asymptotically converges to the optimal solution of (4.37) [83, Teorem 2].

Considering the application framework of this chapter, agents are the C-SUP regulators implemented at the top of the C-MPC layer. Therefore, a C-SUP agent is defined for each cluster $k \in \{1, \dots, n_c\}$, as reported in Figure 4.1. The optimization problem (4.36) is convex, while the communication graph is defined to be connected. In fact, it is assumed that each cluster can interact with all its direct neighbours and, moreover, there are not isolated clusters, as they are all part of the same distribution network.

The definition of the DC-ADMM algorithm is based on duality theory, which plays a central role in the distribution of multi-agent optimization problems, see [68].

The Lagrangian function of (4.37) is defined as follows

$$\begin{aligned} L(x_1, \ldots, x_{n_c}, \lambda) \;&=\; \sum_{k=1}^{n_c} f_k(\, x_k\,) \;+\; \lambda \left(\sum_{k=1}^{n_c} E_k x_k - q \right) \;= \\ &= \sum_{k=1}^{n_c} \left\{ \; f_k(\, x_k\,) \;+\; \lambda\, E_k\, x_k \;-\; \lambda \frac{q}{n_c} \; \right\}, \end{aligned} \tag{4.38}$$

which is obtained by adding to the cost function of (4.37) a penalizing term for the violation of coupling constraint, weighted by the dual variable λ. At this stage, the dual problem of (4.37) is defined as

$$\max_{\lambda} \sum_{k=1}^{n_c} \min_{x_k \in X_k} \left\{ \; f_k(\, x_k\,) \;+\; \lambda\, E_k\, x_k \;-\; \lambda \frac{q}{n_c} \; \right\}, \tag{4.39}$$

which can be easily solved using standard distributed optimization methods, as the dual sub-gradient algorithm, see [68, Section 6.3]. These methods rely on a central entity that iteratively updates the dual variable based on the local solutions of the agents until convergence is reached and the coupling constraint is respected. Conversely, the DC-ADMM entitles the agents themselves to update local copies of the dual variable, without the need of a central entity. The problem (4.39) is equivalent to solve

$$\min_{\lambda} \; \sum_{k=1}^{n_c} \Bigg[\lambda \frac{q}{n_c} \; \underbrace{- \min_{x_k \in X_k} \left\{ \; f_k(\, x_k\,) \;+\; \lambda\, E_k\, x_k \; \right\}}_{\phi_k(\lambda)} \Bigg], \tag{4.40}$$

which becomes

$$\min_{\lambda} \; \sum_{k=1}^{n_c} \left(\lambda \frac{q}{n_c} \;+\; \phi_k(\lambda) \right). \tag{4.41}$$

Since the undirected communication graph among agents is connected, the problem (4.41) can be equivalently written as

$$\min_{\lambda_1,\ldots,\lambda_{n_c}} \quad \sum_{k=1}^{n_c} \left(\lambda_k \frac{q}{n_c} + \phi_k(\lambda_k) \right) \tag{4.42a}$$

subject to

$$\lambda_k = \lambda_j, \quad \forall k \in \mathcal{V}, \ \ \forall j \in \mathcal{N}_k \,. \tag{4.42b}$$

Defining (4.42), each agent k can optimize the cost function (4.42a) with respect to the local copy of the dual variable λ, denoted as λ_k. These local copies of the dual variable, at convergence, must be equal among neighbouring agents through the coupling constraints (4.42b).

The DC-ADMM algorithm is obtained by applying a standard algorithm, i.e. the Consensus ADMM (C-ADMM) [86], to the dual problem formulated as in (4.42). Indeed, agents, exchanging information among neighbours, must reach a the consensus on the local copies of the dual variable, so that they all converge to the optimal solution (4.39). The details of the C-ADMM and the corresponding mathematical steps to derive the DC-ADMM are omitted here, and they are reported in [83, Section IV-A]. The final form of the DC-ADMM algorithm to solve (4.37) is depicted in Algorithm 3. Although more details are needed to fully understand each step of the algorithm, a general explanation is here given.

All agents act in parallel, iteratively solving Steps 7-8-9. Precisely, Step 7 finds the optimal value of the local optimization variable x_k^i, where i is the iteration number. At each step, agent k uses as external information just local dual variables of the neighbouring agents at the previous iteration, i.e. λ_j^{i-1} with $j \in \mathcal{N}_k$. The local dual variable λ_k^i is updated in Step 8. An additional auxiliary variable is also considered, i.e. p_k^i, which is updated in Step 9 based on the differences of the dual variable of agent k and the ones of its neighbours, so as to induce the dual variables of neighbouring agents to be equal.

As it will be shown in the numerical results, the DC-ADMM algorithm allows to find an optimal solution of (4.36) in a very reduced number of iterations. This is also due to the fact that most of the model and problem complexity is addressed at the C-MPC layer, while the C-SUP is formulated as a simple static problem, aiming to quickly define the optimal power exchanges among clusters.

Algorithm 3 Dual Consensus ADMM for solving C-SUP problem (4.36)

Select $c > 0$ as a tuning parameter

$\lambda_k^0 = 0 \quad \forall\, k \in \mathcal{V}$

$p_k^0 = 0 \quad \forall\, k \in \mathcal{V}$

$i = 1$

repeat

for $\forall\, k \in \mathcal{V}$, in parallel, **do**

$$x_k^i = \underset{\mathbf{x}_k \in X_k}{\operatorname{argmin}} \left\{ f_k(\, x_k\,) + \frac{c}{4\, n_k} \left\| \frac{1}{c} \left(E_k\, x_k - \frac{q}{n_c} \right) - \frac{1}{c} p_k^{i-1} + \right. \right.$$

$$\left. \left. + \sum_{j \in \mathcal{N}_k} \left(\lambda_k^{i-1} - \lambda_j^{i-1} \right) \right\|_2^2 \right\}$$

$$\lambda_k^i = \frac{1}{2\, n_k} \left(\sum_{j \in \mathcal{N}_k} \left(\lambda_k^{i-1} - \lambda_j^{i-1} \right) - \frac{1}{c} p_k^{i-1} + \frac{1}{c} \left(E_k x_k^i - \frac{1}{n_c} q \right) \right)$$

$$p_k^i = p_k^{i-1} + c \sum_{j \in \mathcal{N}_k} \left(\lambda_k^i - \lambda_j^i \right)$$

$i \leftarrow i + 1$

end for

until a predefined stopping criterion is satisfied.

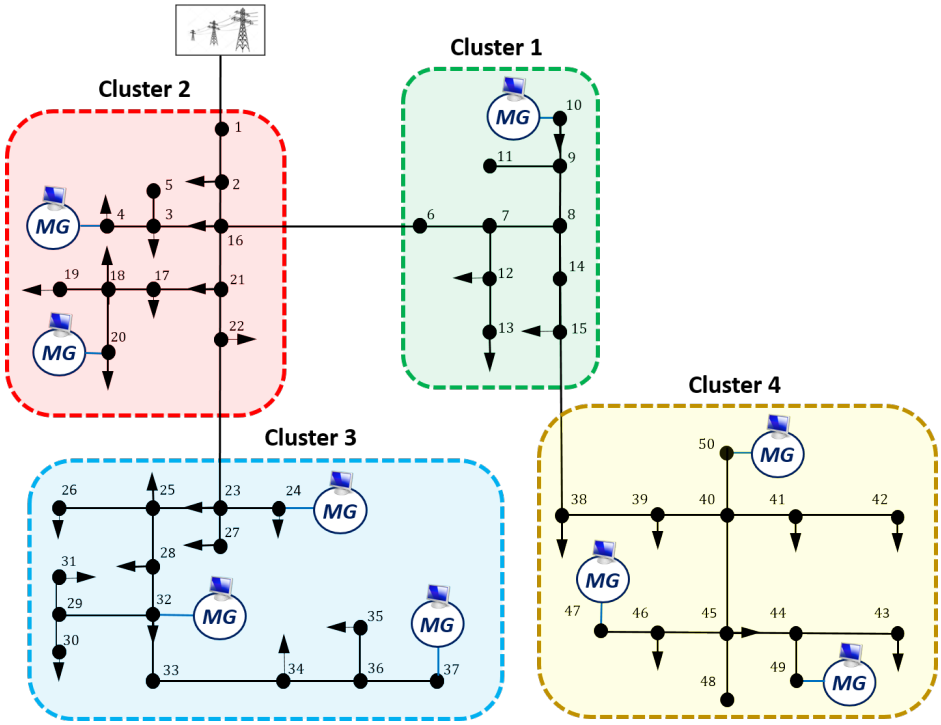

Figure 4.3: Distribution network benchmark partitioned in 4 clusters.

4.2.4 Numerical results

The proposed control system has been tested using the distribution network depicted in Figure 4.3, consisting in the interconnection of the IEEE 37-bus (nodes 1 to 37) and IEEE 13-bus test feeders, the first including nodes 1 to 37 and the second nodes 38 to 50, respectively.

The overall network has been simulated in MATLAB, while CPLEX has been used to solve the optimization problems. The distribution network has been arbitrary partitioned in $n_c = 4$ different clusters, and it includes 9 MGs and 32 non-dispatchable elements. MGs are designed using the characteristics shown in the previous chapters (e.g. see Table 2.2), while their pre-scheduled power profiles and reserves are computed using the methods described in Chapter 2.

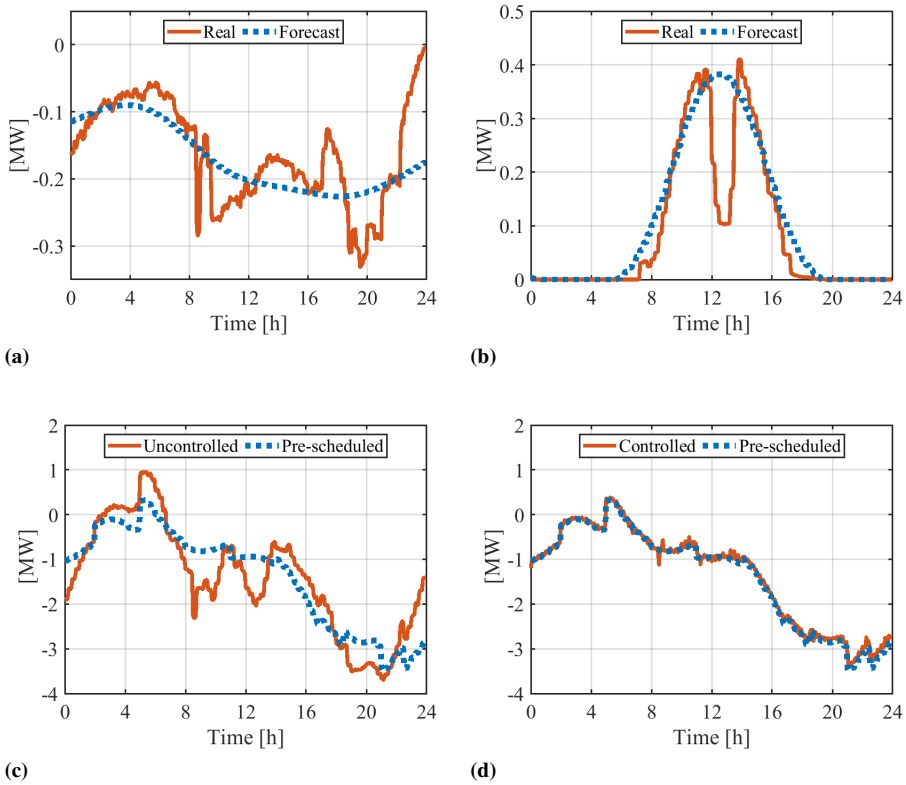

Figure 4.4: (a) Power output of the load connected to node 26; (b) Power output of the PV system connected to node 10; (c) Power exchange with the main utility in the uncontrolled case; (d) Power exchange with the main utility in the controlled case.

Loads' and RESs' power profiles and forecasts have been provided by RSE S.p.A. and were measured from the secondary substations and PhotoVoltaic (PV) systems located in Milan, Italy. The actual power outputs and forecasts of a single load and PV system are shown in Figure 4.4(a)-(b). It is evident that the actual power output can be quite different with respect to the forecasted one, and these fluctuations call for a balancing control system.

Indeed, in case unexpected power variations are not balanced, the power exchanged with the main utility exhibits serious deviations with respect to the programmed profile, see Figure 4.4(c). On the contrary, if the proposed control structure is applied, each grid cluster is able to track its programmed power profile, and therefore the programmed exchange with the main grid is respected, see Figure 4.4(d).

To assess the performances of the proposed control scheme, the trends of the aggregated disturbance and of the dispatched control inputs in cluster 1 are shown in Figure 4.5(a), limitedly to the time range 15:00-22:00 for convenience. Note that just the variables of the MG connected to node 10 are depicted, denoted as MG_{10}, since it is the only MG in cluster 1. As evident from Figure 4.5(b), in the interval 15:00-18:30, the BESS provides a fast power set-point modulation, while the mGEN power reference changes smoothly, owing to the penalization of the variation rate in (4.27).

However, between 18:30 and 21:00, the aggregated disturbance acting on Cluster 1 becomes significantly large, forcing the C-MPC to saturate the dispatchable mGEN, see Figure 4.5(b), and to request additional power to compensate the power variability, see Figure 4.5(c). It is worth noticing that, the BESS output power is set close to zero since the terminal constraint (4.25) would be compromised to balance such large power variation. As the C-MPC of cluster 1 issue the power request, the C-SUP layer is activated to dispatch the needed power to the other clusters. In Figure 4.5(d), the C-SUP final decisions are depicted, showing that clusters 2, 3 and 4 are requested to increase their output power between 18:30 and 21:00 to compensate the large disturbance in cluster 1. It is also evident from Figure 4.5(d), the C-SUP commits cluster 1 to absorb extra-power with respect to the one requested, since $\Delta P_1^{sup} < 0$ between 20:15 and 21:00. This is due to the fact that clusters' reserves must be always larger in magnitude than a selected threshold as reported in Figures 4.5(e) and (f). Precisely, considering Figure 4.5(f), the upward power reserve of cluster 1 is actually maintained above the threshold between 20:15 and 21:00 thanks to the extra amount of power committed by the C-SUP layer.

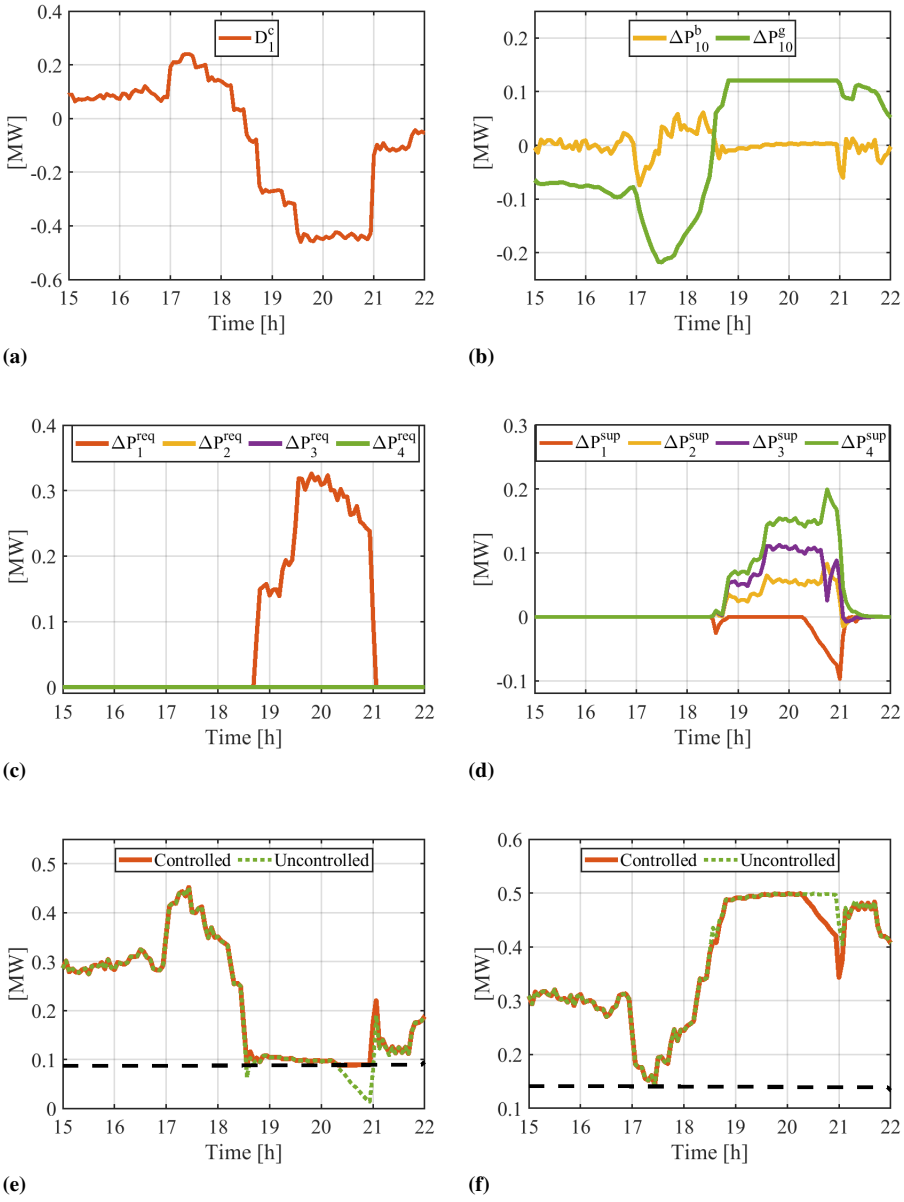

Figure 4.5: (a) Total disturbance in cluster 1; (b) Power variations of MG_{10}'s mGENs and BESSs; (c) C-MPC power requests; (d) C-SUP committed power variations to clusters; (e) Upward power reserve in cluster 1; (e) Downward power reserve in cluster 1.

The pre-scheduled output power of dispatchable mGENs and the overall profile of the BESSs of MG_{10} are represented in Figure 4.6(a)-(b), together with the corresponding reserves. Figure 4.6(c) reports the modulation of the output power of the mGENs of MG_{10} with respect to the pre-scheduled profile; it is evident that the power variations are contained in the offered power reserves depicted in Figure 4.6(a). Concerning BESS, the almost zero-mean power adjustments, see Figure 4.5(b), along with the terminal constraint (4.25), allow to contain the deviations of energy profiles and to restore the scheduled stored energy within the end of the day, as shown in Figure 4.6(d).

The C-SUP distributed layer is implemented to solve Algortihm 3 by allowing communication just between directly connected clusters, for example C-SUP agent of cluster 3 can interact just with the C-SUP agent of cluster 2 (see Figure 4.3).
Figure 4.7 shows the performances of DC-ADMM algorithm for solving the C-SUP layer, at the time instant 21:00. The DC-ADMM achieves the same optimal cost of the centralized solution in around 10 iterations, as shown in Figure 4.7(a). Figure 4.7(b) reports the trends of the local dual variables, and it is evident that the agents (i.e. the C-SUP regulators) eventually reach the consensus, finding the optimal dual variable which solves (4.39). Figure 4.7(c) shows the committed power variations by the C-SUP layer, while Figure 4.7(d) report the optimal reserve slack variables, which are practically null as the reserves are always above the threshold (see Figure 4.5(e)-(f)).

Considering the computational time, the C-MPC computes the optimal solution in around 1 sec, while the C-SUP layer in a average of 2 sec. This witnesses the potentiality of the proposed approach, conversely to centralized and pure distributed methods, make it particularly suited to be applied to large-scale networked systems.

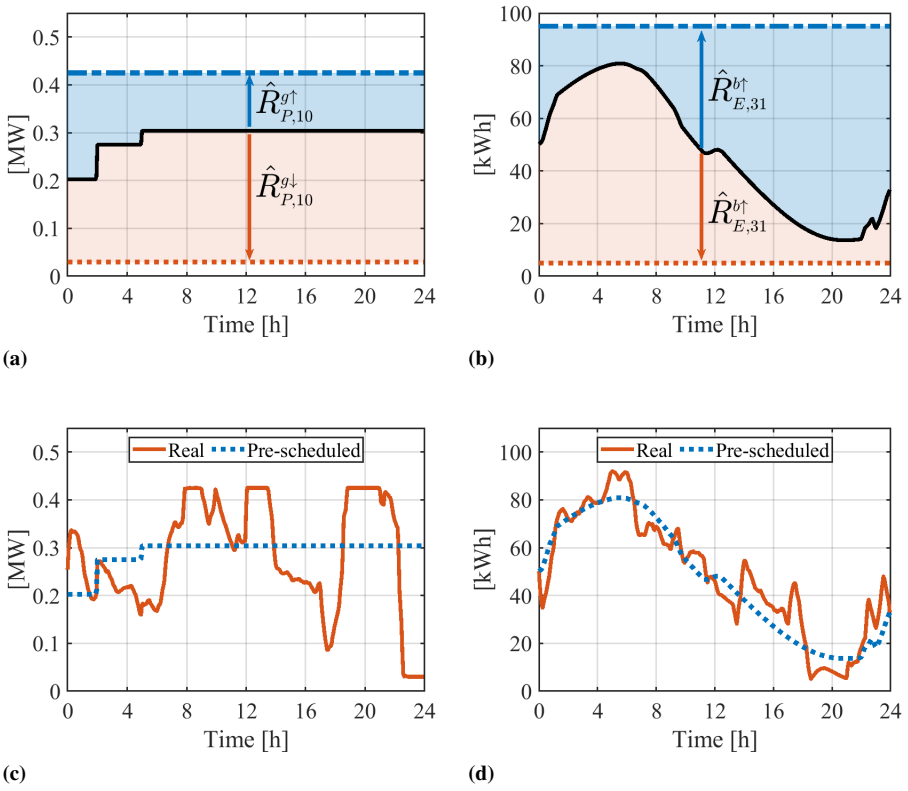

Figure 4.6: MG_{10} power trends: (a) Pre-scheduled power reserves for mGENs; (b) Pre-scheduled energy reserves for BESSs; (c) mGENs overall output power; (d) BESSs overall energy profile.

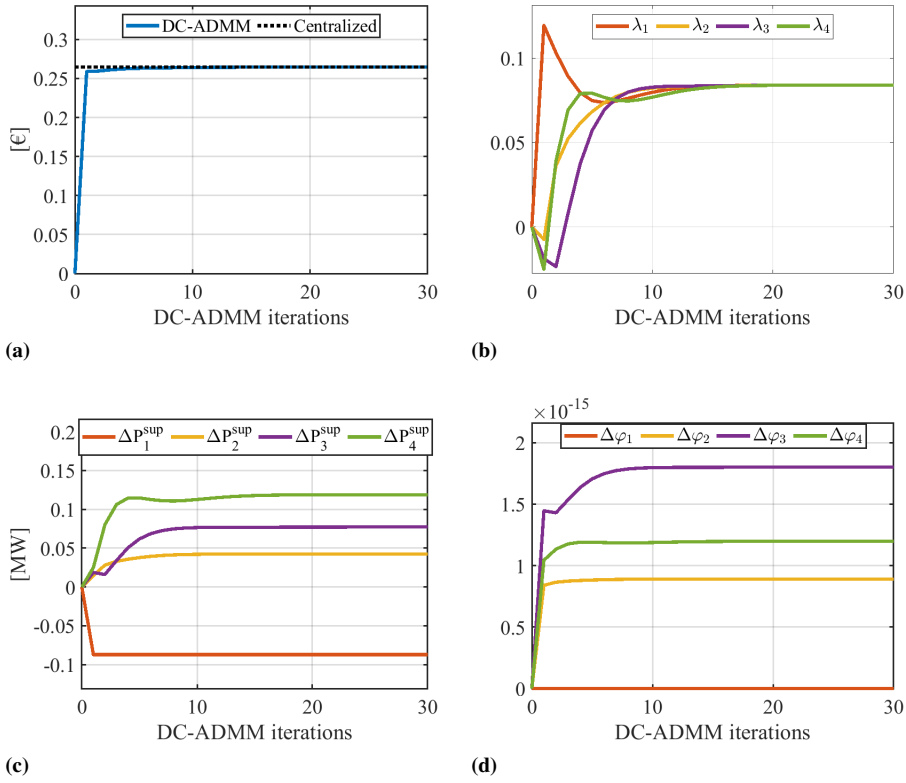

Figure 4.7: DC-ADMM performances at 21:00: (a) Optimal cost function of (4.36); (b) Local dual variables for each cluster; (c) Power variations committed by C-SUP to each cluster; (d) Slack variables for clusters' reserves.

4.3 A clustering technique for large-scale networks with shared resources

The previous section concerned the control of a network previously decomposed into grid areas, with the objective of balancing the local power variability in clusters. Moreover, clusters were also regulated to exchange power between them, supporting each other in case of necessity.

In this Section, it is shown how a network can be partitioned in clusters, using a novel procedure, with the objective of creating clusters as self-sufficient as possible. The partitioning approach is defined for networks composed of dispatchable and non-dispatchable elements, the first generally denoted as sources, while the second as sinks.
The method is described from a conceptual point view rather than focusing on a specific application, since it can be adopted for decomposing different types of networks, as the ones depicted in Figure 4.8. For instance, considering drinking water networks, sources correspond to the water pumps extracting the groundwater, while sinks are the water consumers. In district heating systems, diverse controllable sources of heat can be manipulated (e.g. waste heat from power plants or dedicated heating plants), while the residential houses operate as sinks.
With reference to electricity networks, the designed partitioning algorithm is eventually tested for decomposing large-scale electrical grids, as it will be shown in Paragraph 4.3.4.

The primary objective of the proposed method is the creation of clusters with the highest possible degree of independence, requiring for external assistance just in a few unlikely extreme scenarios, using for instance the control architecture proposed in Section 4.2. Another desired feature of the algorithm is to obtain "compact" clusters, keeping the distance between any individual pair of nodes within each cluster as small as possible. In this ways, the flows among long lines are reduced and most exchanges are addressed within clusters. Obviously, the network must be partitioned so that each cluster is as self-sufficient of possible, having enough sources to be able to balance most of the local sinks' demand.

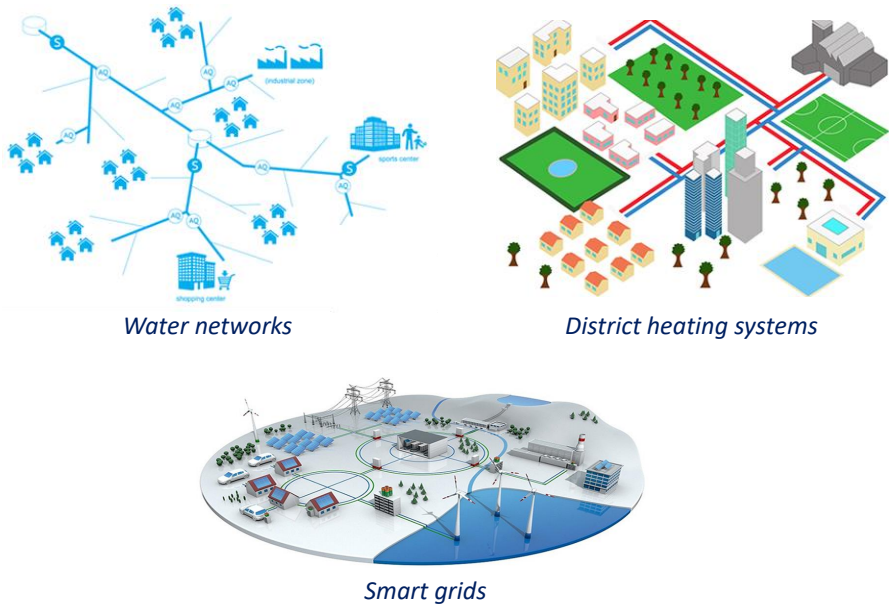

Figure 4.8: Three common examples of networked systems.

The proposed clustering procedure is structured as follows.

- The first step consists in associating sources to sinks, defining the optimal flow transactions between them. This is pursued through a properly defined optimization problem, aiming to minimize the total cost associated to the transactions, considering also constraints related to the capability of sources and the demand trends of sinks. The cost of transactions depends on the amount of resource exchanged and on a proper distance measure between sources and sinks. Since the network is assumed to be connected, each source can be associated to any sink of the network, defining the optimal flow transaction between them. Moreover, each source can be associated to more than one sink, and each sink demand can be satisfied by multiple source nodes.

- Once the optimal flow transactions between sources and sinks have been identified, these are projected onto the real network graph. As it will be explained in the next paragraphs, the transactions are mapped considering the shortest path which connects a source and a sink, in order to achieve clusters as compact as possible. The projection of transactions into the real network serves to define the weight of each edge, and consequently its importance in the network operations.
- Finally, the network graph is partitioned in a way to minimise the edge-cut, i.e. the sum of the weights of the edges connecting individual clusters. This is a specific instance of the so-called *k-way* partitioning problem, in which a given graph is divided into a predetermined amount of balanced, connected and non-overlapping clusters [87]. This task is here performed using the well-known software tool METIS [88], designed for graph partitioning problems.

The proposed partitioning procedure is described in the following.

4.3.1 Definition of optimal transactions between sources and sinks

First, define the set of sources as $\mathcal{S}$ and the set of sinks as $\mathcal{D}$. The variable x_{ij} denotes the amount of resource flowing from source $i \in \mathcal{S}$ to sink $j \in \mathcal{D}$, i.e. the flow transaction between the nodes. A slack variable is also introduced for feasibility issues, i.e. x_{sj}, identifying the amount of demand of sink j that is not provided by sources in $\mathcal{S}$. If the network to be partitioned is not isolated, e.g. connected to main utility as for the electrical case, $\sum_{j\in\mathcal{D}} x_{sj}$ corresponds to the total demand of resources satisfied by external sources.

The optimal transactions between sources and sinks can be defined according two approaches. The first computes the transactions such that sources satisfy the nominal demand of sinks. The second approach determines the transactions such that sources balance the worst-case variations of sinks' demand with respect to the nominal one. This distinction leads to the definition of two different procedures to compute the optimal transactions.

Transactions definition for nominal demand of sinks

In the following, the maximum and minimum capabilities of source i are denoted as $S_i^{\uparrow}$ and $S_i^{\downarrow}$, respectively, while the nominal demand of a sink j is denoted as D_j. Both the source capacities and sink demands are modelled as positive. For the sake of clarity, it is initially supposed that sources capabilities and sinks demands are defined as constant quantities. This assumption will be removed later, extending the approach to the time-varying case.
To compute the optimal transactions between sources and sinks, the following optimization problem is stated

$$\min_{x_{ij},x_{sj}} \sum_{i\in\mathcal{S}}\sum_{j\in\mathcal{D}} c_{ij}\,|x_{ij}| + \sum_{j\in\mathcal{D}} c_s\,|x_{sj}| \tag{4.43a}$$

subject to:

$$\sum_{j\in\mathcal{D}} x_{ij} \leq S_i^{\uparrow}, \quad \forall i \in \mathcal{S} \tag{4.43b}$$

$$\sum_{j\in\mathcal{D}} x_{ij} \geq S_i^{\downarrow}, \quad \forall i \in \mathcal{S} \tag{4.43c}$$

$$\sum_{i\in\mathcal{S}} x_{ij} + x_{sj} = D_j, \quad \forall j \in \mathcal{D}\,. \tag{4.43d}$$

Constraints (4.43b)-(4.43c) impose that the total transactions for each source i must respect its capability limits, while constraint (4.43d) ensures that the nominal demand of each sink is provided. Notice that the demand of sink j can be satisfied by different sources. For the sake of generality, it is assumed that transactions x_{ij} can be either positive or negative, therefore their absolute value is considered in the cost function (4.43a). The terms c_{ij} and c_s express the cost associated with transactions. Costs c_{ij} are defined as the distance between the node i and the node j, considering the real network graph. If a proper physical distance between the nodes is not available, c_{ij} can be also defined as the number of edges of the shortest path connecting source i and sink j. The variable x_{sj} must be used as a proper slack variable, i.e. just if local sources are not able to satisfy the nominal sinks demand, implying that $c_s > c_{ij}$, $\forall i \in \mathcal{S}$ and $\forall j \in \mathcal{D}$.

As (4.43) is solved, the optimal transactions between each source i and each sink j are computed, denoted as x^*_{ij}.

Remark 4.4. *It is important to note that* (4.43) *does not take into account any information on the underlying graph structure. This means that the obtained optimal transactions do not take into account any physical constraints of the network. This could imply that the transactions lead to exceed the capacity of the network lines. For the sake of simplicity, these constraints have been neglected here. However, these limits can be dealt with by considering an appropriate projection (mapping) of the transactions onto the network, while solving problem* (4.43).

Transactions definition for balancing worst-case demand variations

Consistently with the main purpose of the chapter, sources can be associated to sinks so as to balance the demand variability. Here, a worst-case approach is considered, supposing that the maximum upward and downward demand variation are available for each sink[2].
For each source i, the maximum upward and downward possible flow variations with respect to their nominal output are denoted as $\Delta s_i^{\uparrow}$ and $\Delta s_i^{\downarrow}$. On the other hand, $\Delta d_j^{\uparrow}$ and $\Delta d_j^{\downarrow}$ denote the maximum upward and downward demand variation, respectively, for each sink j. Since the mentioned variables are variations with respect to nominal values, these are defined such that $\Delta s_i^{\uparrow} \geq 0,\ \Delta s_i^{\downarrow} \leq 0$ and $\Delta d_j^{\uparrow} \geq 0,\ \Delta d_j^{\downarrow} \leq 0$.
The variable $x_{ij}^{\uparrow}$ is introduced, denoted as upward transaction, to define the flow transactions in case all sinks are characterized by the maximum demand variation, while $x_{ij}^{\downarrow}$, denoted as downward transaction, is used in case all sinks absorb the minimum demand. Following the same reasoning, also the slack variables $x_{sj}^{\uparrow}$ and $x_{sj}^{\downarrow}$ are introduced. The optimal transactions in the two cases can be computed through the following problems

[2]Depending on the information available, an alternative approach could rely on a stochastic reasoning in which a probability can be associated to each demand scenario. However, this approach could lead to a very complex problem statement (extremely high number of possible scenarios, especially in the presence of correlated behaviour of the sinks).

$$\min_{x_{ij}^{\uparrow}, x_{sj}^{\uparrow}} \sum_{i \in \mathcal{S}} \sum_{j \in \mathcal{D}} c_{ij} x_{ij}^{\uparrow} + \sum_{j \in \mathcal{D}} c_s x_{sj}^{\uparrow}$$

subject to:

$$\begin{aligned}
&\sum_{j \in \mathcal{D}} x_{ij}^{\uparrow} \leq \Delta s_i^{\uparrow}, \quad \forall i \in \mathcal{S} \\
&\sum_{i \in \mathcal{S}} x_{ij}^{\uparrow} + x_{sj}^{\uparrow} = \Delta d_j^{\uparrow}, \quad \forall j \in \mathcal{D} \\
&x_{ij}^{\uparrow} \geq 0, \quad \forall i \in \mathcal{S}, \;\; j \in \mathcal{D} \\
&x_{sj}^{\uparrow} \geq 0, \quad \forall j \in \mathcal{D},
\end{aligned} \tag{4.44}$$

and

$$\min_{x_{ij}^{\downarrow}, x_{sj}^{\downarrow}} \sum_{i \in \mathcal{S}} \sum_{j \in \mathcal{D}} -c_{ij} x_{ij}^{\downarrow} + \sum_{j \in \mathcal{D}} -c_s x_{sj}^{\downarrow}$$

subject to:

$$\begin{aligned}
&\sum_{j \in \mathcal{D}} x_{ij}^{\downarrow} \geq \Delta s_i^{\downarrow}, \quad \forall i \in \mathcal{S} \\
&\sum_{i \in \mathcal{S}} x_{ij}^{\downarrow} + x_{sj}^{\downarrow} = \Delta d_j^{\downarrow}, \quad \forall j \in \mathcal{D} \\
&x_{ij}^{\downarrow} \leq 0, \quad \forall i \in \mathcal{S}, \;\; j \in \mathcal{D} \\
&x_{sj}^{\downarrow}, \leq 0 \quad \forall j \in \mathcal{D}.
\end{aligned} \tag{4.45}$$

The optimal upward and downward transactions computed by the two problems are denoted as $x_{ij}^{\uparrow *}$ and $x_{ij}^{\downarrow *}$, respectively. At this stage, the overall transaction between source i and sink j is defined as

$$x_{ij}^{*} = x_{ij}^{\uparrow *} - x_{ij}^{\downarrow *}. \tag{4.46}$$

This "overall transaction" can be interpreted as the amount of control resource a source i has to deliver to balance the demand variation of a sink j, in the worst-case scenario. The higher this value, the more important source i is for the balancing of sink j variation.

A further refinement can be obtained if some prediction of the temporal evolution of the worst-case demands is available. Indeed, if a sink for instance has a very high possible worst-case demand at a specific time but is "well-behaved" otherwise, collocating it with a very potent source just to compensate for this one event may be undesirable. Suppose that the known trends are defined with a proper sampling time τ_c from the time instant t_0 to the time instant T_c. Therefore, the optimization problems (4.44) and (4.45) can be extended to the time-variant case as follows

$$\min_{x_{ij}^{\uparrow}(t),x_{sj}^{\uparrow}(t)} \sum_{t=t_0}^{T_c} \left(\sum_{i\in\mathcal{S}} \sum_{j\in\mathcal{D}} c_{ij} x_{ij}^{\uparrow}(t) + \sum_{j\in\mathcal{D}} c_s x_{sj}^{\uparrow}(t) \right)$$

$$\begin{aligned} \text{s.t.}, \forall t \in \{t_0, \dots, T_c\}, & \\ & \sum_{j\in\mathcal{D}} x_{ij}^{\uparrow}(t) \leq \Delta s_i^{\uparrow}(t)\,, \quad \forall i \in \mathcal{S} \\ & \sum_{i\in\mathcal{S}} x_{ij}^{\uparrow}(t) + x_{sj}^{\uparrow}(t) = \Delta d_j^{\uparrow}(t)\,, \quad \forall j \in \mathcal{D} \\ & x_{ij}^{\uparrow}(t) \geq 0\,, \quad \forall i \in \mathcal{S},\ j \in \mathcal{D} \\ & x_{sj}^{\uparrow}(t) \geq 0\,, \quad \forall j \in \mathcal{D}\,, \end{aligned} \tag{4.47}$$

and

$$\min_{x_{ij}^{\downarrow}(t),x_{sj}^{\downarrow}(t)} -\sum_{t=t_0}^{T_c} \left(\sum_{i\in\mathcal{S}} \sum_{j\in\mathcal{D}} c_{ij} x_{ij}^{\downarrow}(t) + \sum_{j\in\mathcal{D}} c_s x_{sj}^{\downarrow}(t) \right)$$

$$\begin{aligned} \text{s.t.}, \forall t \in \{t_0, \dots, T_c\}, & \\ & \sum_{j\in\mathcal{D}} x_{ij}^{\downarrow}(t) \leq \Delta s_i^{\downarrow}(t)\,, \quad \forall i \in \mathcal{S} \\ & \sum_{i\in\mathcal{S}} x_{ij}^{\downarrow}(t) + x_{sj}^{\downarrow}(t) = \Delta d_j^{\downarrow}(t)\,, \quad \forall j \in \mathcal{D} \\ & x_{ij}^{\downarrow}(t) \leq 0\,, \quad \forall i \in \mathcal{S},\ j \in \mathcal{D} \\ & x_{sj}^{\downarrow}(t) \leq 0\,, \quad \forall j \in \mathcal{D}\,. \end{aligned} \tag{4.48}$$

The optimal transactions computed by problems (4.47) and (4.48), denoted as $x_{ij}^{\uparrow *}(t)$ and $x_{ij}^{\downarrow *}(t)$, are therefore condensed as follows

$$X_{ij}^{\uparrow *} = \sum_{t=t_0}^{T_c} x_{ij}^{\uparrow *}(t), \qquad X_{ij}^{\downarrow *} = \sum_{t=t_0}^{T_c} x_{ij}^{\downarrow *}(t)\,, \tag{4.49}$$

representing the cumulative transactions over the whole prediction horizon between the source i and the sink j. The overall transaction is then defined as

$$x_{ij}^{*} = X_{ij}^{\uparrow *} - X_{ij}^{\downarrow *}. \tag{4.50}$$

4.3.2 Transactions projection onto shortest path

The obtained optimal overall transactions between sources and sinks are now mapped onto the graph representing the actual network. This operation serves to identify the weights of each edge, which will then essentially determine which edges will be cut by the partitioning algorithm.
The transactions projection can be performed using different methods. For instance, the physical equations governing the network could be used to obtain the flows in each edge of the network, leading however to a complex and not generalizable procedure.
Here, it is proposed to project the optimal transaction between the source i and the sink j on the shortest path connecting the nodes. Other than being a general and easily-implementable approach, this has the further advantage of obtaining clusters as compact as possible. It is worth noticing that the definition of shortest path makes sense just for meshed networks, since in the radial case each node is connected to another just by a unique path.

The projection of the optimal transactions onto the shortest path can be mathematically defined as follows.
First, denote the set of all nodes in the network with $\mathcal{V} = \{1, ..., N\}$ and the set of undirected edges as $\mathcal{E} \subseteq \mathcal{V} \times \mathcal{V}$. An edge l is denoted $l = (a, b) = (b, a)$, where $a, b \in \mathcal{V}$. Then, the shortest path between a source i and a sink j can be defined as the set of edges

$$\mathcal{L}_{ij} = \{(i, a_1), (a_1, a_2), (a_2, a_3), ..., (a_n, j)\}\,, \tag{4.51}$$

where $a_m \in \mathcal{V}$ and $(a_m, a_n) \in \mathcal{E}$, such that there is no path between i and j with less than $n+1$ edges.
It should be noted that the shortest path between two nodes may not be unique, in which case $\mathcal{L}_{ij}$ is chosen arbitrarily among the shortest paths. Several algorithms for identifying a shortest path between two nodes exist, such as Dijkstra's algorithm [89].

In order to be able to consider transactions with opposite direction on the same edge, a reference orientation must be assigned to each edge. Considering that each edge $l \in \mathcal{E}$ is characterized by two end-nodes, the orientation is here defined from the node with the lower index to the one with the higher index. Furthermore, for a given edge $l \in \mathcal{E}$ and a given transaction x_{ij}, the end-node of l closer to source i is denoted as a_i, while the one closer to sink j is denoted as a_j.

It is now possible to properly define the projection of the optimal transaction x^*_{ij} onto any edge l of the graph, denoted as $x_{ij,l}$. Introducing $\perp_{sp}$ as the "shortest path projection" operator, this is defined as

$$x_{ij,l} = x_{ij} \perp_{sp} l = \begin{cases} 0 & \text{if} \quad l \notin \mathcal{L}_{ij} \\ x^*_{ij} & \text{if} \quad a_i < a_j \\ -x^*_{ij} & \text{if} \quad a_i > a_j \end{cases} . \tag{4.52}$$

Indeed, if the transaction x_{ij}, defined as directed from the source towards the sink, crosses the edge with the same orientation of the edge (i.e. from the end-node with the lower index to the one with the higher index), the projection is equal to the effective value of the transaction. In the opposite case, the projection of the transaction corresponds to its negative.
At this stage, the total flow on each edge l, under the shortest path assumption, can be defined as follows

$$w_l = \left| \sum_{i \in \mathcal{S}} \sum_{j \in \mathcal{D}} x_{ij,l} \right| = \left| \sum_{i \in \mathcal{S}} \sum_{j \in \mathcal{D}} x^*_{ij} \perp_{sp} l \right| , \tag{4.53}$$

defining therefore the weight of each edge of the network based on the transactions between sources and sinks.

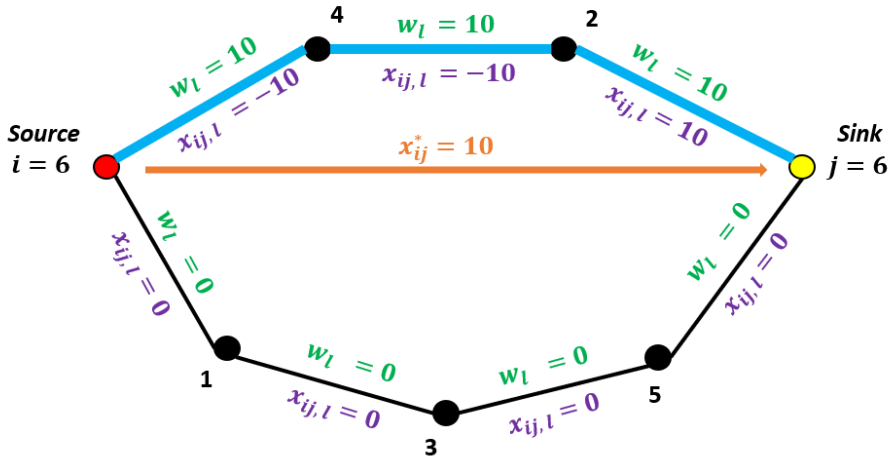

Figure 4.9: A simple illustration of the transaction projection onto the shortest path in the case of a single transaction.

Figure 4.9 gives a simple illustration of the described procedure to map transactions on shortest paths. Node indices ranging from 1 to 7 are given by standard face black numbers. The optimal transaction $x^*_{ij} = 10$ between source $i = 6$ and sink $j = 7$ is depicted with an orange line (note that this is *not* an edge of the graph). The shortest path connecting the source and the sink is indicated with a thick light blue line and it is given by the following edges: $\mathcal{L}_{ij} = \{(6, 4), (4, 2), (2, 7)\}$. The projections $x_{ij,l} = x_{ij} \perp_{sc} l$ following equation (4.52) are indicated in purple while the final w_l terms, computed according to equation (4.53) are indicated in green. At this stage, consider edge $l = (4, 2)$. Following the described definition, for this node $a_i = 4$ (being the end-node closer to the source) and $a_j = 2$ (being the end-node closer to the sink). Therefore, $a_i > a_j$, it implies that $x_{ij,l} = -x_{ij} = -10$. Although this procedure may seem sophisticated, it is an effective tool to properly compute the weights when more transitions with opposite directions cross the same edge.

4.3.3 Minimal edge-cut partitioning using METIS

The terms w_l defined in (4.53) identify the weights of each edge of the network, which are then used to carry out the *k-way* partitioning of the graph. The overall network is decomposed by minimizing the edge-cut, i.e. the sum of the weights of the edges connecting individual clusters.
This procedure is carried out supposing to define a-priori the number of clusters. In fact, determining both the size and the optimal number of clusters is a complex problem, and some heuristic approaches have been proposed in the literature, as in [90], Graph partitioning and clustering problems arise in many fields of science and technology and have been studied extensively. Therefore, the use of the already existing tool METIS [88] to perform the partitioning is proposed here. For more details on METIS, the reader is referred to [91] and [92].

4.3.4 Numerical results

The proposed procedure has been tested to partition two large-scale electrical networks: the IEEE 118 and the IEEE 123 bus systems.
The first is a meshed network, as shown in Figure 4.10, and it is based on a real transmission network in the United States with 91 loads and 19 generators [93]. The IEEE 118 bus system has been decomposed trying to define clusters as self-sufficient as possible, i.e. where sources nominally satisfy the sink demands. This is accomplished defining the transactions through the problem expressed in (4.43). The data set in [93] provides a stable operating point of the network for a given demand of the loads, as well as the maximum rate of the generators.
Figure 4.11 gives an indication of the computed optimal transactions between sources and sinks, whose numerical values are not shown for reasons of legibility. Then, all the transactions are projected onto the shortest paths connecting each source to the associated sink, and the weights w_l are determined as in (4.53). Finally, the METIS toolbox has been applied, specifying a predefined number of 4 clusters. The generated clusters are illustrated in Figure 4.12, which show to be compact and well in agreement with the transactions depicted in Figure 4.11.

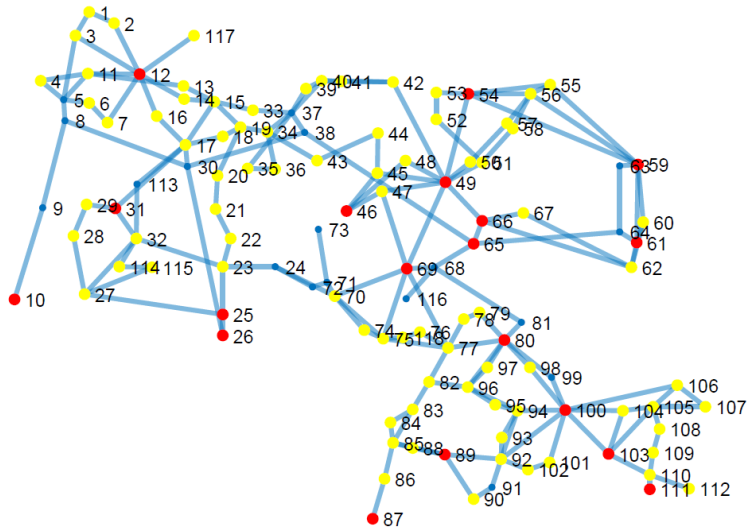

Figure 4.10: The IEEE-118 transmission network (generators in red, loads in yellow).

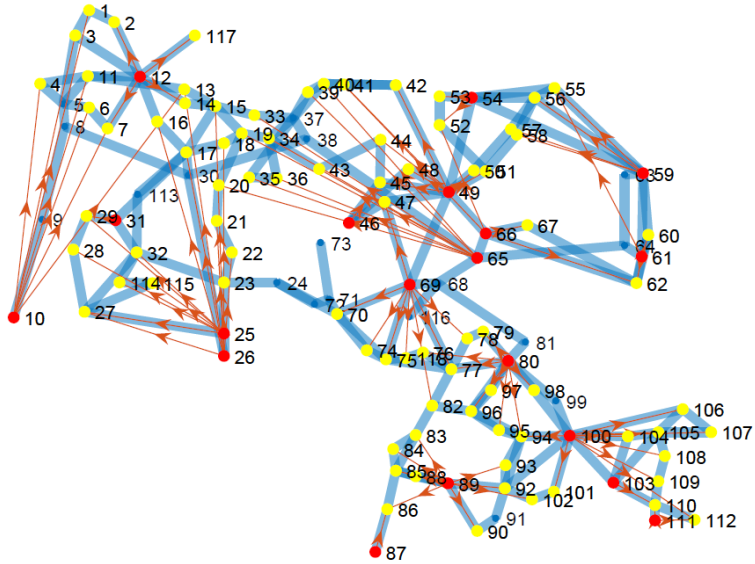

Figure 4.11: Indication of the optimal regulatory transactions for the IEEE-118 transmission network.

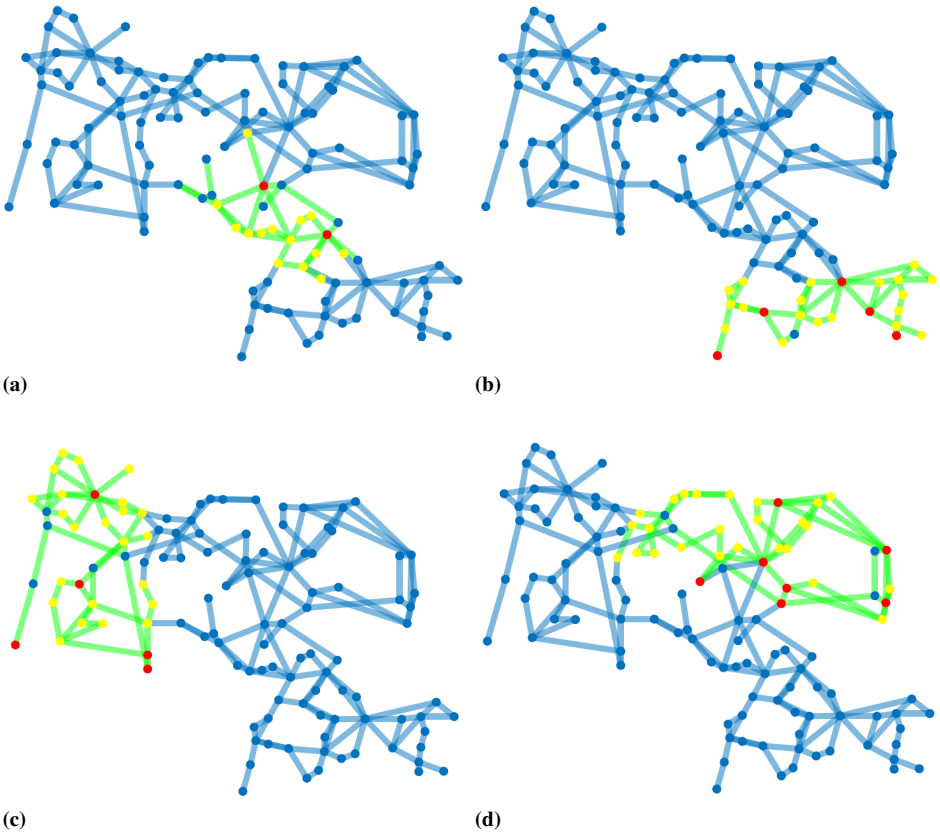

Figure 4.12: Clusters obtained by partitioning the IEEE-118 transmission network with the self-sufficient clusters objective. Nodes in the respective cluster are highlighted according to the previous colour scheme with edges connecting nodes in the respective cluster highlighted in green.

The proposed procedure is also applied to the IEEE-123 bus system, which is a radial distribution feeder composed of 123 nodes and 85 loads. A schematic diagram is shown in Figure 4.13. However, the original distribution feeder does not contain any generators, and therefore a number of generators has to be placed in the network as proposed in [94]; the original network data for loads are instead taken from [95]. This network, conversely to the previous test-case, is decomposed so that sources are able to balance the maximum and minimum demand variations of each sink with respect to the nominal one. The scheduled reserves of the generators and the forecasted worst-case deviations of the loads are based on the data given in [94] and [95] according to the following formula

$$\Delta s_i^{\uparrow} = 0.55\,(0.8 + 0.4 r_i) \cdot P_i^{data} \qquad \forall i \in \mathcal{G} \tag{4.54}$$

$$\Delta s_i^{\downarrow} = -0.55\,(0.8 + 0.4 r_i) \cdot P_i^{data} \qquad \forall i \in \mathcal{G} \tag{4.55}$$

$$\Delta d_j^{\uparrow} = (0.8 + 0.4 r_j) \cdot P_j^{data} \qquad \forall j \in \mathcal{L} \tag{4.56}$$

$$\Delta d_j^{\downarrow} = -\,(0.8 + 0.4 r_j) \cdot P_j^{data} \qquad \forall j \in \mathcal{L}, \tag{4.57}$$

where $r_{i/j}$ are random numbers, defined between zero and one, while $P_{i/j}^{data}$ correspond to the the nominal powers from the dataset. The upward and downward optimal transactions between sources and sinks have been therefore computed solving problems (4.44) and (4.45), respectively, and then the overall optimal transactions are defined using (4.46). The optimal transactions are depicted in 4.14, where it can be noted that some loads, such as those located at nodes 85, 113 or 114, are not involved in any transactions. This is a natural consequence of the proposed approach which includes a slack node, and it can be a realistic situation where the available reserves in local sources are not sufficient to balance the overall load variability. Being a radial network, the transactions can be uniquely mapped in the network graph, since it exists only one path between each source and sink.
Finally, the METIS toolbox is applied to partition the network, predefining a number of 6 clusters. Figure 4.15 shows the final partitioning, where notably all clusters are defined as connected and compact portions of the overall network.

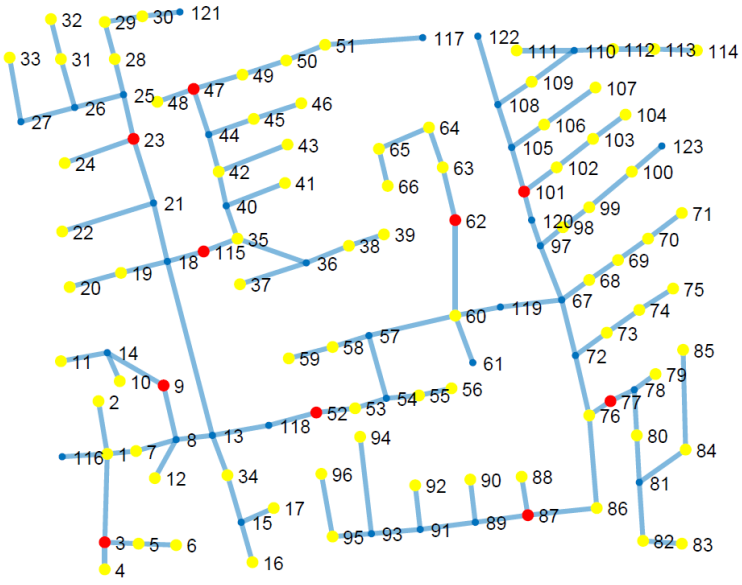

Figure 4.13: The IEEE-123 test feeder (generators in red, loads in yellow).

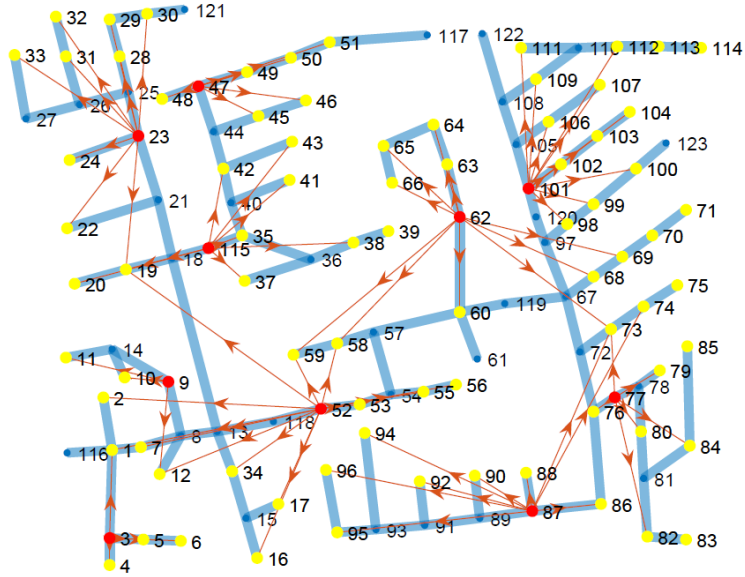

Figure 4.14: Indication of the optimal regulatory transactions computed for the IEEE-123 test feeder.

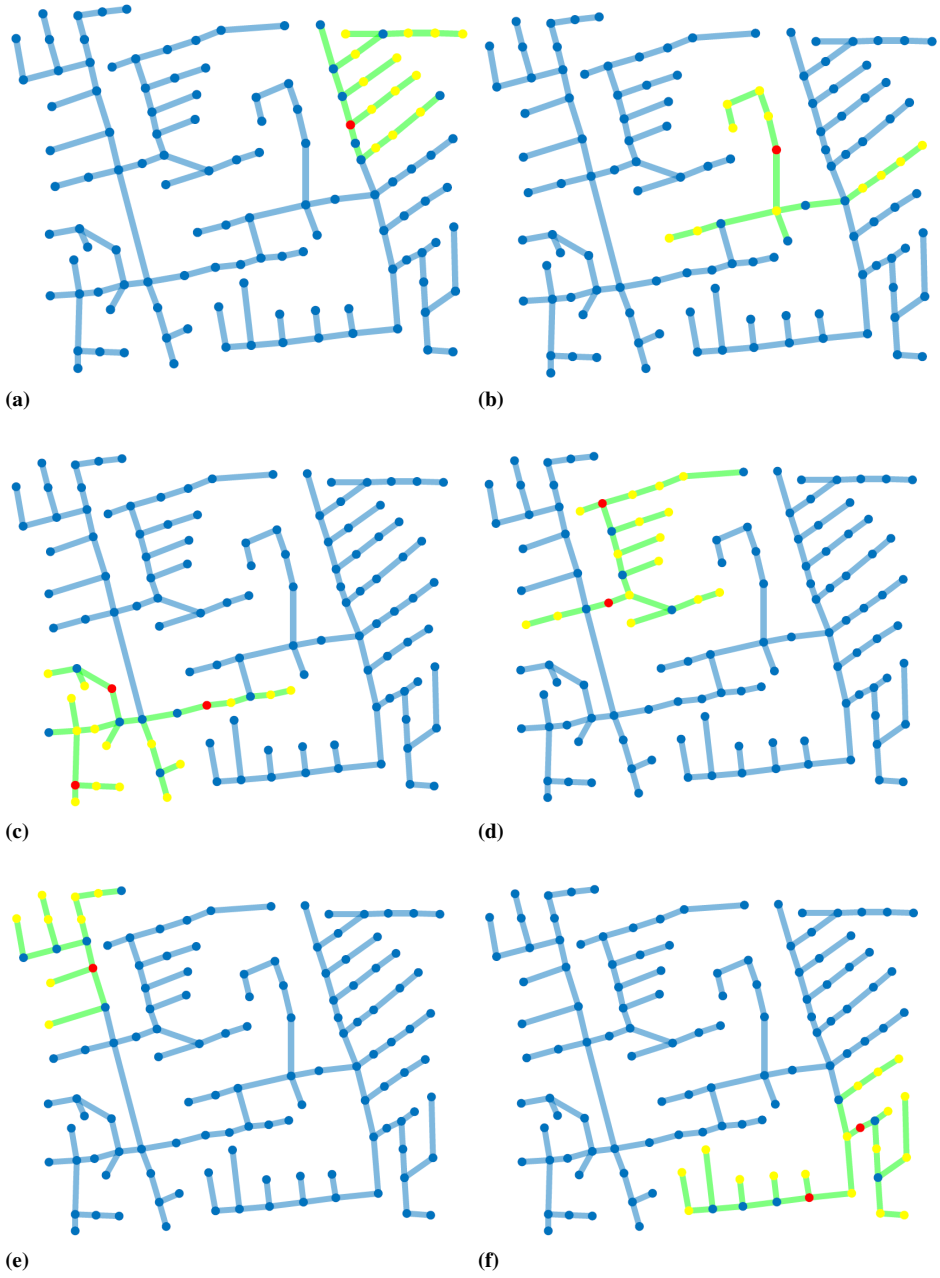

Figure 4.15: Clusters obtained by partitioning the IEEE-123 test feeder.

4.4 Conclusions

This chapter concerned two main problems. In Section 4.2 a novel supervised MPC control architecture has been proposed to coordinate different grid areas. The main objective is to balance the power variability in the distribution network using the offered reserves in MGs, so as to respect a predefined power exchange with the main utility. The numerical results witness the potentiality of the proposed approach, ensuring both the quick compensation of power imbalances and enhanced scalability proprieties.

Section 4.2 describes a new partitioning algorithm, applied to distribution grids, but actually generalizable to other types of networks. The method shows to be very efficient in decomposing large-scale networks, allowing to obtain compact and self-sufficient partitions, where sources and sinks are clustered to ensure the overall balance.

CHAPTER 5

A data-driven approach to estimate microgrids internal scheduling

5.1 Introduction

In Chapter 2, it has been shown how Microgrids Aggregators (MG-AGs) can be coordinated by a supervisory system, i.e. the Aggregator Supervisor (AGS), to optimally schedule their units based on the energy price trends, providing also the required amount of power reserves to provide balancing services to the main utility. To protect Microgrids (MGs) internal information and to reduce the overall problem complexity, a distributed optimization strategy was proposed where the AGS iteratively updates some internal prices, i.e. the dual variables, such that the overall optimal scheduling of the MG-AGs is obtained.
The proposed procedure is an effective tool to be applied when energy prices have been already defined through the day-ahead and intra-day

markets. On the other hand, the AGS could also directly participate to the auction processes of energy markets to effectively define the energy prices, submitting the supply/demand bids for the whole MG-AGs. Performing this operation, without relying on centralized approaches, implies that the distribution optimization algorithm discussed in Chapter 2 must be repetitively executed in order to assess the MG-AG optimal power output for each realization of the energy prices, resulting in a quite long and inefficient procedure. Because of this, an estimation procedure is proposed in this chapter, which allows the AGS to efficiently evaluate how much its MG-AG is going to produce/absorb for a given trend of energy prices. Precisely, an approximated data-based model of each MG is derived, using just historical data of output power vs. energy prices, which are available to the AGS.

5.1.1 Proposed solution

It is assumed that the AGS has no information on the layout of each MG and on the power trends of the non-dispatchable units (e.g. renewable sources and loads). The main contribution is the use of a nonlinear Set Membership (SM) estimation approach [96] to perform the described estimation problem. This identification technique provides both a nominal estimate and guaranteed uncertainty bounds. This is a significant advantage, since the AGS can have knowledge of not only a nominal estimate of the MG power trend as a function of the energy prices, but also of certified power deviation bounds, accounting for the uncertainty.
An important feature of the proposed method is that it requires rather mild assumptions on the uncertain components of produced/consumed power, which are simply required to be bounded. This suits very well the considered application, since the trends of loads and renewable sources, although unknown to the AGS, are for sure bounded by their maximum power production/absorption values. The considered SM technique features tuning parameters that have to be chosen by the user: the assumed Lipschitz constant γ of the function to be learned, and the bound ϵ on the additive uncertainty. Without any a-priori knowledge on the system, the tuning of (γ, ϵ) might be time-consuming, see [96] for a discussion. As an additional contribution of this chapter, an optimization-based tuning

procedure is proposed for (γ, ϵ) that aims to minimize the uncertainty interval associated with the nominal predicted power output, which is the most important feature in the considered application context. This chapter represents a first study to evaluate the applicability of the proposed method, its accuracy and conservativeness.

5.2 Problem formulation

Each MG schedules the power set-points for its generating units and controllable loads, aiming to maximize its internal profit, considering also the effect of the non-dispatchable units (see the MG model described in Paragraph 3.2.1). Therefore, considering the standard 15-minutes sampling interval, the scheduled power output y of each MG can be expressed as

$$y(t, \mathbf{p_e}) = f_t(\mathbf{p_e}) + d(t),\ t = 1, \dots, T, \tag{5.1}$$

where t is the discrete time variable, $T = 96$ is the number of considered time instants (i.e. one full day), $\mathbf{p_e} = \{p_e(1), \dots, p_e(T)\}^\top \in \mathbb{R}^T$ is the course of energy prices at 15-min intervals along the day ($^\top$ denotes the matrix transpose operator and bold-faced quantities denote vectors). Finally, $d(t)$ is an additive disturbance term, accounting for the effect of the non-dispatchable units and loads. For notational simplicity, in the remainder a single MG is considered; the whole approach presented in the chapter can be then applied in parallel to all the MGs associated with the MG-AG. The AGS needs a model of the form (5.1) for each MG, i.e. an estimate $\tilde{y}(t, \mathbf{p_e}) \approx y(t, \mathbf{p_e})$. It is proposed to learn a separate model for each time instant. Moreover, a finite data-set is assumed to be available, given by the following two sequences

$$\begin{aligned} Y_t &= \{\tilde{y}^{(1)}(t, \tilde{\mathbf{p}}_\mathbf{e}^{(1)}), \dots, \tilde{y}^{(N)}(t, \tilde{\mathbf{p}}_\mathbf{e}^{(N)})\} \\ P_e &= \{\tilde{\mathbf{p}}_\mathbf{e}^{(1)}, \dots, \tilde{\mathbf{p}}_\mathbf{e}^{(N)}\} \end{aligned} \tag{5.2}$$

where $\tilde{x}$ denotes a sampled data point of the generic variable x, $\tilde{y}^{(j)}(t)$ is the observed power that the MG provides at instant t in response to the energy price sequence $\tilde{\mathbf{p}}_\mathbf{e}^{(j)}$, and N is the total number of data points. Note that, due to the mentioned uncertainty in Renewable Energy Sources

(RESs) and non-controllable loads, for any $\tilde{\mathbf{p}}_{\mathbf{e}}^{(j)} = \tilde{\mathbf{p}}_{\mathbf{e}}^{(k)}$, $j \neq k$, it may occur to have $\tilde{y}^{(j)}(t) \neq \tilde{y}^{(k)}(t)$.
In the described scenario, the main goal of the proposed procedure is summarized as follows.

Problem 1. From the available data set Y_t, P_e, derive $T = 96$ approximating functions $f_t : \mathbb{R}^T \to \mathbb{R}$ such that

$$\hat{y}(t, \mathbf{p_e}) = \hat{f}_t(\mathbf{p_e}),\ t = 1, \dots, T. \tag{5.3}$$

Moreover, for each considered t, derive two additional functions, $\bar{f}_t$ and $\underline{f}_t$, and an additive uncertainty bound, ϵ_t, providing guaranteed upper and lower bounds on $y(t)$

$$\underline{f}_t(\mathbf{p_e}) - \epsilon_t \leq y(t, \mathbf{p_e}) \leq \bar{f}_t(\mathbf{p_e}) + \epsilon_t,\ t = 1, \dots, T. \tag{5.4}$$

The estimators $\hat{f}_t(\mathbf{p_e})$ and the guaranteed uncertainty intervals $\overline{f}_t(\mathbf{p_e}) - \underline{f}_t(\mathbf{p_e}) + 2\epsilon_t$, $t = 1, \dots, T$, could be then used by the AGS in the day-ahead bidding process. This part is not treated in this chapter, whose main focus is instead on **Problem 1**. In Section 5.4 the use of SM identification to solve this problem is proposed, together with a novel tuning procedure for the identification routine. The designed procedure is applied to synthetic data, produced by simulating the optimization problem that a real MG would solve to schedule its elements. This allows to evaluate two aspects: 1) whether at a theoretical level the working assumptions of the considered SM technique are satisfied, and 2) the estimation accuracy that can be achieved in an ideal scenario. The employed MG model is described in the following.

5.3 Microgrid optimal scheduling model

A generic MG is considered, equipped with n^g Micro-Generators (mGENs), n^b Battery Energy Storage Systems (BESSs), n^r RESs and n^l non-dispatchable loads. Moreover, also the presence of controllable loads (CLs) is assumed, for simplicity modelled with continuous vari-

Table 5.1: MG optimization variables and parameters

Symbol	Description
p^g	mGEN active power set-point [kW]
p^b	BESS active power set-point [kW]
s^b	State of charge (SOC) [%]
p^{sl}	Shifting load active power output [kW]
p^{rl}	Reducible load effective active power output [kW]
d^l	Non-dispatchable load active power output [kW]
d^r	RES active power output [kW]
y^{mg}	MG active power output [kW]
C^b	BESS capacity [kWh]
$\bar{e}^{sl}$	Shifting loads energy demand [kWh]
$\bar{\tau}^{sl}$, $\underline{\tau}^{sl}$	Shifting loads time limits [h]
$\hat{d}^{rl}$	Reducible load predefined active power output [kW]
$\Delta\bar{d}^{rl}$	Max reducible loads power reduction [kW]
$\bar{\tau}^{rl}$, $\underline{\tau}^{rl}$	Reducible loads time limits [h]
c^{rl}	Reducible load cost [€/kWh^2]
c^b	BESS usage cost [€/kWh^2]
a^g, b^g, c^g	mGEN cost coefficients [€/kWh^2, €/kWh, €]
p_e	Energy price [€/kWh]

ables. Precisely, the generic MG is modelled with n^{rl} reducible loads and n^{sl} shifting loads, where the first allow to reduce the load demand, while the second can be shifted, but it must maintain the pre-defined energy demand. The variables and parameters of the MG elements are described in Table 5.1. For the sake of simplicity, the active power reserves of MGs are not modelled in this chapter. Moreover, as a convention, all the power values are positive if delivered and negative if absorbed, while maximum and minimum limits of each variable are denoted with a bar over or below the variable, respectively.
Considering mGENs and BESSs, their output power at time step t is constrained by the capability limits. Therefore, $\forall j \in \{1, \ldots, n^g\}$ and

$\forall i \in \{1, \dots, n^b\}$, it follows

$$\underline{p}_j^g \;\leq\; p_j^g(t) \;\leq\; \bar{p}_j^g, \qquad \underline{p}_i^b \;\leq\; p_i^b(t) \;\leq\; \bar{p}_i^b \,. \tag{5.5}$$

The state of charge (SOC) of BESSs is modelled as a pure integrator and it is bounded by predefined limits. Moreover, it is supposed that the SOC at the end of the day must be equal to the one at the beginning, in order to start the next day with the same initial storage conditions. Therefore, $\forall j \in \{1, \dots, n^b\}$,

$$s_j^b(t+1) \;=\; s_j^b(t) \;-\; 100\,\frac{\tau}{C_j^b}\,u_j^b(t)\,, \tag{5.6a}$$

$$\underline{s}_j^b \;\leq\; s_j^b(t) \;\leq\; \bar{s}_j^b, \quad s_j^b(T) = s_j^b(0)\,. \tag{5.6b}$$

The shiftable, or deferrable, loads are usually characterized by active power limits and, moreover, they can be activated just in a predefined time range where a specific amount of energy demand must be satisfied. Therefore, the following constraints are imposed, $\forall j \in \{1, \dots, n^{sl}\}$,

$$\underline{p}_j^{sl} \;\leq\; |p_j^{sl}(t)| \;\leq\; \bar{p}_j^{sl}\,, \quad \forall\, t \;\in \{\underline{\tau}_j^{sl}, \bar{\tau}_j^{sl}\}\,, \tag{5.7a}$$

$$p_j^{sl}(t) \;=\; 0\,, \qquad\qquad \forall\, t \;\notin \{\underline{\tau}_j^{sl}, \bar{\tau}_j^{sl}\}\,, \tag{5.7b}$$

$$\sum_{\forall\, t \in \{\underline{\tau}_j^{sl}, \bar{\tau}_j^{sl}\}} |p_j^{sl}(t)|\,\tau = \bar{e}_j^{sl}\,. \tag{5.7c}$$

The reducible loads allow the MG operator to reduce their consumption in certain time slots, with respect to the predefined fixed demand $\hat{d}^{rl}$, within a maximum reduction limit,$\forall j \in \{1, \dots, n^{rl}\}$,

$$|\hat{d}_j^{rl}(t) \;-\; p_j^{rl}(t)| \;\leq\; \Delta\bar{d}^{rl}\,, \qquad \forall\, t \;\in \{\underline{\tau}_j^{rl}, \bar{\tau}_j^{rl}\}\,, \tag{5.8a}$$

$$|\hat{d}_j^{rl}(t) \;-\; p_j^{rl}(t)| \;=\; 0\,, \qquad \forall\, t \;\notin \{\underline{\tau}_j^{rl}, \bar{\tau}_j^{rl}\}\,. \tag{5.8b}$$

For simplicity, the sum of all active power setpoints of the dispatchable units (i.e. the MG decision variables) and the sum of active power values

of non-dispatchable units (i.e. the disturbance variables) are collected in two vectors, $\mathbf{u}$ and $\mathbf{d}$, respectively

$$\begin{aligned}
\mathbf{u} &= [u(1), \dots, u(T)]^\top \in \mathbb{R}^T , \\
u(t) &= \sum_{j=1}^{n^g} p_j^g(t) + \sum_{j=1}^{n^b} p_j^b(t) + \sum_{j=1}^{n^{sl}} p_j^{sl}(t) + \sum_{j=1}^{n^{rl}} p_j^{rl}(t) , \\
\mathbf{d} &= [d(1), \dots, d(T)]^\top \in \mathbb{R}^T , \\
d(t) &= \sum_{j=1}^{n^l} d_j^l(t) + \sum_{j=1}^{n^r} d_j^r(t) .
\end{aligned}$$

The cost function to be minimized is now introduced (see Table 5.1 for the involved parameters) as

$$\begin{aligned}
J = & \underbrace{\sum_{t=1}^{T} \sum_{j=1}^{n^g} (a_j^g \tau^2 (p_j^g(t))^2 + b_j^g \, \tau \, p_j^g(t) + c_j^g)}_{\alpha} + \\
& + \underbrace{\sum_{t=2}^{T} \sum_{j=1}^{n^b} c_j^b \tau^2 \left(p_j^b(t) - p_j^b(t-1)\right)^2}_{\beta} + \\
& + \underbrace{\sum_{t=1}^{T} \sum_{j=1}^{n^{rl}} c_j^{rl} \tau^2 (d_j^{rl}(t) - p_j^{rl}(t))^2}_{\eta} \\
& - \sum_{t=1}^{T} \tau (\underbrace{p_e(t)}_{\gamma} (u(t) + d(t))) ,
\end{aligned} \tag{5.9}$$

where all the costs/prices are multiplied by the sampling time τ, since they are commonly referred to the amount of energy generated/consumed. The mGENs cost α is modelled with a quadratic polynomial function, as common in the literature. Although BESSs do not have an effective cost, the term β is expressed to penalize the square of the power variation to avoid excessive charges and discharges which may reduce the BESS life.

Since the load reducible usually leads to some discomfort issues, their power reduction will be characterized by a cost expressed by the term η, as in [97]. Finally, the term γ indicates the net output power of the MG. In this study, the MG management system is supposed to solve the following optimization problem

$$\begin{aligned} &\min_{\mathbf{u}} \quad J \\ &\text{subject to} \quad (5.5) \text{ - } (5.8) \end{aligned} \tag{5.10}$$

Note that (5.10) is a convex quadratic program (QP), for which a global minimizer can be efficiently computed. Moreover, under reasonable assumptions on the MG constraints and weights in the cost function, the problem is strictly convex and such a minimizer is unique. Let us denote with $\mathbf{u}^*(\mathbf{p_e}) = [u^*(1, \mathbf{p_e}), \dots, u^*(T, \mathbf{p_e})]^\top$ a global minimizer of (5.10). Then, by the internal power balance, the MG power output at each time t is given by

$$y(t, \mathbf{p_e}) = u^*(t, \mathbf{p_e}) + d(t). \tag{5.11}$$

Remark 5.1. *Note that the terms $d(t)$, $t = 1, \dots, T$ do not affect the value $\mathbf{u}^*(\mathbf{p_e})$, since in (5.9) they contribute to an additive offset that doesn't depend on the optimization variables. Thus, the solution of (5.10) depends only on the predicted prices $\mathbf{p_e}$, and (5.11) can be equivalently expressed as*

$$y(t, \mathbf{p_e}) = \underbrace{f_t(\mathbf{p_e})}_{u^*(t, \mathbf{p_e})} + d(t), \tag{5.12}$$

which is consistent with the problem setup, see (5.1). Moreover, by the implicit function theorem, strict convexity of (5.10) results in Lipschitz continuity of functions $f_t(\mathbf{p_e})$, $t = 1, \dots, T$. Finally, the additive term $d(t)$ accounts for all uncertain, non-controllable sources and loads, and it is a bounded quantity with generally unknown bounds, that can however be estimated from data.

Overall, the features highlighted in Remark 5.1 fit perfectly with the prior assumptions of the adopted SM identification approach, recalled in the next section.

To generate the data that will be used for the estimation procedures, the problem (5.10) is solved with a finite number N of energy price courses $\tilde{\mathbf{p}}_{\mathbf{e}}^{(j)}$ and uncertain (e.g. random) values of $\tilde{d}(t)^{(j)}$, and the resulting values of $\tilde{y}(t, \tilde{\mathbf{p}}_{\mathbf{e}}^{(j)})$ computed as in (5.12), for all $t = 1, \dots, T$ and $j = 1, \dots, N$ are stored. Then, this data is collected in the sequences $Y_t,\ P_e$, see (5.2).

5.4 Identification procedure

The SM identification approach proposed in [96] is summarized, and then employed here to solve **Problem 1**. Moreover, the novel proposed optimization-based tuning procedure is introduced. For notational simplicity, a fixed value of t is considered and the notation $t = 1, \dots, T$ is dropped, since it is implicit that the whole identification process has to be carried out at each value of t. Thus, the main objective is to derive from the available data $Y_t,\ P_e$ an approximation of function $f_t(\mathbf{p_e})$ and guaranteed upper and lower bounds. This is achieved in three steps, described in the following sub-sections.

Before proceeding further, the available data are subdivided as $Y_t = \{Y_{t,A}\,, Y_{t,C}\}$ and $P_e = \{P_{e,A}\,, P_{e,C}\}$, where the subscripts $_A$, $_C$ stand for approximation and calibration, respectively. Moreover, the sets of integers $\mathcal{N}_A = \{1, \dots, N_A\}$ and $\mathcal{N}_C = \{N_A + 1, \dots, N_A + N_C\}$, where N_A and N_C are the cardinalities of $Y_{t,A}$ and $Y_{t,C}$, are also defined.

5.4.1 First step: compute a preliminary approximating function

An estimate $f'_t \approx f_t$ is firstly derived, using the approximation data set $Y_{t,A},\ P_{e,A}$. In this step, one can choose the functional forms of f' among many existing possibilities (linear regression, polynomials, neural nets, etc.), as long as it enjoys Lipschitz continuity. Here, a linear regression is adopted (as done also e.g. in [98])

$$f'_t(\mathbf{p_e}) = \hat{\theta}^\top \mathbf{p_e}, \tag{5.13}$$

whose parameters $\hat{\theta}$ are computed with a ℓ_1-norm regularization approach

$$\hat{\theta} = \underset{\theta}{\text{argmin}}\{ \sum_{\forall i \in \mathcal{N}_A} ||\tilde{y}_t^{(i)} - \theta^\top \tilde{\mathbf{p}}_\mathbf{e}^{(i)}||_2^2 + \lambda \|\theta\|_1 \}, \tag{5.14}$$

where the scalar $\lambda > 0$ is a tuning parameter.

5.4.2 Second step: define the residual function, collect the related data points, and compute the feasible parameter region

Using the obtained preliminary approximation (5.13), the residual function Δ_t is defined as

$$\Delta_t(\mathbf{p_e}) = f_t(\mathbf{p_e}) - \hat{\theta}^\top \mathbf{p_e}. \tag{5.15}$$

Then, (5.1) can be alternatively written as

$$y(t, \mathbf{p_e}) = \hat{\theta}^\top \mathbf{p_e} + \Delta_t(\mathbf{p_e}) + d(t). \tag{5.16}$$

The derivation of an approximating function $\hat{\Delta}_t \approx \Delta_t$ is now addressed, using the nonlinear SM approach of [96]. The following prior knowledge is available:

1. Lipschitz continuity of Δ_t (thanks to Lipschitz continuity of both f_t and f_t', see Remark 5.1 and (5.13)):

$$\begin{aligned} &|\Delta_t(\mathbf{p_e}^{(j)}) - \Delta_t(\mathbf{p_e}^{(k)})| \leq \gamma_t \|\mathbf{p_e}^{(j)} - \mathbf{p_e}^{(k)}\|_2, \\ &\forall \mathbf{p_e}^{(j)}, \, \mathbf{p_e}^{(k)} \in P \end{aligned} \tag{5.17}$$

2. Boundedness of $d(t)$ (see Remark 5.1):

$$|d(t)| \leq \epsilon_t \ , \tag{5.18}$$

where $P \subset \mathbb{R}^T$ is a compact set containing all the possible energy price courses over the day. The positive scalars γ_t, ϵ_t in (5.17)-(5.18) are not known, and shall be estimated from data as well. To do so, let's start by computing the *feasible parameter region* $\mathcal{B} \subset \mathbb{R}^+ \times \mathbb{R}^+$. Namely, this is the set of (γ_t, ϵ_t) pairs such that the prior knowledge is consistent with the

available data. Using the data-set, the samples of the residuals $\tilde{\Delta}_t^{(i)}$ are obtained as

$$\tilde{\Delta}_t^{(i)} = \tilde{y}_t^{(i)} - \hat{\theta}^\top \tilde{\mathbf{p}}_\mathbf{e}^{(i)} \qquad i = 1, \dots, N \tag{5.19}$$

Then, for a given pair (γ_t, ϵ_t), the following functions are introduced

$$\bar{\Delta}_t(\mathbf{p}_\mathbf{e}) \doteq \min_{\forall j=1,\dots,N} (\tilde{\Delta}_t^{(j)} + \epsilon_t + \gamma_t \|\mathbf{p}_\mathbf{e} - \tilde{\mathbf{p}}_\mathbf{e}^{(j)}\|_2) \tag{5.20}$$

$$\underline{\Delta}_t(\mathbf{p}_\mathbf{e}) \doteq \min_{\forall j=1,\dots,N} (\tilde{\Delta}_t^{(j)} - \epsilon_t - \gamma_t \|\mathbf{p}_\mathbf{e} - \tilde{\mathbf{p}}_\mathbf{e}^{(j)}\|_2) \tag{5.21}$$

Now, it is possible to compute $\mathcal{B}$ by exploiting the following result (*Theorem 1* in [96]):

A necessary and sufficient condition for the prior knowledge to be validated is:

$$\bar{\Delta}_t(\tilde{\mathbf{p}}_\mathbf{e}^{(i)}) > \tilde{\Delta}_t^{(i)} - \epsilon_t \quad \forall i \in \mathcal{N}_A \cup \mathcal{N}_C \tag{5.22}$$

The feasible parameter set is defined as

$$\mathcal{B} = \{(\gamma_t, \epsilon_t) : \text{ condition (5.22) holds}\} . \tag{5.23}$$

Note that the set $\mathcal{B}$ is unbounded, since it is always possible to satisfy condition (5.22) with large enough values of γ_t and/or ϵ_t. On the other hand, it is of interest to compute the "lower boundary" $\underline{\gamma}_t(\epsilon_t)$:

$$\begin{aligned} \underline{\gamma}_t(\epsilon_t) \quad = \quad & \arg\min_{\gamma} \gamma \\ & \text{s.t.} (\gamma, \epsilon_t) \in \mathcal{B} . \end{aligned} \tag{5.24}$$

Figure 5.1 presents a qualitative example of set $\mathcal{B}$. This curve is used to select suitable estimates $\hat{\gamma}_t, \hat{\epsilon}_t$ and eventually obtain the approximating function and error bounds, as described next.

5.4.3 Third step: select an estimate of the Lipschitz constant and error bound, and derive the approximating function $\hat{f}_t$

To derive the wanted approximating functions, one has to select a pair $(\hat{\gamma}_t, \hat{\epsilon}_t)$ inside the set $\mathcal{B}$. Assuming that these estimates have been chosen, then the corresponding functions $\bar{\Delta}_t(\mathbf{p}_\mathbf{e})$ and $\underline{\Delta}_t(\mathbf{p}_\mathbf{e})$ in (5.20)-(5.21)

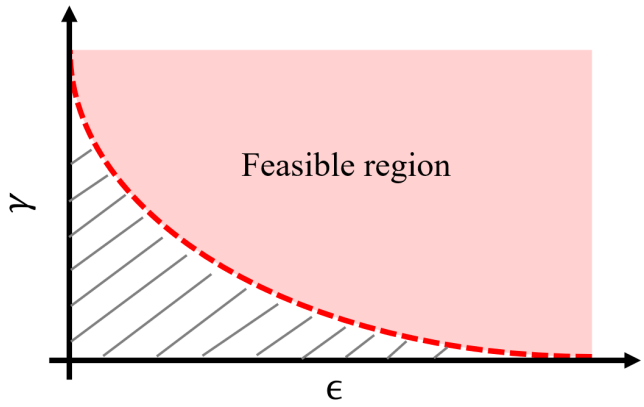

Figure 5.1: Example of γ_t-ϵ_t feasible parameter set

represent the upper and lower bounds of $\Delta_t(\mathbf{p_e})$. Moreover, if the prior knowledge is valid, the interval $\left[\underline{\Delta}(\mathbf{p_e}),\ \bar{\Delta}_t(\mathbf{p_e})\right]$ is guaranteed to include the true function $\Delta(\mathbf{p_e})$ [96]. As a result, for a given price prediction $\mathbf{p_e} \in P$, the output $y(t, \mathbf{p_e})$ (5.16) is guaranteed to be bounded by the following functions

$$\underline{y}(t, \mathbf{p_e}) \leq y(t, \mathbf{p_e}) \leq \bar{y}(t, \mathbf{p_e}) \tag{5.25}$$

$$\begin{array}{rcl} \bar{y}(t, \mathbf{p_e}) & = & \theta^\top \mathbf{p_e} + \bar{\Delta}_t(\mathbf{p_e}) + \epsilon_t \\ \underline{y}(t, \mathbf{p_e}) & = & \theta^\top \mathbf{p_e} + \underline{\Delta}_t(\mathbf{p_e}) - \epsilon_t \end{array} \tag{5.26}$$

and the estimated uncertainty interval is given by

$$\bar{y}(t, \mathbf{p_e}) - \underline{y}(t, \mathbf{p_e}) = \bar{\Delta}_t(\mathbf{p_e}) - \underline{\Delta}_t(\mathbf{p_e}) + 2\epsilon_t > 0 \tag{5.27}$$

In the literature, it is often the case that the pair (γ, ϵ) is selected in the feasible region using some prior knowledge on the system to be identified. When this knowledge is not available, one has to choose these parameters using the available input-output data, which can be a time-consuming task. To this end, a possible approach is to choose the optimal parameters in the feasible region by minimizing the identification error with respect to the calibration data. This method can achieve a small approximation error on average, however the resulting uncertainty interval can be rather

large. On the other hand, in the application considered here it is more reasonable to select estimates $\hat{\gamma}_t, \hat{\epsilon}_t$ such that the uncertainty interval (5.27) is as small as possible. Therefore, it is proposed to choose $(\hat{\gamma}_t, \hat{\epsilon}_t)$ by solving the following optimization problem, which involves the calibration dataset:

$$(\hat{\gamma}_t, \hat{\epsilon}_t) = \underset{(\gamma,\epsilon)\in\mathcal{B}}{\operatorname{argmin}}\{ \sum_{\forall j\in\mathcal{N}_C} (\bar{y}(t, \tilde{\mathbf{p}}_{\mathbf{e}}^{(j)}) - \underline{y}(t, \tilde{\mathbf{p}}_{\mathbf{e}}^{(j)}))^2\} \tag{5.28}$$

Having computed the parameters $(\hat{\gamma}_t, \hat{\epsilon}_t)$, the wanted approximating function (see (5.3)) is given by:

$$\hat{y}(t, \mathbf{p_e}) = \hat{f}_t(\mathbf{p_e}) \quad = \quad \theta^\top \tilde{\mathbf{p}}_{\mathbf{e}} + \frac{\bar{\Delta}_t(\tilde{\mathbf{p}}_{\mathbf{e}}) + \underline{\Delta}_t(\tilde{\mathbf{p}}_{\mathbf{e}})}{2}$$

while the guaranteed power bounds can be computed as in (5.26). Function $\hat{f}_t(\mathbf{p_e})$ is the central (or optimal) approximation, i.e. it provides the smallest worst-case approximation error for the given data-set and chosen $(\hat{\gamma}_t, \hat{\epsilon}_t)$, equal to half the uncertainty bound (radius of information, see e.g. [96]).

5.5 Numerical results

The numerical results have been carried out considering a MG composed of different generation units and loads, whose parameters are reported in Table 5.2. Considering the identification data set, the non-dispatchable power trends of load absorption and of renewable sources production are reported in Figure 5.2(a) and 5.2(b), respectively. The daily prices profiles are reported in Figure 5.2(c): their trends are defined considering the real daily prices of the Italian Day-Ahead Market, which can be found in [99]. In Figure 5.2(d) the resulting sampled data of MG output power are depicted, which have been computed according to the optimization framework described in Section 5.3. As described in Section 5.4, the identification data set is divided in two different sets as follows: $N_A = 30$ approximation data, and $N_C = 120$ calibration data. The identification process is performed as described in Section 5.4 and the optimal tuning parameters $(\hat{\gamma}_t, \hat{\epsilon}_t)$ are computed.

In Figure 5.3, the feasible region for $t = 40$ is shown, together with the optimal solution of (5.28). Then, the performance of the identification process are evaluated using an additional *validation data* set, denoted as $\mathcal{N}_\mathcal{V}$, with $N_V = 60$ data points. Before proceeding to the description of the numerical results, the following variables are defined $\mathbf{y}(\mathbf{p_e})$, $\hat{\mathbf{y}}(\mathbf{p_e})$, $\bar{\mathbf{y}}(\mathbf{p_e})$, $\underline{\mathbf{y}}(\mathbf{p_e})$, which express the daily MG output power, the corresponding estimate and the upper and lower bounds, respectively.
The following variable is also introduced, expressing the average output power of the MG

$$y_m(\mathbf{p_e}) = \sum_{t=1}^{T} y(t, \mathbf{p_e})$$

To properly evaluate the achieved performance, the following indexes are computed $\forall i \in \mathcal{N}_\mathcal{V}$

$$IE^{(i)} = \frac{||\mathbf{y}(\mathbf{p_e}^{(i)}) - \hat{\mathbf{y}}(\mathbf{p_e}^{(i)})||_2}{\sqrt{T}}, \qquad IE^{(i)}_{\%} = \frac{100\, IE^{(i)}}{y_m(\mathbf{p_e}^{(i)})}$$

$$MD^{(i)} = \frac{||\bar{\mathbf{y}}(\mathbf{p_e}^{(i)}) - \underline{\mathbf{y}}(\mathbf{p_e}^{(i)})||_\infty}{2}, \quad MD^{(i)}_{\%} = \frac{100\, MD^{(i)}}{y_m(\mathbf{p_e}^{(i)})}$$

where IE corresponds to the identification error computed for the whole daily period, while MD represents the maximum possible deviation of the output with respect to the estimate, considering the computed power bounds. For the sake of completeness, also the values normalized with respect to the average output power y_m are computed, i.e. $IE_{\%}$ and $MD_{\%}$. The achieved performance indicators have been computed considering the whole validation data set $\mathcal{N}_\mathcal{V}$ and the results are reported in Table 5.3. The reported results witness the effectiveness of the proposed approach both in terms of reduced identification error and of capability to provide guaranteed bounds for the MG output power. To better highlight the advantage of the proposed SM approach, the results obtained with two exemplary validation data trends are presented in Figure 5.4. Precisely, Figure 5.4(a)(b) shows a case when a small identification error is achieved, $IE = 2.16\, kW$; it is worth noticing that the real MG output

Table 5.2: MG parameters and constraints

mGENs	$(\underline{p}^g, \bar{p}^g)$	a^g	b^g	c^g
p_1^g	$(20, 100)$	$1.25e-5$	$1.25e-3$	$3e-2$
p_2^g	$(20, 50)$	$2.25e-5$	$7.5e-4$	$3.5e^{-3}$
BESSs	$(\underline{p}^b, \bar{p}^b)$	$(\underline{s}^b, \bar{s}^b)$	C^b	c^b
p_1^b	$(-50, 50)$	$(0.2, 0.8)$	40	$2.5e^{-2}$
p_2^b	$(-40, 40)$	$(0.2, 0.8)$	50	$2.5e^{-2}$
Shifting loads	$(\underline{p}^{sl}, \bar{p}^{sl})$	$(\underline{\tau}^{sl}, \bar{\tau}^{sl})$	$\bar{e}^{sl}$	–
p_1^{sl}	$(0, 20)$	$(9, 12)$	20	–
p_2^{sl}	$(0, 20)$	$(16, 19)$	20	–
Reducible loads	$\lvert\hat{d}^{rl}(\forall t)\rvert$	$(\underline{\tau}^{rl}, \bar{\tau}^{rl})$	Δd^{rl}	c^{rl}
p_1^{rl}	20	$(12, 16)$	10	$3.13e-2$

Table 5.3: Identification performances

	mean	min	max
IE	4.79 kW	2.16 kW	8.20 kW
$IE_{\%}$	7.1%	3%	14.7%
MD	14.62 kW	11.62 kW	20.17 kW
$MD_{\%}$	20%	17.3%	30%

power is fully contained in the computed bounds, see Figure 5.4(b). On the other hand, Figure 5.4(c)-(d) show a case where a larger estimation error is obtained, with $IE = 8.2\,kW$. Notwithstanding the estimation error, also in this second case the true power output is still contained in the computed bounds, see Figure 5.4(d). The knowledge of such bounds can be thus effectively used to account for the uncertainty in the day-ahead energy price definition process.

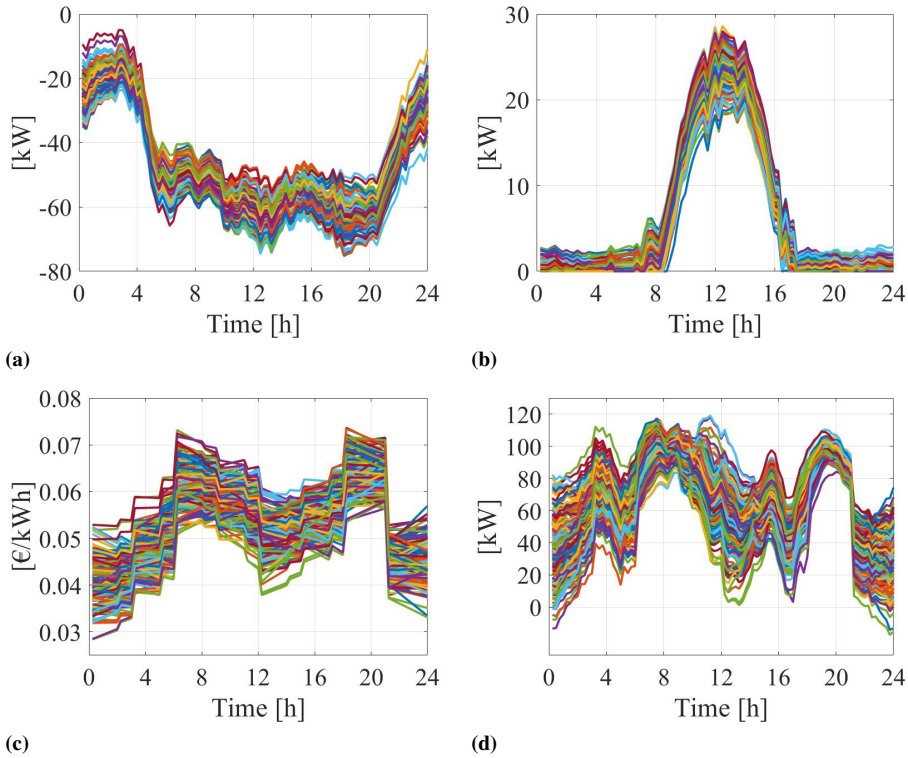

Figure 5.2: Identification data: (a) Non-dispachable load power trends, (b) Renewable energy sources power trends, (c) Energy prices trends, (d) MG output power trends.

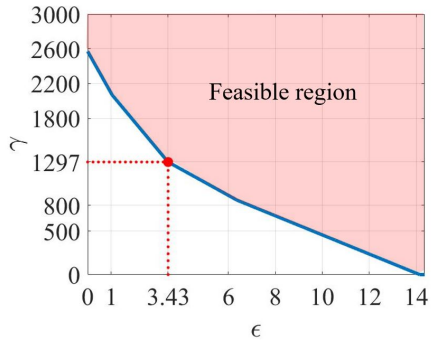

Figure 5.3: γ-ϵ feasible region at $t = 40$ and selected optimal $(\hat{\gamma}_t, \hat{\epsilon}_t)$ (red dot).

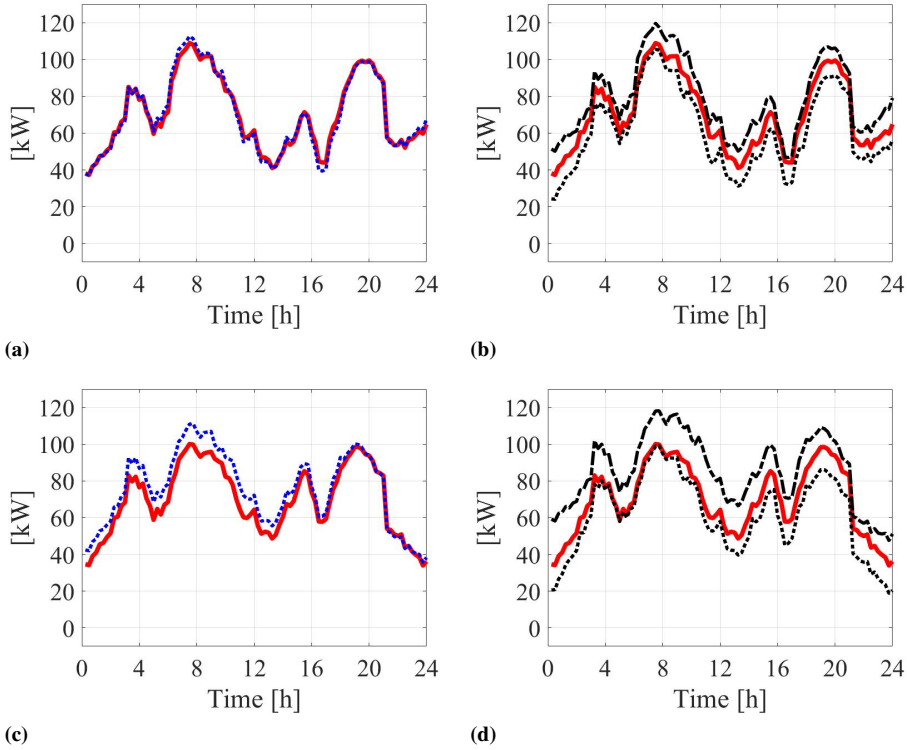

Figure 5.4: Example of validation outcome with small estimation error and large estimation error: (a)&(c) real MG output power trend (solid line), estimated MG output power (dotted line), (b)&(d) higher power bound (dashed line), lower power bound (dotted line), real MG output power (solid line).

5.6 Conclusions

The problem of deriving from data an estimate of the price-based power scheduling of microgrids has been considered. AGS can use the obtained models to optimize their trading process with the system operator, by better predicting the power output of each one of the associated microgrids as a function of the predicted energy prices. The proposed method is based on the Set Membership theory and provides also guaranteed error bounds, which can be exploited by the aggregator to improve robustness of its decisions. A novel tuning approach is proposed, based on numerical optimization, that aims to minimize the estimated uncertainty interval.

Part II

Hierarchical Model Predictive Control architectures for islanded microgrids

CHAPTER 6

Two-layer control of AC islanded microgrids with energy storage systems

6.1 Introduction

Microgrids (MGs), being sites of both generation and consumption, can either be operated connected to the overall grid system or in islanded mode. This last condition is the most critical one since, given the presence of non-deterministic units as Renewable Energy Sources (RESs) and loads, significant power unbalances may occur, which lead to voltages and frequency deviations. Moreover, this becomes a crucial problem in case the MG is not supported by traditional rotating generators but just by electronically-interfaced sources, e.g. Battery Energy Storage Systems (BESSs) and RESs, since the overall network inertia considerably decreases. This requires the design of dedicated control architectures, entitled of the quick regulation of the internal frequency and voltages, as

well as efficiently managing the available Distributed Energy Resources (DERs). To accomplish these tasks, a centralized control architecture is not an effective solution since different time-scales are involved, as well as different control objectives. Therefore, a novel two-layer control architecture is proposed in this chapter, used for regulating an Alternating Current islanded MG (AC-iMG), supported just by BESSs and RESs units.

6.1.1 Literature Review

Inspired by the traditional electric regulation systems, AC-iMGs controllers are usually constituted by a hierarchical structure where control layers are characterized by different tasks and time scales [100]. The so-called *primary control* is designed to locally regulate generation units in order to ensure voltage and frequency stability. For this control layer, *droop control*, which is based on a decentralized proportional regulators, is often considered; in [101] and [38] the stability of this control approach is analysed. Nevertheless a proportional control action, even though properly designed, is not sufficient to keep voltages and frequency at their nominal values. A traditional solution to this problem is the implementation of a *secondary control* layer which restores nominal frequency at a slower time scale, as proposed in [102]. However, if all DERs of the AC-iMG are mostly interfaced through electronic power converters, an alternative approach is possible to avoid frequency deviations. One inverter-based generation unit, thanks to its fast dynamics, denoted as *slack generator*, can be controlled to maintain both the reference frequency for the whole AC-iMG network and also the voltage at its connection node. Meanwhile, other DERs, named as *PQ generators*, are regulated to provide properly defined power references, so as to support the slack generator in its operation, see [103]- [104]. The advantage of this approach is that frequency disturbances are avoided, since frequency is directly imposed by the inverter-interface of the slack node, and this is beneficial for loads (e.g. in case of presence of asynchronous motors directly connected to the network). On the other hand, the drawback is that unexpected load variations are compensated by the slack generator only, having it to maintain the nodal voltage and the network frequency at the reference values. What is more, if the slack generator output saturates at its capability

limits, it could not be able to generate a proper reference nodal voltage. The mentioned issues motivate the design of a proper supervising control layer. The high-level controller should consider the units and grid physical constraints, the system efficiency, the forecasts of loads and renewable sources power trends, if available. In the literature, some high level optimization algorithms concerning islanded microgrids have been developed, even though with a reduced attention to the interaction with the low-level control layers [105], [42].

6.1.2 Proposed solution

This chapter presents the design of a hierarchical control architecture which integrates fast decentralized low-level controllers and a centralized high-level Model Predictive Control (MPC) regulator. This two-layer approach allows to coordinate PQ generators such that the slack generator is properly operated and all the nodal voltages of the AC-iMG are maintained in the predefined bounds despite unexpected changes in load demand. Moreover, the high level optimization problem is stated to minimize overall line losses and to properly coordinate DERs operations. The control structure is derived considering an AC-iMG equipped with BESSs and RESs, where it is assumed that the total generation capability is sufficient to satisfy the overall load demand. The islanded condition is expected to last a limited time period, given the fact that the available DERs are either non-dispatchable or with limited stored energy.
The chapter is structured as follows: in Section 6.2 the low-level controllers are described, while in Section 6.3 the high-level network model is defined and the optimization problem is stated. Finally, Section 6.4 presents the simulation results and in Section 6.5 final conclusions are discussed. The main variables and parameters used in this chapter are described in Table 6.1. All the power values are positive if delivered and negative if absorbed, while maximum and minimum limits of each variable are denoted with a bar over or below the variable, respectively. The first order derivative with respect to time is expressed with a dot over the variable, e.g. $\dot{p}$, while the second order derivative with two dots, e.g. $\ddot{p}$. If derivatives are expressed for vectors, the operation must be intended element-wise.

Table 6.1: Main variables and parameters

Symbol	Description
i_L	Output converter current [A]
v_c	Output converter voltage [V]
i_G	Grid current at converter output [A]
v_G	Grid voltage at converter output [V]
C, L	Capacitor and inductance at converter output filter [F, H]
P, Q	Nodal active and reactive power [W, VAR]
s^b	BESS state of charge
C^b	BESS capacity [Wh]
$\Delta\bar{P}^d$, $\Delta\bar{Q}^d$	Maximum load active and reactive power variations [W, VAR]
V	Nodal voltage magnitude [V]
δ	Nodal voltage phase [V]
P^L	Active power line losses [W]

6.2 Decentralized voltage and frequency control

It is assumed that each generation node is supported by a BESS interfaced with a voltage-source electronic converter, characterized as common by a L-C-L output filter [106]. The equivalent circuit of the converter is depicted in Figure 6.1, where electrical variables are supposed to be three-phase, symmetrical and balanced.

Modulation techniques for direct current tracking are available in the literature, as the ones in [107, 108], therefore it is possible to use the output converter current, denoted as i_L, as a direct control variable both for the slack and the PQ generators (see again Figure 6.1). At this stage, two different control strategies need to be implemented for the low layer. The slack generator must be designed to track the reference of the output converter voltage, i.e. v_c, since the frequency can be assumed to be automatically imposed by its converter. The PQ nodes must be regulated to track the pre-defined active and reactive power references, by regulating the output current i_G.

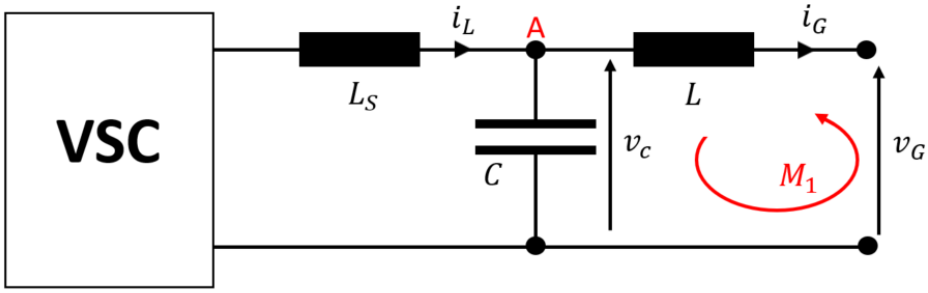

Figure 6.1: Voltage Source Converter (VSC) equivalent circuit

6.2.1 Slack generator control

Since the reference frequency, denoted as ω_n, is directly imposed by the slack converter, it is possible to apply the Park Transformation with an arbitrary initial phase reference, defining all electrical variables in the dq reference frame [109]. Applying Kirchhoff current law at node A in Figure 6.1 and considering the capacitor constitutive equation, the following dynamical equation holds

$$\begin{cases} \dot{v}_{c,d} &= \omega_n v_{c,q} + \frac{1}{C} i_{L,d} - \frac{1}{C} i_{G,d} \\ \dot{v}_{c,q} &= -\omega_n v_{c,d} + \frac{1}{C} i_{L,q} - \frac{1}{C} i_{G,q} \end{cases}, \tag{6.1}$$

where C is the filter capacitance of the slack generator system. For the sake of clarity, the dq components of each electrical variable are stacked in a unique vector denoted in bold, e.g. $\mathbf{v_c} = [v_{c,d}, v_{c,q}]'$.
Therefore, (6.1) can be expressed as

$$\dot{\mathbf{v}}_\mathbf{c} = A_{\omega_n} \mathbf{v_c} + \frac{1}{C} \mathbf{i_L} - \frac{1}{C} \mathbf{i_G}, \quad A_{\omega_n} = \begin{bmatrix} 0 & \omega_n \\ -\omega_n & 0 \end{bmatrix}. \tag{6.2}$$

To design the control system, an approach inspired by Sliding Mode control theory has been adopted, as discussed in [110]. Therefore, defining the output voltage error $\epsilon_\mathbf{v} = \mathbf{v_c}^o - \mathbf{v_c}$, where $\mathbf{v_c^o}$ corresponds to the reference output voltage, the following function is expressed

$$\sigma_{\mathbf{v}} = \epsilon_{\mathbf{v}} + T_1 \frac{d\epsilon_{\mathbf{v}}}{dt} + \frac{1}{T_2} \int \epsilon_{\mathbf{v}}\, dt \ , \tag{6.3}$$

where T_1 and T_2 are design parameters. Following the approach in [110], imposing that $\sigma_{\mathbf{v}} = \mathbf{0}$ and combining (6.2)-(6.3), an equivalent control law can be obtained

$$\mathbf{i_L} = K_p\, \epsilon_{\mathbf{v}} \ + \ K_i \int \epsilon_{\mathbf{v}}\, dt \ - \ C A_{\omega_n}\, \mathbf{v_c} + \mathbf{i_G} + C\, \dot{\mathbf{v}}_{\mathbf{c}}^{\mathbf{o}} \ . \tag{6.4}$$

Looking at (6.4), it is possible to notice a proportional and a integral action with respect to voltage error $\epsilon_{\mathbf{v}}$, a direct feedback from output voltage $\mathbf{v_c}$ and a compensation of grid current $\mathbf{i_G}$, assumed to be a measurable disturbance. Since the slack generator imposes a fixed voltage reference, i.e. $\dot{\mathbf{v}}_{\mathbf{c}}^{\mathbf{o}} = \mathbf{0}$, the last term in (6.4) is zero. The gains K_p and K_I must be tuned both to ensure the system stability, considering the state-space equation (6.2) and the control law (6.4), and to obtain the desired dynamical performances.
It is worth noticing that uncompensated load variations may have a significant impact on the output current $\mathbf{i_G}$, implying that the slack generator is forced to work close to its capability limits to maintain the reference of $\mathbf{v_c}$. This condition should be avoided because it may compromise the modulation of the output current of the converter (6.4). This is pursued thanks to the high-level MPC action, properly modulating the PQ generators power set-points, so as to properly distribute the load demand.

6.2.2 PQ control

PQ generator converters are designed to work in strict synchronization with the network. This is possible by equipping them with a Phase Lock Loop system (PLL), which provides the reference phase to apply the Park transformation such that $v_{G,q} = 0$ [111]. In this condition, the PQ control loop can be designed to track the output current reference, which can be defined as a function of power set-points, named as P^o and Q^o, and of $v_{G,d}$, assumed to be measurable.

$$i^o_{G,d} = \frac{2}{3}\frac{P^o}{v_{G,d}} \ , \qquad i^o_{G,q} = \frac{2}{3}\frac{Q^o}{v_{G,d}} \ . \tag{6.5}$$

Considering the inductor constitutive equation and the Kirchhoff voltage law in mesh M_1 (see Figure 6.1), the output current model can be obtained

$$\dot{\mathbf{i}}_{\mathbf{G}} = A_{\omega_n}\mathbf{i}_{\mathbf{G}} + \frac{1}{L}\mathbf{v}_{\mathbf{c}} - \frac{1}{L}\mathbf{v}_{\mathbf{G}} \ , \tag{6.6}$$

which, combined with (6.2), gives the overall model for the PQ generators control. Similarly to the approach described in [110], the output current error is defined, i.e. $\epsilon_{\mathbf{i}} = \mathbf{i}^{\mathbf{o}}_{\mathbf{G}} - \mathbf{i}_{\mathbf{G}}$, and the following function is introduced

$$\sigma_{\mathbf{i}} = \epsilon_{\mathbf{i}} + T_1\frac{d\epsilon_{\mathbf{i}}}{dt} + T_2\frac{d^2\epsilon_{\mathbf{i}}}{dt^2} + \frac{1}{T_3}\int \epsilon_{\mathbf{i}}\, dt \ , \tag{6.7}$$

where the second derivative of the error is included in order to have explicit dependency on the control variable $\mathbf{i}_{\mathbf{L}}$. Imposing $\sigma_{\mathbf{i}} = \mathbf{0}$ and considering system equations (6.2) and (6.6), the equivalent control law can be computed

$$\begin{aligned}\mathbf{i}_{\mathbf{L}} =& K_p\,\epsilon_{\mathbf{i}} + K_i\int \epsilon_{\mathbf{i}}\, dt + K_d\frac{d\epsilon_{\mathbf{i}}}{dt} + \Gamma_{v_c}\mathbf{v}_{\mathbf{c}} + \\ &+ \Gamma_{i_G}\mathbf{i}_{\mathbf{G}} + \Gamma_{v_G}\mathbf{v}_{\mathbf{G}} + \Gamma_{\dot{v}_G}\dot{\mathbf{v}}_{\mathbf{G}} + \Gamma_{\ddot{i}_G}\ddot{\mathbf{i}}^{\mathbf{o}}_{\mathbf{G}} \ ,\end{aligned} \tag{6.8}$$

where K_p, K_i, K_d are control design parameters, while the Γ matrices, which for the sake of compactness are not explicitly expressed, depend on the network angular frequency and on the filter parameters. For the actual implementation of the control law in (6.8), it is considered that $\dot{\mathbf{v}}_{\mathbf{G}} \approx 0$ since $\mathbf{v}_{\mathbf{G}}$ can be assumed to be constant with respect to the PQ control time dynamics. Moreover, it can be also assumed that $\ddot{\mathbf{i}}^{\mathbf{o}}_{\mathbf{G}} \approx 0$ since references are implemented to be either constant or varying as ramp signals, implying that their second derivative is null. Also in this case, the control design parameters have been tuned to obtain the desired transient performances and to ensure the stability of the overall closed loop system.

6.3 Design of supervising MPC control layer

A high-level control system is employed to coordinate DERs operations during the islanded condition. This task can be efficiently accomplished by a MPC algorithm, easily incorporating constraints, like generators power capabilities, and resource management strategies to optimally distribute the power flows. Before describing the MPC design for this specific application, a system model must be derived. This has been defined as a discrete time model, with time index k and sampling time τ_s, chosen such that the network can be considered at steady-state at the MPC level, thanks to the prompt action of the low-level controllers described in Section 6.2.

6.3.1 Microgrid high-level electrical modelling

The iMG modelling must consider both the network variables, e.g. voltages, and the DERs variables, such as output powers and states of charge. Therefore, the description of overall model is structured in the following paragraphs.

Network model

The network can be represented by an undirected graph $\mathcal{G} = (\mathcal{N}, \mathcal{E})$, where $\mathcal{N}$ denotes the set of nodes and $\mathcal{E} \subseteq \mathcal{N} \times \mathcal{N}$ defines the set of interconnection lines. Each of the $n = |\mathcal{N}|$ nodes can correspond either to a generation unit, a load or a transit node. As a convention, the slack generator node is numbered as the first node of the network. Moreover, the sets $\mathcal{N}_u \subseteq \mathcal{N} \setminus \{1\}$ and $\mathcal{N}_d \subseteq \mathcal{N} \setminus \{1\}$, with $n_u = |\mathcal{N}_u|$ and $n_d = |\mathcal{N}_d|$, correspond to PQ generators nodes and to non-dispatchable nodes, respectively.
Since the network frequency is imposed by the inverter-based slack generation system and a three-phase balanced and symmetrical system is considered, the phasor approach can be adopted [109]. Therefore, each nodal voltage is represented by its magnitude, V_i, and by its phase displacement with respect to the slack node voltage, δ_i, with $i \in (1, \ldots, n)$.

The power flow equations hold for the i-th node

$$\begin{aligned} P_i &= f_i^P(\mathbf{V},\, \boldsymbol{\delta}) = V_i \sum_{j=1}^{n} V_j |\mathrm{Y}_{ij}| \cos\left(\delta_i - \delta_j - \angle Y_{ij}\right) , \\ Q_i &= f_i^Q(\mathbf{V},\, \boldsymbol{\delta}) = V_i \sum_{j=1}^{n} V_j |\mathrm{Y}_{ij}| \sin\left(\delta_i - \delta_j - \angle Y_{ij}\right) , \end{aligned} \tag{6.9}$$

where $\mathbf{V} = [V_2,\, \ldots,\, V_n]'$ and $\boldsymbol{\delta} = [\delta_2,\, \ldots,\, \delta_n]'$ (the dependency with respect to the slack node voltage is not expressed since V_1 and δ_1 are fixed), Y_{ij} corresponds to the (i, j) position of the *network admittance matrix* and (P_i, Q_i) represent the nodal active and reactive powers. Given that each node can be associated to a PQ generator, to a non-dispatchable unit or both, the following power balances can be expressed

$$\begin{cases} P_i \;=\; f_i^P(\mathbf{V},\, \boldsymbol{\delta}) \;=\; P_i^u + P_i^d \\ Q_i \;=\; f_i^Q(\mathbf{V},\, \boldsymbol{\delta}) \;=\; Q_i^u + Q_i^d \end{cases} , \quad \forall i \in (2, ..., n) , \tag{6.10}$$

where $(P_i^u,\, Q_i^u)$ and $(P_i^d,\, Q_i^d)$ correspond to the output powers of PQ generators and of non-dispatchable units connected to the i-th node, respectively. Moreover, it follows that

$$P_i^u = Q_i^u = 0 \quad \text{if } i \notin \mathcal{N}_u, \qquad\qquad P_i^d = Q_i^d = 0 \quad \text{if } i \notin \mathcal{N}_d \, .$$

For the sake of compactness, the following vectors are defined

$$\tilde{\mathbf{x}} = \; [\mathbf{V}', \boldsymbol{\delta}'], \quad \mathbf{f^P}(\tilde{\mathbf{x}}) = [f^P_{2,..,n}, f^Q_{2,..,n}]'$$

$$\mathbf{P} = [P_{2,..,n}, Q_{2,..n}]', \quad \mathbf{P^u} = [P^u_{2,..,n}, Q^u_{2,..,n}]', \quad \mathbf{P^d} = [P^d_{2,..,n}, Q^d_{2,..,n}]' \, .$$

Therefore, equation (6.10) can be expressed as

$$\mathbf{P} = \mathbf{f}^{\mathbf{P}}(\tilde{\mathbf{x}}) = \left(\boldsymbol{\Theta}_{\mathbf{u}}\,\mathbf{P}^{\mathbf{u}} + \boldsymbol{\Theta}_{\mathbf{d}}\,\mathbf{P}^{\mathbf{d}}\right), \tag{6.11}$$

where $\boldsymbol{\Theta}_{\mathbf{u}}, \boldsymbol{\Theta}_{\mathbf{d}} \in \mathbb{R}^{2(n-1),2(n-1)}$ are properly defined diagonal matrices, selecting the active and reactive powers of PQ generators and non-dispatchable units in the nodes where they are effectively located. Precisely, these are defined as

$$\begin{aligned}\boldsymbol{\Theta}_{\mathbf{u}} &= \text{diag}\{\theta_2^u, \ldots, \theta_n^u, \theta_2^u, \ldots, \theta_n^u\}\ ,\\ \boldsymbol{\Theta}_{\mathbf{d}} &= \text{diag}\{\theta_2^d, \ldots, \theta_n^d, \theta_2^d, \ldots, \theta_n^d\}\ ,\end{aligned}$$

where

$$\begin{cases}\theta_i^u = 1 & \forall i \in \mathcal{N}_u\\ \theta_i^u = 0 & \forall i \notin \mathcal{N}_u\end{cases} \qquad \begin{cases}\theta_i^d = 1 & \forall i \in \mathcal{N}_d\\ \theta_i^d = 0 & \forall i \notin \mathcal{N}_d\end{cases}\ .$$

To derive an approximated dynamical model that expresses the electrical variables evolution caused by external power variations, the nonlinear equations in (6.11) are linearized around the actual network steady-state equilibrium, denoted as $\tilde{\mathbf{x}}(k)$,

$$\Delta\mathbf{P}(k) \;=\; \left.\frac{\partial \mathbf{f}^{\mathbf{P}}}{\partial \tilde{\mathbf{x}}}\right|_{\tilde{\mathbf{x}}(k)} \Delta\tilde{\mathbf{x}}(k)\ , \tag{6.12}$$

where variables are expressed as variations with respect to the network condition at the k-time instant. Introducing a time discretization, these variations are defined as $\Delta\mathbf{P}(k) = \mathbf{P}(k+1) - \mathbf{P}(k)$ and $\Delta\tilde{\mathbf{x}}(k) = \tilde{\mathbf{x}}(k+1) - \tilde{\mathbf{x}}(k)$ and, combining (6.11) and (6.12), the following model can be obtained

$$\tilde{\mathbf{x}}(k+1) = \tilde{\mathbf{x}}(k) + \left[\left.\frac{\partial \mathbf{f}^{\mathbf{P}}}{\partial \tilde{\mathbf{x}}}\right|_{\tilde{\mathbf{x}}(k)}\right]^{-1} \left(\boldsymbol{\Theta}_{\mathbf{u}}\,\Delta\mathbf{u}(k) + \boldsymbol{\Theta}_{\mathbf{d}}\,\Delta\mathbf{d}(k)\right), \tag{6.13}$$

where $\Delta\mathbf{u} = [\Delta P^u_{2,..,n},\ \Delta Q^u_{2,..,n}]'$ and $\Delta\mathbf{d} = [\Delta P^d_{2,..,n},\ \Delta Q^d_{2,..,n}]'$.

To better understand (6.13), it is worth noting that each power variation, either caused by the high-level MPC acting on the PQ generators set-points, described by $\Delta\mathbf{u}$, or by the loads, described by $\Delta\mathbf{d}$, results in a transient for the network electrical variables until they reach a new steady state condition, thanks the low-level control action. This new equilibrium point is sampled by the MPC controller at the next iteration $k+1$. Through this procedure, the voltage dynamics can be described as a state-space equation, so that its prediction can be evaluated by the MPC regulator.

Remark 6.1. *It's worth noticing that modelling the network as in (6.13) has the advantage of considering just the variations of disturbances $\Delta\mathbf{d}$ and not their total amplitude. This means that, if the future profiles of non-dispatchable elements are not known, it can be reasonably assumed that $\Delta\mathbf{d}(k) = 0$, meaning that the loads are supposed to not vary between two consecutive time steps. As it will be discussed in Section 6.4, if a reduced sampling time is used, this approximation turns out to be very effective, allowing to control the AC-iMG with any knowledge on the load power absorptions.*

Line losses

The MPC control layer is designed to also minimize the active power line losses, ensuring an efficient management of the AC-iMG power flows. Combining the equations (6.13), it is possible to recover a nonlinear function expressing each line power losses based on nodal voltages magnitude and phases of adjacent nodes, as described in [57]. It follows that

$$\mathbf{P^L} = \mathbf{f^L}(\tilde{\mathbf{x}}) \ , \tag{6.14}$$

where the vector $\mathbf{P^L}$ includes all active power losses $P^L_{(i,j)}\ \forall\,(i,j) \in \mathcal{E}$, while $\mathbf{f^L}(\tilde{\mathbf{x}})$ denotes the vector of line losses nonlinear functions. Also in this case, a linearization procedure is performed considering the network equilibrium condition at the general time index k.

It follows that

$$\Delta \mathbf{P^L}(k) \;=\; \left.\frac{\partial \mathbf{f^L}}{\partial \tilde{\mathbf{x}}}\right|_{\tilde{\mathbf{x}}(k)} \Delta \tilde{\mathbf{x}}(k)\;. \tag{6.15}$$

Similarly to the previous paragraph and combining the equations (6.13) and (6.15), a discrete-time linear model can be obtained

$$\begin{aligned}\mathbf{P^L}(k+1) = \;& \mathbf{P^L}(k) + \\ &+ \left[\frac{\partial \mathbf{f^L}}{\partial \tilde{\mathbf{x}}}\left(\frac{\partial \mathbf{f^P}}{\partial \tilde{\mathbf{x}}}\right)^{-1}\right]\Bigg|_{\tilde{\mathbf{x}}(k)} \left(\mathbf{\Theta_u}\Delta\mathbf{u}(k) + \mathbf{\Theta_d}\,\Delta\mathbf{d}(k)\right)\;.\end{aligned} \tag{6.16}$$

PQ generators active and reactive powers

As mentioned, the high-level MPC regulator is designed to vary the power set-points of PQ generators. Given that the low-level control layer acts with a negligible time constant with respect to the MPC action, the output power of the PQ generators can be assumed to be equal to the references. Because of this, simple power models are defined such that it is possible to easily express capability constraints and State Of Charge (SOC) dynamics of BESSs. It follows that

$$\mathbf{P^u}(k+1) \;=\; \mathbf{P^u}(k) \;+\; \mathbf{\Theta_u}\Delta\mathbf{u}(k)\;. \tag{6.17}$$

The same reasoning cannot be applied to the slack generator. Indeed, since it is designed to impose the reference voltage and frequency, its output active and reactive powers are determined by the power imbalances in the AC-iMG network. Therefore, the slack power output at time $k+1$ is defined to be equal power balance of the network at time k, as follows

$$P_1(k+1) = P_1(k) \;- I_P\left(\mathbf{\Theta_u}\Delta\mathbf{u}(k) + \mathbf{\Theta_d}\Delta\mathbf{d}(k)\right)\;, \tag{6.18a}$$

$$Q_1(k+1) = Q_1(k) - I_Q\left(\mathbf{\Theta_u}\Delta\mathbf{u}(k) + \mathbf{\Theta_d}\Delta\mathbf{d}(k)\right)\;, \tag{6.18b}$$

where I_P and I_Q are suitably defined to properly sum the active and reactive powers given by the PQ generators and loads units.

State of charges in BESSs

Concerning the SOC dynamics, a simple model based on the discrete integration of the output active power has been adopted, neglecting the charging and discharging efficiencies. For PQ generators, the following equation is stated

$$\mathbf{s^b}(k+1) = \mathbf{s^b}(k) + \tau_s \, \tilde{\mathbf{C}}^{\mathbf{b}} \, \tilde{\mathbf{\Theta}}_{\mathbf{u}} (\mathbf{P^u}(k) + \Delta \mathbf{u}(k)) \; , \tag{6.19}$$

where $\mathbf{s^b} = \{s_1^b, \ldots, s_{n_u}^b\}$ includes the SOCs of all PQ generators, while $\tilde{\mathbf{C}}^{\mathbf{b}}$ is defined as $\tilde{\mathbf{C}}^{\mathbf{b}} = \text{diag}\{\frac{1}{C_1^b}, \ldots, \frac{1}{C_{n_u}^b}\}$, where C_j^b corresponds to the energy capacity of the j-th PQ generator BESS, with $j \in \mathcal{N}_u$. Also in this case, an additional matrix has been introduced, i.e. $\tilde{\mathbf{\Theta}}_{\mathbf{u}} = \text{diag}\{\theta_2^u, \ldots, \theta_n^u, 0, \ldots, 0\} \in \mathbb{R}^{2(n-1),2(n-1)}$, such that just the output active powers of BESS units are selected in (6.19).

The SOC of the slack generator, denoted as s_s^b, is modelled in a slightly different form since the corresponding output active power depends also on the external disturbances, see (6.18a). Therefore it follows

$$s_s^b(k+1) \; = s_s^b(k) \; + \; \frac{\tau_s}{C_s^b} (\, P_1(k) + I_P(\mathbf{\Theta_u} \Delta \mathbf{u}(k) + \mathbf{\Theta_d} \Delta \mathbf{d}(k) \,) \; , \tag{6.20}$$

where C_s^b corresponds to slack generator storing capacity.

6.3.2 Optimization problem formulation

The high-level MPC controller is applied at the generic time instant $\bar{k}$, following the standard receding horizon technique [112]. Defining with N the prediction horizon, the optimal input sequence $\Delta \mathbf{U}(\bar{k}) = [\Delta \mathbf{u}(\bar{k}), \ldots, \Delta \mathbf{u}(\bar{k} + N - 1)]$ is initially computed through the optimization problem defined in the following; then, just the first input step is implemented. The procedure is periodically performed at each sampling time τ_s.

The input sequence $\Delta\mathbf{U}(\bar{k})$ is computed so as to respect the system constraints for the whole horizon, which are now described.

First of all, the nodal voltage magnitudes must be maintained within a predefined range, defined as $(1 \pm \alpha_v)V^o$, where V^o is the network nominal voltage and $\alpha_v > 0$ is a tuning parameter defining the maximum allowed deviation. Therefore it follows that

$$\epsilon_v + (1 - \alpha_v)V^o \leq V_i(k) \leq (1 + \alpha_v)V^o + \epsilon_v \,, \quad \forall i \in \mathcal{N} \,, \tag{6.21}$$

where ϵ_v is a slack variable, introduced for avoid unfeasibility issues. Indeed, it is good practice to not hardly constrain variables that are not directly controlled by the MPC regulator, as it is for the voltages, as discussed in [112].
PQ generators must be operated such that the active and reactive powers limits are respected, as well as the limitations on maximum and minimum SOCs. Therefore, the following constraints are stated

$$\underline{\mathbf{P}}^{\mathbf{u}} \leq \mathbf{P}^{\mathbf{u}}(k) \leq \overline{\mathbf{P}}^{\mathbf{u}} \,, \tag{6.22}$$

$$\underline{\mathbf{s}}^{\mathbf{b}} \leq \mathbf{s}^{\mathbf{b}}(k) \leq \bar{\mathbf{s}}^{\mathbf{b}} \,. \tag{6.23}$$

Concerning the slack generator power constraints, the parameters $\Delta\bar{P}^d$ and $\Delta\bar{Q}^d$ are initially introduced, representing the maximum unexpected power variation by non-deterministic units. Therefore, its active power capability limits are defined as

$$P_1(k) \leq \min\left\{\frac{(s_s^b(k) - \underline{s}_s^b)C_s^b}{\tau_s}, \quad \bar{P}_1\right\} - \Delta\bar{P}^d + \epsilon_p \,, \tag{6.24}$$

$$P_1(k) \geq -\min\left\{\frac{(\bar{s}_s^b - s_s^b(k))C_s^b}{\tau_s}, -\underline{P}_1\right\} + \Delta\bar{P}^d - \epsilon_p \,. \tag{6.25}$$

The first term of expression (6.24), and of (6.25), serves to quantify the maximum power that the slack generator can deliver, or absorb, based

both on the BESS power limits and the stored energy at time k. Then, this quantity is subtracted by the maximum possible power deviation of loads, so as to be sure that the slack generator has always enough power margin to compensate unexpected power imbalances. Finally, a slack variable ϵ_p is also considered.
Similarly, the reactive power constraints of the slack generator can be stated as follows

$$-\epsilon_q + \Delta\bar{Q}^d + \underline{Q_1} \leq Q_1(k) \leq \bar{Q}_1 - \Delta\bar{Q}^d + \epsilon_q \,, \tag{6.26}$$

where ϵ_q is a slack variable.

Since there is no precise knowledge of the duration of the islanding condition, the SOC of the slack generator is constrained to evolve in a smaller range with respect to the maximum capacity limits, as follows

$$-\epsilon_s + \alpha_s \underline{s}_s^b \leq s_s^b(k) \leq (1-\alpha_s)\,\overline{s}_s^b + \epsilon_s \,, \tag{6.27}$$

where $\alpha_s > 0$ is a design parameter; also this constraint is defined as a soft one through the slack variable ϵ_s.

Having defined all the units constraints, the cost function of the MPC problem follows

$$\begin{aligned} J(\bar{k}) = \sum_{k=\bar{k}}^{\bar{k}+N} & w_L \mathbf{P^L}(k)'\mathbf{P^L}(k) + w_u \Delta\mathbf{u}(k)'\Delta\mathbf{u}(k) + \\ & + w_\epsilon \left(\epsilon_v^2 + \epsilon_s^2 + \epsilon_p^2 + \epsilon_q^2\right) , \end{aligned} \tag{6.28}$$

where $w_L > 0$ is used for the power losses minimization, while $w_u > 0$ is used to avoid unnecessary changes of the control inputs. Finally, the term w_ϵ is introduced to discourage the use of the slack variables, therefore $w_\epsilon >> w_u, w_L$.

At the generic time $\bar{k}$, the high-level MPC samples the network states, indicated by the state-space equations in (6.13)-(6.20), and it performs the linearization procedure described in Section 6.3.1.

Line power losses are supposed to be not measurable, as they can computed through (6.14) using the measured electrical variables at the time instant $\bar{k}$.

Therefore, the MPC optimization problem is stated

$$\begin{aligned} &\min_{\substack{\Delta\mathbf{U}(\bar{k}),\\ \epsilon_v,\epsilon_s,\epsilon_p}} J(\bar{k}) \\ \text{subject to} \quad & \\ & (6.13)\text{-}(6.27), \\ & \forall\, k = \{\bar{k}, \ldots, \bar{k}+N-1\}\ . \end{aligned} \tag{6.29}$$

Remark 6.2. *It should be noted that a modelling approximation is introduced by the fact that the linearized model at $\bar{k}$ is used for the whole prediction horizon for solving (6.29). Nevertheless, numerical results show that the approximation is acceptable if a limited prediction horizon is adopted.*

6.4 Numerical results

The considered AC-iMG benchmark is depicted in Figure 6.2. It consists of a 6-nodes 20 kV network, where line lengths are reported in Figure 6.2 and specific impedances are assumed to be $Z = 1.5 + j0.4\ \Omega/km$. Since a small-size AC-iMG is considered, line impedances are more resistive than in an usual medium-voltage grid; nevertheless, numerical results show that power losses and voltage drops are acceptable. The system has been simulated for 1 hour, using the Simscape Power Systems MATLAB toolbox, particularly suited for these applications. The primary controllers, espressed in (6.4) and (6.8), are implemented directly in the simulation environment, while MPC regulator is periodically solved, based on the systems measures, using the CPLEX solver.
The AC-iMG is supported by three BESS generation units, whose capabilities are presented in Table 6.2. Non-dispatchable power trends,. i.e. the two loads and the PV generator, are shown in Figures 6.3(a) and (b). The high-level MPC has been designed to act with a time sample

Table 6.2: Storage generation units

	$(\underline{P}, \bar{P})$ [MW]	$(\underline{Q}, \bar{Q})$ [MVAR]	C^b [MWh]
Slack generator	$(-2, +2)$	$(-2, +2)$	1
PQ generator 1, 2	$(-1, +1)$	$(-1, +1)$	0.5

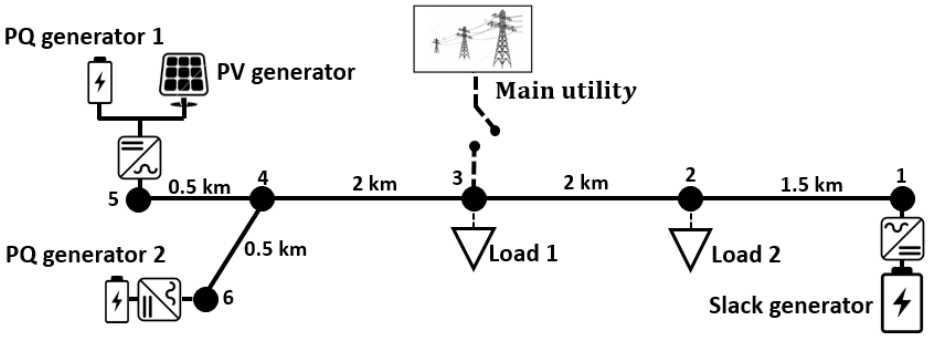

Figure 6.2: AC islanded microgrid benchmark

$\tau_s = 10\,s$, much larger than low-level control transients, and with a prediction horizon $N = 12$, i.e. corresponding to two minutes.

Considering the optimization problem, the tolerance ranges for nodal voltages and slack generator SOC are set $\alpha_v = 1\%$ and $\alpha_s = 20\%$, respectively; on the other hand, the maximum non-dispatchable power variation is assumed to be equal to $\Delta\bar{P}^d = 0.5\,\text{MW}$ and $\Delta\bar{Q}^d = 0.4$ MVAR. Figures 6.3(c) and (d) show the generated active and reactive power trends of BESSs, respectively, while Figure 6.3(e) reports the evolution of their SOCs. It is possible to notice that during the first 30 minutes, the control system distributes quite homogeneously the load demand between the slack generator, located at the network right-side, and the two PQ generators, located at the left-side. In particular, due to non-dispatchable generation from the PV system in node 5, the BESS of PQ generator 1 is charged while the BESS in node 6 delivers a limited amount of active power. This power distribution minimizes line power losses while maintaining nodal voltages in the predefined band. The same reasoning holds for the dispatch of generators reactive powers, depicted in Figure 6.3(b).

After the first 30 minutes, the slack generator's SOC reaches the minimum lower bound, i.e. 20%, and therefore the MPC system coordinates the other PQ generators such that the slack generator substantially does not generate active power. This results in the discharge of the BESS in node 6 at time 45 min, which is then compensated by an increase of the active power reference for the BESS unit in node 5. Figure 6.3(f) shows the overall power losses normalized with respect to the total generated active power: it can be noted that, as long as SOC constraints are not violated, the control system efficiently manages the power references achieving a reduced amount of power losses (around 1%). It should be underlined that, considering a real application, it is usually expected that islanded condition ends before BESS units are fully discharged.

Concerning nodal voltages, the effect of the load step at time 5 min is depicted in Figure 6.4. In particular, two simulations have been carried out, depending on load predictions availability. As it possible to notice from Figure 6.4(a), the MPC arranges the PQ generation units making the nodal voltages increase, in order to avoid violating the predefined voltage band when the foreseen load step occurs. On the other hand, if load predictions are not available, the control system can not prevent voltages to violate the lower bound but, at the following MPC iteration, voltages are forced back in the predefined range, see Figure 6.4(b).

Being the high-level model obtained through a linearization procedure, having no predictions means to assume that non-dispatchable units do not vary their power output during the MPC prediction horizon, i.e. in the next 120 seconds; this is a quite reasonable assumption for practical implementation of the proposed hierarchical control structure.

Finally, the performances of the low-level controllers described in Section 6.2 are reported: Figure 6.4(c) shows the slack generator voltage transient due to the load step occurring at 5 min, while Figure 6.4(d) reports the tracking of the PQ generators' active and reactive power references, fed as ramp-wise signals.

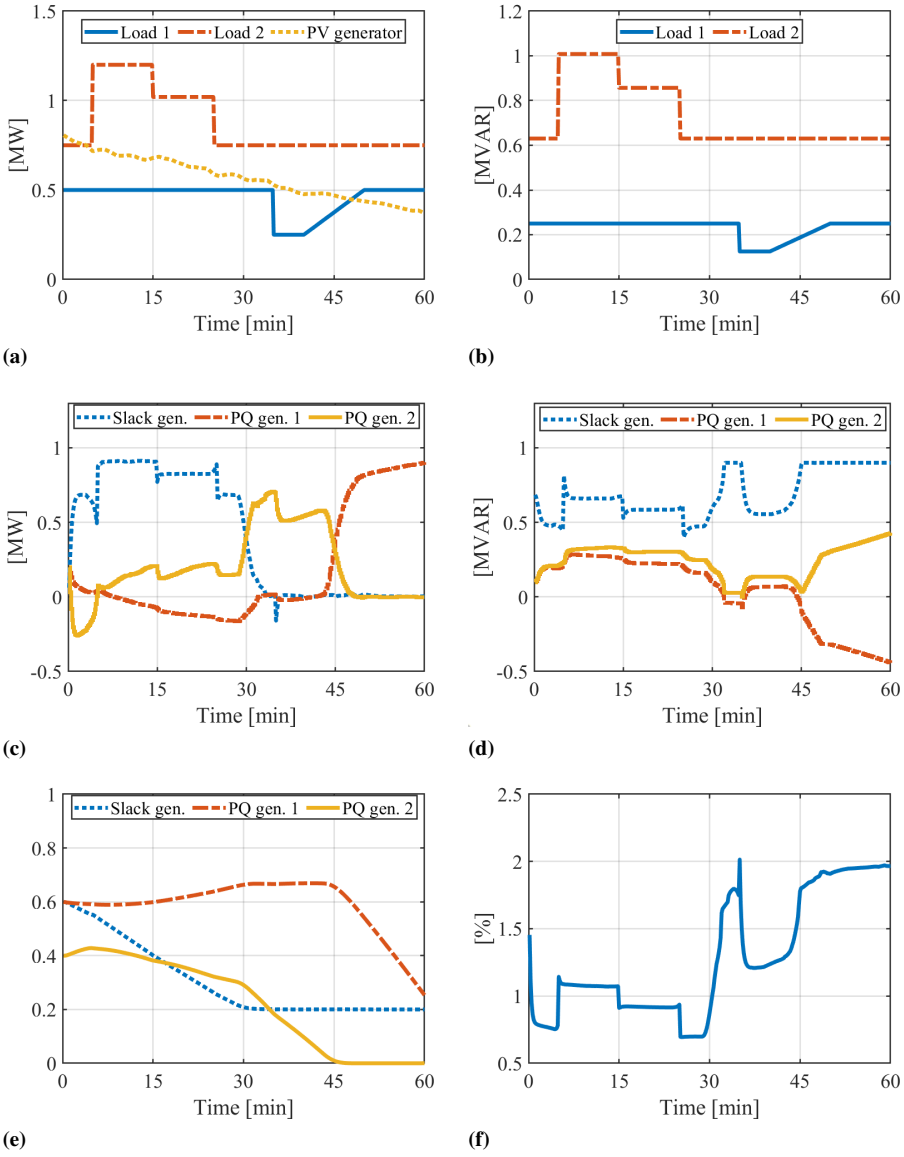

Figure 6.3: (a) Non-dispatchable active power profiles; (b) non-dispatchable reactive power profiles; (c) dispatchable active power profiles; (d) dispatchable reactive power profiles; (e) states of charge of BESS; (f) total power losses (expressed in percentage with respect to the total active power generation)

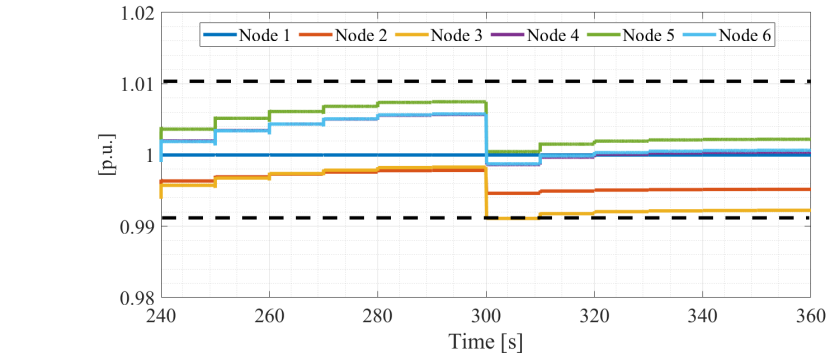

(a)

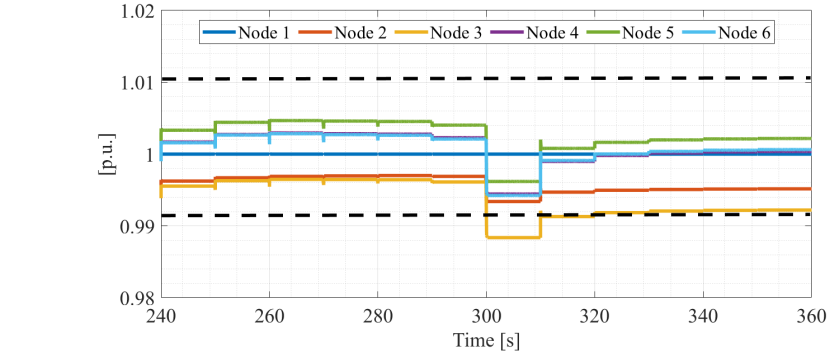

(b)

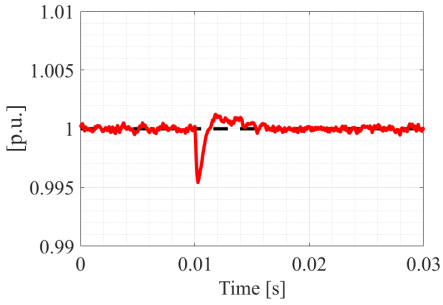

(c)

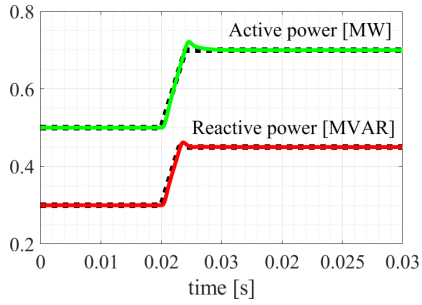

(d)

Figure 6.4: Voltages in case of (a) available load predictions and (b) unavailable load predictions: nodal voltages (continuous line) and voltage tolerance band (dashed line). (c) Slack output voltage and (d) PQ generator output powers at $t = 5$ min: measured (continuous line), references (dashed-line).

6.5 Conclusion

This chapter concerned the design of a hierarchical control structure for an islanded microgrid with AC network. This involves a low-level decentralized control layer, allowing to achieve stable operation of the slack and of the PQ generation nodes, and a high-level MPC managing the PQ units considering voltages deviation, units capabilities and overall power losses. Simulation results witness the potentialities of the proposed approach, even if load power demand is not known.

CHAPTER 7

Three-layer control of DC islanded microgrids with flexible structure

7.1 Introduction

During recent years, a growing interest is raising for Direct Current (DC) Microgrids (MGs), due to their ability to interface naturally with several Renewable Energy Sources (RESs), Battery Energy Storage Sources (BESSs), and electronic loads (LEDs, Electric Vehicles, etc.), as discussed in [113]. DC MGs can be also operated in islanded mode, relying on their local Distributed Generation Units (DGUs), requiring however dedicated control architectures to be properly operated [114].
With respect to the solution proposed in Chapter 6, here the design of a flexible control architecture allowing for a more efficient resource management is proposed (considering a prediction horizon of hours instead of minutes), where DGUs can be disconnected and reconnected, without

affecting the MG stable operation in the islanded condition.

7.1.1 Literature Review

The overall control of a DC Islanded Microgrid (DC-iMG) is a multi-objective problem spanning different control stages, time scales, and physical layers. For a stable and economic operation, a hierarchical control scheme is generally employed, [113–115]. The primary control layer, acting at the component level, is responsible for voltage stability, which is crucial for DC iMGs. Many research studies have aimed to define decentralized stabilizing primary controllers, implemented at each DGU to track suitable voltage references, based on different control techniques, such as droop control [114, 116], plug-and-play [117, 118], and sliding-mode [39].
Primary controllers, however, are unable to account for various operational and economic constraints necessary for continuous and proper functioning of the DC-iMG. High-level supervisory control architectures are, therefore, necessary to coordinate the voltage references provided to the primary layers. Consensus-based controllers assigning appropriate voltage references to guarantee proportional load sharing and voltage balancing are discussed in [119, 120]. Despite their distributed structure, these controllers assume load satisfiability and unsaturated inputs at all times.
These limitations can be overcome by designing a proper Energy Management System (EMS), which can meet specified power and energy objectives while respecting system constraints. Flowchart-based EMS encompassing multiple case scenarios are discussed in [121, 122] whereas the use of optimization methods and predictive algorithms to design EMS is discussed in [123]. In general, EMS for MGs, for example based on stochastic or mixed-integer optimization algorithms, utilize power balance equations and provide the optimal power generations set-points to the DGUs [124–127]. Nevertheless, when the primary layer is voltage controlled, standard EMSs cannot be directly implemented, as the optimal power references need to be translated into suitable voltage set-points for the DGUs. Such a translation is not straightforward for MGs with meshed topologies and, effectively, requires the solution of power-flow

equations. Moreover, considering that the voltages can solely be enforced at the DGUs nodes thanks to the primary controllers, a unique voltage equilibrium may fail to exist at the load nodes, especially in the presence of nonlinear loads [128].

7.1.2 Proposed solution

These issues motivated the design of a novel three-layered hierarchical control architecture for the operation of a DC-iMG with arbitrary topology. A schematic of the proposed architecture is depicted in Figure 7.2, and it is structured as follows.

- An EMS sits at the upper level, denoted as tertiary level, designed with a Model Predictive Control (MPC) strategy to define the optimal power references for the DGUs based on the system constraints and objectives. Moreover, the MPC is formulated as a mixed-integer optimization problem, allowing to switch ON, or OFF, dispatchbale DGU units, to consider different operation modes for BESS and to switch the PV DGUs between Maximum Power Point Tracking (MPPT) and the voltage-controlled modes [1].

- Then, a secondary control layer is devised, which can be considered the main contribution of the chapter. This acts as an interface between the primary and the tertiary layer, converting the optimal power references from the EMS into voltage set-points, which are then tracked by the primary voltage regulators. This power-voltage conversion is performed by a properly defined optimization problem, which is based on the power-flow equations and takes into account the converter and network losses.
  Although the optimization problem is nonlinear and non-convex, it is here proved that the problem is always feasible if nodal voltages and power injections are not bounded. The existence of a solution to the power-flow equations has been addressed in [130, 131], considering however fixed DGUs voltages. Conversely, here the DGU

[1] The Maximum Power Point Tracking is a well-know strategy for controlling PV generators, acting on the converter interface to maximize the producible power given the actual solar radiation [129].

voltage references are decision variables not known *a priori*. Furthermore, as a complement, a necessary condition for the solvability of the optimization problem is proposed and proved in this chapter. It is worth noticing that the voltages can only be enforced at DGU nodes and therefore, the uniqueness of voltages at the load nodes is necessary for attaining the predefined operational objectives. Indeed, if the voltages appearing at the load nodes are different from the ones anticipated by the secondary layer, permissible voltage limits may be violated and the DGUs fail to track the power set-points provided by the EMS. In this respect, a novel condition for the uniqueness of load voltages and DGU power injections is provided and proved in this chapter. The uniqueness of voltages has also been addressed in [130], where the deduced condition depends on the generator voltages and the topological parameters of the network. Here, a novel and simpler condition is stated, depending only on local load parameters and that can be easily taken into account while designing the DC-iMG network.

- Finally, the low-level is constituted by the primary voltage controllers. It is assumed that all DGUs are equipped with voltage primary controllers, even though the analysis can be extended to scenarios where some DGUs are current-controlled [132], without compromising the validity of the approach. The implemented primary voltage controllers are designed based on the Plug-and-Play paradigm, which allows the disconnection, and the reconnection, of DGUs without spoiling the overall voltage stability. The structure and design of the primary layer, along with stability certificates and proofs, are not provided in this chapter, as a detailed analysis can be found in [118, 133].

Different from [121, 122, 127], the proposed control architecture can be applied to DC iMGs with generic topology and in the presence ZIP loads (constant impedance, constant current, and constant power), characterized by a non-linear dependence on the nodal voltages.

The structure of the iMG along with the proposed hierarchical control scheme is described in Section 7.2. The EMS-based tertiary layer and

its interaction with the secondary control layer is detailed in Section 7.3. The in-depth functioning of the secondary layer and the related theoretical derivations are presented in Section 7.4. Simulations validating theoretical results are provided in Section 7.5. Finally, conclusions are drawn in Section 7.6.

7.1.3 Preliminaries and notation

Sets, vectors, and functions: We let $\mathbb{R}$ (resp. $\mathbb{R}_{>0}$) denote the set of real (resp. strictly positive real) numbers. Given $x \in \mathbb{R}^n$, $[x] \in \mathbb{R}^{n\times n}$ is the associated diagonal matrix with x on the diagonal. The inequality $x \leq y$ for vectors $x, y \in \mathbb{R}^n$ is component-wise, that is, $x_i \leq y_i, \ \ \forall i \in 1, ..., n$. For a finite set $\mathcal{V}$, let $|\mathcal{V}|$ denote its cardinality. Given a matrix $A \in \mathbb{R}^{n\times m}$, $(A)_i$ denotes the i^{th} row. The notation $A \succ 0$, $A \succeq 0$, $A > 0$, and $A \geq 0$ represents a positive definite, positive semidefinite, positive, and nonnegative matrix, respectively. Throughout, $\mathbf{1}_n$ and $\mathbf{0}_n$ are the n-dimensional vectors of unit and zero entries, and $\mathbf{0}$ is a matrix of all zeros of appropriate dimensions. Given a weighted directed graph $\mathcal{G}(\mathcal{V}, \mathcal{E})$, with $\mathcal{V}$ the set of nodes and $\mathcal{E}$ the set of edges, its Laplacian matrix $L \in \mathbb{R}^{|\mathcal{V}|\times|\mathcal{V}|}$ is defined as

$$L = A\,\mathbf{1}_{|\mathcal{V}|} - A,$$

where A is the adjacency matrix of $\mathcal{G}$ collecting edges weights and is defined as

$$a_{ij} = \begin{cases} w_{ij} & \text{if } (i,j) \in \mathcal{E} \\ 0 & \text{otherwise} \end{cases}.$$

Moreover, all the power values are defined to be positive if delivered from a DGU, while the upper and lower bounds of each variable are denoted with superscripts max and min, respectively. The upper bar is instead used to define constant quantities.

7.2 DC microgrid structure and hierarchical control scheme

In this section, the DC-iMG structure is described and an outline of the hierarchical control structure is provided.

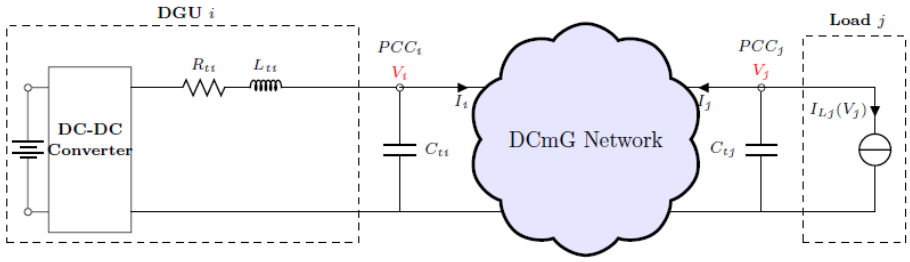

Figure 7.1: Representative diagram of the DC-iMG network with DGUs and loads.

Structure of the DC-iMG: The electric interconnections in a DC-iMG are modelled as an undirected connected graph $m\mathcal{G} = (\mathcal{V}, \mathcal{E})$. $\mathcal{V}$ is partitioned into two sets: $\mathcal{G}$ is the set of DGUs and $\mathcal{L}$ is the set of loads. The edges represent the interconnecting lines of the DC-iMG. As shown in Figure 7.1, each DGU and load is interfaced with the DC-iMG through a point of common coupling (PCC).

Distributed generation units (DGUs): The DGUs comprise a DC voltage source, a DC-DC converter, and a series RLC filter. Additionally, depending upon the type of DC voltage source, $\mathcal{G}_D$ is defined as the set of dispatchable DGUs, $\mathcal{G}_B$ as the set of DGUs interfaced with BESSs, and $\mathcal{G}_P$ as the set of DGUs connected to PV panels, where $\mathcal{G}_D \cup \mathcal{G}_B \cup \mathcal{G}_P = \mathcal{G}$.

Load model: Depending upon the type of load, the functional dependence on the PCC voltage changes and the term $I_{Lj}(V_j)$ takes different expressions. Prototypical load models that are of interest include the following:

1. constant-current loads: $I_{LI,j} = \bar{I}_{L,j}$,
2. constant-impedance loads: $I_{LZ,j}(V_j) = Y_{L,j}V_j$, where $Y_{L,j} = 1/R_{L,j} > 0$ is the conductance of the j^{th} load, and
3. constant-power loads:

$$I_{LP,j}(V_j) = V_j^{-1}\bar{P}_{L,j}, \tag{7.1}$$

where $\bar{P}_{L,j} > 0$ is the power demand of the load j.

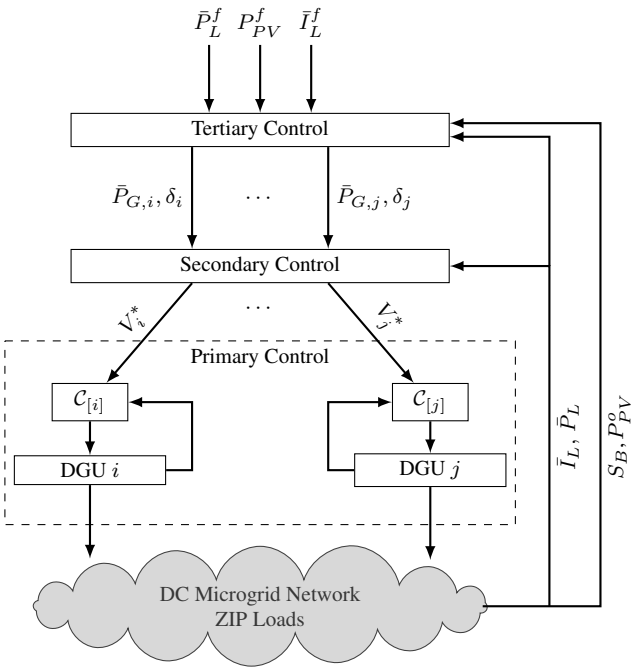

Figure 7.2: Hierarchical control scheme for DC microgrids.

To refer to the three load cases above, the abbreviations "I", "Z", and "P" are often used [134]. The analysis presented in this chapter focuses on the general case of a parallel combination of the three loads, thus on the case of "ZIP" loads, which are modeled as

$$I_{L,j}(V_j) = \bar{I}_{L,j} + Y_{L,j}V_j + V_j^{-1}\bar{P}_{L,j}. \tag{7.2}$$

The net power absorbed by the j^{th} load is given as

$$P_{L,j} = \bar{I}_{L,j}V_j + Y_{L,j}V_j^2 + \bar{P}_{L,j}. \tag{7.3}$$

7.2.1 Hierarchical control in DC microgrids

The proposed hierarchical control architecture, depicted in Figure 7.2, is constituted by three distinct layers: primary, secondary, and tertiary.
Each DGUs is equipped with local voltage regulators (not shown in Figure 7.1) forming the *primary control layer*. The main objective of these

controllers is to ensure that the voltage at each DGU's PCC tracks a reference voltage V_i^* provided by the secondary control layer.

Assumption 7.1 (Stability under primary voltage control)**.** *It is assumed that the primary controllers, under constant voltage reference $V_i^*, i \in \mathcal{G}$, achieve offset-free voltage tracking and guarantee the stability of the entire DC-iMG network. Moreover, the stability is preserved even though DGU units are connected and disconnected, as the primary layer is implemented according to the Plug-and-Play approach. The reader is referred to [113, 118, 133] for further details concerning the design of Plug-and-Play stabilizing decentralized voltage controllers.*

The EMS sits at the tertiary level, and utilizes the forecasts of PV power production P_{PV}^f, and of loads' power and current absorption $\bar{P}_L^f$, $\bar{I}_L^f$. At each sampling time, the EMS measures the nominal PV generation power P_{PV}^o, the State Of Charge (SOC) of BESSs S_B and the power and current absorption of ZIP loads $\bar{P}_L, \bar{I}_L$. Solving a MPC optimization problem, the EMS generates optimal power references $\bar{P}_{G,i}, i \in \mathcal{G}$ for the DGUs. In addition, it produces decision variables $\delta_i \in \{0, 1\}, i \in \mathcal{G}$, which can either turn on/off DGUs or change their operation mode. Since the primary layer operates only with voltage references, the secondary control layer translates the power references into appropriate voltage references V^*. The detailed structure and functioning of the secondary and tertiary control layers are discussed in Sections 7.4 and 7.3, respectively.

It is highlighted that different layers work at different time scales. In a typical scenario, the primary controllers operates in a range varying from 10^{-6} to 10^{-3} s, the secondary layer ranges from 100 to 300 s, and the tertiary layer ranges from 5 to 15 mins. At each high level sampling time, the controller provides a reference to its corresponding lower layer.

7.3 Tertiary control layer: the EMS

This section details the functioning of the MPC-based EMS, sitting at the top of the proposed hierarchical structure. The forecasts, parameters, and decision variables are described in Table 7.1.

Table 7.1: Optimization variables and system parameters for the EMS

Symbol	Description
P_{DH}, P_{CH}	Charging and discharging power of the BESS [kW]
P_B	Power output of BESS DGUs [kW]
P_D	Power output of dispatchable DGUs [kW]
P_{PV}	Power output of PV DGUs [kW]
P_{PV}^o	Nominal power production of PV DGUs [kW]
P_{PV}^f	Power production forecast of PV DGUs [kW]
P_L^o	Nominal total power absorption for ZIP loads [kW]
$\bar{I}_L^f$	Current absorption forecast for I component of ZIP loads [kVar]
$\bar{P}_L^f$	Power absorption forecast for P component of ZIP loads [kW]
S_B	State of charge (SOC) of BESS
S_B^o	Nominal SOC of BESS
η_{CH}, η_{DH}	Charging and discharging efficiency of BESS
C_B	MG BESS capacity [kWh]
V^o	Nominal network voltage [V]
δ_B	Operation mode of BESS DGU [boolean]
δ_D	Operation mode of dispatachable DGU [boolean]
δ_{PV}	Operation mode of PV DGU [boolean]
V	Nodal voltage magnitude [V]
I	Nodal current magnitude [A]

7.3.1 MPC-based EMS for islanded DC MGs

The MPC-based EMS controller is responsible for energy management and coordination of resources in the DC-iMG. The core of this controller is a receding horizon optimization problem, which enables load satisfiability, optimal scheduling of dispatchable and BESS DGUs, and maximum possible utilization of PV DGUs. The EMS is formulated as a mixed integer optimization problem, executed at the generic time instant k, with a finite prediction horizon $[k, \ldots, k+N]$, where N indicates the number of prediction steps. In the following discussion, the index i is used to define variables and constraints spanning all prediction horizon, i.e. $i \in [0, \ldots, N]$.

The MPC-based EMS is implemented according the standard *receding horizon* approach [112]. Therefore, at each time step, the EMS defines an optimal plan is formulated on power dispatch and operational modes of the units for the whole prediction horizon. However, only the first sample of the input sequence is implemented and subsequently the horizon is shifted. At the next sampling time, using updated information on forecasts and DC-iMG initial condition, a new optimization problem is solved. Next, the EMS is described in detail.

1. *DGUs*: Based upon the type of voltage source, the DGUs are characterized differently for the EMS.

   a) BESS DGUs: For these DGUs, a BESS serves as the voltage source. The SOC dynamics of a BESS $b \in \mathcal{G}_B$, considering both the charging and discharging efficiencies, are given as

   $$\begin{aligned} S_{B,b}(k+1+i) \;&=\; S_{B,b}(k+i) \;+ \\ -\; \frac{\tau}{C_{B,b}} &\Big(\frac{1}{\eta_{DH,b}} P_{DH,b}(k+i) + \eta_{CH,b} P_{CH,b}(k+i)\Big), \end{aligned} \tag{7.4}$$

   with BESS power output

   $$P_{B,b}(k+i) = P_{DH,b}(k+i) - P_{CH,b}(k+i). \tag{7.5}$$

   Since BESS DGUs can operate either in charging or discharging mode, the following constraints are stated

   $$0 \leq P_{DH,b}(k+i) \;\leq\; P^{max}_{B,b}(k+i)\,\delta_{B,b}(k+i), \tag{7.6}$$
   $$0 \leq P_{CH,b}(k+i) \;\leq\; -P^{min}_{B,b}(k+i)\,(1-\delta_{B,b}(k+i)), \tag{7.7}$$

   where $\delta_{B,i} = 1$ indicates discharging mode while $\delta_{B,i} = 0$ represents the charging mode. The SOC is constrained between minimum and maximum bounds

   $$S^{min}_{B,b} \;\leq\; S_{B,b}(k+i) \;\leq\; S^{max}_{B,b}. \tag{7.8}$$

   The constraints (7.4)-(7.8) must hold $\forall i \in [0, \ldots, N-1]$. To avoid complete charging or discharging of BESSs, not ideal for guaranteeing voltage stability and load satisfiability for all

possible contingencies, a terminal constraint on the SOC is imposed

$$S_{B,b}(k+N) = S^{o}_{B,b} + \Delta S_{B,b}\,, \tag{7.9}$$

where $\Delta S_{B,b}$ is a slack variable introduced to ensure feasibility.

b) Dispatchable DGUs: These DGUs are interfaced with a dispatchable units, as micro-generator (mGEN) units. These DGUs can be turned off or on based on the power necessity of the DC-iMG. The operational mode is governed by the variable $\delta_{D,d}, d \in \mathcal{D}_{\mathcal{D}}$, with values 1 and 0 indicating on and off states, respectively. The power produced by the dispatchable DGU must lie within a range defined by lower and upper bounds

$$\delta_{D,d}(k+i)P^{min}_{D,d} \leq P_{D,d}(k+i) \leq P^{max}_{D,d}\,\delta_{D,d}(k+i), \quad d \in \mathcal{G}_D, \tag{7.10}$$

defined $\forall i \in [0,\ldots,N-1]$.

c) PV DGUs: These DGUs can be operated in two distinct modes: MPPT and the power curtailment mode. The MPPT is the standard mode of PV systems, where the maximum possible power is injected into the grid. However, in case there an excess of power in the DC-iMG, the power curtailment mode is activated, where the EMS reduces the power produced by the PV DGU. In the power curtailment mode, the DGU is voltage-controlled using the voltage set-points computed by the secondary layer, so that to track the power reduction reference provided by the EMS. Considering the actual PV generation P^{o}_{PV} and the forecast P^{f}_{PV}, and the effective PV power output is expressed as

$$P_{PV,p}(k) = P^{o}_{PV,p}(k) - \Delta P_{PV,p}(k), \quad p \in \mathcal{G}_P, \tag{7.11}$$

$$P_{PV,p}(k+i) = P^{f}_{PV,p}(k+i) - \Delta P_{PV,p}(k+i), \tag{7.12}$$

defined for $\forall i \in [0,\ldots,N-1]$.
The variable $\Delta P_{PV,p}$ expresses the amount of curtailed power. The curtailed power cannot be arbitrary and it must fulfil the

following constraints

$$\begin{aligned}
\Delta P_{PV,p}(k) &\geq (1-\delta_{PV,p}(k))\,\epsilon, && (7.13)\\
\Delta P_{PV,p}(k) &\leq (1-\delta_{PV,p}(k))\,P^{o}_{PV,p}(k), && (7.14)\\
\Delta P_{PV,p}(k+i) &\geq (1-\delta_{PV,p}(k+i))\,\epsilon, && (7.15)\\
\Delta P_{PV,p}(k+i) &\leq (1-\delta_{PV,p}(k+i))\,P^{f}_{PV,p}(k+i), && (7.16)
\end{aligned}$$

defined for $\forall i \in [1,\ldots,N-1]$.

The parameter $\epsilon > 0$ is chosen at a sufficiently small number and $\delta_{PV,p}$ is a decision variable. The rationale behind constraints (7.13)-(7.16) is not only to limit power curtailment but also to enable one to distinguish between the operation modes. Clearly, if $\delta_{PV,p} = 1$ the MPPT is activated, i.e. $\Delta P_{PV,p}$ is forced to zero, whereas if $\delta_{PV,p} = 0$ the power curtailment mode, it must be strictly greater than zero and lower than the nominal PV power production. For more details on logic and mixed-integer constraints, the reader is referred to [135].

2. *Loads:* The nominal power absorption of the l^{th} ZIP load, $l \in \mathcal{L}$, is computed at nominal voltage by utilizing the current state of the system for the first time step

$$P^{o}_{L,l}(k) = \bar{I}_{L,l}(k)V^{o} + Y_{L,l}V^{o2} + \bar{P}_{L,l}(k),\ l \in \mathcal{L}, \qquad (7.17)$$

while forecasts are used for future time instants

$$P^{o}_{L,l}(k+i) = \bar{I}^{f}_{L,l}(k+i)V^{o} + Y_{L,l}V^{o2} + \bar{P}^{f}_{L,l}(k+i), \qquad (7.18)$$

defined $\forall i \in [1,\ldots,N-1]$.
It is worth noticing that $P^{o}_{L,l}$ is just an estimate, as net power absorption of ZIP loads depends on the actual DC-iMG voltages, as expressed in (7.3).

3. *Power balance:* In a DC-iMG, the internal power balance must be maintained. Hence, the following constraint is expressed

$$\sum_{b\in\mathcal{D}_\mathcal{B}} P_{B,b}(k+i) \;+\; \sum_{d\in\mathcal{D}_\mathcal{D}} P_{D,d}(k+i) \;+\; \sum_{p\in\mathcal{D}_\mathcal{P}} P_{PV,p}(k+i) \;+$$
$$+\; \sum_{l\in\mathcal{L}} P^{o}_{L,l}(k+i) \;=\; 0,$$

(7.19)

which is stated $\forall i \in [0,\ldots,N-1]$.
It is worth noticing that the converters and network losses are neglected at the EMS level.

4. *Cost function:* The aim is to minimize the cost of satisfying the electrical loads, hence the cost function is

$$\begin{aligned} J(k) = &\sum_{b\in\mathcal{D}_\mathcal{B}} (\Delta S_{B,b})^2\, w_{S,b} \;+ \sum_{i=0}^{N-1} \sum_{b\in\mathcal{D}_\mathcal{B}} (P_{B,b}(k+i))^2\, w_{B,b} + \\ &+ \sum_{i=0}^{N-1} \sum_{d\in\mathcal{D}_\mathcal{D}} (P_{D,d}(k+i))^2\, w_{D,d} + \\ &+ \sum_{i=0}^{N-1} \sum_{p\in\mathcal{D}_\mathcal{P}} (\Delta P_{PV,p}(k+i))^2\, w_{PV,p} + \\ &+ \underbrace{\sum_{i=0}^{N-1} \sum_{p\in\mathcal{D}_\mathcal{P}} (\delta_{PV,p}(k+i) - \delta_{PV,p}(k+i-1))^2\, w\delta_{PV,p}}_{\alpha} + \\ &+ \underbrace{\sum_{i=0}^{N-1} \sum_{b\in\mathcal{D}_\mathcal{B}} (\delta_{B,b}(k+i) - \delta_{B,b}(k+i-1))^2\, w\delta_{B,b}}_{\beta} + \\ &+ \underbrace{\sum_{i=0}^{N-1} \sum_{d\in\mathcal{D}_\mathcal{D}} (\delta_{D,d}(k+i) - \delta_{D,d}(k+i-1))^2\, w\delta_{D,d}}_{\gamma} \quad , \end{aligned}$$

(7.20)

where $w_S, w_{PV}, \ldots$ are positive weights. The EMS is designed keeping BESSs close to their nominal SOCs and using power curtailment as the last resort. Thus, the weights $w_{S,B}$ and w_{PV} are set to much higher values with respect to others, enabling $\Delta S_{B,b}$ and $\Delta P_{PV,p}$ to be nonzero only when necessary for preserving feasibility. The terms α, β and γ are included in the cost to avoid frequent changes in modes of operation of different DGUs.

At every EMS time instant, the following optimization is solved

$$\min J(k) \tag{7.21a}$$

subject to

$$(7.4) - (7.19). \tag{7.21b}$$

and the optimal power set points $\bar{P}_{B,i}, \bar{P}_{D,j}, \bar{P}_{PV,p}$ and decision variables $\bar{\delta}_{B,i}$, $\bar{\delta}_{D,j}$, $\bar{\delta}_{PV,p}$ are obtained.

7.3.2 Interaction between tertiary and secondary layers

The EMS produces power references as well as decision variables, both of which are passed down to the secondary control layer. The value of these decision variables essentially determines the topology of the DC-iMG network. This is due to the fact that dispatchable generators can be connected/disconnected from the network based on the value of $\delta_{D,j}$. Moreover, based on the value of $\delta_{PV,p}$, the PV DGUs can either inject maximum power or undergo power curtailment. While injecting maximum power, the PV DGU is governed by MPPT algorithms and automatically alters its output voltage in order to inject maximum power. Thus, in this mode, the DGU operates as a P load injecting power. When the DGU experiences a power curtailment, it injects the requested power and operates as a voltage-controlled DGU.
As mentioned earlier, the EMS power references are not directly perceivable by the primary controllers. Thus, a power-to-voltage translation is performed by the secondary controller by utilizing topology-based power-flow equations (see Section 7.4). Therefore, at every EMS time instant, the secondary controller uses the decision variables to update the DC-iMG

topology in order to accommodate the turning ON/OFF of dispatchable generators as well as operation mode of PV DGUs.

Remark 7.1. *(Connectivity of the DC-iMG network) It is assumed that the turning ON/OFF of dispatchable DGUs does not impact the connectivity of the rest of the DC-iMG network. In other words, addition or removal of a dispatchable DGUs must not split the remainder of the network into two or more disjoint iMGs. In case, critical DGUs affecting the connectivity of graph are present in the network, one can restrict their operation modes by adding additional constraints to the EMS optimization problem (see Section 7.5 for an example). As shown in [135], the variable δ_D can be used to deduce relevant constraints.*

7.4 Secondary control based on power-flow equations

The secondary control is designed to make DGUs track the power references provided by the EMS, here condensed in the vector $\bar{P}_G$. The decision variables communicated by the EMS at a given sampling instant define the topology of the network over the next EMS sampling period.

Remark 7.2. *The secondary layer, operating on a faster time scale in comparison to the EMS, utilizes a fixed topology over an EMS sampling period to perform power-voltage translation. The DC-iMG topology is updated when a new set of decision variables is received.*

To perform the power-to-voltage translation, such that proper references can be sent to primary controllers, the equations linking power and voltage are firstly deduced. The relation between power and voltage in a DC-iMG is defined by the power-flow equations dependent on DC-iMG parameters and topology.

The undirected connected graph $\tilde{\mathcal{G}} = (\tilde{\mathcal{V}}, \tilde{\mathcal{E}})$ is introduced, defining the topology of the DC-iMG for a specified EMS sampling period. The set $\tilde{\mathcal{V}}$ is partitioned into two sets: $\tilde{\mathcal{G}} = \{1, \ldots, n\}$ is the set of DGUs and $\tilde{\mathcal{L}} = \{n+1, \ldots, n+m\}$ is the set of loads. The set $\tilde{\mathcal{G}} = \tilde{\mathcal{G}}_D \cup \tilde{\mathcal{G}}_B \cup \tilde{\mathcal{G}}_P^G$, where $\tilde{\mathcal{G}}_D$ is the set of connected dispatchable DGUs, $\tilde{\mathcal{G}}_B$ is the set of BESSs, and $\tilde{\mathcal{G}}_P^G$ is the set of voltage-controlled PV DGUs. In steady

state, the inductances and capacitances can be neglected and the current-voltage relation is given by the identity $I = B\Gamma B^T V = YV$, where $B \in \mathbb{R}^{(n+m)\times|\mathcal{E}|}$ is the incidence matrix of $m\tilde{\mathcal{G}}$, I is the vector of PCC currents, V is the vector containing PCC voltages, Γ is the diagonal matrix of line conductances, and $Y \in \mathbb{R}^{(n+m)\times(n+m)}$ is the network admittance matrix [136].

On partitioning the nodes into DGUs and loads, the relation can be rewritten as

$$\begin{bmatrix} I_G \\ I_L \end{bmatrix} = \begin{bmatrix} B_G R^{-1} B_G^T & B_G R^{-1} B_G^T \\ B_L R^{-1} B_G^T & B_L R^{-1} B_G^T \end{bmatrix} \begin{bmatrix} V_G \\ V_L \end{bmatrix} := \begin{bmatrix} Y_{GG} & Y_{GL} \\ Y_{LG} & Y_{LL} \end{bmatrix} \begin{bmatrix} V_G \\ V_L \end{bmatrix}, \tag{7.22}$$

where $V_G = [V_1, \ldots, V_n]^T$, $V_L = [V_{n+1}, \ldots, V_{n+m}]^T$, $I_G = [I_1, \ldots, I_n]^T$, and $I_L = [I_{n+1}, \ldots, I_{n+m}]^T$. The subscripts G and L indicate the voltage-controlled DGUs and loads, respectively. Throughout this chapter, the following assumption is made.

Assumption 7.2. *The PCC voltage V_i is strictly positive for all $i \in \mathcal{V}$.*

It is underlined that Assumption 7.2 is not a limitation, and rather reflects a common constraint in MGs operation. Notice that, in Figure 7.1, one end of the load is connected to the PCC and the other to the ground, assumed be at zero potential by convention. Since the electric current and hence power flows from higher to lower potential, negative references and PCC voltages would reverse the role of loads and make them power generators. In order to ensure power balance in the network, this power would be absorbed by the generators. This, in effect, defeats the fundamental goal of the DC-iMG, that is, the satisfiability of the loads by virtue of the power generated by the DGUs. Furthermore, if $V_i \in \mathbb{R}^N$, then a zero-crossing for the voltages may take place. At zero voltage, the power consumed by the ZIP loads tends to infinity.

Based on the current directions depicted in Figure 7.1, it is evident that

$I_{L,j}(V_j) = -I_j,\ j \in \mathcal{L}$. Using (7.2), one can simplify (7.22) as

$$I_G = Y_{GG} V_G + Y_{GL} V_L \tag{7.23a}$$

$$-Y_L V_L - \bar{I}_L - [V_L]^{-1} \bar{P}_L = Y_{LG} V_G + Y_{LL} V_L, \tag{7.23b}$$

where $Y_L \in \mathbb{R}^{m \times m}$ is the diagonal matrix of load admittances. The vectors $\bar{I}_L$ and $\bar{P}_L$ collect consumptions of I and P loads, respectively.

The power $P_{G,i}, i \in \tilde{\mathcal{G}}$ produced by an individual DGU can be divided in the sum of power injected into the network and the filter losses. Equivalently,

$$P_G = [V_G] I_G + [I_G] R_G I_G \tag{7.24}$$

where $R_G \in \mathbb{R}^{n \times n}$ is a diagonal matrix collecting filter resistances and I_G is the vector of DGU filter currents. On pre-multiplying (7.23a) with $[V_G]$, and by using (7.24), one can rewrite (7.23) as

$$\begin{aligned} f_G(V_G, V_L, P_G) = [V_G] Y_{GG} V_G + [V_G] Y_{GL} V_L \\ + [I_G] R_G I_G - P_G = 0, \end{aligned} \tag{7.25}$$

$$\begin{aligned} f_L(V_G, V_L) = Y_{LG} V_G + Y_{LL} V_L + Y_L V_L \\ + Y_L V_L + \bar{I}_L + [V_L]^{-1} \bar{P}_L = 0. \end{aligned} \tag{7.26}$$

The equations (7.25) and (7.26) fundamentally depict the power balance and current balance at DGU and load nodes, respectively. These equations depend on the topology-dependent Y matrix, and are updated once a new set of decision variable is received. In order to translate the power references into suitable voltage references, the secondary layer solves an optimization problem, whose objective is to minimize the difference between the reference power $\bar{P}_G$ and the DGU input power P_G under the equilibrium relations (7.25) and (7.26). Firstly, a simplified version of the optimization problem is presented, where constraints on voltages and generator power are neglected. Unlike the EMS, the secondary controllers consider only the DGUs and loads connected at a given time instant, and their respective operating modes. the current topology, i.e, of the DC-iMG to perform the power-voltage translation. The secondary layer, operating

on faster time scale, utilize this topology to perform power-voltage translation until a new set of decision variables are received.

Secondary Power Flow (SPF):

$$J_{SPF}(\bar{P}_G, \bar{P}_L, \bar{I}_L) = \min_{V_G, V_L, P_G} \; ||P_G - \bar{P}_G||_2 \tag{7.27a}$$

subject to

$$f_G(V_G, V_L, P_G) = 0 \tag{7.27b}$$

$$f_L(V_G, V_L) = 0\ . \tag{7.27c}$$

As noticeable from Figure 7.2, the SPF layer requires the updated load consumption $(\bar{P}_L, \bar{I}_L)$ and the power references $\bar{P}_G$ in order to solve (7.27). The set $\mathcal{X}$ is introduced, as the set of all (V_G, V_L, P_G) that satisfy (7.27b)-(7.27c) simultaneously. Hereafter, necessary and sufficient conditions are discussed, ensuring that the set $\mathcal{X}$ is nonempty. Two preliminary Lemmas are firstly introduced.

Lemma 7.1. *The matrix Y_{LL} can be written as*

$$Y_{LL} = \hat{Y}_{LL} + [-Y_{LG}\mathbf{1}_n], \tag{7.28}$$

where $\hat{Y}_{LL}$ is a Laplacian matrix .

Proof. The network admittance matrix Y is a Laplacian with zero row sum [136]. Matrix Y_{LL}, a submatrix of Y, is symmetric with positive diagonal and non-negative off-diagonal entries. Since the network graph $\mathcal{G}$ is connected, Y_{LL} has at least one row with strictly positive row sum. Y_{LL} is a Laplacian matrix with self loops [137] and, therefore, can be written as (7.28). □

Lemma 7.2. *The matrix $-(Y_{LL} + Y_L)^{-1} Y_{LG}$ has no rows with all zero entries and is nonnegative.*

Proof. The matrix $-Y_{LG}$ is a non-negative matrix and, since the graph is connected, has at least one row with non-zero row sum. The statement of the above Lemma follows from the fact that $Y_{LL} + Y_L$ is a Laplacian matrix with self loops and its inverse is strictly positive [137]. □

Next, it is shown that **SPF** is always feasible.

Proposition 7.1. *The feasible set $\mathcal{X}$ is non-empty . In particular, for all $\bar{P}_L \in \mathbb{R}^m$ and $\bar{I}_L \in \mathbb{R}^m$, the following statements hold:*

1. *The equation (7.27c) is always solvable.*
2. *The solvability of (7.27c) implies that (7.27b) is solvable.*

Proof. Under Assumption 7.2, the equation (7.27c) can be written as follows:

$$[V_L]\,\tilde{Y}_{LL}\,V_L + [V_L]\,Y_{LG}\,V_G + [V_L]\,\bar{I}_L + \bar{P}_L = 0, \tag{7.29}$$

where $\tilde{Y}_{LL} = Y_{LL} + Y_L$. Using Banach fixed-point theorem, as shown in [130], it can be proven that for a fixed V_G, a corresponding V_L solving (7.27c) exists if

$$\Delta = ||P_{crit}^{-1}\,\bar{P}_L||_\infty \;<\; 1 \tag{7.30}$$

where

$$P_{crit} = \frac{1}{4}\,[\tilde{V}]\,\tilde{Y}_{LL}\,[\tilde{V}] \tag{7.31}$$

and

$$\tilde{V} = -\tilde{Y}_{LL}^{-1}\,Y_{LG}V_G - \tilde{Y}_{LL}^{-1}\bar{I}_L. \tag{7.32}$$

Different from [130], here V_G is a free variable. Therefore, for the solvability of (7.27c), it is enough to show that a V_G can be always found such that (7.30) is satisfied for any $\bar{I}_L$ and $\bar{P}_L$.
Consider $V_G^\alpha = \alpha\,\mathbf{1}_n$, with $\alpha \in \mathbb{R}_{>0}$. Therefore,

$$\tilde{V}^\alpha = -\tilde{Y}_{LL}^{-1}\,Y_{LG}V_G^\alpha - \tilde{Y}_{LL}^{-1}\bar{I}_L = \alpha(-\tilde{Y}_{LL}^{-1}\,Y_{LG}\mathbf{1}_n) - \tilde{Y}_{LL}^{-1}\bar{I}_L.$$

Given Lemma 7.2, $(-\tilde{Y}_{LL}^{-1}\,Y_{LG}\mathbf{1}_n)$ is a positive vector. Hence, there exists an $\bar{\alpha} \in \mathbb{R}_{>0}$ such that $\tilde{V}^\alpha > 0 \;\; \forall \alpha > \bar{\alpha}$.
Considering $i, j \in \mathcal{L}$, any element (i,j) of the matrix $(P_{crit}^\alpha)^{-1}$ can be expressed as follows

$$(P_{crit}^\alpha)_{ij}^{-1} \;=\; 4\,(\tilde{Y}_{LL})_{i,j}^{-1}/(\tilde{V}_i^\alpha\;\tilde{V}_j^\alpha). \tag{7.33}$$

It is evident that $(P_{crit}^\alpha)_{ij}^{-1}$ is inversely proportional to the parameter α, for $\alpha > \bar{\alpha}$. As a result, it is always possible to increase α such that (7.30) is verified for any $\bar{P}_L$ and $\bar{I}_L$. Consequently, a voltage solution (V_G^*, V_L^*) of (7.27c) always exists, proving statement 1.

Regarding statement 2, it is evident that (7.27b) is linear with respect to P_G. This implies that, for any solution (V_G^*, V_L^*) of (7.27c), a corresponding P_G^* solving (7.27b) always exists. □

Proposition 7.1 guarantees the feasibility of **SPF**. Now, its optimality is discussed. If **SPF** achieves the optimal cost $J_{SPF}^* = 0$, it implies that a voltage solution exists such that the power references $\bar{P}_G$ are exactly tracked by the DGUs. This condition can not be achieved for any value of $(\bar{P}_L, \bar{I}_L, \bar{P}_G)$. The following proposition, inspired by [138], presents a necessary condition that must hold for $J_{SPF}^* = 0$. The proof nonetheless is different as DGU filter losses are also taken into account.

Proposition 7.2. *If the **SPF** achieves the optimal cost $J_{SPF}^* = 0$, then*

$$\sum_{\forall i \in \mathcal{D}} \bar{P}_G \geq \sum_{\forall i \in \mathcal{L}} \bar{P}_L - \frac{1}{4} \bar{I}_L^T \tilde{Y}_{GG}^{-1} \bar{I}_L, \tag{7.34}$$

where $\tilde{Y}_{GG} = Y_{GG} - Y_{GL}^T (Y_{LL} + Y_L) Y_{GL}$.

Proof. Under Assumption 1, equations (7.27b) and (7.27c) can be expressed in a single matrix equality as follows

$$\begin{aligned} f(V, P_G) = [V]\, \tilde{Y}\, V \;+\; [V] \widetilde{I} \;+ \begin{bmatrix} [I_G]\, R\, I_G \\ \mathbf{0} \end{bmatrix} \\ + \begin{bmatrix} -P_G \\ \bar{P}_L \end{bmatrix} = \mathbf{0}_{n+m}, \end{aligned} \tag{7.35}$$

where $\widetilde{I} = \begin{bmatrix} \mathbf{0}_n^T & \bar{I}_L^T \end{bmatrix}^T$, and $\tilde{Y} = Y + \begin{bmatrix} \mathbf{0} & \mathbf{0} \\ \mathbf{0} & Y_L \end{bmatrix}$. To achieve $J_{SPF}^* = 0$, a solution (V, P_G) to **SPF** must exist such that $P_G = \bar{P}_G$ and

$$f(V, \bar{P}_G) = \mathbf{0}_{n+m}. \tag{7.36}$$

On multiplying the above equation by $\mathbf{1}_{n+m}^T$ on both sides, one obtains

$$\begin{aligned} \mathbf{1}_{n+m}^T\, f(V, \bar{P}_G) = \; & V^T\, \tilde{Y}\, V \;+\; V^T\, \widetilde{I} \;+\; I_G^T\, R\, I_G \\ & - \mathbf{1}_n^T\, P_G \;+\; \mathbf{1}_m^T\, \bar{P}_L \;=\; 0\,. \end{aligned} \tag{7.37}$$

If the solution exists for (7.35), then, one can also verify (7.36). Using simple computations, equation (7.37) can be rewritten as

$$\begin{aligned}(V + \frac{1}{2}\tilde{Y}^{-1}\widetilde{I})^T\,\tilde{Y}\,(V + \frac{1}{2}\tilde{Y}^{-1}\widetilde{I}) + I_G^T\,R_G\,I_G \\ = \frac{1}{4}\,\widetilde{I}^T\,\tilde{Y}^{-1}\,\widetilde{I} + \sum_{\forall i \in \mathcal{D}} \bar{P}_G - \sum_{\forall i \in \mathcal{L}} \bar{P}_L.\end{aligned} \tag{7.38}$$

Note that the matrices $\tilde{Y} \succ 0$ and $R_G \succ 0$, and hence, if a voltage solution V exists, then

$$(V + \frac{1}{2}\tilde{Y}^{-1}\widetilde{I})^T\,\tilde{Y}\,(V + \frac{1}{2}\tilde{Y}^{-1}\widetilde{I}) + I_G^T\,R\,I_G \geq 0. \tag{7.39}$$

We highlight that I_G is a function of V (see (7.23a)). This further implies that

$$\frac{1}{4}\,\widetilde{I}^T\,\tilde{Y}^{-1}\,\widetilde{I} + \sum_{\forall i \in \mathcal{D}} \bar{P}_G - \sum_{\forall i \in \mathcal{L}} \bar{P}_L \geq 0. \tag{7.40}$$

Using standard results on the inverse of block matrices, the expression $\widetilde{I}^T\,\tilde{Y}^{-1}\,\widetilde{I}$ can be simplified as $\bar{I}_L^T\,(\,\tilde{Y}_{GG}\,)^{-1}\,\bar{I}_L$, where $\tilde{Y}_{GG}$ is the Schur complement of $\tilde{Y}$ [139]. The matrix $\tilde{Y}^{-1}$ can be represented as a block matrix

$$\tilde{Y}^{-1} = \begin{bmatrix} A & B \\ C & D \end{bmatrix} \tag{7.41}$$

Using the properties of block matrices inversion, it can be proven that D corresponds to the Schur complement of $\tilde{Y}$, i.e. $D = (\tilde{Y}_{GG} - Y_{GL}^T\,Y_{LL}^{-1}Y_{GL})^{-1}$, as discussed in [140]. Therefore, equation (7.40) can be written as follows

$$\sum_{\forall i \in \mathcal{D}} \bar{P}_G \geq \sum_{\forall i \in \mathcal{L}} \bar{P}_L - \frac{1}{4}\,\bar{I}_L^T\,(\tilde{Y}_{GG} - Y_{GL}^T\,Y_{LL}^{-1}Y_{GL})^{-1}\,\bar{I}_L \tag{7.42}$$

which expresses the necessary condition for the existence of a solution V to (7.36). □

Remark 7.3. *It is highlighted that the necessary condition (7.42) depends only on the network parameters and load consumption. Therefore, it can be incorporated in the EMS optimization problem as a constraint for the choice of the power references* $\bar{P}_G$.

In a real DC-iMG, the power output P_G is constrained by physical limits of the DGUs. Moreover, the components of the DC-iMG are designed to operate around the nominal voltage. Hence, both nodal voltages and DGU powers must respect certain constraints, which are not incorporated in the aforementioned **SPF**. Consequently, the following optimization problem is introduced with additional operational constraints.

Secondary Constrained Power Flow (SCPF):

$$J_{SCPF}(\bar{P}_G, \bar{P}_L, \bar{I}_L) = \min_{V_G, V_L, P_G} ||P_G - \bar{P}_G||_2 \tag{7.43a}$$

subject to

$$f_G(V_G, V_L, P_G) = 0 \tag{7.43b}$$
$$f_L(V_G, V_L) = 0 \tag{7.43c}$$
$$V_G^{min} \leq V_G \leq V_G^{max} \tag{7.43d}$$
$$V_L^{min} \leq V_L \leq V_L^{max} \tag{7.43e}$$
$$P_G^{min} \leq P_G \leq P_G^{max} \ . \tag{7.43f}$$

If (7.43d)-(7.43f) are not considered, the feasibility of (7.43a)-(7.43c) is theoretically guaranteed by Proposition 7.1. Nevertheless, if the DC-iMG is properly designed, a feasible solution should always exist also if voltages and power constraints are considered. In fact, the infeasibility of the **SCPF** would imply the absence of sufficient power generation to satisfy the load demand and losses in the allowed voltage range, which a problem related to the DC-iMG physical design.

Given the above motivations, and the stated Proposition 7.1, it is assumed that a solution of (7.43) always exist, as it will be shown by the numerical results.

At this stage, the properties of the optimal solution $\mathbf{x}^* = (V_G^*, V_L^*, P_G^*)$ of **SCPF** are analysed, assuming it exists.
As mentioned before, the secondary control layer acts as an interface between the EMS (tertiary layer) and the local voltage regulators (primary layer). The voltage V_G^* obtained from the **SCPF** is transmitted as a reference to the primary voltage controllers of the DGUs. It is highlighted that just the component V_G^* of $\mathbf{x}^*$ can be directly imposed in the DC-iMG, since the load nodes are not equipped with voltage controllers and the generators are not controlled to track power references.

Therefore, it is important to guarantee that, for a given voltage reference V_G^* at the DGU nodes, it results that P_G^* is the power produced by the DGUs and V_L^* appears at the load nodes.
This implies that for a fixed V_G^*, the unique solution satisfying the power flow equation (7.25)-(7.26) must be $V_L = V_L^*,\ P_G = P_G^*$. This uniqueness property is stated by means of the following theorem.

Theorem 7.1. *Consider the optimal solution* $\boldsymbol{x}^* = (V_G^*, V_L^*, P_G^*)$ *of* (7.43). *For a fixed* V_G^*, *the pair* (V_L^*, P_G^*) *is the unique solution of* (7.25)-(7.26) *in the set* $\mathcal{Y} = \{(V_L, P_G) : V_L > V_L^{min},\ P_G \in \mathbb{R}^n\}$ *if*

$$\bar{P}_{L,i} < (V_i^{min})^2\, Y_{L,i}, \quad \forall i \in \tilde{\mathcal{L}}. \tag{7.44}$$

Proof. For a fixed V_G^*, the power-flow equations (7.25)-(7.26) can be rewritten as

$$\begin{aligned} \tilde{f}_G(V_L, P_G) = \ f_G(V_G, V_L, P_G)\Big|_{V_G = V_G^*} \ = \ [V_G^*] Y_{GG} V_G^* \\ + \ [V_L] Y_{LG} V_L + [I_G] R_G I_G - P_G = 0, \end{aligned} \tag{7.45}$$

$$\begin{aligned} \tilde{f}_L(V_L) = f_L(V_G, V_L)\Big|_{V_G = V_G^*} = Y_{LG}\, V_G^* \ + Y_{LL}\, V_L \\ + Y_L V_L + \bar{I}_L + \ [V_L]^{-1}\, \bar{P}_L = 0. \end{aligned} \tag{7.46}$$

First of all, equation (7.46) is analysed. Note that $\tilde{f}(V_L^*) = 0$ since V_L^* is a feasible solution obtained from the **SCPF**. Moreover, if the function $\tilde{f}_L(V_L)$ is injective, then V_L^* is the unique solution of (7.46).
To show the injectivity of $\tilde{f}_L(V_L)$, we first evaluate its Jacobian with respect to V_L, given as

$$\mathcal{J}(V_L) = \frac{\partial \tilde{f}_L(V_L)}{\partial V_L} = Y_{LL} + Y_L - \left[[V_L]^{-2}\bar{P}_L\right]. \tag{7.47}$$

As stated in [141, Theorem 6], if the Jacobian (7.47) of the function $\tilde{f}_L(V_L)$ is symmetric and positive definite in a convex region Ω, then $\tilde{f}_L(V_L)$ is injective in Ω. Note that $\mathcal{J}(V_L)$ is symmetric by construction. Moreover, using Lemma 7.1, one can split (7.47) into

$$\mathcal{J}(V_L) = \hat{Y}_{LL} + \underbrace{[-Y_{LG}\mathbf{1}_n] + Y_L - \left[[V_L]^{-2}\bar{P}_L\right]}_{\widetilde{M}}, \tag{7.48}$$

where $\hat{Y}_{LL} \succeq 0$ and $-Y_{LG}$ is a nonnegative matrix. For $\mathcal{J}(V_L)$ to be positive definite, it is sufficient to show that $\tilde{M} \succ 0$. Since $\tilde{M}$ is a diagonal matrix,

$$-\sum_{j\in\mathcal{D}} Y_{ij} + Y_{L,i} - \bar{P}_{L,i}V_i^{-2} > 0, \quad \forall i \in \tilde{\mathcal{L}}. \tag{7.49}$$

We remark that $-\sum_{j\in\mathcal{D}} Y_{ij}$ is positive only if load i is connected directly to at least one DGU, and is otherwise zero. Hence, if

$$\bar{P}_{L,i} < V_i^2\, Y_{L,i}, \tag{7.50}$$

then (7.49) is automatically satisfied and consequently $\mathcal{J}(V_L) \succ 0$. Using (7.50), one can deduce that $\tilde{f}_L(V_L)$ is injective in Ω given as

$$\Omega = \{\, V_i :\ V_i > \sqrt{\frac{\bar{P}_{L,i}}{Y_{L,i}}}, \quad \forall i \in \tilde{\mathcal{L}}\,\}.$$

Since $V_{Li}^* \in [\, V_{Li}^{min}, V_{Li}^{max}\,]$ and (7.44) holds, V_L^* always belongs to Ω. The uniqueness of V_L^* in Ω follows from the injectivity of $\tilde{f}_L(V_L)$; moreover, given (7.44), V_L^* is unique in $\mathcal{Y}$. Consequently, considering that $\tilde{f}_G(V_L^*, P_G^*) = 0$, it is evident that $P_G = P_G^*$ is the unique solution of (7.45) if $V_G = V_G^*$ and $V_L = V_L^*$. □

Remark 7.4. *(Condition (7.44) and stability) The uniqueness condition (7.44) essentially limits the power consumption of P loads. As shown in [118], due to the negative impedance introduced by the P loads, their power consumption* $P_{L,i} < (V_i^*)^2 Y_{L,i}, i \in \tilde{\mathcal{L}}$ *in order to guarantee stability. Since* V_i^* *is the solution of* ***SCPF****,* $V_i^* \geq V_i^{min}$*, by satisfying (7.44), one can simultaneously guarantee the uniqueness of load voltages and the stability of the DC-iMG.*

7.5 Numerical Results

The aim of this section is to show the performance of the proposed hierarchical control scheme via simulation studies conducted in MATLAB. The 16-bus DC feeder in meshed stand-alone configuration described in [142] is considered, equipped with three BESS DGUs, two dispatchable DGUs, a PV DGU, and ten ZIP loads (see Figure 7.3). The DC-iMG is operated at a nominal voltage $V^o = 100$ V with nodal voltages lying between $V^{min} = 0.9V^o$ and $V^{max} = 1.1V^o$. The DGU parameters utilized by the EMS are given in Table 7.2.

Three types of loads are considered, denoted by subscripts A, B, and C, based on different consumption patterns. The daily evolution of the constant current and constant power terms of the loads are shown in Figure 7.4 (a) and (b), while the admittances are set as $Y_{L,A} = 0.8$ S, $Y_{L,B} = 0.7$ S, $Y_{L,C} = 0.6$ S. Figures 7.4 (c)-(f) show the total power absorption of loads and the total production of the PV DGU, at the nominal voltage and according to the available forecasts.

The DGUs are interfaced with synchronous Buck converters and controlled by the primary voltage controllers studied in [118].
It is evident that turning off dispatchable DGUs at nodes 1 and 2 simultaneously splits the network into two separate iMGs (see Figure 7.3). This can be circumvented by adding the simple constraint $\delta_{D,1}(k) + \delta_{D,2}(k) \geq 1$ to the EMS optimization problem (7.21).

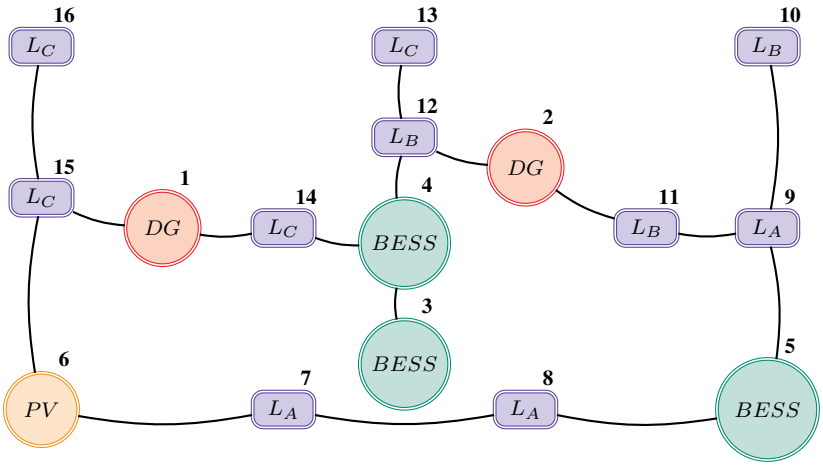

Figure 7.3: DC-iMG based on the modified 16-bus feeder [142]. The letters DG, $BESS$, and PV denote Dispatchable Generators, Battery Energy Storage Systems, and Photovoltaic DGUs, respectively. The letter L indicates Loads with subscripts A, B, and C defining different consumption patterns.

DGU	$(P^{min},\ P^{max})$	C^B	(η_{CH}, η_{DH})	$(S_B^{min},\ S_B^{max})$	S_B^o
DG 1	$(+10, +80)$	–	–	–	–
DG 2	$(+10, +80)$	–	–	–	–
BESS 3	$(-40, +40)$	150	(0.9, 0.9)	(0.1, 0.9)	0.5
BESS 4	$(-50, +50)$	150	(0.9, 0.9)	(0.1, 0.9)	0.6
BESS 5	$(-60, +60)$	250	(0.9, 0.9)	(0.1, 0.9)	0.4

Table 7.2: DGU parameters used by the EMS. DG and $BESS$ stands for Dispatchable Generator and Battery Energy Storage System DGUs, while the number indicates the node of connection.

The MPC-based EMS schedules the optimal power set-points of DGUs every 15 minutes, using a prediction horizon of 5 hours, i.e. $N = 20$. The secondary layer runs with a sampling time of 3 minutes with the goal of tracking the received power references despite the aforementioned load variations. In the ensuing discussion, the behaviour of various DC-iMG components is described, controlled by the proposed hierarchical controller over a span of 24 hours.

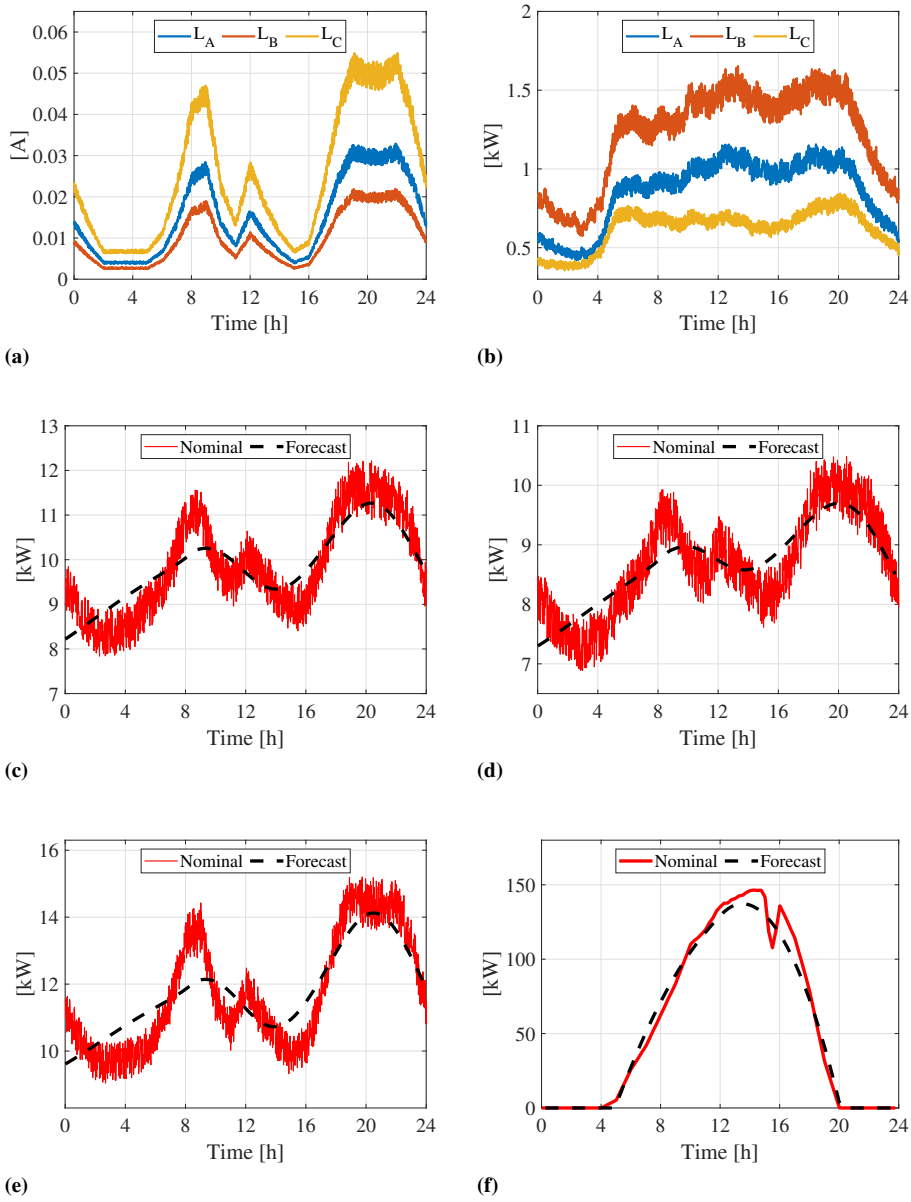

Figure 7.4: (a) Current term profile of ZIP loads; (b) Power term profile of ZIP loads. (c) Total power absorption of Load A; (d) Total power absorption of Load B; (e) Total power absorption of Load C; (f) Power production of PV.

Dispatchable DGUs: As shown in Figures 7.5 (a) and (b), DGUs DG1 and DG2 track the power references provided by the EMS. During the day, when PV generation starts picking up (see Figure 7.4 (f)), the EMS turns off DGU DG1 to ensure economic optimality and maintain DC-iMG power balance. DGU DG2, although producing minimum permissible power during the period of peak PV generation, remains operational throughout the day in order to maintain connectivity of the DC-iMG.

BESS DGUs: In Figures 7.5 (c), (d) and (e), it can be noticed that BESS DGUs follow power references provided by the EMS. Abrupt charging and discharging, and frequent switching between these two modes work to the detriment of BESS's longevity, and are prevented by the EMS. As for the SOCs, reported in Figure 7.6, they evolve respecting the operational constraints. Moreover, the EMS tries to store all the possible surplus energy during periods of peak PV generation (see Figure 7.4(f)). This energy is released in the last part of the day during which the PV generation declines, since the SOCs return around their nominal value, see Figure 7.6.

PV DGU: As reported in Figure 7.4(f), so as to be consistent with a real operation scenario, the simulations have been conducted with a mismatch between nominal PV generation and forecasts. At a sampling instant, the EMS utilizes the nominal PV generation and the forecast not only to generate power references but also to decide whether to operate the PV DGU in MPPT or power curtailment mode. As seen from Figure 7.5 (f), the power injected by the PV generators into the DC-iMG tracks the EMS power references. Notice that the PV DGU operates in MPPT mode during the first and the last hours of the simulation, whereas it curtails power during the central part of the day. Clearly, a power curtailment is inevitable considering that the SOCs are going to hit their upper bound, DGU DG2 is injecting minimum power, and DGU DG1 is nonoperational.

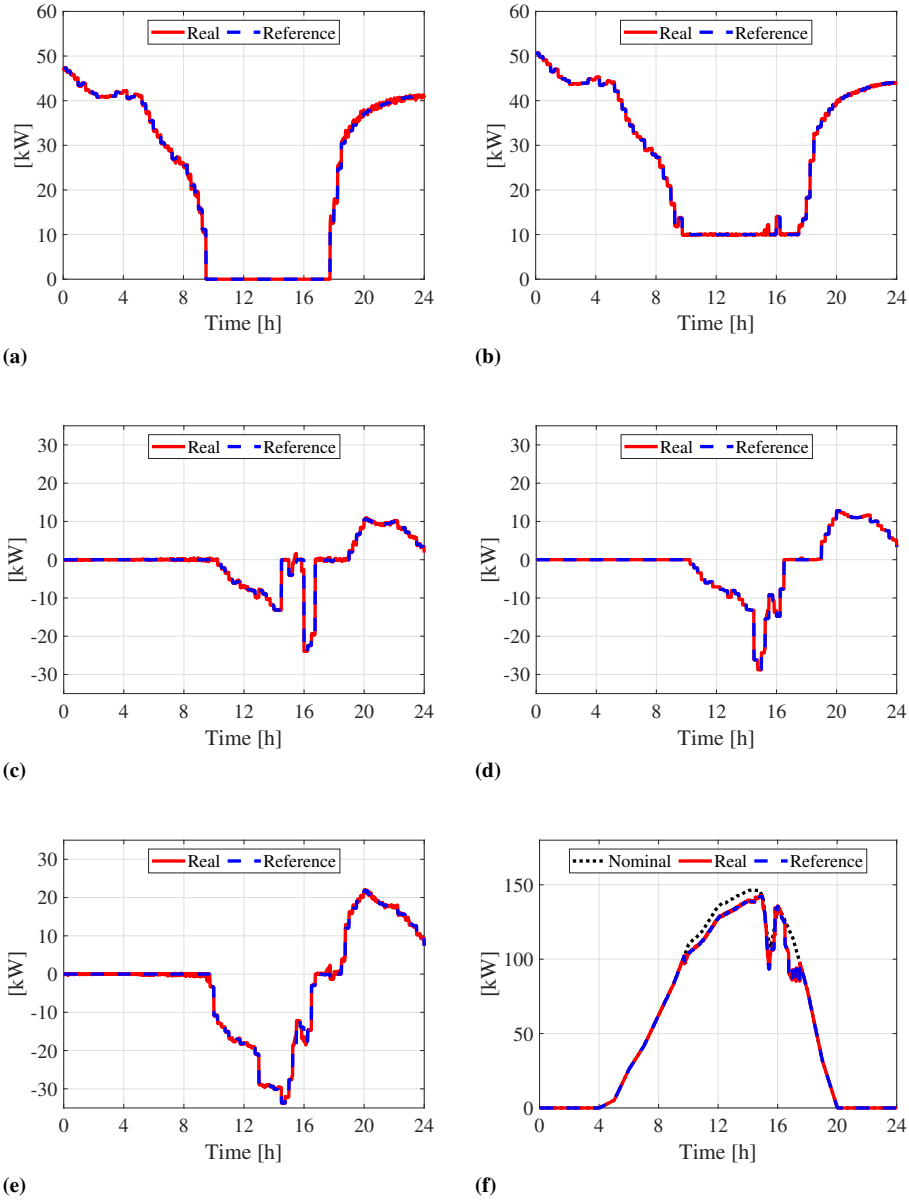

Figure 7.5: (a) Power output of DG 1; (b) Power output of DG 2; (c) Power output of BESS 3; (d) Power output of BESS 4; (e) Power output of BESS 5; (f) Power output of PV 6.

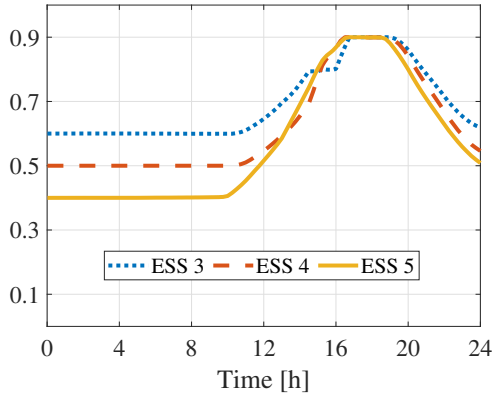

Figure 7.6: SOCs of BESS DGUs.

It is underlined that, during the simulation, the condition (7.44) always holds for all load nodes, ensuring the uniqueness of solution for load voltages and the perfect tracking of DGUs power injections.

The secondary control layer manipulates the voltage references of the DGUs every three minutes, and maintains the voltages in the allowed range, as shown in Figure 7.7(a). As a consequence of new power references received from the EMS, a clear change in voltages can be observed every 15 minutes.

Finally Figures 7.7(b) and (c) report the performance of primary voltage controllers when the dispatchable DGU DG1 is turned off by the EMS. It is evident that the transients quickly die out and voltages are forced back to desired reference values, although a DGU unit is being detached by the DC-iMG. The overall voltage stability is preserved thanks to the implemented Plug-and-Play voltage primary controllers, described in details in [118].

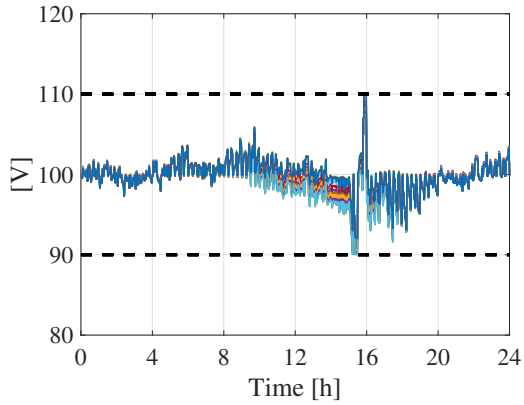

(a)

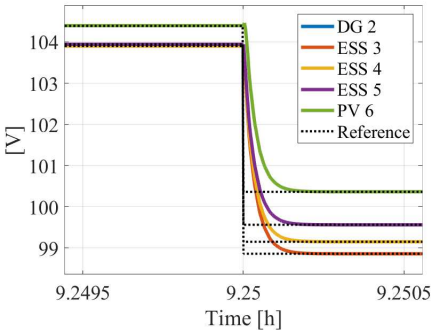

(b)

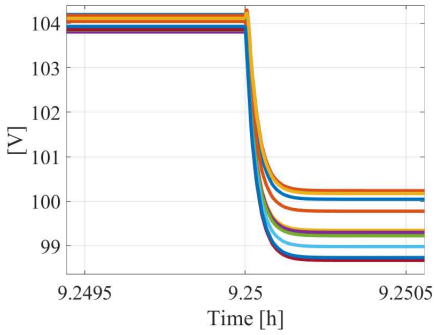

(c)

Figure 7.7: (a) Power output of DG 1; (b) Power output of DG 2; (c) Power output of BESS 3; (d) Power output of BESS 4; (e) Power output of BESS 5; (f) Power output of PV 6.

7.6 Conclusions

A top-to-bottom hierarchical control structure for a DC-iMG has been proposed. By utilizing an MPC-based EMS at tertiary layer, optimal power references are generated. The secondary layer translates these power signals into voltage references for the primary layer. More specifically, the voltage references are generated by solving an optimization problem at the secondary layer, which can incorporate practical operational constraints. Furthermore, the well-posedness of the secondary optimization problem has been studied, discussing its feasibility and deduced a novel condition for the uniqueness of generator voltages and DGU power injections. Lastly, it has been numerically shown that the multiple layers of the hierarchical controller achieve satisfactory results in terms of DGUs management and voltage regulation, allowing the proper operation of a DC-MG in islanded mode.

CHAPTER 8

Conclusions and Future Research

This doctoral thesis aimed to define a comprehensive framework of control algorithms and architectures for the integration of smart microgrids into the electrical system, considered as the key-solution for enhancing the diffusion of renewable energy sources (RESs). Indeed, the collocation of RESs with storage systems, controllable loads and other dispatchable units, allows to better exploit their potentiality, if properly coordinated by adequate control strategies.
As extensively discussed in the first part of this thesis, a significant advantage of microgrids is related to their flexibility, possibly adapting the internal scheduling of their units to support the overall electrical system through the provision of ancillary services. This is a fundamental and widely discussed aspect of today energy market mechanisms and regulations, due to the increasing intermittency and power variability caused by RESs and by the raising world power demand.

Nevertheless, microgrids would have a negligible impact on the electrical system if autonomously operated, and they would not be able to meet the minimum requirements for the ancillary services provision. Therefore, coordination and multi-agents optimization control strategies have been designed and proposed, so as to coordinate multiple microgrids as part of a unique aggregator, able to participate in the energy markets and to effectively provide ancillary services.

Another peculiar advantage of collocating RESs, storage devices and controllable loads in microgrids, is that these entities can also autonomously operate as proper electrical islands. This is an effective solution to electrify rural areas or to ensure a secure supply in case of faults in the main grid system. The second part of this thesis concerned the design of dedicated and structured control architectures for the islanded operation mode, allowing an efficient management of local resources and the stable regulation of the internal frequency and voltages.

Future research directions

To enhance the energy transition to a more decentralized and sustainable electrical paradigm, the presented research can be continued through the following paths.

Data-based control of distributed energy resources

Most of the control and coordination algorithms designed and described in this thesis consider the available forecasts on the RESs production and the loads absorption. Nevertheless, it must be considered that an enormous number of historical data is available about these quantities, recorded day by day during the normal systems operation. It would be interesting to investigate how this information can be properly classified and exploited to improve the management and control of distributed energy resources, both at the microgrid and at the aggregator level. A preliminary solution to develop estimation models from data with very mild assumptions is described in Chapter 5, and this could be integrated with a proper management and control algorithm for microgrids.

Coordination and multi-agent algorithms for generic optimization problems

The multi-agent coordination of multiple microgrids and energy sources is one of the core topics of this thesis. Nevertheless, the performances of existing distributed optimization algorithms significantly depend on the problem structure and they are not generalizable. In Chapter 2 a distributed optimization algorithm for convex problems has been presented, while Chapter 3 focused on coordination strategies for the balancing service provision in presence of mixed-integer variables. However, the distributed algorithm described in Chapter 3 still applies to a specific class of problems, i.e. the mixed-integer linear problems. It would be interesting to investigate the design of multi-agent optimization strategies which do not require any assumption or knowledge on the agent internal structure, allowing to anyhow find a convergent solution, hopefully with reduced sub-optimality. In fact, microgrids can be equipped with different types of units and they can be internally controlled according to different optimization strategies, constraints and objectives. This should not affect their coordination in efficiently supporting the overall electrical system.

Clustering and multi-clusters control architectures for networked systems

Chapter 4 addressed the problem of coordinating large-scale networks with a prompt and scalable control action. The main idea of the proposed solution relies on firstly partitioning the network in areas, and then coordinating their operations through a novel fully distributed two-layer architecture. An interesting development is to further improve the proposed network partitioning algorithm and to integrate it with the designed two-layer control architecture, so that the boundaries of network areas are iteratively updated based on the control performances and availability of resources. Moreover, the overall framework can be defined from a more conceptual point of view, so as to be applied to different networked applications.

Improving the integration of high-level management strategies and low-level control structures in islanded microgrids

Chapter 6 and 7 concerned the islanded microgrid operation with AC and DC networks, aiming to close the gap between the well-studied optimization-based management algorithms and the existing low-level control techniques for the voltages and frequency stabilization. This integration is in fact of crucial importance for ensuring the efficient operation of real islanded microgrids. The designed approaches achieve satisfactory results, relying however on the measurement of voltage magnitudes and phases (for Chapter 6) and of loads consumption (for Chapter 7), and on the knowledge of some network parameters. An interesting research path is to further improve the designed control architectures in a more flexible fashion, requiring the sampling of just few electrical variables, and then internally developing reliable estimation models of the islanded microgrid system. This would facilitate the implementation of the designed control solutions into real microgrids.

Bibliography

[1] United Nations Framework Convention on Climate Change, "The Paris Agreement." https://unfccc.int/process-and-meetings/the-paris-agreement/the-paris-agreement, 2015.

[2] European Union, *Directive (EU) 2018/2001 of the European Parliament and of the Council of 11 December 2018 on the promotion of the use of energy from renewable sources*. 2018.

[3] P. Kundur, N. J. Balu, and M. G. Lauby, *Power system stability and control*, vol. 7. McGraw-hill New York, 1994.

[4] International Energy Agency, *World Energy Outlook 2018*. 2018.

[5] G. Joos, B. Ooi, D. McGillis, F. Galiana, and R. Marceau, "The potential of distributed generation to provide ancillary services," in *2000 Power Engineering Society Summer Meeting (Cat. No. 00CH37134)*, vol. 3, pp. 1762–1767, IEEE, 2000.

[6] N. Hatziargyriou, A. Anastasiadis, A. Tsikalakis, and J. Vasiljevska, "Quantification of economic, environmental and operational benefits due to significant penetration of microgrids in a typ-

ical LV and MV greek network," *European Transactions on Electrical Power*, vol. 21, no. 2, pp. 1217–1237, 2011.

[7] R. Lasseter, A. Akhil, C. Marnay, J. Stephens, J. Dagle, R. Guttromsom, A. S. Meliopoulous, R. Yinger, and J. Eto, "Integration of distributed energy resources. the certs microgrid concept," tech. rep., Lawrence Berkeley National Lab.(LBNL), Berkeley, CA (United States), 2002.

[8] S. R. Cominesi, M. Farina, L. Giulioni, B. Picasso, and R. Scattolini, "A two-layer stochastic model predictive control scheme for microgrids," *IEEE Transactions on Control Systems Technology*, vol. 26, no. 1, pp. 1–13, 2017.

[9] A. Lefort, R. Bourdais, G. Ansanay-Alex, and H. Guéguen, "Hierarchical control method applied to energy management of a residential house," *Energy and Buildings*, vol. 64, pp. 53–61, 2013.

[10] R. H. Lasseter, "Smart distribution: Coupled microgrids," *Proceedings of the IEEE*, vol. 99, no. 6, pp. 1074–1082, 2011.

[11] R. H. Lasseter and P. Piagi, "Microgrid: A conceptual solution," in *IEEE Power Electronics Specialists Conference*, vol. 6, pp. 4285–4291, Citeseer, 2004.

[12] Navigant Research, "Microgrid Deployment Tracker 4Q18." https://www.navigantresearch.com/reports/microgrid-deployment-tracker-4q18, 2018.

[13] "Proposal for a regulation of the European Parliament and of the Council on the internal market for electricity." https://eur-lex.europa.eu/legal-content/EN/TXT/?uri=celex:52016PC0861.

[14] T. Gomez, I. Herrero, P. Rodilla, R. Escobar, S. Lanza, I. de la Fuente, M. L. Llorens, and P. Junco, "European union electricity markets: Current practice and future view," *IEEE Power and Energy Magazine*, vol. 17, no. 1, pp. 20–31, 2019.

[15] "Commission Regulation (EU) 2017/2195 of 23 November 2017 establishing a guideline on electricity balancing." https://eur-lex.europa.eu/legal-content/EN/TXT/?uri=CELEX:32017R2195.

[16] ENTSO-E, "Electricity balancing in europe - november 2018." https://docstore.entsoe.eu/Documents/Network%20codes%20documents/NC%20EB/entso-e_balancing_in%20_europe_report_Nov2018_web.pdf.

[17] K. Poplavskaya and L. de Vries, "Distributed energy resources and the organized balancing market: A symbiosis yet? case of three european balancing markets," *Energy Policy*, vol. 126, pp. 264–276, 2019.

[18] "Directive 2009/72/EC of the European Parliament and of the Council of 13 July 2009 concerning common rules for the internal market in electricity and repealing Directive 2003/54/EC." https://eur-lex.europa.eu/legal-content/EN/TXT/?uri=CELEX:32009L0072.

[19] "Directive 96/92/EC of the European Parliament and of the Council of 19 December 1996 concerning common rules for the internal market in electricity." https://eur-lex.europa.eu/legal-content/EN/TXT/?uri=CELEX:31996L0092.

[20] "Directive 2003/54/EC of the European Parliament and of the Council of 26 June 2003 concerning common rules for the internal market in electricity and repealing Directive 96/92/EC." https://eur-lex.europa.eu/legal-content/EN/TXT/?uri=CELEX:32003L0054.

[21] A. M. Carreiro, H. M. Jorge, and C. H. Antunes, "Energy management systems aggregators: A literature survey," *Renewable and Sustainable Energy Reviews*, vol. 73, pp. 1160–1172, June 2017.

[22] E. Koliou, C. Eid, J. P. Chaves-Ávila, and R. A. Hakvoort, "Demand response in liberalized electricity markets: Analysis of aggregated load participation in the german balancing mechanism," *Energy*, vol. 71, pp. 245–254, 2014.

[23] R. A. van der Veen and R. A. Hakvoort, "The electricity balancing market: Exploring the design challenge," *Utilities Policy*, vol. 43, pp. 186–194, 2016.

[24] L. Hirth and I. Ziegenhagen, "Balancing power and variable renewables: Three links," *Renewable and Sustainable Energy Reviews*, vol. 50, pp. 1035–1051, 2015.

[25] International Energy Agency, *Repowering markets*. 2016.

[26] Terna, "Grid code." http://www.terna.it/en-gb/sistemaelettrico/codicedirete.aspx.

[27] N. Lidula and A. Rajapakse, "Microgrids research: A review of experimental microgrids and test systems," *Renewable and Sustainable Energy Reviews*, vol. 15, no. 1, pp. 186–202, 2011.

[28] P. Olivella-Rosell, P. Lloret-Gallego, Í. Munné-Collado, R. Villafafila-Robles, A. Sumper, S. Ottessen, J. Rajasekharan, and B. Bremdal, "Local flexibility market design for aggregators providing multiple flexibility services at distribution network level," *Energies*, vol. 11, no. 4, p. 822, 2018.

[29] ARERA, "Delibera 422/2018/R/eel." https://www.arera.it/it/docs/18/422-18.htm, Aug. 2018.

[30] Terna, "Regolamento recante le modalità per la creazione, qualificazione e gestione di unità virtuali abilitate miste al mercato dei servizi di dispacciamento." http://download.terna.it/terna/0000/1117/96.PDF.

[31] I. Lampropoulos, M. van den Broek, E. van der Hoofd, K. Hommes, and W. van Sark, "A system perspective to the deployment of flexibility through aggregator companies in the netherlands," *Energy policy*, vol. 118, pp. 534–551, 2018.

[32] R. Minciardi and M. Robba, "A bilevel approach for the stochastic optimal operation of interconnected microgrids," *IEEE Transactions on Automation Science and Engineering*, vol. 14, no. 2, pp. 482–493, 2016.

[33] A. Ouammi, H. Dagdougui, L. Dessaint, and R. Sacile, "Coordinated model predictive-based power flows control in a cooperative network of smart microgrids," *IEEE Transactions on Smart grid*, vol. 6, no. 5, pp. 2233–2244, 2015.

[34] M. Balandat, F. Oldewurtel, M. Chen, and C. Tomlin, "Contract design for frequency regulation by aggregations of commercial buildings," in *Communication, Control, and Computing (Allerton), 2014 52nd Annual Allerton Conference on*, pp. 38–45, IEEE, 2014.

[35] E. Vrettos, F. Oldewurtel, and G. Andersson, "Robust energy-constrained frequency reserves from aggregations of commercial buildings," *IEEE Trans. PS*, vol. 31, no. 6, pp. 4272–4285, 2016.

[36] W. Mai and C. Chung, "Economic mpc of aggregating commercial buildings for providing flexible power reserve," *IEEE transactions on power systems*, vol. 30, no. 5, pp. 2685–2694, 2014.

[37] C. Yuen, A. Oudalov, and A. Timbus, "The provision of frequency control reserves from multiple microgrids," *IEEE Transactions on Industrial Electronics*, vol. 58, no. 1, pp. 173–183, 2011.

[38] J. W. Simpson-Porco, F. Dörfler, and F. Bullo, "Synchronization and power sharing for droop-controlled inverters in islanded microgrids," *Automatica*, vol. 49, no. 9, pp. 2603–2611, 2013.

[39] M. Cucuzzella, S. Rosti, A. Cavallo, and A. Ferrara, "Decentralized sliding mode voltage control in dc microgrids," in *2017 American Control Conference (ACC)*, pp. 3445–3450, IEEE, 2017.

[40] X. Guo, Z. Lu, B. Wang, X. Sun, L. Wang, and J. M. Guerrero, "Dynamic phasors-based modeling and stability analysis of droop-controlled inverters for microgrid applications," *IEEE Transactions on Smart Grid*, vol. 5, no. 6, pp. 2980–2987, 2014.

[41] M. Tucci, S. Riverso, J. C. Vasquez, J. M. Guerrero, and G. Ferrari-Trecate, "A decentralized scalable approach to voltage control of dc islanded microgrids," *IEEE Transactions on Control Systems Technology*, vol. 24, no. 6, pp. 1965–1979, 2016.

[42] C. A. Hans, P. Sopasakis, A. Bemporad, J. Raisch, and C. Reincke-Collon, "Scenario-based model predictive operation control of islanded microgrids," in *Decision and Control (CDC), 2015 IEEE 54th Annual Conference on*, pp. 3272–3277, IEEE, 2015.

[43] S. Oh, S. Chae, J. Neely, J. Baek, and M. Cook, "Efficient model predictive control strategies for resource management in an islanded microgrid," *Energies*, vol. 10, no. 7, p. 1008, 2017.

[44] J. J. Justo, F. Mwasilu, J. Lee, and J.-W. Jung, "Ac-microgrids versus dc-microgrids with distributed energy resources: A review," *Renewable and sustainable energy reviews*, vol. 24, pp. 387–405, 2013.

[45] H. Kim and M. Thottan, "A two-stage market model for microgrid power transactions via aggregators," *Bell Labs Technical Journal*, vol. 16, no. 3, pp. 101–107, 2011.

[46] R. W. Brehm, H. Ramezani, and J. Jouffroy, "Distributed coordination of energy-storage capacities in virtual microgrids," in *2018 European Control Conference (ECC)*, pp. 1124–1129, IEEE, 2018.

[47] F. Rey, X. Zhang, S. Merkli, V. Agliati, M. Kamgarpour, and J. Lygeros, "Strengthening the group: Aggregated frequency reserve bidding with ADMM," *IEEE Trans. SG*, 2018.

[48] D. K. Molzahn, F. Dörfler, H. Sandberg, S. H. Low, S. Chakrabarti, R. Baldick, and J. Lavaei, "A survey of distributed optimization and control algorithms for electric power systems," *IEEE Transactions on Smart Grid*, vol. 8, no. 6, pp. 2941–2962, 2017.

[49] B. Houska, J. Frasch, and M. Diehl, "An augmented lagrangian based algorithm for distributed nonconvex optimization," *SIAM Journal on Optimization*, vol. 26, no. 2, pp. 1101–1127, 2016.

[50] S. Magnússon, P. C. Weeraddana, and C. Fischione, "A distributed approach for the optimal power-flow problem based on ADMM and sequential convex approximations," *IEEE Transactions on Control of Network Systems*, vol. 2, no. 3, pp. 238–253, 2015.

[51] T. Morstyn, B. Hredzak, R. P. Aguilera, and V. G. Agelidis, "Model predictive control for distributed microgrid battery energy storage systems," *IEEE Trans. CST*, vol. 26, no. 3, pp. 1107–1114, 2018.

[52] W. Shi, X. Xie, C.-C. Chu, and R. Gadh, "A distributed optimal energy management strategy for microgrids," in *2014 IEEE International Conference on Smart Grid Communications*, pp. 200–205, IEEE, 2014.

[53] S. Boyd, N. Parikh, E. Chu, B. Peleato, J. Eckstein, *et al.*, "Distributed optimization and statistical learning via the alternating direction method of multipliers," *Foundations and Trends® in Machine Learning*, vol. 3, no. 1, pp. 1–122, 2011.

[54] Y. Sönmez, "Estimation of fuel cost curve parameters for thermal power plants using the abc algorithm," *Turkish Journal of Electrical Engineering & Computer Sciences*, vol. 21, no. Sup. 1, pp. 1827–1841, 2013.

[55] S. R. Cominesi, M. Farina, L. Giulioni, B. Picasso, and R. Scattolini, "A two-layer stochastic model predictive control scheme for microgrids," *IEEE Transactions on Control Systems Technology*, vol. 26, no. 1, pp. 1–13, 2018.

[56] D. P. Bertsekas and J. N. Tsitsiklis, *Parallel and distributed computation: numerical methods*, vol. 23. Prentice hall Englewood Cliffs, NJ, 1989.

[57] R. Marconato, *Electric power systems*. CEI, 2002.

[58] W. H. Kersting, "Radial distribution test feeders," in *Power Engineering Society Winter Meeting, 2001. IEEE*, vol. 2, pp. 908–912, IEEE, 2001.

[59] L. Fabietti, F. A. Qureshi, T. T. Gorecki, C. Salzmann, and C. N. Jones, "Multi-time scale coordination of complementary resources for the provision of ancillary services," *Applied Energy*, vol. 229, pp. 1164 – 1180, 2018.

[60] E. Vrettos and G. Andersson, "Scheduling and provision of secondary frequency reserves by aggregations of commercial buildings," *IEEE Transactions on Sustainable Energy*, vol. 7, pp. 850–864, April 2016.

[61] A. Papavasiliou, H. Hindi, and D. Greene, "Market-based control mechanisms for electric power demand response," in *49th IEEE Conference on Decision and Control (CDC)*, pp. 1891–1898, IEEE, 2010.

[62] W. Pei, Y. Du, W. Deng, K. Sheng, H. Xiao, and H. Qu, "Optimal bidding strategy and intramarket mechanism of microgrid aggregator in real-time balancing market," *IEEE Transactions on Industrial Informatics*, vol. 12, no. 2, pp. 587–596, 2016.

[63] S.-J. Kim and G. B. Giannakis, "Scalable and robust demand response with mixed-integer constraints," *IEEE Transactions on Smart Grid*, vol. 4, no. 4, pp. 2089–2099, 2013.

[64] S. Mhanna, A. C. Chapman, and G. Verbič, "A distributed algorithm for demand response with mixed-integer variables," *IEEE Transactions on Smart Grid*, vol. 7, no. 3, pp. 1754–1755, 2016.

[65] T. Samad, E. Koch, and P. Stluka, "Automated demand response for smart buildings and microgrids: The state of the practice and research challenges," *Proceedings of the IEEE*, vol. 104, no. 4, pp. 726–744, 2016.

[66] A. Falsone, K. Margellos, and M. Prandini, "A decentralized approach to multi-agent MILPs': finite-time feasibility and performance guarantees," *Automatica*, vol. 103, pp. 141–150, 2019.

[67] A. Bemporad and C. Filippi, "An algorithm for approximate multiparametric convex programming," *Computational optimization and applications*, vol. 35, no. 1, pp. 87–108, 2006.

[68] D. P. Bertsekas, "Nonlinear programming," *Journal of the Operational Research Society*, vol. 48, no. 3, pp. 334–334, 1997.

[69] N. Z. Shor, *Minimization methods for non-differentiable functions*. Springer, 1985.

[70] T. Hong and F. de León, "Controlling non-synchronous microgrids for load balancing of radial distribution systems," *IEEE Transactions on Smart Grid*, vol. 8, no. 6, pp. 2608–2616, 2017.

[71] A. Majzoobi and A. Khodaei, "Application of microgrids in providing ancillary services to the utility grid," *Energy*, vol. 123, pp. 555–563, 2017.

[72] G. Hug-Glanzmann, "Coordination of intermittent generation with storage, demand control and conventional energy sources," in *2010 IREP Symposium Bulk Power System Dynamics and Control-VIII (IREP)*, pp. 1–7, IEEE, 2010.

[73] G. Hug-Glanzmann and G. Andersson, "Decentralized optimal power flow control for overlapping areas in power systems," *IEEE Transactions on Power Systems*, vol. 24, no. 1, pp. 327–336, 2009.

[74] K. Baker, J. Guo, G. Hug, and X. Li, "Distributed MPC for efficient coordination of storage and renewable energy sources across control areas," *IEEE Transactions on Smart Grid*, vol. 7, no. 2, pp. 992–1001, 2016.

[75] G. Hug-Glanzmann and G. Andersson, "Coordinated control of facts devices in power systems for security enhancement," in *2007 iREP Symposium - Bulk Power System Dynamics and Control - VII. Revitalizing Operational Reliability*, pp. 1–10, Aug 2007.

[76] C. A. Cortes, S. F. Contreras, and M. Shahidehpour, "Microgrid topology planning for enhancing the reliability of active distribution networks," *IEEE Transactions on Smart Grid*, vol. 9, no. 6, pp. 6369–6377, 2018.

[77] E. Cotilla-Sanchez, P. D. Hines, C. Barrows, S. Blumsack, and M. Patel, "Multi-attribute partitioning of power networks based on

electrical distance," *IEEE Transactions on Power Systems*, vol. 28, no. 4, pp. 4979–4987, 2013.

[78] J. Li, C.-C. Liu, and K. P. Schneider, "Controlled Partitioning of a Power Network Considering Real and Reactive Power Balance," *IEEE Transactions on Smart Grid*, vol. 1, no. 3, pp. 261 – 269, 2010.

[79] S. A. Arefifar, Y. A.-R. I. Mohamed, and T. H. M. El-Fouly, "Supply-Adequacy-Based Optimal Construction of Microgrids in Smart Distribution Systems," *IEEE Transactions on Smart Grid*, vol. 3, no. 3, pp. 1491 – 1502, 2012.

[80] T. Tanjo, K. Minami, and H. Maruyama, "Graph partitioning of power grids considering electricity sharing," *International Journal of Smart Grid and Clean Energy*, vol. 5, no. 2, pp. 112 – 120, 2016.

[81] A. Di Nardo, M. Di Natale, C. Giudicianni, D. Musmarra, G. F. Santonastaso, and A. Simone, "Water Distribution System Clustering and Partitioning Based on Social Network Algorithms," *Procedia Engineering*, vol. 119, pp. 196 – 205, 2015.

[82] C. Ocampo-Martinez, D. Barcelli, V. Puig, and A. Bemporad, "Hierarchical and decentralised model predictive control of drinking water networks: Application to barcelona case study," *IET control theory & applications*, vol. 6, no. 1, pp. 62–71, 2012.

[83] T.-H. Chang, M. Hong, and X. Wang, "Multi-agent distributed optimization via inexact consensus admm," *IEEE Transactions on Signal Processing*, vol. 63, no. 2, pp. 482–497, 2014.

[84] T.-H. Chang, "A proximal dual consensus admm method for multi-agent constrained optimization," *IEEE Transactions on Signal Processing*, vol. 64, no. 14, pp. 3719–3734, 2016.

[85] G. Banjac, F. Rey, P. Goulart, and J. Lygeros, "Decentralized resource allocation via dual consensus admm," in *2019 American Control Conference (ACC)*, pp. 2789–2794, IEEE, 2019.

[86] G. Mateos, J. A. Bazerque, and G. B. Giannakis, "Distributed sparse linear regression," *IEEE Transactions on Signal Processing*, vol. 58, no. 10, pp. 5262–5276, 2010.

[87] G. Karypis and V. Kumar, "Multilevel k-way hypergraph partitioning," *VLSI design*, vol. 11, no. 3, pp. 285–300, 2000.

[88] G. Karypis and V. Kumar, *METIS: A Software Package for Partitioning Unstructured Graphs, Partitioning Meshes, and Computing Fill-Reducing Orderings of Sparse Matrices*. University of Minnesota, Department of Computer Science, 1998.

[89] E. W. Dijkstra, "A Note on Two Problems in Connexion With Graphs," *Numerische Mathematik*, vol. 1, no. 1, pp. 269 – 271, 1959.

[90] D. Kiran, A. R. Abhyankar, and B. K. Panigrahi, "Hierarchical Clustering Based Zone Formation in Power Networks," in *2016 National Power Systems Conference (NPSC)*, 2016.

[91] G. Karypis and V. Kumar, "A fast and high quality multilevel scheme for partitioning irregular graphs," *SIAM Journal on Scientific Computing*, vol. 20, no. 1, pp. 359 – 392, 1998.

[92] G. Karypis and V. Kumar, "Multilevel algorithms for multi-constraint graph partitioning.," tech. rep., University of Minnesota, 1998.

[93] "IEEE-118 bus system data source." https://al-roomi.org/power-flow/118-bus-system.

[94] Z. Wang, J. Wang, and C. Chen, "A Three-Phase Microgrid Restoration Model Considering Unbalanced Operation of Distributed Generation," *IEEE Transactions on Smart Grid*, vol. 9, no. 4, pp. 3594 – 3604, 2018.

[95] "IEEE-123 test feeder data source." http://sites.ieee.org/pes-testfeeders/resources/.

[96] M. Milanese and C. Novara, "Set membership identification of nonlinear systems," *Automatica*, vol. 40, no. 6, pp. 957–975, 2004.

[97] A. Parisio and L. Glielmo, "Energy efficient microgrid management using model predictive control," in *Decision and Control and European Control Conference (CDC-ECC), 2011 50th IEEE Conference on*, pp. 5449–5454, IEEE, 2011.

[98] M. Milanese and C. Novara, "Model quality in nonlinear sm identification," in *Decision and Control, 2003. Proceedings. 42nd IEEE Conference on*, vol. 6, pp. 6021–6026, IEEE, 2003.

[99] "Gestore mercati energetici." http://www.mercatoelettrico.org/En/Default.aspx.

[100] D. E. Olivares, A. Mehrizi-Sani, A. H. Etemadi, C. A. Cañizares, R. Iravani, M. Kazerani, A. H. Hajimiragha, O. Gomis-Bellmunt, M. Saeedifard, R. Palma-Behnke, *et al.*, "Trends in microgrid control," *IEEE Transactions on smart grid*, vol. 5, no. 4, pp. 1905–1919, 2014.

[101] A. Bolzoni, G. Foglia, L. Frosio, M. Iacchetti, and R. Perini, "Impact of line and control parameters on droop stability in inverters for distributed generation," *IEEE Transactions on Smart Grid*, 2017.

[102] J. W. Simpson-Porco, Q. Shafiee, F. Dörfler, J. C. Vasquez, J. M. Guerrero, and F. Bullo, "Secondary frequency and voltage control of islanded microgrids via distributed averaging," *IEEE Transactions on Industrial Electronics*, vol. 62, no. 11, pp. 7025–7038, 2015.

[103] S. Negri, E. Tironi, and D. S. Danna, "Integrated control strategy for islanded operation in smart grids: Virtual inertia and ancillary services," in *Environment and Electrical Engineering and 2017 IEEE Industrial and Commercial Power Systems Europe (EEEIC/I&CPS Europe), 2017 IEEE International Conference on*, pp. 1–6, IEEE, 2017.

[104] M. Cucuzzella, G. P. Incremona, and A. Ferrara, "Design of robust higher order sliding mode control for microgrids," *IEEE Journal*

on Emerging and Selected Topics in Circuits and Systems, vol. 5, no. 3, pp. 393–401, 2015.

[105] D. E. Olivares, C. A. Cañizares, and M. Kazerani, "A centralized energy management system for isolated microgrids," *IEEE Transactions on smart grid*, vol. 5, no. 4, pp. 1864–1875, 2014.

[106] J. Rocabert, A. Luna, F. Blaabjerg, and P. Rodríguez, "Control of power converters in ac microgrids," *IEEE Transactions on Power Electronics*, vol. 27, pp. 4734–4749, Nov 2012.

[107] M. Carmeli, F. Castelli-Dezza, and G. Superti-Furga, "Smart modulation: a new approach to power converter control," in *9th European Conference on Power Electronics and Applications*, pp. 27–29, 2001.

[108] M. Carmeli, F. Castelli-Dezza, and G. Superti-Furga, "Constant frequency current modulation algorithm based on linkage flux," in *Power Electronics Specialist Conference, 2003. PESC'03. 2003 IEEE 34th Annual*, vol. 1, pp. 195–200, IEEE, 2003.

[109] N. Mohan, T. M. Undeland, and W. P. Robbins, *Power electronics: converters, applications, and design*. John wiley & sons, 2003.

[110] M. Carmeli, F. Castelli-Dezza, and G. Superti-Furga, "Sliding mode control for an innovative universal power conditioner with ups function," in *Industrial Electronics, 2005. ISIE 2005. Proceedings of the IEEE International Symposium on*, vol. 2, pp. 651–656, IEEE, 2005.

[111] L. Piegari and P. Tricoli, "A control algorithm of power converters in smart-grids for providing uninterruptible ancillary services," in *Harmonics and Quality of Power (ICHQP), 2010 14th International Conference on*, pp. 1–7, IEEE, 2010.

[112] J. B. Rawlings and D. Q. Mayne, *Model predictive control: Theory and design*. Nob Hill Pub., 2009.

[113] L. Meng, Q. Shafiee, G. Ferrari-Trecate, H. Karimi, D. Fulwani, X. Lu, and J. M. Guerrero, "Review on control of DC microgrids

and multiple microgrid clusters," *IEEE Journal of Emerging and Selected Topics in Power Electronics*, vol. 5, no. 3, pp. 928–948, 2017.

[114] T. Dragičević, X. Lu, J. C. Vasquez, and J. M. Guerrero, "DC microgrids part I: A review of control strategies and stabilization techniques," *IEEE Transactions on Power Electronics*, vol. 31, no. 5, pp. 4876–4891, 2016.

[115] A. Bidram and A. Davoudi, "Hierarchical structure of microgrids control system," *IEEE Transactions on Smart Grid*, vol. 3, pp. 1963–1976, Dec 2012.

[116] Q. Shafiee, J. M. Guerrero, and J. C. Vasquez, "Distributed Secondary Control for Islanded Microgrids : A Novel Approach," *IEEE Transactions on Power Electronics*, vol. 29, no. 2, pp. 1018–1031, 2014.

[117] A. Martinelli, P. Nahata, and G. Ferrari-Trecate, "Voltage stabilization in MVDC microgrids using passivity-based nonlinear control," in *2018 IEEE Conference on Decision and Control (CDC)*, pp. 7022–7027, Dec 2018.

[118] P. Nahata, R. Soloperto, M. Tucci, A. Martinelli, and G. Ferrari-Trecate, "A passivity-based approach to voltage stabilization in islanded DC microgrids with ZIP loads," tech. rep., 2017.

[119] M. Tucci, L. Meng, J. M. Guerrero, and G. Ferrari-Trecate, "Stable current sharing and voltage balancing in dc microgrids: A consensus-based secondary control layer," *Automatica*, vol. 95, pp. 1 – 13, 2018.

[120] S. Trip, M. Cucuzzella, X. Cheng, and J. Scherpen, "Distributed averaging control for voltage regulation and current sharing in dc microgrids," *IEEE Control Systems Letters*, vol. 3, pp. 174–179, Jan 2019.

[121] M. Kumar, S. C. Srivastava, and S. N. Singh, "Control strategies of a DC microgrid for grid connected and islanded operations," *IEEE Transactions on Smart Grid*, vol. 6, pp. 1588–1601, July 2015.

[122] T. Dragičević, J. M. Guerrero, and J. C. Vasquez, "Supervisory control of an adaptive-droop regulated dc microgrid with battery management capability," *IEEE Transactions on Power Electronics*, vol. 29, pp. 695–706, Feb 2014.

[123] M. Marzband, F. Azarinejadian, M. Savaghebi, and J. M. Guerrero, "An optimal energy management system for islanded microgrids based on multiperiod artificial bee colony combined with markov chain," *IEEE Systems Journal*, vol. 11, no. 3, pp. 1712–1722, 2017.

[124] C. A. Hans, P. Sopasakis, A. Bemporad, J. Raisch, and C. Reincke-Collon, "Scenario-based model predictive operation control of islanded microgrids," in *2015 54th IEEE Conference on Decision and Control (CDC)*, pp. 3272–3277, Dec 2015.

[125] A. Parisio, E. Rikos, and L. Glielmo, "Stochastic model predictive control for economic/environmental operation management of microgrids: An experimental case study," *Journal of Process Control*, vol. 43, pp. 24–37, 2016.

[126] S. R. Cominesi, A. La Bella, M. Farina, and R. Scattolini, "A multilayer control scheme for microgrid energy management," *IFAC-PapersOnLine*, vol. 49, no. 27, pp. 256–261, 2016.

[127] A. Iovine, T. Rigaut, G. Damm, E. De Santis, and M. D. Di Benedetto, "Power management for a dc microgrid integrating renewables and storages," *Control Engineering Practice*, vol. 85, pp. 59–79, 2019.

[128] A. S. Matveev, J. E. Machado, R. Ortega, J. Schiffer, and A. Pyrkin, "On the existence and long-term stability of voltage equilibria in power systems with constant power loads," *arXiv preprint arXiv:1809.08127*, 2018.

[129] D. Hohm and M. E. Ropp, "Comparative study of maximum power point tracking algorithms," *Progress in photovoltaics: Research and Applications*, vol. 11, no. 1, pp. 47–62, 2003.

[130] J. W. Simpson-Porco, F. Dörfler, and F. Bullo, "Voltage collapse in complex power grids," *Nature communications*, vol. 7, p. 10790, 2016.

[131] S. Taheri and V. Kekatos, "Power flow solvers for direct current networks," *arXiv preprint arXiv:1807.03936*, 2018.

[132] R. Han, M. Tucci, A. Martinelli, J. M. Guerrero, and G. Ferrari-Trecate, "Stability analysis of primary plug-and-play and secondary leader-based controllers for DC microgrid clusters," *IEEE Transactions on Power Systems*, vol. 34, pp. 1780–1800, May 2019.

[133] M. Tucci, S. Riverso, and G. Ferrari-Trecate, "Line-independent plug-and-play controllers for voltage stabilization in dc microgrids," *IEEE Transactions on Control Systems Technology*, vol. 26, pp. 1115–1123, May 2018.

[134] P. Kundur, *Power System Stability and Control*. McGraw-Hill, 1994.

[135] A. Bemporad and M. Morari, "Control of systems integrating logic, dynamics, and constraints," *Automatica*, vol. 35, no. 3, pp. 407 – 427, 1999.

[136] F. Dörfler, J. W. Simpson-Porco, and F. Bullo, "Electrical networks and algebraic graph theory: Models, properties, and applications," *Proceedings of the IEEE*, vol. 106, no. 5, pp. 977–1005, 2018.

[137] F. Dörfler and F. Bullo, "Kron reduction of graphs with applications to electrical networks," *IEEE Transactions on Circuits and Systems I: Regular Papers*, vol. 60, no. 1, pp. 150–163, 2013.

[138] S. Sanchez, R. Ortega, R. Grino, G. Bergna, and M. Molinas, "Conditions for existence of equilibria of systems with constant power loads," *IEEE Transactions on Circuits and Systems I: Regular Papers*, vol. 61, no. 7, pp. 2204–2211, 2014.

[139] T.-T. Lu and S.-H. Shiou, "Inverses of 2 by 2 block matrices," *Computers and Mathematics with Applications*, vol. 43, no. 1, pp. 119 – 129, 2002.

[140] F. Zhang, *The Schur complement and its applications*, vol. 4. Springer Science & Business Media, 2006.

[141] D. Gale and H. Nikaido, "The Jacobian matrix and global univalence of mappings," *Mathematische Annalen*, vol. 159, no. 2, pp. 81–93, 1965.

[142] J. Li, F. Liu, Z. Wang, S. H. Low, and S. Mei, "Optimal power flow in stand-alone DC microgrids," *IEEE Transactions on Power Systems*, vol. 33, pp. 5496–5506, Sep. 2018.

About the author

Alessio La Bella was born in Erice (TP), Italy, in 1992. He received the Bachelor and the Master of Science in Automation and Control Engineering from Politecnico di Milano in 2013 and in 2015, respectively. He received the Alta Scuola Politecnica Diploma, together with the Master of Science in Mechatronics Engineering from Politecnico di Torino in 2016. From January to October 2016, he worked at the research center RSE SpA, developing electrical simulators for assessing the integration of renewable sources in small islands. From November 2016 to October 2019, he was enrolled as a Ph.D. candidate in Information Technology at Politecnico di Milano. From September to December 2018, he was a visiting researcher at the Automatic Control Lab of the École Polytechnique Fédérale de Lausanne. From November 2019, he has been a post-doctoral researcher at the Department of Electronics, Information and Bioengineering of Politecnico di Milano. His main research interests concern the design of optimization-based control algorithms for the efficient management of energy and electrical systems, e.g. microgrids and renewable sources.

The list of publications of Alessio La Bella is hereafter reported.

Journal papers

- A. La Bella, M. Farina, C. Sandroni, R. Scattolini. (in press) *Design of aggregators for the day-ahead management of microgrids providing active and reactive power services*. IEEE Transactions on Control Systems Technology. Extensive version available at https://arxiv.org/abs/1804.02195.

- N. Rathod, A. La Bella, A. Rossetti, C. Sandroni, R. Scattolini. (2019) *Modelling and predictive control of a solar cooling plant with flexible configuration*. Journal of Process Control, 76, 74-86.

- A. La Bella, S. Raimondi Cominesi, C. Sandroni, R. Scattolini. (2017) *Hierarchical predictive control of microgrids in islanded operation*. IEEE Transactions on Automation Science and Engineering, 14(2), 536-546.

- A. La Bella, A. Falsone, D. Ioli. M. Prandini, R. Scattolini. *A mixed-integer distributed approach to prosumers aggregation for providing balancing services*. IEEE Transactions on Smart Grid, (under review).

- P. Nahata, A. La Bella, R. Scattolini, G. Ferrari-Trecate. *Hierarchical Control in Islanded DC Micogrids with Flexible Structures*. IEEE Transactions on Control Systems Technology (under review). Technical Report available at https://arxiv.org/pdf/1910.05107.

- F. Bonassi, A. La Bella, R. Lazzari, C. Sandroni, R. Scattolini. *A supervised MPC architecture for power balance restoration in hybrid AC-DC grids*. International Journal of Electric Power and Energy Systems, Elsevier (under review).

International conference papers

- A. La Bella, F. Bonassi, K. Pascal, R. Scattolini. *A fully distributed control scheme for power balancing in distribution networks*. IFAC World Congress 2020 - Berlin (Germany), (under review).
- A. La Bella, F. Bonassi, C. Sandroni, L. Fagiano, R. Scattolini. *A hierarchical approach for balancing service provision by microgrids aggregators*. IFAC World Congress 2020 - Berlin (Germany), (under review).
- A. La Bella, P. Nahata, G. Ferrari-Trecate. *A Supervisory Control Structure for Voltage-Controlled Islanded DC Microgrids*. IEEE Conference on Decision and Control - Nice (France), 11-13 December 2019.
- A. La Bella, F. Bonassi, M. Farina, R. Scattolini. *Two-layer model predictive control of independent systems with shared control sources*. IFAC Symposium on Large Scale Complex Systems - Delft (Netherlands), 26-28 May 2019.
  Conferred with the *IFAC Young Author Award*.
- A. Martinelli, A. La Bella, R. Scattolini. *Secondary control strategies for DC islanded microgrids operations*. European Control Conference - Naples (Italy), 24-28 June 2019.
- A. La Bella, L. Fagiano, R. Scattolini. *Set-membership identification of day-ahead microgrids scheduling*. European Control Conference - Naples (Italy), 24-28 June 2019.
- A. La Bella, S. Negri, R. Scattolini, E. Tironi. *A two-layer control architecture for islanded AC microgrids with storage devices*. IEEE Conference on Control Technology and Applications - Copenhagen (Denmark), 21-24 August 2018.
- A. La Bella, M. Farina, C. Sandroni, R. Scattolini. *Microgrids aggregation management providing ancillary services*. European Control Conference (ECC) - Limassol (Cyprus), 12-15 June 2018.

- A. La Bella, M. Farina, C. Sandroni, R. Scattolini. *On the design of a microgrids aggregation framework to provide ancillary services*. CIRED Workshop on "Microgrids and local communities"- Ljubjana (Slovenia), 2-8 June 2018.
- S. Raimondi Cominesi, A. La Bella, M. Farina, R. Scattolini, *A multi-layer control scheme for microgrid energy management*, IFAC Workshop on Control of Transmission and Distribution SmartGrids - Prague (Czech Republic), 11-13 October 2016.
- A. Bolzoni, A. La Bella et al. *Object based modelling of hybrid electrical vehicle and power management control* Research and Technologies for Society and Industry, IEEE 1st International Forum on - Turin (Italy), 16-18 September 2015.